Seismic Fragility Assessment of Highway Bridges

By

Seyyed Nima Mahmoudi

Department of Civil Engineering and Applied Mechanics

McGill University

Montreal, Quebec, Canada

January, 2015

A thesis submitted to McGill University in partial fulfillment of the requirements of the degree of Doctor of Philosophy

ABSTRACT

Fragility curves are useful tools for reliability evaluation of structures as well as for identifying the most vulnerable components. This study focuses on the seismic fragility analysis of highway bridges. Two main approaches are used for this purpose: component-based and system-based fragility analyses. The seismic vulnerability of two existing bridges located in Montreal are assessed as case studies.

The main goal of this study is to develop reliable seismic fragility curves for highway bridge structures considering all significant uncertainties involved. Uncertainties include those associated with modelling structural behavior, seismic inputs and definition of component capacities. The procedures are implemented for the fragility assessment of two existing bridges as case studies. For this purpose, deterioration due to corrosion of reinforcing steel and its effects on structural behavior are included, as well as validation of the Finite Element Model using dynamic properties obtained from ambient noise measurements. Proposed methods for the selection of appropriate set of ground motion records, the type of model analysis and probabilistic modeling of component capacities are presented and illustrated for the two case studies.

Two stochastic methods are proposed for validating the Finite Element Model of a bridge. The first method is based on classical hypothesis testing procedures while the second uses a Bayesian updating approach. The stochastic methods are also used to update the input parameters, detect probable major damage in the bridges and determine the confidence interval on model responses as a function of laboratory test data and field observations.
In order to limit the uncertainties involved in seismic inputs, a state-of-the-art ground motion record selection procedure based on Conditional Mean Spectrum (CMS) is used. Incremental Dynamic Analysis (IDA) is performed to evaluate the record to record variability in seismic responses and to capture the nonlinearity in structural component behaviors.

The first part of the thesis describes the application of component-based fragility analysis for the seismic vulnerability assessment of highway bridge structures. IDA is performed on the validated Finite Element model of the structure using an appropriate set of ground

motion records. The results are used for estimating the relationships between ground motion intensity measures and component demands. A Joint Probabilistic Seismic Demand Model (JPSDM) is fitted to the results in order to develop component and system fragility curves of the structure.

Since the component based fragility analysis of complex structures comprising a large number of components requires enormous computational efforts, in the second part of this study, a system-based approach for developing seismic system fragility curves is proposed which uses Support Vector Machines (SVM). SVM is a state-of-the-art machine learning technique which is used to discover patterns in highly dimensional and complex data sets. In this application, SVM is used to determine the relationship between ground motion intensity measures and peak structural responses. Seismic fragility curves are developed using Probabilistic SVM (PSVM). Finally, the efficiency of the proposed PSVM method for its application to vector-valued ground motion Intensity Measures (IM) as well as traditional single-valued IM are investigated.

RÉSUMÉ

Les courbes de fragilité sont utilisées afin d'évaluer la fiabilité des structures ainsi que pour identifier les composants les plus vulnérables. Cette recherche porte sur les analyses de fragilité sismique des ponts. Deux approches principales sont utilisées : 1) une analyse basée sur les courbes de fragilité de chaque composant et 2) une analyse basée sur la courbe de fragilité du système. Ces deux approches sont démontrées par la suite pour l'évaluation de deux ponts existants situés à Montréal. Les courbes de fragilité sont développées en considérant toutes les sources d'incertitudes aléatoire et épistémique, soit : le modèle de comportement structural, les sollicitations sismiques et la résistance des composants. L'évaluation de la fragilité des ponts existants comprend un modèle de détérioration associé à la corrosion des aciers d'armature ainsi qu'une validation du modèle structural à partir des caractéristiques dynamiques obtenues des mesures du bruit ambiant. De nouvelles procédures pour la sélection optimale des sollicitations sismiques et des méthodes d'analyse probabiliste pour la résistance des composants sont présentées et illustrées pour deux cas types. Deux méthodes stochastiques sont développées et proposées pour valider le modèle en éléments finis d'un pont. La première est basée sur les tests d'hypothèses statistiques classiques tandis que la deuxième est basée sur une approche bayésienne. Les méthodes stochastiques sont également utilisées afin d'actualiser les propriétés du système, identifier les causes les plus probables de défaillance et de définir un intervalle de confiance sur le comportement structural en fonction des résultats d'essais effectués en laboratoire ou sur le terrain. Afin de réduire l'incertitude sur les sollicitations sismiques à utiliser pour l'analyse, l'approche basée sur le spectre moyen conditionnel (Conditional Mean Spectrum - CMS) est utilisée. Des analyses dynamiques par incréments (ADI) sont effectuées afin d'estimer la variabilité du comportement sismique non-linéaire en fonction des caractéristiques des sollicitations. Dans un premier temps, un modèle de fiabilité est développé sur la base des courbes de fragilité par composant. Les courbes de fragilité sont dérivées à partir des analyses ADI en fonction de divers paramètres caractérisant les sollicitations sismiques et les demandes correspondantes sur chaque composant. Une distribution probabiliste conjointe des demandes sismiques (DPCDS) est estimée afin de dériver les courbes de fragilité pour les

composants ainsi que pour l'ensemble du pont (système). Un désavantage de l'approche par composant est la complexité et la quantité des analyses à effectuer lorsque le système comprend plusieurs composants. Une approche alternative basée sur l'analyse des systèmes est également proposée. Celle-ci est basée sur la théorie des Support Vector Machines (SVM), une méthode innovante d'apprentissage par simulation. Cette technique permet d'identifier les relations entre plusieurs variables à partir de l'analyse d'un grand nombre de données. Dans ce cas-ci, le SVM est utilisé afin d'établir la relation entre les mesures d'intensité des sollicitations sismiques et le comportement structural. Les courbes de fragilité sont développées par la technique de PSVM (Probabilistic Support Vector Machines). Finalement, la performance de la procédure est évaluée pour des analyses basées sur une approche multi-variable pour la caractérisation des sollicitations sismiques ainsi que sur les analyses traditionnelles à une variable.

PREFACE

I would like to express the deepest appreciation to my supervisor, Professor Luc Chouinard for his advice, support and encouragement throughout this study. He continually and persuasively conveyed a spirit of adventure in regard to this research and this dissertation would not have been possible without his continuous guidance.

I would also like to gratefully acknowledge the advice and assistance of Professor Denis Mitchell. His nice, friendly and inspiring attitude during my study is greatly appreciated. I am truly thankful for the financial support provided by the City of Montreal, Canadian Seismic Research Network (CSRN) and McGill University through VP and MIDA awards.

I also wish to specially thank my friend and officemate, Dr Payam Tehrani, for his technical and nontechnical supports. I would also like to give thanks to Dr Salman Saeed and Alireza Rouhi who accompanied and assisted me in conducting the Ambient Vibration Tests.

My special gratitude is extended to my parents and my sister for their endless love and unconditional support. I could not go this far without their unwavering support and confidence in my abilities.

My deepest and heartfelt gratitude goes to my beloved wife, Nasim, for her ceaseless love, support and sacrifice. I am truly blessed to have her by my side and to her I not only give my thanks but also my love.

CONTRIBUTION OF AUTHORS

I would like to express my sincere gratitude to the City of Montreal for providing detailed information about the studied bridge in chapter 5 and 6.

I would also wish to thank Dr. Payam Tehrani and Dr. Alejandro de la Puente for providing the finite element model of the bridge structure studied in chapters 3 and 4.
I am also grateful to Professor Denis Mitchell for his technical reviews and constructive comments on the articles in chapter 3 and 4.

Last but certainly not least, I wish to thank Professor Luc Chouinard for his supervision of research, technical reviews and helpful comments on the articles and this dissertation.

STATEMENT OF ORIGINAL CONTRIBUTIONS

- Application of ambient vibration survey in model validation, parameter updating and damage detection of highway bridge structures:
  It is shown that applying the proposed stochastic methods to analyze the ambient vibration test results can reduce the parameter uncertainties of the model. Moreover, this methodology is applicable for detecting structural damages which affect the overall stiffness of the structure as well as validating the structural model to reduce the model uncertainties.

- Investigation of the effect of component retrofits on system behavior and reliability of a typical highway bridge:
  Seismic fragility curves of a typical bridge located in Montreal are developed for both existing and retrofitted structure and the effect of retrofitting a frame component on the overall behavior and vulnerability of the structure is investigated.

- Developing reliable component-based and system-based seismic fragility curves of highway bridge structures considering all the significant uncertainties involved:
  All significant sources of parameter, model and numerical uncertainty which arise from seismic demand and component limit state estimation, modeling and fragility analysis are addressed in this study and where applicable, practical solutions are proposed to reduce the associated uncertainties.

- Introducing a novel methodology for seismic reliability assessment of structures based on Support Vector Machine (SVM) learning method:
  A new approach to develop fragility curves is proposed which provides more reliable estimations, minimizes the numerical uncertainties of fragility analysis and requires significantly less computational efforts.

I would like to dedicate this work to my wife, Nasim, for her never-ending support, patience and encouragement.

TABLE OF CONTENTS

Chapter 1: Introduction 1

1.1 Problem Description 1

1.2 Research Objectives 3

1.3 Thesis Organization 4

Chapter 2: Review of Relevant Concepts 7

2.1 Model Validation and Parameter Updating 7

2.1.1 Uncertainty Propagation (UP) 9

2.1.2 Classic Hypothesis Test 10

2.1.3 Bayesian Hypothesis Test 11

2.2 Ambient Vibration Test 13

2.2.1 Measurement Scheme 15

2.2.2 Synchronization 16

2.2.3 System Identification 16

2.3 Corrosion Effect 18

2.3.1 Corrosion Initiation 20

2.3.2 Corrosion Propagation 21

2.4 Ground Motion Record Selection 22

2.4.1 MR- Based Approach 24

2.4.2 Epsilon (ε) Based Approach 24

2.4.3 Uniform Hazard Spectrum (UHS) Based Approach 26

2.4.4 CMS Based Approach 26

2.5 IDA Method 29

2.5.1 Introduction 29
2.5.2 Intensity Measure (IM) and Engineering Demand Parameter (EDP) Selection 30
2.5.2.1 Efficiency 31
2.5.2.2 Practicality 32
2.5.2.3 Sufficiency 32
2.5.2.4 Hazard computability 33
2.6 Fragility Curves 34
2.6.1 Introduction 34
2.6.2 Fragility Analysis Approaches 35
2.6.2.1 System-Based Fragility 37
2.6.2.2 Component-Based Fragility: 39
2.6.3 Component Importance Measure 41
2.7 SVM learning 42
2.7.1 Introduction 42
2.7.2 Linear Binary SVM Classification for Separable and Non-separable Data 44
2.7.3 Nonlinear SVM Classification 47
2.7.4 SVM Model Selection 48
2.7.5 Multiclass SVMs 49
2.7.6 Probabilistic Support Vector Machines (PSVM) 50
Chapter 3: Manuscript 1 53
Abstract 53
3.1 Introduction 54
3.2 Structure and Structural Components Description 55
3.3 Finite Element Modeling and Laboratory test 57

3.4 Finite Element Model Validation 59
3.4.1 Classic Hypothesis Approach 60
3.4.2 Bayesian Model Validation Approach 63
3.5 Incremental Dynamic Analysis (IDA) 65
3.5.1 Selection of Ground Motion Records 65
3.5.2 Selection of EDPs and IM 67
3.5.3 IDA Results 69
3.6 Fragility Curves 69
3.6.1 Component Fragility 70
3.6.2 System Fragility 72
3.7 Conclusion 75
Chapter 4: Manuscript 2 77
Abstract 77
4.1 Introduction 78
4.2 Structure and Structural Components Description 79
4.3 Corrosion Effect 80
4.4 Bridge retrofitting strategy 83
4.5 Finite Element Modeling and Laboratory test 84
4.6 Finite Element Model Validation 86
4.6.1 Classic Hypothesis Approach 87
4.6.2 Bayesian Model Validation Approach 89
4.7 Incremental Dynamic Analysis (IDA) 92
4.7.1 IDA Results 93
4.8 Fragility Curves 94
4.8.1 Component Fragility 94

4.8.2 System Fragility 95
4.9 Conclusion 98
Chapter 5: Manuscript 3 100
Abstract: 100
5.1 Introduction 100
5.2 Finite Element Modeling and ambient vibration test 101
5.3 Finite Element Model Validation 105
5.3.1 Classic Hypothesis Approach 106
5.3.2 Bayesian Approach 107
5.4 Conclusion 109
Chapter 6: Manuscript 4 111
Abstract 111
6.1 Introduction 111
6.2 Review on SVMs 114
6.2.1 SVM Classification 114
6.2.2 Probabilistic Support Vector Machines (PSVM) 116
6.2.3 Model Selection 117
6.3 Case Study 117
6.3.1 Bridge Description and Finite Element Modeling 118
6.3.2 Ground Motion Selection and IDA 119
6.3.3 Fragility Curves 121
6.3.3.1 Component-Based Fragility Analysis 122
6.3.3.2 PSVM-Based Fragility Analysis 123
6.4 Results and Discussion 123
6.4.1 Fragility Curves using single-valued IM 123

6.4.2 Fragility Curves using Vector-valued IM 126
6.4.3 Multi-class reliability assessment 127
6.5 Conclusion 128
Chapter 7: Conclusions and Recommendations 130
Appendix A: Analytical Model of Highway Bridge Component 134
A.1 Superstructure 134
A.2 Steel Bearings 137
A.2.1 Low-type Fixed Bearings 139
A.2.2 High-type Expansion Bearings at the Abutments 140
A.2.3 High-type Expansion Bearings at the Columns 141
A.3 Reinforced Concrete Columns 142
A.4 Abutments 143
A.4.1 Longitudinal Direction 145
A.4.2 Passive Soil Behavior at Abutments 145
A.4.3 Pile Behavior 147
A.4.4 Transverse Direction 148
Appendix B: Ambient Vibration Test 149
B.1 Test Equipment and Measurement Scheme 149
B.2 Results of the System Identification Analysis 149
Appendix C: Ground Motion Selection 157
C.1 Deaggregation of Montreal Seismic Hazard 157
C.2 MATLAB Program for CMS Based Ground Motion Selection 159
C.2.1 Program Inputs 159
C.2.2 Program Outputs 159
C.3 Detailed Information of the Selected Ground Motion Records 168

Appendix D: Detailed Results of Incremental Dynamic Analysis of the Studied Bridge in Chapters 5 and 6 169

D.1 Ground Motion Intensities Corresponding to Different Component Failures .. 169

D.2 Component probabilistic Demand and Capacity Models at Selected Ground Motion Intensities 172

References 186

LIST OF FIGURES

Figure 2-1. Classic Hypothesis test for (A) Single Observation (B) Multiple observations 11
Figure 2-2. Model Validation of univariate system using Bayesian hypothesis approach 13
Figure 2-3. Tutti model of degree of corrosion in a deteriorating structure 20
Figure 2-4. Average response spectra for different ε values 25
Figure 2-5. Normalized average response spectra for various ε at a period of 0.4 sec .. 26
Figure 2-6. Comparison of PGA and Sa as candidate IM 32
Figure 2-7. Typical IDA results accompanied by median and 16 and 84 percentile responses for cases presenting a) softening and b) Weaving behaviour 34
Figure 2-8. A typical fragility curve 36
Figure 2-9. Fragility curve and the sample cumulative distribution (stepped curve) 38
Figure 2-10. Probabilistic Seismic Demand Model (PSDM) (Nielson, 2005) 40
Figure 2-11. Visual comparison of system fragility versus component fragility curves 42
Figure 2-12. Margin based loss function for SVM classification 45
Figure 2-13. Linearly separable SVM classification 46
Figure 2-14. Non-separable SVM classification 47
Figure 3-1. Frame elevation of bridge 55
Figure 3-2. Details of as-built bridge components: (a) Column cross section (b) Beam cross section 56
Figure 3-3. Deterioration in one of the bridge columns 56
Figure 3-4. Structural idealization of moment-resisting frame (Left side) 58
Figure 3-5. Predicted Component Response: (a) Force- Displacement of Columns (b) Moment- Curvature of Columns (c) Force- Displacement of Beams (d) Moment-Curvature of Beams 59
Figure 3-6. Relationships of the variables which are considered in RSM 63
Figure 3-7. Model Validation using classic hypothesis approach 63
Figure 3-8. Model Validation using Bayesian hypothesis approach 66

Figure 3-9. Epsilon values of all records and mean epsilon values computed using the AB06 GMPE for Eastern North America (Tehrani and Mitchell, 2012) 67
Figure 3-10- Comparison of PGA and Sa as candidate IM for ATC-63 ground motions for an Interior Column Component (Element 5). 69
Figure 3-11. IDA results associated with the 16, 50 and 84 percentiles for: (a) Beam Component (Element 13) (b) Interior Column Component (Element 5). 70
Figure 3-12. Comparison of the fragility curves of a Beam Component (Element 13), an Interior Column Component (Element 5) and an Exterior Column Component (Element 1) under ATC36 ground motion records 71
Figure 3-13. Comparison of component fragility curve for three different ground motion set: (a) Beam component (Element 13) (b) Interior column (Element 5)..... 72
Figure 3-14. Correlations between natural logarithm of demands for elements 1, 5 and 13 (Exterior Column, Interior Column and Beam) over a range of Sa..... 73
Figure 3-15. System fragility curve with confidence and prediction intervals under ATC63 ground motion records 74
Figure 3-16. Contribution of component failures in system failure under ATC63 records (a) Visual comparison of system fragility versus component fragility curves (b) CIM of components over Sa 75
Figure 3-17. Comparison of system fragility curve for three different ground motion sets of: ATC-63 (natural records), Atkinson-6C2 (artificial records) and Atkinson-7C2 (artificial records) 76
Figure 4-1. Lateral view of the bridge 80
Figure 4-2. Details of as-built bridge components: (a) Column cross section (b) Beam cross section 81
Figure 4-3. Deterioration in one of the bridge columns 82
Figure 4-4. Histogram of: a) time to initiation of corrosion (T_i) b) ratio of the area of the remaining reinforcing bars to the area of intact bars after 50 years of service life. . 83
Figure 4-5. Predicted force-displacement response of as-built column: a) Intact b) Spalled and corroded 84
Figure 4-6. Detail of a) Retrofitted beam section b) Retrofitted beam at joint location. 85
Figure 4-7. Predicted force-displacement response of a) as-built beam b) Retrofitted

beam 85
Figure 4-8. Structural idealization of the moment-resisting frame (Left side) 86
Figure 4-9. Model Validation using classic hypothesis testing based on: a)F_1 b)F_2 89
Figure 4-10. a) Classic Hypothesis test for multiple observations of F_1 and F_2 b) Power of the test 90
Figure 4-11. Power of Bayesian Test 92
Figure 4-12. Domain of observations which result in acceptance of the finite element model 93
Figure 4-13- IDA results associated with the 16, 50 and 84 percentiles for: (a) Exterior Column (Element 1) (b) Interior Column Component (Element 5) (c) Beam Component (Element 13) 95
Figure 4-14- Comparison of the fragility curves of interior and exterior columns (Element 5 and 1) under ATC36 ground motion records 96
Figure 4-15. Correlations between natural logarithm of demands for elements 1 and 5 and 13 (an exterior Colum and an interior Column) over a range of Sa 97
Figure 4-16. System fragility curve with confidence and prediction intervals under ATC63 ground motion records 98
Figure 4-17. Contribution of component failures in system failure under ATC63 records (a) Visual comparison of system fragility versus component fragility curves (b) CIM of components over Sa 99
Figure 4-18. Comparison of the system fragility curves of the existing and the retrofitted structures underATC36 ground motion records 99
Figure 5-1. Three Dimensional view of Finite Element model 103
Figure 5-2. Force-Displacement relationship in a) Abutments b) Bearings 104
Figure 5-3. Results of EFDD analysis for the (a) first, (b) second and (c) third mode shapes of the bridge 105
Figure 5-4. Model Validation using classic hypothesis approach (a) Free rotation at the bearings (b) Fixed rotation at the bearings 108
Figure 5-5. Model Validation using Bayesian hypothesis approach 110
Figure 6-1. Binary SVM classification 116
Figure 6-2. Three Dimensional view of Finite Element model of the bridge 120

Figure 6-3. Force-Displacement relationship in a) Abutments b) Bearings 120
Figure 6-4. a)CMS and UHS b)CMS and Sa of the top ten selected ground motion records 122
Figure 6-5. IDA results associated with the 16, 50 and 84 percentiles for: (a) Bearing at the second abutment (b) First Column 122
Figure 6-6. Prediction errors of the PSVM in fragility analysis with single-valued IM 125
Figure 6-7. System fragility curves based on PSVM method (RBF kernel function) and the sample cumulative distribution (stepped curve) a) Serviceability limit state b) Onset of Collapse limit state 126
Figure 6-8. Decision hyper-planes for (a) serviceability and (b) collapse limit states . 127
Figure 6-9. Fragility contours for a) serviceability b) onset of collapse limit states 128
Figure 6-10. Probability of sustaining various damage states assuming Sa as the IM . 128
Figure 6-11.Probability of sustaining various damage states assuming (Sa,ε) as the IM 129
Figure A-1. Typical cross-section geometry of the bridge 135
Figure A-2. Typical Superstructure Section Definition in SAP2000 136
Figure A-3. Elevation View Bridge Superstructure 136
Figure A-4. As-built plans of the bearings a) low-type fixed bearing b) High-type expansion bearing (I) c) High-type expansion bearing (II) d) high-type expansion bearing (at the abutments) 140
Figure A-5. Current condition of the bearings a) at an abutment b) at an interior column 141
Figure A-6. ABAQUS model of the bearing located at abutment of the bridge 141
Figure A-7. Failure mechanism of the fixed bearing 142
Figure A-8. Failure mechanism of high-type expansion bearings at the abutments 143
Figure A-9. Force-Displacement Relationship in Bearings 143
Figure A-10. As-built plans of a typical pier 144
Figure A-11. Typical pier model in SAP2000 144
Figure A-12. Force-Displacement curves of a typical pier in a) transverse b) longitudinal directions 145

Figure A-14. Abutment supported by pile group a) plan view b) elevation view 146
Figure A-15. Hyperbolic force-displacement behavior of abutment backfill soil as suggested by Shamsabadi et al. (2007) 148
Figure A-16. Force-displacement relationship of the abutments backfill soil 149
Figure B-1. Schematic representation of setups for ambient vibration measurements 152
Figure B-2. Singular value plot obtained from EFDD analysis 153
Figure B-3. First structural mode shape obtained from EFDD analysis 154
Figure B-4. Second structural mode shape obtained from EFDD analysis 154
Figure B-5. Third structural mode shape obtained from EFDD analysis 155
Figure B-6. Fourth structural mode shape obtained from EFDD analysis 155
Figure B-7. Fifth structural mode shape obtained from EFDD analysis 156
Figure B-8. Sixth structural mode shape obtained from EFDD analysis 156
Figure B-9. Seventh structural mode shape obtained from EFDD analysis 157
Figure B-10. Eighth structural mode shape obtained from EFDD analysis 157
Figure B-11. Ninth structural mode shape obtained from EFDD analysis 158
Figure B-12. Tenth structural mode shape obtained from EFDD analysis 158
Figure C-1. Deaggregation of Montreal for the probability of 2% in 50 years for various periods (Halchuk and Adam, 2007) 160
Figure D-1. Probabilistic models of the demand and capacity of bearing 1 for serviceability limit state, given that a) Sa=0.09, b) Sa=0.24 and c) Sa=0.39 175
Figure D-2. Probabilistic models of the demand and capacity of bearing 2 for serviceability limit state, given that a) Sa=0.09, b) Sa=0.24 and c) Sa=0.39 176
Figure D-3. Probabilistic models of the demand and capacity of bearing 3 for serviceability limit state, given that a) Sa=0.09, b) Sa=0.24 and c) Sa=0.39 177
Figure D-4. Probabilistic models of the demand and capacity of bearing 4 for serviceability limit state, given that a) Sa=0.09, b) Sa=0.24 and c) Sa=0.39 178
Figure D-5. Probabilistic models of the demand and capacity of bearing 5 for serviceability limit state, given that a) Sa=0.09, b) Sa=0.24 and c) Sa=0.39 179
Figure D-6. Probabilistic models of the demand and capacity of bearing 6 for serviceability limit state, given that a) Sa=0.09, b) Sa=0.24 and c) Sa=0.39 180
Figure D-7. Probabilistic models of the demand and capacity of column 1 for

serviceability limit state, given that a) Sa=0.51, b) Sa=0.99 and c) Sa=1.5 181
Figure D-8. Probabilistic models of the demand and capacity of column 2 for serviceability limit state, given that a) Sa=0.51, b) Sa=0.99 and c) Sa=1.5 182
Figure D-9. Probabilistic models of the demand and capacity of column 3 for serviceability limit state, given that a) Sa=0.51, b) Sa=0.99 and c) Sa=1.5 183
Figure D-10. Probabilistic models of the demand and capacity of column 4 for serviceability limit state, given that a) Sa=0.51, b) Sa=0.99 and c) Sa=1.5 184
Figure D-11. Probabilistic models of the demand and capacity of the pile group for serviceability limit state, given that a) Sa=0.51, b) Sa=0.99 and c) Sa=1.5 185
Figure D-12. Probabilistic models of the demand and capacity of bearing 1 for collapse limit state, given that a) Sa=0.51, b) Sa=0.99 and c) Sa=1.5 186
Figure D-13. Probabilistic models of the demand and capacity of bearing 4 for collapse limit state, given that a) Sa=0.51, b) Sa=0.99 and c) Sa=1.5 187
Figure D-14. Probabilistic models of the demand and capacity of bearing 6 for collapse limit state, given that a) Sa=0.51, b) Sa=0.99 and c) Sa=1.5 188

LIST OF TABLES

Table 2-1. Formulation of Kernel Functions 48
Table 3-1. Parameters of the input variable distributions in prior and posterior states .. 61
Table 3-2. Parameters of the input and output variable distributions in prior and posterior states 65
Table 3-3. Mean epsilon values at different hazard levels from seismic deaggregation for Montreal (Tehrani and Mitchell, 2012)..... 67
Table 4-1. Parameters of the input variable distributions in corrosion effect prediction 83
Table 4-2. Parameters of the input variable distributions in prior and posterior states .. 91
Table 4-3. Distribution values used in developing component fragility curves under ATC63 records..... 96
Table 5-1. Comparison of natural periods obtained by ambient vibration test and the Finite Element model..... 106
Table 5-2. Parameters of the input variable distributions in prior and posterior states 110
Table 6-1. Formulation of Kernel Functions 117
Table 6-2. Quantitative Limit states for structural components 123
Table 6-3. Optimal SVM parameters and associated prediction errors in classifications 125
Table 6-4. Results of Kolmogorov–Smirnov goodness of fit test 126
Table A-1. Section Properties of the Superstructure at End Spans and the Middle Span 137
Table A-2. Selected geotechnical parameters for passive soil behaviour modeling 148
Table A-3. Model properties of soil passive action 149
Table A-4. Model properties of soil passive action 150
Table B-1. Structural natural periods obtained from EFDD analysis..... 153
Table C-1. Detailed information of 40 selected ground motion records for dynamic time history analysis of the studied bridge 170
Table D-1. Spectral Accelerations at which the bearings exceed serviceability limit state 172
Table D-2. Spectral Accelerations at which the bearings exceed collapse limit state.. 173

SYMBOLS AND ABBREVIATIONS

A_0	Area of intact bars
ASC	Advanced simulation and computing
A (t)	Area of the remaining reinforcing bars at time t
ATC	Applied technology council
AVT	Ambient vibration testing
b	Bias term
B	Bayes factor
C	Chloride ion concentration, SVM penalty parameter
C_0	Chloride concentration at the surface
C_{cr}	Critical chloride concentration
CIM_i	Importance measure of component *i*
CMS	Conditional mean spectrum
COV	Coefficient of variation
CPSD	Computation of the cross-power spectral density
CSCE	Canadian society of civil engineering
D_0	initial diameter of the bar
DAS	Data acquisition systems
D_c	Diffusion coefficient
DDAG	Decision directed acyclic graph
D (t)	Diameter of the corroding bar at time t
ECC	Engineered cementitious composites
EDP	Engineering demand parameter
$\widehat{EDP}$	Median demand at the given intensity measure
EFDD	Enhanced frequency domain decomposition
erf	Gaussian error function
ERM	Empirical risk minimization
F	Faraday's constant, 96500 A.S.

f_c	Compressive strength of concrete
FDD	Frequency domain decomposition
FEM	Finite element method
f_i	Failure event of component *i*
FORM	First order reliability method
f_{sys}	System failure event
FRP	Fiber-reinforced polymer
F_{ult}	maximum abutment force
FVT	Forced vibration testing
f (x)	Prior probability density function, the classification decision score in SVM
f_y	Yielding stress of reinforcing bars
f (θ_i)	Prior probability density function of the input parameter θ_i
GMPE	Ground motion prediction equation
GWN	Gaussian white noise
H_0	Null hypothesis
H_1	Alternative hypothesis
H	Abutments back wall height
i_{corr}	Corrosion current density in the media
IDA	Incremental dynamic analysis
IM	Intensity measure
IUQ	Inverse uncertainty quantification
JPSDM	Joint probabilistic seismic demand model
K	Average soil stiffness
K_{eff}	effective stiffness
K-S test	Kolmogorov-Smirnov test
K (x_i,x_j)	Kernel function of two variables in the input space
L_d	Axial dead load of bridge deck
ln S_a(T)	Natural logarithm of the spectral acceleration at period T
LS	Limit state of the bridge or bridge components
LSSVR	Least square support vector regression

$L(y \mid \theta_i)$	Likelihood of observations given the parameter θ_i
M	Ground motion magnitude
$\bar{M}$	Mean ground motion magnitude
MCS	Monte Carlo simulation
m_{Fe}	Atomic weight of Fe (56g)
MSR	Matrix-based system reliability
NN	Neural networks
NNSA	National nuclear security administration
OVA	One-vs-all binerization technique
OVO	One-vs-one binerization technique
PGA	Peak ground acceleration
PP	Peak picking
PSDM	Probabilistic seismic demand model
PSHA	Probabilistic seismic hazard analysis
PSVM	Probabilistic support vector machine
R^2	Coefficient of determination
RBF	Radial basis function
r_{corr}	rate of corrosion
r_{ij}	Binary SVMs of the i^{th} and j^{th} classes
R_p	Polarization resistance
RSM	Response surface method
S_a	Spectral acceleration
S_c	Median of capacity for the selected limit state
SORM	Second order reliability method
SRA	Seismic risk assessment
SRM	Structural risk minimization
SSE	Sum of squared errors
SVM	Support vector machine
UHS	Uniform hazard spectrum
UP	Uncertainty propagation
V_{s30}	Average shear wave velocity of soil

V_c	Shear resistance of beam
y	Vector of observations
y_{max}	Maximum displacement
α	Level of significance of the test
β	Reliability index
β_c	Logarithmic standard deviation of capacity uncertainties
$\beta_{(EDP \mid IM)}$	Logarithmic standard deviation of component demand
β_F	Logarithmic standard deviation of fitted cumulative distribution
β_M	Logarithmic standard deviation of modelling uncertainties
β_{tot}	Combined logarithmic standard deviation of fragility curves
γ	Kernel parameter
ε	Epsilon, the number of logarithmic standard deviations by which a target ground motion differs from a median ground motion
$\varepsilon(T_1)$	Value of Epsilon at the first natural period of the structure
$\bar{\varepsilon}(T_1)$	Mean value of Epsilon at the first natural period of the structure
λ (D)	Mean annual frequency of exceeding a level of demand
λ (IM)	Mean annual frequency of exceeding a given intensity measure
θ_i	Input variable
$\mu_{lnSa(T)}$	Predicted mean of $\ln(S_a)$ at period T
ξ_i	Slack variable
$\sigma_{lnSa(T)}$	Standard deviation of $\ln(S_a)$ at period T
Φ (x_i)	Function that maps data from input space into a higher dimensional feature space
Σ	Covariance matrix

CHAPTER 1: INTRODUCTION

1.1 PROBLEM DESCRIPTION

Historic seismic events such as the Saguenay (M_s 5.8) and Ungava (M_s 6.3) earthquakes in 1988 and 1989 aroused an awareness that seismic hazards extend beyond the seismic regions of western Canada. Seismic issues of highway bridges have been traditionally neglected in eastern Canada and seismic deficiencies of existing bridges must be assessed and addressed.

Uncertainties involved in determining the demands from earthquakes and in evaluating the capacity of structures under cyclic loads are important inputs to probabilistic methods for evaluating the reliability of structures. The seismic reliability of a structure can be evaluated by combining seismic hazards at the location of the structure and the fragility function of the structure. Fragility curves represent the state-of-the-art in seismic risk assessment (SRA) and are defined as the conditional probability that a structure will meet or exceed a certain level of damage for a given ground motion intensity.

Fragility curves can be developed for structural components as well as for the structure as a whole system. By considering variability in seismic inputs, structure response, and material capacity into account, component fragility curves are useful tools to identify weak parts of the structure and to guide the efficient allocation of funds to strengthen or retrofit an existing structure while system fragility curves are useful in seismic risk assessment of the structure.

Fragility curves can also be used in the post-earthquake evaluation of bridges. Immediately following an earthquake, the damage state of bridges located in the affected area can be estimated rapidly using fragility curves knowing the intensity measures of ground motions to effectively assist the functional assessment stage of recovery. In addition, after a detailed inspection of the bridge components, fragility curves can be updated based on observations and using probabilistic methods.

Analytical fragility curves are developed through seismic response data from the analysis of bridges. The fragility analysis generally includes the following major steps;

1) Modeling of the bridge structure considering the uncertainty in its properties.
2) Selection or simulation of ground motions representing the effect of soils and earthquakes
3) Analysis of the structure subjected to ground motions
4) Performing analyses to estimate the fragility curves from the response of the bridge model.

In modeling of existing bridge structures, the effects of aging, deteriorations and corrosions should be considered. According to Tavares et. al. (2010), 75% of Quebec's bridges have more than thirty years of service life. Moreover, they are subject to the frequent use of deicing salts in winter and their columns are exposed to splash and mist from service roads adjacent to the bridges. Deicing salts are sources of chloride ions which may result in corrosion of the reinforcing steel and spalling of the concrete cover. Moreover, it is important to validate the structural models based on available test data of the actual bridge in a probabilistic context in order to minimize the uncertainties in modeling and probable model errors.

For ground motion record selection, various techniques have been suggested and used which are generally based on matching a spectral response to a target spectrum. The target spectrum should be based on the seismic hazard and soil characteristics at the location of the bridge and the dynamic behavior of the bridge structure.
In order to reach the highest level of accuracy, most fragility curves are developed based on nonlinear time history analysis of the structures for a given set of ground motion records. The results of the structural analysis provide the data to define the relationship between ground motion intensity and the Engineer Demand Parameter (EDP) as well as the record-to-record variability.

Two approaches have been used in developing fragility curves for a structural system: System-based and Component-based fragility analyses. In system-based fragility analysis, the damage state is defined for the system and the system fragility is defined as the probability of sustaining a certain level of damage in the system at a given ground motion intensity. However, in component based fragility analysis, the probability of exceeding the defined limit state for the given ground motion intensity is calculated for

each component and the probability of system failure is estimated considering the dependencies between the components.

Component-based fragility analysis of structures comprising a large number of components requires enormous computational effort. The application of Machine Learning and Soft Computing methods such as Support Vector Machines (SVM) is an alternative for discovering patterns in highly dimensional and complex data sets such as the relationship between ground motion intensities and peak structural responses.

1.2 RESEARCH OBJECTIVES

The main objective of this thesis is to propose methodologies to develop reliable fragility curves for highway bridges accounting for all significant uncertainties involved. Although the proposed methodologies are only applied to the reliability assessment of two existing reinforced concrete highway bridges located in Montreal as case studies, the general concepts are applicable to other bridge types and materials. The first case study is a typical three-span bridge with total length of 68.8 meters which is supported by rigid frames comprising 12 slender columns. The assessment of this case study can be broken down into the following steps:

- Developing a 3-Dimensional non-linear analytical model. (de la Puente Altez, 2005).
- Model validation and parameter updating based on available laboratory test results of a half-scale model provided by Itagawa (2005)
- Estimation of corrosion effect on behavior of structural components.
- Identify a set of synthetic ground motion records which are representative of the seismic hazard for the Montreal region.
- Performing Incremental Dynamic Analysis (IDA) of the structure with selected ground motions
- Generate probabilistic seismic demand models for various bridge components and obtain joint distribution of component demands for any given ground motion intensity.
- Investigate the effect of using various earthquake intensity measures on the

probabilistic seismic demand models

- Developing seismic fragility curves for critical components.
- Developing system fragility curve of the bridge
- Investigate the effect of a suggested retrofit strategy (proposed by de la Puente Altez, 2005) on fragility curves for the bridge by following the previous steps for the retrofitted structure.

The second case study is a fragility assessment of a bridge with 5 spans with a total length of 232 meters which is supported by hammerhead piers. The specific tasks that are completed for this case study are as follows:

- Develop a 3-Dimentional non-linear analytical model of the bridge including detailed analytical models of the various bridge components.
- Performing ambient vibration tests on the bridge.
- Model validation based on results obtained from ambient vibration tests.
- Ground motion selection by using Conditional Mean Spectrum (CMS) as the target spectra
- Incremental Dynamic Analysis (IDA) of the bridge for selected ground motion records
- Develop component-based fragility curves for the structure
- Develop system fragility curve of the structure using SVM learning

1.3 THESIS ORGANIZATION

After the first introductory chapter, an overview of the main concepts which are required in fragility analysis of highway bridges is presented in chapter 2. This chapter reviews concepts of model validation and parameter updating, ambient vibration test, corrosion effect, ground motion record selection, IDA method, fragility analysis and SVM learning method.

Chapter 3 is a journal article by the author which deals with component based fragility analysis of supporting frames of a typical existing highway bridge located in Montreal. This article adopts two stochastic model validation methods for finite element model validation of the structure using a single observation. The results of a laboratory test on a

half scale model of a supporting frame conducted by Itagawa (2005) are used in model validation process. The results obtained from IDA are used in comparison of the effectiveness of two IM candidates (Spectral Acceleration (Sa) and Peak Ground Acceleration (PGA)) and are used to develop component and system fragility curves. It is demonstrated that the bridge has several major deficiencies such as absence of shear reinforcement in support beams which causes a brittle failure in cap beams of the supporting rigid frames.

Chapter 4 contains a second journal paper by the author which is a companion-paper to the previous article. This article investigates the effectiveness of a retrofit strategy proposed by de la Puente Altez (2005) and presents the influence of the retrofit on the fragility and reliability of the bridge structure. This article also applies the introduced stochastic model validation methods in finite element model validation of the structure using multiple observations. The results of a laboratory test on a half scale model of a supporting frame conducted by Coulombe (2007) are used in the model validation process. Corrosion effects on structural components is also investigated in this article.
Chapter 5 presents a paper accepted in the Canadian Society of Civil Engineering (CSCE) conference (Mahmoudi and Chouinard, 2013). This article deals with finite element modeling and model validation of the second case study. Ambient vibration test results (Saeed, 2013) are used in model validation and parameter updating in this case.

The final journal article by the author presented in Chapter 6 introduces SVMs and presents the application of the Probabilistic Support Vector Machine learning method in developing system fragility curves and demonstrates the superiority of this method to conventional fragility analysis methods. It is indicated that developing fragility curves using the PSVM method results in more reliable estimations, minimizes the numerical uncertainties of fragility analysis and requires significantly less computational efforts. This article also describes a methodology for ground motion selection using Conditional Mean Spectrum (CMS) as the target spectrum.
Chapters 3 to 6 are prepared as individual articles; therefore, the overlap seen in the content of these Chapters is to maintain their technical integrity and completeness. Contributions of the co-authors of the first two journal papers include finite element

modeling of the structure in Ruaumoko 3D (Carr, 2001), supervision of research, technical review of the articles and the contribution of the co-author of the other papers includes supervision and technical review of the articles.

Conclusions of this study and recommendations for future work are presented in Chapter 7.

Appendices:
Appendix A: provides more details regarding structural modeling of the bridge studied in Chapters 5 and 6.

Appendix B: provides more details regarding ambient vibration tests of the bridge studied in Chapters 5 and 6.

Appendix C: provides more information and data regarding CMS based ground motion selection

Appendix D: provides more detailed analysis results for the bridge studied in Chapters 5 and 6.

CHAPTER 2: REVIEW OF RELEVANT CONCEPTS

A typical seismic analytical fragility analysis of a structure includes modeling the structure, ground motion selection, dynamic analysis and a procedure to develop fragility curves from the response of the bridge model. This chapter presents a detailed overview of the concepts and methodologies adopted in this study as well as a review of the existing literature in each relevant field.

2.1 MODEL VALIDATION AND PARAMETER UPDATING

It is infeasible and uneconomical to estimate the reliability of a structure by performing full-scale tests. So, model-based computations are becoming increasingly popular in reliability assessments. However, model predictions are influenced by physical, statistical and model uncertainties. Hence, it is imperative to validate model predictions using some benchmarks. In model validation, the benchmarks are high-quality experimental measurements of the response of the system or subsystem and component level models. Traditionally, computer models have been verified using subjective or quantitative comparison approaches (Chen et. al., 2004). The former is based on visual comparison of the plots or contours of the predicted model and observations. This approach neither presents the uncertainties involved in the prediction model nor demonstrates the level of confidence in the model. The latter uses some measures as the ratio of the results obtained from the model and observations. However, a prescribed acceptable measure cannot be found in the literature for every case.

Kleijnen (1995A, 1995B) proposed two methods for model validation. The first method investigates whether the model predictions and experimental data demonstrate positive correlation and moreover have the same mean values. The other method uses Monte Carlo Simulation (MCS) and sensitivity analysis to find out whether the model inputs have effects on the model outputs that agree with the experts' intuition. Although these methods use statistical methods and offer more information regarding the model, they still rely on prescribed acceptable measures and do not demonstrate the confidence of the model.

During the last decade, large scientific computing projects, such as those led by the US

National Nuclear Security Administration (NNSA) and the Advanced Simulation and Computing (ASC) program, have developed methods to improve project oriented validation experiments (Pilch *et. al.*, 2001; Trucano *et. al.*, 2002; Oberkampf *et. al.*, 2004; Pilch *et. al.*, 2004).

Uncertainties arising from the selection of the conceptual model, the formulation of the mathematical model and the computations of the simulation are mathematically mapped and propagated to uncertainties in the simulation results. Using a probabilistic context for system properties and inputs is a proper approach to address these uncertainties. When the system properties and load conditions are random variables, the outputs also become random variables. Hence, an Uncertainty Propagation (UP) technique is required to obtain the distribution and confidence bounds of the system output. The available methods for UP are briefly discussed in the following section.

Oberkampf and Barone (2006) use statistical confidence intervals to propose validation metrics for interpolation and regression of experimental data. Oberkampf and Trucano (2002) demonstrated the construction of validation metrics based on experimental error and discussed benchmarks for model validation metrics. Hills and Leslie (2003) developed a validation metric which normalizes the difference between the model prediction and the experimental observations to compute a relative error norm.

Using classic hypothesis analysis is also an appropriate option for building and quantifying confidence intervals, as well as for the demonstration of the goodness-of-fit of a model. According to Hills and Trucano (1999), if an experiment falls inside a given confidence bound of the predicted model, the experiment and the model are consistent; otherwise the model will be rejected. This test is applicable for both univariate and multivariate systems and is the foundation of the methods which reject incorrect models. Chen et. al. (2004) has adapted this methodology for model validation of univariate and multivariate systems.

Another approach is developed by Mahadevan and Rebba (2005) and Rebba and Mahadevan (2006) which focuses on accepting appropriate models using Bayesian hypothesis testing. In this methodology a model is accepted if the observation favors the

model. In other words, if the probability density of the predicted value increases as the condition of the new observation, the model will be acceptable.

It is noted that there may not be a unique acceptable model and every model validation method accepts a variety of models. However, the mentioned methods present statistics which can be a representation of the goodness of each model. For this purpose, classical hypothesis test uses the confidence bound or p-value of the test while Bayesian hypothesis approach introduces the Bayes factor.

Finite element models of the highway bridges in this study are validated by classic hypothesis tests and Bayesian hypothesis tests. Hence, these methodologies are explained in detail in the following section.

2.1.1 UNCERTAINTY PROPAGATION (UP)

A lot of effort has been made to develop UP methods in various fields. Hence, there are numerous available methods which are designed for different purposes. Various aspects such as the required level of uncertainty quantification, accuracy or confidence level and the computational cost or efficiency should be considered for UP method selection. Lee and Chen (2009) have classified and investigated the applicability and merits of various UP methods.

Simulation based methods such as MCS is the most frequently used category of UP methods. Madsen et. al. (2006), Christensen and Baker (1982) and Kiureghian (1996) have applied MCS for UP analysis. This method offers the highest accuracy but requires the highest computational cost. Alternative sampling techniques such as Halton sequence (Halton, 1960), Hammersley sequence (Hammersley, 1960) and Latin supercube sampling (Owen, 1998) can be used to reduce the computational cost. However, none of these methods is feasible for systems that require complex computer simulations.

An alternative category of UP methods is the local expansion-based methods. These methods simplify the relationship between the system output and the inputs and develop metamodels of the system using methods such as Taylor series or perturbation method. Madsen et. al. (2006), Christensen and Baker (1982), Kiureghian (1996) and Ghanem and

Spanos (1991) adopted this category of UP methods. Methods in this category are generally computationally efficient but weak against the large variability of inputs and nonlinearity of the system. However, their performance can be improved by using more complicated metamodels. Chen et. al. (2004) has suggested Response Surface Method (RSM) to develop metamodels in order to perform UP analysis. RSM was initially introduced by Box and Wilson (1951) and investigates the relationships between explanatory system inputs and one or more system responses. UP analysis in this study is performed as suggested by Chen et. al. (2004).

Other available UP methods in the literature are functional expansion-based methods such as Polynomial Chaos Expansion and Wavelet Expansions, Most probable point-based methods such as first-order reliability method (FORM) and second-order reliability method (SORM) and Numerical integration-based methods such as Full factorial numerical integration method. (Lee and Chen, 2009)

2.1.2 CLASSIC HYPOTHESIS TEST

In order to validate a model by classic hypothesis test, confidence bounds of the system output(s) at a specified significance level are calculated based on the results from UP analysis of the system. Then, experimental observations are compared to the confidence bounds. A model is acceptable if the observations fall inside the given confidence bound of the predicted model. The main steps for performing classic hypothesis test model validation are as follows:

- Identifying the sources of uncertainty in the system output
- Forming experiments
- Defining the probabilistic distributions of system inputs
- Employing efficient UP analysis
- Calculating multivariate probabilistic distribution of system outputs
- Determine the appropriate level of significance of the test (α) and corresponding confidence bounds.
- Model validation through comparison

Figure 2-1 illustrates model validation for univariate and multivariate systems using

classic hypothesis testing.

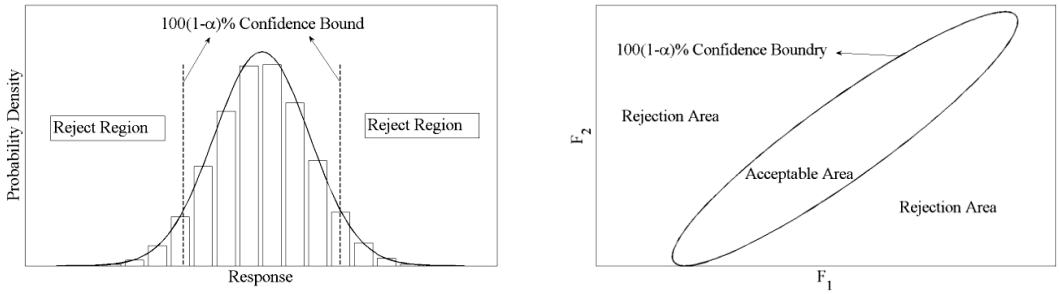

(A) (B)

Figure 2-1. Classic Hypothesis test for (A) Single Observation (B) Multiple observations

Model validation based on classic hypothesis testing approaches provides a powerful method to represent the confidence of the model. However, Edwards et. al. (1963) demonstrates that the classical approaches are often prone to rejecting the null hypothesis on account of the data that do not greatly detract from its credibility because this approach neglects the prior distribution under the alternative hypothesis. In other words, this approach considers how unlikely an observation is if the null hypothesis is true, but do not consider whether the observation is even less likely if the null hypothesis is false. Hence, models are also validated based on Bayesian hypothesis approach in this study.

2.1.3 BAYESIAN HYPOTHESIS TEST

Bayesian Hypothesis testing compares the likelihood of the experimental observations under the null hypothesis (H_0) and the alternative hypothesis (H_1). In this approach, a model is acceptable if the observations favor the model (null hypothesis). The Bayes factor (B) is defined as shown in equation (2-1) and the models with a Bayes factor higher than one are acceptable.

$$B(x_0) = \frac{P(y|H_0: x = x_0)}{P(y|H_1: x \neq x_0)} \tag{2-1}$$

In equation (2-1) y and x_0 represent the observation and the model prediction respectively. This approach was first used in mechanical model validation by Zhang and Mahadevan

(2000). Mahadevan and Rebba (2005) demonstrated that for a single observation test the Bayes factor can be calculated from equation (2-2):

$$B(x_0) = \frac{f(x|y)}{f(x)}|_{x=x_0} \tag{2-2}$$

In which f(x) and f(x|y) represent the prior and posterior Probability Density Functions (PDF) respectively. From equation 2-2, it is inferred that a model is acceptable if the probability density of the model prediction increases with the condition of the new observation. Similarly, for multivariate systems, the Bayes factor is equal to the ratio of the posterior Joint Probability Density Function (JPDF) to the prior JPDF as suggested by Rebba and Mahadevan (2006).

In order to calculate $B(x_0)$ in equation (2-2), the prior and posterior PDF of the system input are required. The prior PDF (f(x)) is obtained by a UP analysis as explained in section 2-1-1. In order to calculate the posterior PDF (f(x|y)), first, the PDF of input variables of the system are updated through an Inverse Uncertainty Quantification (IUQ). Then, the posterior PDF of the system output is obtained by a UP analysis and using the updated PDF of input variables.

In this study, IUQ is also done under the Bayesian framework. Equation (2-3) is used to update the PDF of the input variables given the observations ($\underline{y}$).

$$f(\theta_i|\underline{y}) = \frac{L\left(\underline{y}\middle|\theta_i\right).f(\theta_i)}{\int_{\theta_i} L\left(\underline{y}\middle|\theta_i\right).f(\theta_i)\ d\theta_i} \tag{2-3}$$

In which θ_i represents the input variables, $L(\underline{y}|\theta_i)$ is the likelihood of the observations in prior system and $f(\theta_i)$ represents the prior PDF of the inputs. Generally, IUQ analysis based on equation (2-3) is computationally troublesome and requires numerical integration. However, since the metamodel of the system is used in this study, equation (2-3) can be calculated conveniently by MCS or analytically.

Figure 2-2 shows the Bayesian Hypothesis model validation for a univariate system.

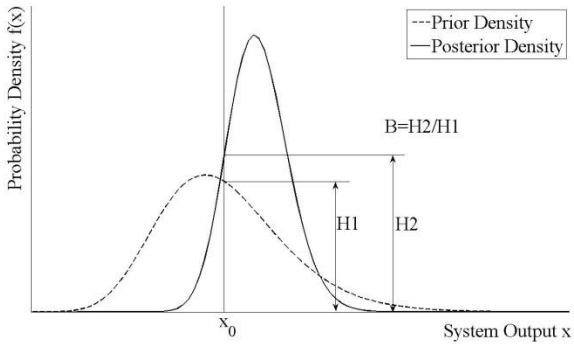

Figure 2-2. Model Validation of univariate system using Bayesian hypothesis approach

2.2 AMBIENT VIBRATION TEST

Various test and survey procedures have been used in bridge inspection which can be applied in model validation analysis. The appropriate test should be selected for every case based on the applications, advantages, limitations, cost and accuracy of the available surveys.

The process in which structural parameters are determined based on measurements is called System Identification (Juang & Pappa, 1994). System identification analysis have been successfully implemented in various applications such as model validation (Kleijnen (1995) and Ren et. al. (2004a)), parameter updating (Zhang and Mahadevan (2000), Soize et. al. (2008) and Wu and Li (2004)), damage detection (Gentile & Saisi (2007), Siddique et. al. (2007), Zhang (2007)) and seismic vulnerability assessments (Boutin et. al. (2005), Herak (2009), Gosar (2012) and Michel et. al. (2012)).

Modal testing is a non-destructive survey of structures which provides modal information of the structure such as natural frequencies, damping and vibration mode shapes. Modal testing was first developed in aerospace and mechanics and later adapted for civil engineering applications. However, implementation of these methods in civil structures has challenges that should be addressed (Sohn and Law, 2000):

- The modal properties of civil structures are highly dependent on environmental conditions such as temperature, loading and humidity. Hence the uncertainties involved in modal assessment of these structures are typically higher than other types of structures

or machines. According to Sohn et. al. (1999), natural frequencies of a structure may change by as much as 5% during a day as the result of temperature changes. Hence, the variability in modal properties of a structure may be several times higher that changes in modal properties due to structural damage.

- Civil structures are typically highly redundant, geometrically complex and consisting of several types of materials. As a result, multiple non-unique acceptable models may exist which are compatible with modal measurements.

- The spatial extent of civil structures and maintaining their functionality during testing increases the cost of certain types of surveys.

Modal test can be categorized into two classes based on the nature of the excitations: Forced Vibration Testing (FVT) and Ambient Vibration Testing (AVT). In FVT, an artificial excitation device is used to impose an external force to the structure. The main advantage of FVT is that input excitations are controlled and precisely measured (Huang, 2007). However, this method of modal test is rather expensive, intrusive and may cause minor damages to the structure in some cases.

In AVT, the system identification is based on operational dynamic excitations or environmental ambient excitations due to wind, human activity or micro-tremors. AVT has recently become a popular method for assessing the dynamic behaviour of full-scale structures. Ambient vibration surveys are non-intrusive because no excitation equipment is needed which translates into minimal interference with the normal function of the structure.

The input excitation in AVT is not measured but assumed to be a Gaussian White Noise (GWN). The frequency domain representation of GWN is a function with constant power (Bendat and Piersol, 1993). It is noted that since the amplitude of input excitations are very small at all frequencies, the components of structural displacements are small and are representative of linear elastic behavior.

Hans et. al. (2005) demonstrated that the AVT provides reliable and efficient data and results obtained from AVT and FVT are in good agreement when comparing the

structural responses from ambient vibrations, harmonic excitation or shock loading.

AVT is especially suited to flexible systems such as long highway bridges. According to Farrar and James (1997), the first application of AVT on a bridge was carried out by McLamore et. al. (1971) and since then, AVT of highway bridges has been performed in numerous studies (Sloan et. al. (1992), Harik et. al. (1997), Farrar and James (1997), Brown- John et. al. (1999), Sohn and Law (2000), Cunha et. al. (2001), Gentile and Martinez y Cabrera (2004), Ren et. al. (2004a and 2004b), Gentile and Gallino (2007) and Conte et. al. (2008)).

System identification by AVT is typically performed by the following steps:
- Define the measurement scheme
- Synchronization of measurements
- System Identification

2.2.1 MEASUREMENT SCHEME

Sensors are used in AVT to measure the velocity or accelerations resulting from ambient excitements. The sensors may have built-in Data Acquisition Systems (DAS) to record the data and radio transceivers.

The first step in an ambient vibration survey is to select the points at which the response is measured. The selection of the points should be done in a way such that the points are accessible and the survey does not interrupt the normal activities of the structure. With those restrictions in mind, the points which define a proper modal model should be selected so that the estimated modal shapes can be detected with sufficient resolution.
For large structures such as high-rise buildings and highway bridges, there may be a need to plan multiple setups due to the limitation in number of available sensors. In that case, some sensors are designated as reference sensors and remain at the same location during the survey while the rest of the sensors (roving sensors) move along the structure for various setups. Reference sensors are required in order to synchronize and assemble the data recorded by the roving sensors.

It is recommended that the reference devices be located in the positions with the highest

amplitude of vibration. For bridges, a node in vicinity of the middle point of the interior span is suggested for the reference point.

The data recording frequency (sampling frequency) should be determined at this stage. The sampling frequency depends on the method of data synchronization. In the case when synchronization is done by GPS time marker technique, a high sampling frequency would be used. However, after the synchronization, the recorded data can be decimated to reduce the computational effort for system identification.

2.2.2 SYNCHRONIZATION

If the sensors have built-in radio transceivers, they can communicate to synchronize their internal clocks within a millisecond precision. Hence, the recorded data in such sensors are synchronized.

However, if sensors with radio transceivers are not available, a synchronization procedure is required. An option for synchronization of the data is to use GPS time markers.
In this study, TROMINO® velocity-meters are used which have built-in data acquisition systems with radio transceivers. Hence, a synchronization procedure is not required in this study. For more information regarding data synchronization, refer to Saeed (2013).

2.2.3 SYSTEM IDENTIFICATION

System identification methods based on AVT can be categorized in different ways. Ewins (2000) and Maia and Silva (1997) conducted a thorough investigation on various techniques of system identification. These methods can be divided based on their domain of analysis (Time Domain or Frequency Domain).

Frequency domain methods are based on an extension of the Fourier analysis while for the time domain analysis, autocorrelation functions are used to determine natural frequencies, modal shapes, and the logarithmic decrement concept is adapted to estimate damping coefficients. Frequency domain methods are more commonly used due to their simpler implementation and interpretation. However, both approaches have benefits and disadvantages and the appropriate method should be selected based on the case under

study.

According to Saeed (2013), Time domain methods demonstrate higher precision when the data contain a large range of frequencies or a large number of modes while the frequency domain methods tend to provide higher accuracy when the range of frequencies of interest is limited and the number of modes is relatively small.

Peak Picking (PP) is the simplest and most widely used procedure in frequency domain methods. PP involves a discrete Fourier transformation of recoded data in the time domain. The peaks on the resulting spectrum correspond to the Eigenvalues of the system or natural frequencies of the structure and each column (or row) in the spectrum matrix represents the corresponding Eigenvector or a mode shape of the structure. If the detected Eigenvalues are not well separated, the corresponding Eigenvector may be a linear combination of multiple mode shapes.

In practice, noise in the structural response measurements makes the peak selection very difficult because the peaks are not clear and some peaks may correspond to the noise. Hence, Brincker et. al. (2001) introduced the Frequency Domain Decomposition (FDD) and Baker et. al. (2001) proposed the Enhanced Frequency Domain Decomposition (EFDD) methods to improve the PP approach. System identification using FDD or EFDD generally involves the following steps:

- Computation of the Cross-Power Spectral Density (CPSD) Matrix
- Singular Value Decomposition
- System assembly for multiple setups

CPSD is developed at each frequency and represents the power distribution per unit frequency. CPSD is an estimate of the Fourier transformation of the correlation matrix of recorded channels. The correlation between two channels is higher when they are in-phase or out of phase (the difference between their oscillation phase is either 0 or 180). The CPSD matrix is obtained from equation (2-4):

$$S_{j,k}(\omega) = E[X_j(\omega)^*.X_k(\omega)] \qquad (2\text{-}4)$$

where * represents the complex conjugate and X_j is the Fourier transform of the recorded

velocity time history of the j^{th} channel (x_j) and is calculated by equation (2-5).

$$X_j(\omega) = \int_0^T x_j(t).e^{-2\pi i\omega t}dt \quad (2\text{-}5)$$

The Singular Value Decomposition of CPSD matrix at each frequency is performed based on equation (2-6).

$$S(\omega_i) = [U_i][\Sigma_i][V_i] \quad (2\text{-}6)$$

in which Σ is a diagonal matrix including Eigenvalues and U is the matrix representing the corresponding Eigenvectors.

In order to assemble the responses of every recorded channel in AVT, several methods have been proposed which are investigated thoroughly by Parloo et. al. (2003). The main concept of these methods is to form the CPSD matrix and corresponding Singular Value Decomposition matrices of every channel with the reference channel and assemble the normalized results to obtain the assembled dynamic properties of the structure. For more detailed information regarding FDD and EFDD analysis refer to Saeed (2013).

2.3 CORROSION EFFECT

Reinforcement corrosion is the main cause of damage and early failure of reinforced concrete structures. Hence, corrosion effects should be carefully assessed in the reliability analysis of existing structures especially when the structures under study are old and exposed to aggressive environments. The severity and duration of the winter periods in Montreal and the large quantities of deicing salts which are used for preparing bare pavements for motorists make the highway bridges prone to corrosion and deterioration.

The adverse effect of corrosion on the behavior of reinforced concrete members is highlighted in several publications. According to Lounis (2003), the corrosion of the reinforcement reduces the cross sectional area of the steel and produces corrosive products with a much larger volume than the original steel material which cause expansive stresses in the concrete. The stresses cause cracking, delamination, spalling of the concrete cover and weakening of the bond between the concrete and reinforcement.

Therefore, corrosion reduces the overall strength and ductility of the structure.

Andrade et. al. (1993a, 1993b) performed a detailed experimental and numerical study on the relationship between reinforcement corrosion and cracking and delamination of concrete covers. They discovered that only a few micrometer of loss in rebar cross-section may cause visible cracks on the cover.

Ismail and Soleymani (2002) conducted an extensive laboratory test on reinforced concretes with various concrete mixtures and monitored the chloride concentration and corrosion rate in the specimens to investigate the environmental effects on corrosion rate in reinforced concrete components.

Li (2004) investigated the effect of corrosion on the behavior of flexural reinforced concrete member which are mainly used in marine environments. He estimated the deflections and strength of components over each phase of service life of corrosion affected members and obtained the probability of failure of components over their service life.

Recently, there have been several studies which investigate the corrosion rate and deterioration effects on reinforced concrete structures in a probabilistic context. Ghosh and Padgett (2010) develop time-dependent seismic fragility curves for highway bridges considering the corrosion effects on the behavior and capacities of reinforced concrete piers, abutments and steel bearings.

Alipour et. al. (2011 and 2013) investigated the chloride ion concentration, corrosion rate and structural degradation mechanisms due to corrosion in a probabilistic framework in order to propose optimum inspection and maintenance strategies to minimize life cycle cost of highway bridges while maintaining the safety level of the bridge. They also presented the time-dependent fragility curves of deteriorating highway bridges.

According to Tutti (1982), the service life of a bridge can be divided into two phases: Phase 1 is the Corrosion Initiation which corresponds to the time period from the completion of the original construction to when a sufficient amount of chloride ions (C_{cr}: Critical Chloride Concentration) accumulates around the steel and corrosion is just about

to begin (T_i). Phase 2 is Corrosion Propagation which is the time period after the corrosion has begun. Figure 2-3 illustrates the Tutti model of corrosion during the service life of a structure.

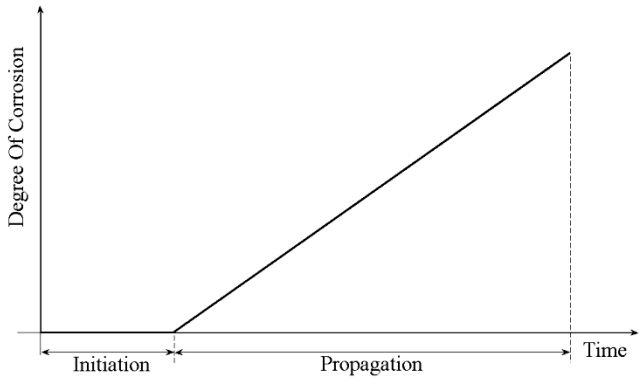

Figure 2-3. Tutti model of degree of corrosion in a deteriorating structure

2.3.1 CORROSION INITIATION

High pH of concrete causes an oxide film to form on the surface of the reinforcing steel when it is placed in the concrete. This passive oxide steel layer is composed of a dense, stable gamma ferric oxide layer which is tightly adhering to the steel surface (Revie 2000). The corrosion process of the reinforcement can only begin once this passive oxide layer has been destroyed. Reactions with chloride ions, as well as moisture and oxygen, destroy the oxide film. The concentration of chloride ions needed to destroy the oxide film is referred to as the critical or threshold chloride ion concentration.

There have been numerous studies on the critical chloride concentration and there is a large variability in the values obtained as variety function of concrete mix type and proportions, pH, cement type, water to cement ratio, relative humidity, and temperature (Stewart and Rosowsky 1998; Duprat 2007).

Corrosion initiation time is the length of time it takes for chloride ions and other substances needed for corrosion, such as water and oxygen, to penetrate the concrete clear cover and reach the depth of reinforcing steel in a sufficient amount to start corrosion of the steel.

Fick's second law of diffusion can be used to predict the progression of chloride ions as a function of time and position within a semi-infinite solid as shown in equation (2-7). (Stewart and Rosowsky 1998).

$$\frac{\partial C(x,t)}{\partial t} = -D_C . \frac{\partial^2 C(x,t)}{\partial x^2} \tag{2-7}$$

in which C represents the chloride ion concentration, D_C is the diffusion coefficient and x represents the depth. The chloride ion diffusion coefficient depends on parameters such as mix proportions, curing time and conditions, compaction, environmental exposure and time effects (Stewart 2003). By re-arranging and modifying equation (2-7), T_i can be obtained from equation (2-8).

$$T_i = \frac{x^2}{4D_C}[erf^{-1}\left(\frac{C_0 - C_{cr}}{C_0}\right)]^{-2} \tag{2-8}$$

in which erf is the Gaussian error function and C_0 represents chloride concentration at the surface.

Lounis et. al. (2004) conducted a probabilistic study of chloride induced corrosion initiation time in reinforced concrete structures. They performed a MCS to estimate the probabilistic distribution of corrosion initiation time in a typical structure located in Ottawa.

Wolofsky (2011) studied the corrosion initiation time in highway bridges located in Montreal in a detailed probabilistic context considering local environment conditions and various corrosion mechanisms.

2.3.2 CORROSION PROPAGATION

Once the corrosion has initiated, the rate of corrosion depends on the availability of water and oxygen in the vicinity of the reinforcement (Duprat 2007) which is affected by the quality and condition of the concrete, and the water to cement ratio of the concrete mix (Lounis, 2003). Since these parameters are unknown at the design stage and vary from structure to structure and within a structure, it is very difficult to accurately predict the

corrosion rate. However, the actual corrosion rate can be determined through field measurements and experiments using, among others, the corrosion current density (Stewart and Rosowsky 1998). The basis of this field test is that the corrosion rate is proportional to the electric current since corrosion involves the transfer of electrons and ions between the metal and the surrounding intersticial solution.

The Half-cell method, DC polarization method and AC impedance method are three most common methods for estimating the rate of corrosion. These methods are based on estimating the polarization resistance (R_p) and subsequently the corrosion current density (i_{corr}) in the media. The corrosion current density is the corrosion current over a unit surface of polarized area of the reinforcing bar.

The conversion of electrochemical parameters into the instantaneous corrosion rate can be made by means of Faraday's law as shown in equation (2-9) (Huang and Yang 1997):

$$r_{corr} = \left(\frac{i_{corr}}{z.F}\right).\left(\frac{M_{Fe}}{\rho_{st}}\right) \tag{2-9}$$

in which z is the number of charges of the ion (equal to 2 for the ferrous ion), F is Faraday's constant, 96500 A.s., M_{Fe} is the atomic weight of Fe (56g) and ρ_{st} is the density of steel (7.81 g/cm^3). It is noted that the rate of corrosion is a time-dependent variable, however, it is assumed to be constant in this study due to lack of data. The diameter of the corroding bar at the time t, D(t) can be estimated from equation (2-10).

$$D(t) = \begin{cases} D_0 & t < T_i \\ D_0 - r_{corr}(t - T_i) & T_i < t < T_i + D_0/r_{corr} \\ 0 & t > T_i + D_0/r_{corr} \end{cases} \tag{2-10}$$

in which D_0 is the initial diameter of the bar.

2.4 GROUND MOTION RECORD SELECTION

In the seismic reliability assessment of structures, the relationship between ground motion intensity and structural response has to be defined. In other words, the goal of structural analysis is to estimate the response of the structure subjected to ground motions with specified intensities so that the conditional probability of exceeding a certain limit state can be calculated at any intensity. However, the structural response is highly dependent

on the set of ground motions which are used in the analyses. Baker and Cornell (2006) and Zareian (2006) demonstrated that using ground motion records with different spectral shapes can change the calculated collapse capacity substantially and in some cases as much as 70%. Hence, appropriate selection of ground motion records is an imperative task in fragility and reliability assessment of structures, which otherwise can result in highly biased predictions.

A realistic and representative set of ground motions should include records with characteristics which are consistent with the site seismicity. Characteristics such as ground motion magnitude (M), distance (R) and spectral shape parameters like epsilon are important characteristics which can influence structural response.

Ground Motion Prediction Equations (GMPE) and seismic hazard deaggregations are key elements of ground motion selection. A GMPE is an empirical equation which predicts a ground motion Intensity Measure (IM), such as response spectra, as a function of ground motion basic characteristics such as earthquake magnitude and distance. GMPEs may require different input parameters such as ground motion magnitude and distance, site condition parameters like average shear wave velocity (V_{s30}) of the soil and fault type and mechanisms. The output of a GMPE may include the predicted mean value and variance of the ground motion IM. GMPEs are required in Probabilistic Seismic Hazard Analyses (PSHA) and seismic hazard deaggregations. GMPE proposed by Atkinson and Boore (2006) and Atkinson (2008) are adapted in this study.

In seismic hazard deaggregation analysis, mean value and variation of ground motion IM is estimated for every possible earthquake scenario with various magnitudes and distances using GMPEs and the results are combined with the probability of occurrence of each event. In order to account for all sources of uncertainty in the results of seismic hazard deaggregation, various GMPEs may be used with uniform or different assigned weights. For example, the Geological Survey of Canada (GSC) (1995 model) uses the GMPE suggested by Atkinson and Boore (1995) for eastern Canada while the updated model suggested by Goda et. al. (2010) applies the GMPEs suggested by Silva et. al. (2002), Campbell (2003), Atkinson and Boore (2006) and Atkinson (2008) with weights of 0.2, 0.3, 0.4 and 0.1 respectively. For the 2015 version of Canadian national Seismic Hazard

Map, Atkinson and Adams (2013) suggest using 3 sets of GMPEs which result in lower, central and upper responses for each type of seismic event to represent the epistemic uncertainty involved in ground motion prediction.

Dehghani and Tremblay (2012) proposes a ground motion selection method which initially selects a set of ground motion records based on seismic hazard deaggregation data. The set is further refined according to their intensity, frequency content and duration.

Many methods have been proposed for ground motion record selection. Tehrani et. al. (2014) investigated the influence of using different ground motion selection approaches on seismic response of a typical bridge in Canada. The most widely used methods typically either choose ground motion with main characteristics close to the seismic characteristics obtained from the seismic hazard deaggregation of the site location or choose records which match some target spectrum. Spectral Acceleration (Sa) at a given period is usually considered as the ground motion IM in order to benefit from having a direct link to a ground motion hazard curve (Cornell et. al., 2002). Tehrani (2012) performed a detailed study on the influence of different earthquake types and various ground motion selection methods on the seismic response of highway bridges.

2.4.1 MR- BASED APPROACH

The simplest method for ground motion selection is to choose records which have similar magnitude, M and distance, R to the mean magnitude and distance obtained from seismic hazard deaggregation of the site. In order to get more diversity, one unit of magnitude can be assumed equivalent to a certain distance. For instance, Baker and Cornell (2006) treat a unit change in magnitude as equivalent to a 40km difference in distance. However, this approach neglects the spectral shape of the ground motions and may result in highly biased predictions.

2.4.2 EPSILON (ε) BASED APPROACH

Epsilon (ε) is the number of logarithmic standard deviations by which a target ground motion differs from a median ground motion and can be obtained by equation (2-11) in

which $\mu_{\ln Sa}(M,R,T)$ and $\sigma_{\ln Sa}(T)$ are the predicted mean and standard deviation of ln(Sa) at given period and ln Sa(T) is the natural logarithm of the spectral acceleration of interest.

$$\varepsilon(T) = \frac{\ln Sa(T) - \mu_{\ln Sa}(M,R,T)}{\sigma_{ln\,Sa}(T)} \tag{2-11}$$

Figure 2-4 shows average response spectra for different ε values.

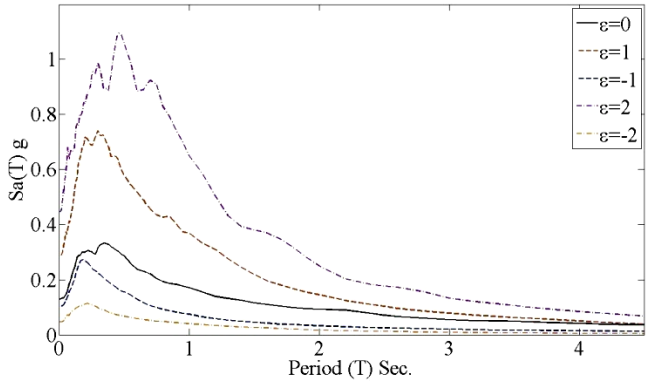

Figure 2-4. Average response spectra for different ε values

It is noted that ε is an indicator of the spectral shape as it shows whether an Sa at a specified period is in a peak or a valley of the spectrum (Baker and Cornell, 2006). Figure 2-5 demonstrates typical normalized average response spectra for various ε at a period of 0.4 sec.

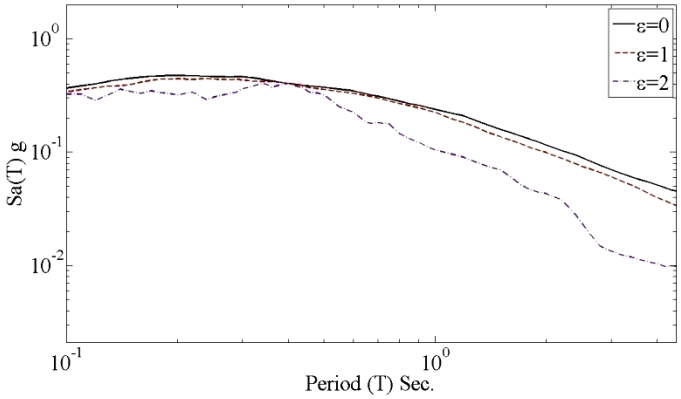

Figure 2-5. Normalized average response spectra for various ε at a period of 0.4 sec

Baker and Cornell (2005) demonstrate the significant influence of ε on structural

responses and use ε as a component of a vector valued ground motion IM to present structural fragility curves. Baker and Cornell (2006) suggest the application of ε in ground motion record selection. Chandramohan et. al. (2013) use ε as an indicator of spectral shape and demonstrate the high influence of ε on the overall seismic risk of collapse of structures.

It has been demonstrated that the selection of the records with similar $\varepsilon(T_1)$ (the value of epsilon at the first natural period of structure) to the mean ε values obtained from the seismic hazard deaggregation results in more realistic predictions in comparison with the MR-based approach.

2.4.3 UNIFORM HAZARD SPECTRUM (UHS) BASED APPROACH

The Uniform Hazard Spectrum (UHS) has been traditionally used as a target spectrum to determine an appropriate set of ground motions which are representative of the site seismicity. In this method, scaled natural records are matched and compared to a target UHS over a range of periods. This range should include the important modes of the structure and consider the period elongation due to inelastic deformation of the structure. A period range from 0.2 to 2 times the first period of the structure is recommended for this purpose.

However, UHS is not the best target spectrum for this purpose because traditional probabilistic seismic hazard analysis ignores the joint probability of exceedance of spectral ordinates at different periods. In other words, UHS conservatively considers the Spectral Accelerations (Sa) with low probability of occurrence at all periods. However, it is unlikely to find a single ground motion record with Sa higher than median over a wide range of periods. In order to solve this problem, Baker and Cornell (2006) introduced the “Conditional Mean Spectrum” (CMS) as a suitable alternative for the target spectrum.

2.4.4 CMS BASED APPROACH

The main purpose of introducing CMS is to provide the expected response spectrum, conditioned on occurrence of a target spectral acceleration value at the period of interest

(e.g. at the first natural period of the structure). CMS based approach takes into account the influence of all three main parameters of M, R and ε in record selection. CMS is defined by the conditional mean and standard deviation of spectral ordinates which are obtained using deaggregation of the seismic hazard function and GMPE models which are based on the observations of correlations between spectral ordinates (Baker and Jayaram 2008).

After CMS is developed as a target spectral shape for a given M, R and ε, the records which have similar spectral shape over a range of target period ($0.2T_1$ to $2T_1$ in this study) will be selected regardless of their actual M, R and ε (Baker and Cornell, 2006).
The main steps for CMS based ground motion selection as proposed by Baker (2011) can be summarized as follows:

1) Determine the target $Sa(T_1)$ and corresponding M,R and ε
The mean value of M and R of earthquakes are determined by deaggregation of the seismic hazard. Seismic hazard deaggregation of Montreal is investigated by Halchuk et. al. (2007) and the results are adapted in this study.

2) Determine the mean value and standard deviation of the response spectrum, given M and R
$\mu_{\ln Sa}(M,R,T)$ and $\sigma_{\ln Sa}(T)$ are obtained from available GMPE. GMPE proposed by Atkinson and Boore (2006) and Boore and Atkinson (2008) are adapted for eastern Canada and used in this study. Soil characteristics at the location of interest are determined based on the seismic microzonation map developed by Chouinard et al. (2011) and are verified by empirical equations offered by CALTRAN (2009) which estimate the soil characteristics based on the result of SPT tests.

3) Estimate ε for all the periods
$\varepsilon(T_1)$ can be obtained from seismic hazard deaggregation only if the target $Sa(T_1)$ is selected from PSHA. In case that $Sa(T_1)$ is chosen otherwise (e.g. based on UHS offered by codes), $\varepsilon(T_1)$ should be calculated based on equation (2-11). The ε at other periods are estimated by multiplying the $\varepsilon(T_1)$ in the inter- period correlation factor as shown in equation (2-12).

$$\mu_{\varepsilon(T_i|T_1)} = \rho(T_i, T_1).\varepsilon(T_1) \quad (2\text{-}12)$$

in which $\mu_{\varepsilon(Ti|T1)}$ represents $\varepsilon(T_i)$ given $\varepsilon(T_1)$ and $\rho(T_i, T_1)$ is the inter-period correlation of spectral accelerations at vibration periods T_i and T_1 and is proposed by Baker and Cornell (2006) as shown in equation (2-13).

$$\rho(T_{Min}, T_{Max}) = 1 - \cos(\frac{\pi}{2} - (0.359 + 0.163 I_{T_{Min}<0.189}.\ln\left(\frac{T_{Min}}{0.189}\right).ln\frac{T_{Max}}{T_{Min}}) \quad (2\text{-}13)$$

in which T_{Min} and T_{Max} denote for the smallest and the largest of the two periods of interest and $I_{Tmin<0.189}$ is an indicator function which is equal to 1 if T_{Min} is less than 0.189 sec and equal to 0 otherwise.

4) Determine CMS

CMS is implemented by using equation (2-14). (Baker, 2011)

$$\mu_{lnS_a(T_i)|lnS_a(T_1)} = \mu_{lnS_a}(\bar{M}, \bar{R}, T_i) + \rho(T_i, T_1)\bar{\varepsilon}(T_1)\sigma_{lnS_a}(T_i) \quad (2\text{-}14)$$

where $\mu_{lnS_a}(\bar{M}, \bar{R}, T_i)$ and $\sigma_{lnS_a}(T_i)$ are the mean and standard deviation of the natural logarithm of Sa at the first period of the structure and $\bar{M}$, $\bar{R}$, and $\bar{\boldsymbol{\varepsilon}}(T_1)$ are the mean magnitude, mean distance and mean value of epsilon at the considered period T_1 respectively.

5) Ground motion selection

Once the CMS is developed, it can be used as the target spectrum to select the set of ground motions for dynamic analysis. For this purpose, a period range from 0.2 to 2 times the first period of the structure is considered to match the CMS. All the ground motion records of the available database are scaled so that their Sa at the first period of the structure ($Sa(T_1)$) matches the target spectral acceleration from the CMS. Then the Sum of Squared Errors (SSE) is calculated for each ground motion record based on equation (2-15) and the records with the lowest SSE are selected as representative earthquakes for dynamic analysis. (Baker, 2011)

$$SSE = \sum_{j=1}^{n} (\ln Sa(T_j) - \ln Sa_{CMS}(T_j))^2 \quad (2\text{-}15)$$

where $\ln Sa(T_j)$ is the natural logarithm of Sa of the ground motion at period T_j and $\ln Sa_{CMS}(T_j)$ is the natural logarithm of CMS value at period T_j. In this study, the PEER-NGA database which offers 3541 ground motion records from 175 earthquakes is used for record selection. In addition, ground motion record set suggested by ATC-63, and some artificial ground motion record sets suggested by Atkinson and Beresnev (1998) which are compatible with the UHS of Montreal are also used in this study.

2.5 IDA METHOD

2.5.1 INTRODUCTION

The increasing processing power of computers makes it possible to make more detailed and realistic computer models and perform more complex and accurate structural analyses. The Incremental Dynamic Analysis (IDA) method which was proposed by Vamvatsikos and Cornell (2002) has become a widely used method in seismic performance prediction of structures. This method has been adapted by some codes and guidelines such as ATC-63 (ATC-63, 2008) in order to estimate the collapse capacity and develop fragility curves of structures. Many researchers have adapted this method in performance and reliability assessment of highway bridges. Mander et. al. (2007) applied IDA in seismic financial risk assessment of bridges; Tehrani and Mitchell (2013) used IDA in order to investigate the influence of different earthquake types on the structural responses of a typical highway bridge; Mackie and Stojadinovic (2004) applied the IDA method in developing component probabilistic seismic demands and fragility assessment of reinforced concrete highway bridges.

The IDA method involves performing nonlinear dynamic analyses of a structural system under a single or a set of ground motion records, each scaled to several Intensity Measure (IM) levels designed to force the structure all the way from elastic response to final global dynamic instability (collapse).

According to Vamvatsikos and Cornell (2002), performing numerous nonlinear dynamic analyses of the structure in the IDA framework has several benefits for a better understanding of the structural behaviour under seismic events and for the reliability assessment of structures;

- IDA presents the seismic demands over a wide range of Intensity Measure (IM) levels including rare and severe ground motions which cause the structure to undergo ultimate performance levels such as collapse.

- IDA analysis estimates the seismic demand on each structural component at any intensity level which can be conveniently used in component based structural reliability and fragility assessments.

- IDA method takes into account the effect of inherent randomness in seismic inputs (record-to-record variability), which is a significant source of aleatory uncertainty in seismic evaluation of structures, on structural responses by using the set of ground motion records. Dolsek (2009) investigated and quantified the aleatory and epistemic uncertainties involved in an IDA of a typical building. He demonstrated that the record-to-record randomness is the most important source of uncertainty in IDA. However, epistemic uncertainties may also have significant influence on collapse capacity despite their inconsiderable effect in the range far from collapse.

2.5.2 INTENSITY MEASURE (IM) AND ENGINEERING DEMAND PARAMETER (EDP) SELECTION

The input of IDA is the structural model and the set of ground motion records and the output is the structural demands, also known as Engineering Demand Parameter (EDP), at various Intensity Measure (IM) levels. The uncertainty involved in IDA results is highly dependent on the selected ground motion set (as discussed in section 2-4) and selected EDP and IM pair.

IM is a nonnegative scalar which is a function of the unscaled ground motion accelerogram and can be monotonically scaled. The intensity level is the multiplication product of the scale factor in the unscaled scalar value (Vamvatsikos and Cornell, 2002). Based on this definition, many quantities which are normally used to demonstrate the earthquake intensities such as moment magnitude, duration, or Modified Mercalli Intensity are not applicable in IDA. Peak Ground Acceleration (PGA) and Spectral Acceleration (Sa) at the first period of the structure are the most popular choices of IM in

the literature (Nielson, 2005).

EDP is a scalar quantity which represents the response of a structure subjected to a seismic event. EDP may correspond to global behaviour of the structure such as interstorey drift or correspond to component responses such as shear force or component ductility demands. Many EDPs have been suggested and implemented in IDA depending on the objective of the analysis. In this study, curvature ductility, axial force and shear force of components are considered as EDPs to account for various failure scenarios in each structural element.

Mackie and Stojadinovic (2003) investigated the efficiency of various IM-EDP pairs and demonstrated that there may not be a single choice which is appropriate for all cases. However, they suggested that out of 23 studied potential IMs, Sa at the first period of the structure tends to be the most efficient IM for highway bridges.

Padgett et. al. (2007) performed a thorough study on optimal IM selection in Probabilistic Seismic Demand Models (PSDM) and suggested efficiency, practicality, sufficiency, and hazard computability as main criteria for proper IM selection.

2.5.2.1 *EFFICIENCY*

The efficiency of IMs are measured based on a dispersion parameter obtained from regression analysis between the natural logarithm of IM and the natural logarithm of EDP. More efficient IMs reduce the uncertainty and variation in the estimated EDP for a given IM value (Giovenale et. al., 2004). It has been suggested by Cornell et. al. (2002) that the estimate of the median demand ($\widehat{\mathrm{EDP}}$) can be represented by a power model as shown in equation (2-16).

$$\widehat{\mathrm{EDP}} = \mathrm{a}.\,\mathrm{IM}^{\mathrm{b}} \tag{2-16}$$

Where a and b are regression coefficients. Given the IM, the demand is assumed to be lognormally distributed with a logarithmic standard deviation $\beta_{EDP|IM}$. Therefore, the logarithm of the demand is normally distributed. Equation 2-13 can be rewritten as equation (2-17)

$$Ln\left(\widehat{EDP}\right) = Ln(a) + b.Ln(IM) \quad (2\text{-}17)$$

The variation about the median ($\beta_{EDP|IM}$) is the measure of effectiveness of the selected IM to estimate the seismic demand. Figure 2-6 compares the efficiency of Sa and PGA for IDA of a typical highway bridge pier.

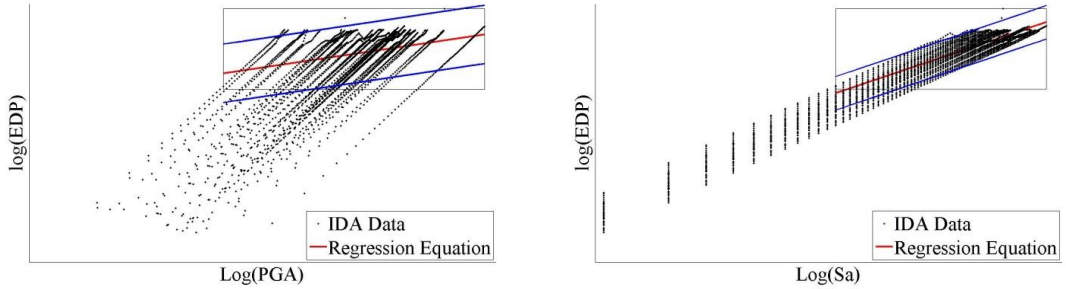

Figure 2-6. Comparison of PGA and Sa as candidate IM

It is noted that in figure 2-6, the variability ($\beta_{EDP|IM}$) for Sa is less than for PGA, in consequence, Sa is the more efficient choice in this case.

2.5.2.2 *PRACTICALITY*

Practicality of IMs is measured based on the correlation between the natural logarithm of the EDP and the natural logarithm of the IM. Hence the parameter *b* (the slope of the regression line) in equation (2-17) is a measure for practicality of IMs. Larger value of *b* for the IM of interest demonstrates higher dependency between studied IM and EDP and demonstrates the high practicality of the IM of interest. If this parameter approaches zero, the IM contribution in EDP is negligible and the IM is not practical. It is noted that in figure 2-6 the slope of the regression line for Sa is higher. So, Sa is the more practical IM in that case.

2.5.2.3 SUFFICIENCY

An IM is deemed sufficient if EDP at a given intensity level is independent of basic earthquake characteristic such as magnitude (M) and distance (R). If an insufficient IM is used in IDA, the traditional application of total probability theorem for Probabilistic

Seismic Demand Analysis (PSDA) will be invalid. In other words, equation (2-18) will not be applicable since exceedance probability should be evaluated as P(D>d|IM,M,R) (Padgett et. al., 2007).

$$\lambda(D) = \int_{IM} P(D \geq d|IM).d\lambda(IM) \qquad (2\text{-}18)$$

In equation 2-18, λ(D) is the mean annual frequency of exceeding a level of demand and λ(IM) represents the mean annual frequency of exceeding each value of IM.
Sufficiency of IM can be investigated by a classic hypothesis test. If there is a significant correlation between the residuals of the regression in equation (2-17) and basic ground motion characteristics such as M or R, the studied IM is insufficient.

2.5.2.4 *HAZARD COMPUTABILITY*

In order to estimate the reliability of a structure and applicability of equation (2-18), the hazard or occurrence probability of the selected IM should be known for various intensity levels. Hazard curves for Sa and PGA are already available. However, application of other IMs requires additional effort to develop hazard functions.

In addition, Baker and Cornell (2005) studied vector- valued ground motion IMs and demonstrated the possibility of achieving higher efficiency by application of vector-valued IMs. They suggested the Sa-ε vector as a proper candidate for IM in PSDAs.

The results obtained by IDA are often presented in IDA curves which demonstrate the EDP at different intensities for the selected records. Figure 2-7 presents two typical IDA results for structural components. IDA curves may indicate softening, mild or severe hardening or weaving behaviour (Vamvatsikos and Cornell, 2002).

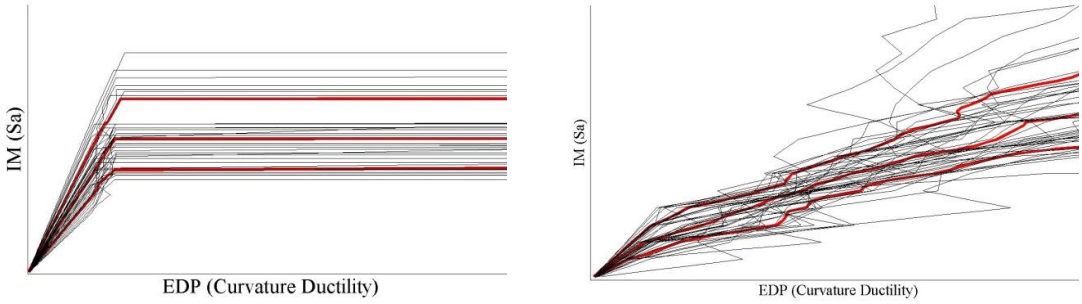

(a) Softening behaviour (b) Weaving behaviour

Figure 2-7. Typical IDA results accompanied by median and 16 and 84 percentile responses for cases presenting a) softening and b) Weaving behaviour

IDA curves usually start with a linear section which ends when the first nonlinearity occurs in the structure. Any nonlinearity in structural behaviour changes the slope of IDA curve. After the linear section, the IDA curve may present softening, which indicates acceleration in demands or damages in structural components, or hardening which demonstrate deceleration of demands. This deceleration can be powerful enough to briefly stop the EDP accumulation or even reverse it. Weaving behavior occurs when the structure experiences alternating softening and hardening behavior which makes the IDA curve a non-monotonic function.

As it is evident in figure 2-7, the IDA results may present high variability due to the record-to-record uncertainty. Hence, in order to summarize the results, Vamvatsikos and Cornell (2002) proposed to use certain percentiles of the obtained results. Based on the lognormal assumption for the structural behavior, 16, 50 and 84 percentiles can be used which correspond to the median and median times $e^{\pm dispersion}$. As it is inferred from figure 2-7, the percentile IDA curves are smoother than the results of individual records and can represent the structural behavior more properly.

2.6 FRAGILITY CURVES

2.6.1 INTRODUCTION

Uncertainties involved in determining the structural demands during earthquakes and in evaluating the capacity of structural components under cyclic loads are important inputs

of probabilistic methods to quantitatively assess the reliability of structures. The seismic reliability of a structure can be evaluated by combining seismic hazards at the location of the structure and the fragility function of the structure. Fragility curves represent the state-of-the-art in seismic risk assessment (SRA) and are defined as the conditional probability that a structure will meet or exceed a certain level of damage for a given ground motion intensity. Equation (2-19) presents the fragility definition

$$P_F = P[LS \mid IM = y] \tag{2-19}$$

where LS is the limit state or damage level of the bridge or bridge component, IM is the ground motion intensity measure and y is the realization of the chosen ground motion intensity measure.

Figure 2-8 presents a typical structural fragility curve.

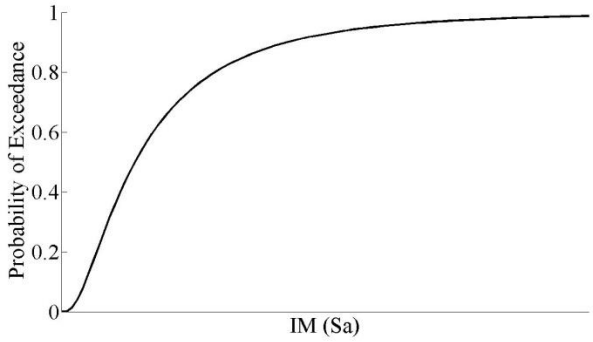

Figure 2-8. A typical fragility curve

Fragility curves can be developed for structural components as well as for the structure as a whole system. Component fragility curves are useful tools to identify weak parts of the structure while system fragility curves are used in seismic risk assessment of the structure.

2.6.2 FRAGILITY ANALYSIS APPROACHES

Fragility analysis was first introduced in the seismic evaluation of nuclear facility vulnerabilities in the late 1970s and early 1980s and since then has expanded into other areas of structural engineering. Fragility analysis are classified into three major

categories; i) Expert based fragility curves, ii) Empirical fragility curves, and iii) Analytical fragility curves.

In the 1980s and early 1990s, fragility curves for various types of structures were developed by a prescriptive approach and based on expert opinion due to the lack of required seismic data.

For instance, Applied Technology Council (ATC) used some questionnaires filled by experts in order to develop expert based fragility curves in ATC-13 and ATC- 25 (ATC, 1991). The resulted fragility curves were highly subjective and biased because of the limited number of experts and limited types of bridges considered in the questionnaires.

Empirical fragility curves were widely used after the 1989 Loma Prieta, 1994 Northridge and 1995 Kobe earthquakes due to the availability of actual ground motions and bridge damage data. Basoz and Kiremidjian (1997) and Basoz et. al. (1999) used logistic regression analysis, Shinozuka et. al. (2000a) applied the maximum likelihood method and Der Kiureghian (2002) utilized a Bayesian approach and the Likelihood function to develop empirical fragility curves based on the data obtained from the bridges which were damaged during the Northridge and Kobe earthquakes. Empirical fragilities also have high uncertainties because of the limited number of each bridge classes in a specific area and their reliance on experts to determine the ground motion intensity at the bridge site and to assign the damage level to each bridge. (Basoz and Kiremidjian, 1997)

Following the progress in computer modeling and availability of detailed computer models and complex analysis methods, analytical fragility curves became increasingly popular. There have been numerous researchers who developed analytical fragility curves for highway bridges. The fragility analysis generally includes the following major parts;

- Simulation of bridge structure considering the uncertainty in its properties
- Performing a set of model analyses in order to obtain structural demands (EDP) at various ground motion intensities
- Evaluate the capacities or limit states of the structure or structural components
- A procedure to develop fragility curves from the response of the bridge model under considered seismic loads.

The most popular analytical method is nonlinear time history analysis (Hwang et. al.,

2000b; Shinozuka et. al., 2000a). However, simplified analysis methods such as elastic spectral analysis (Hwang et. al., 2000a) and nonlinear static analysis (Mander and Basoz, 1999, Shinozuka et. al., 2000b, Hwang et. al. 2000b and Rossetto and Elnashai, 2004) have also been used.

Regarding the procedures to develop analytical fragility curves for structural systems, the methods which have been proposed in the literature can be divided into two different approaches: System-Based Fragility and Component-Based-Fragility.

2.6.2.1 *SYSTEM-BASED FRAGILITY*

In this approach, fragility curves are developed directly from structural analysis data. Hwang and Huo (1998) performed a time history analysis on a bridge structure and used a Bernoulli random variable with 0 and 1 outcomes to show whether or not the bridge sustains the defined damage-state at each level of the ground motion Intensity Measure (IM). They estimated the probability of failure based on the number of zeros and ones at each IM value and fitted a logistic probability distribution to present the fragility curve of the structural system. Shinozuka (1998) also considered the event of bridge damage as a realization from a Bernoulli experiment. However, he applied the maximum likelihood method to fit a lognormal distribution. This approach doesn't directly account for uncertainties in component capacities.

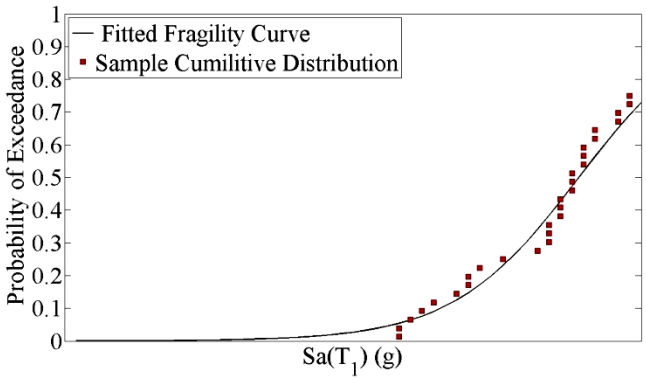

Figure 2-9. Fragility curve and the sample cumulative distribution (stepped curve)

Figure 2-9 presents a system fragility curve fitted to the sample cumulative distribution

points obtained from the analysis of a typical structure.

The main steps in a system-based fragility analysis are as follows:

- Simulation of the bridge structure with median properties
- Evaluation of the median capacities or limit states of the structure or structural components
- Performing a set of model analysis (a set of ground motion records with various scaled or unscaled intensities) in order to obtain structural demands (EDP) at various ground motion intensities
- For every analyzed point, determining if there is any failures in the structure.
- Calculation of the sample cumulative distribution of failure at various ground motion intensities
- developing the system fragility curve by fitting a cumulative distribution function to the obtained sample cumulative distribution.

Wen et. al. (2003) demonstrated that the lognormal distribution is a good fit for the fragility curve and is convenient for calculations using conventional probability theory. In order to consider the uncertainties in modeling and capacities, one can either simulate N nominally identical but statistically different bridge samples and component capacities and pair them with corresponding EDPs in fragility analysis or follow the mentioned steps for median model and capacity variables and apply the total uncertainty to the obtained median value of the fragility curve based on equation (2-20).

$$\beta_{Tot} = \sqrt{{\beta_F}^2 + {\beta_C}^2 + {\beta_M}^2} \qquad (2\text{-}20)$$

in which β_{Tot} represent combined logarithmic standard deviations of the fragility curve, β_F is the logarithmic standard deviation of the fitted cumulative distribution and β_C and β_M are logarithmic standard deviations corresponding to uncertainties in capacities and modeling respectively.

ATC63 proposes the same methodology for developing fragility curves for the design of seismic-force-resisting systems in new building structures. This methodology is

conceptually applicable to the design of any type of new structure, and to the retrofit of seismic-force-resisting systems in existing structures. ATC63 suggests a set of ground motion records for performing an IDA on the structure with median properties and determines the minimum ground motion intensity at which the structure sustains the specified damage-state under half of the scaled ground motion records. Finally, the methodology applies the total uncertainty of the system due to record-to-record, modeling and test data related uncertainties by multiplying the median response in a lognormal random variable with a median of 1 and representing the same uncertainty.

2.6.2.2 *COMPONENT-BASED FRAGILITY:*

The second approach is called component-based method in which a probabilistic model of the seismic demands are obtained at each ground motion intensity and the fragility curve for each structural component is developed by comparing the distributions of demands and capacities at various IM levels as shown in equation (2-21). Hwang et. al. (2000), Bignell et. al. (2004) and Choi et. al. (2004) followed this approach.

$$PF = P[LS\,|IM = y] = P[D/C \geq 1|IM = y] \quad \text{or } P[C - D \leq 0|IM = y] \tag{2-21}$$

The probabilistic seismic demands can be obtained based on the peak structural responses at any given ground motion intensity as shown in figure 2-10.

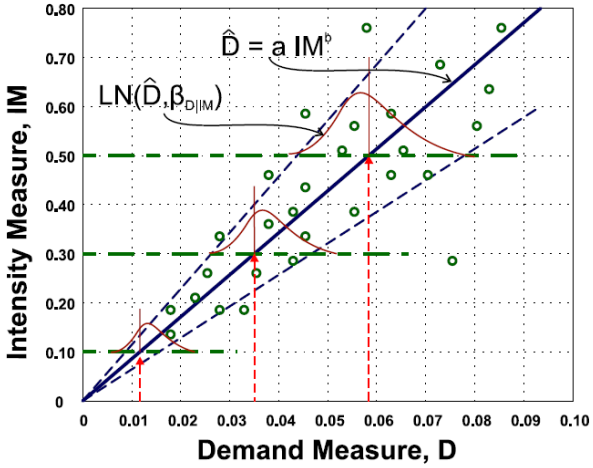

Figure 2-10. Probabilistic Seismic Demand Model (PSDM) (Nielson, 2005)

Regression analysis or parameter estimation techniques like maximum likelihood method can be used in order to obtain Probabilistic Seismic Demand Models (PSDM). Shinozuka et. al. (2003) used the Maximum Likelihood Method (MLE) to model the column responses at the chosen earthquake intensities.

The main steps in a typical probabilistic component fragility analysis are as follows:

- Simulation of bridge structure with median properties
- Determining the distribution of the component capacities or limit states
- Performing a set of model analysis (for a set of ground motion records with various scaled or unscaled intensities) in order to obtain structural demands (EDP) at various ground motion intensities
- Calculating the fragility of the structural component by comparing the distributions of EDP and corresponding capacity as shown in equation (2-21).

According to Kottegoda and Rosso (1997), when the structural capacity and demand roughly fit a normal or lognormal distribution, it can be said that the composite performance will be lognormally distributed. Assuming lognormal distributions for component demand and capacity, component fragility curve can be calculated from equation (2-22).

$$P\left[\frac{D}{C} \geq 1 \mid IM\right] = \Phi\left(\frac{Ln(\widehat{EDP}/S_c)}{\sqrt{\beta_{EDP|IM}{}^2 + \beta_c{}^2}}\right) \qquad (2\text{-}22)$$

in which $\widehat{EDP}$ is the median of demand at the given IM, S_c is the median of capacity for the selected limit state, $\beta_{EDP|IM}$ is the logarithmic standard deviations of the component demand and β_c is the logarithmic standard deviation of the limit state (capacity).

Component fragility curves are very useful tools to identify weak parts of the structure and to guide the efficient allocation of funds to strengthen or retrofit an existing structure. However, the system fragility curve is required in reliability assessment of structures. In order to obtain system fragility curves based on component responses, Nielson and

DesRoches (2006) introduced a component level approach.

In this approach, a Joint Probabilistic Seismic Demand Model (JPSDM) of natural logarithm of the component demands is determined at each ground motion intensity. Then, based on the obtained JPSDMs, component demands and corresponding capacities are simulated using MCS. Finally, the fragility or the conditional probability of failure at a given intensity is the probability of having at least one failure in the simulated system. In order to develop the JPSDM, median, standard deviation and correlations of logarithm of component EDPs are required. Median of logarithm of EDPs and logarithmic standard deviations are obtained by performing a regression analysis on IDA results of each component as explained earlier and shown in equation (2-17) and figure 2-10. Correlations are calculated at each Sa using IDA results which provide a set of demands for each component at each Sa. It is noted that the correlation between logarithm of component EDPs depends on Sa and vary for different levels of damage.

It is noted that the fragility curves developed by this method have lognormal distributions. Tavares et. al. (2010) followed this approach to develop fragility curves for multi-span simply supported concrete highway bridges in Quebec.

Song and Kang (2009) have introduced a Matrix-based System Reliability (MSR) which considers the correlations between components by introducing common source random variables using Dunnett–Sobel correlation coefficient matrix. This method enables the designer to consider different scenarios of failure and progressive collapse in the system. However, fragility analysis of structures comprising a large number of components by this method requires enormous computational effort. Hence, in this study, the approach proposed by Nielson and DesRoches (2006) is adapted.

An advantage of the component-based approach in fragility analysis is that it provides the required information in order to quantify the contribution of each component in the failure of the system.

2.6.3 COMPONENT IMPORTANCE MEASURE

In order to compare the importance of a specific component and its contribution in the

failure of the system, the component and system fragility curves can be visually compared. Figure 2-11 provides an example of component versus system fragility comparison.

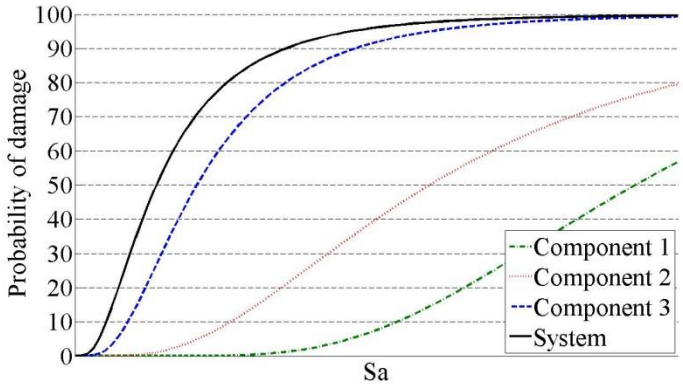

Figure 2-11. Visual comparison of system fragility versus component fragility curves

However, in order to quantify the contribution of each component in system failure, several methods have been proposed in the literature. Kuo and Zhu (2012a, 2012b) performed a thorough study on available component importance measures and their probabilistic perspectives, merits and applicability.

In this study, the Bayesian Reliability Importance Measure is applied to identify the most critical components. Birnbaum (1969) defined the Bayesian Reliability Importance of a component as the probability of failure of that component given the failure of the system. Equation (2-23) demonstrates this definition mathematically.

$$CIM_i = P\left(f_i \middle| f_{sys}\right) = \frac{P(f_i \cap f_{sys})}{P(f_{sys})} \tag{2-23}$$

where CIM_i represents the importance of component i, f_i denotes the event of failure in component i and f_{sys} represents the event of system failure.

2.7 SVM LEARNING

2.7.1 INTRODUCTION

The implicit nature of the limit state function is one of the main challenges in developing

seismic fragility curves for complex structures as it requires determining the conditional probability that the structure exceeds a critical state for any given intensity measure.

Practically, many algorithms used for explicit performance function reliability evaluation cannot be adapted to deal with implicit performance functions. For example, it is difficult to implement gradient based methods such as First Order and Second Order Reliability Methods (FORM/SORM) for the implicit limit state function since they need to calculate the gradient of the performance function. Moreover, it is not feasible to directly use simulation based methods due to their vast computational effort of the implicit performance function call which is usually based on Finite Element Method (FEM).

In order to alleviate these difficulties, regression methods such as Response Surface Method (RSM) have been successfully applied in many engineering cases (Hurtado, 2004, Bucher and Bourgund, 1990, Rajashekhar and Ellingwood, 1993, Unnikrishnan et. al., 2013). These methods which are based on empirical risk minimization (ERM) inductive principle, aim at finding a substitute explicit function for the implicit performance function by fitting it through planned or random samples. Unfortunately, the inflexible nature of response surface function selection under ERM principle severely influences the application range of these methods. (Guan and Melchers, 2001, Hurtado, 2004).

In order to discover patterns in highly dimensional and complex data such as the relationship between ground motion intensities and peak structural responses, Machine Learning and Soft Computing methods such as Support Vector Machines (SVM) can be used. SVM introduced by Vapnik (1995) is an increasingly popular machine learning technique which has widespread applications in classification, regression and density estimation. It is based on structural risk minimization (SRM) inductive principle and aim at minimizing an upper bound of the generalization error (Vapnik, 1995, Cortes and Vapnik, 1995).

The application of SVM in the reliability analysis was first introduced by Rocco and Moreno (2002). Jack and Nandi (2002) and Widodo and Yang (2007) proposed the application of SVM classification for machine condition monitoring and fault diagnosis.

Ge et. al. (2004) compared the efficiency of NN and SVM methods in fault detection in a manufacturing process and demonstrated the superiority of SVM classification method. Hong-Shuang et. al. (2006) proposed SVM based MCS and SVM based FORM analyses for reliability assessment of simple structures. Hurtado and Alvarez (2003) adopted SVM in conjunction with stochastic finite element for performing structural reliability analysis. Zhiwei and Guangchen (2009) introduced the application of least squares support vector machine for regression (LSSVR) into reliability analysis of engineering structures.

2.7.2 LINEAR BINARY SVM CLASSIFICATION FOR SEPARABLE AND NON-SEPARABLE DATA

Consider a set of training data $(x_1,y_1),(x_2,y_2),...,(x_n,y_n)$ where $x_i \in R^n$ is the training data and $y_i \in \{+1,-1\}$ is the class label for x_i. Our goal is to find the optimal hyper plane that separates one class from the other correctly and follows the form of

$$f(w,x) = w.x + b = 0 \qquad (2\text{-}24)$$

Where (.) means inner product of two vectors.

For this purpose SVM implements a margin-based loss function such that most of the training data can be separated perfectly (with zero empirical loss) and the rest of the training data falls within the margin and can only be explained with some uncertainty (non-zero loss). The concept of margin based loss function is indicated in figure 2-12. The best decision boundary achieves the optimal balance between two conflicting goals of predictive learning (Cherkassky and Mulier, 2007):

1. Minimizing the total empirical loss for the samples that lie within the margin.
2. Achieving maximum separation (margin) between training samples that are perfectly classified by the model.

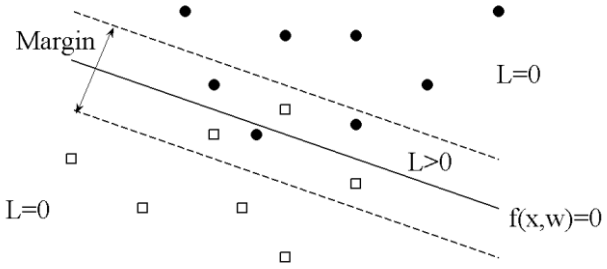

Figure 2-12. Margin based loss function for SVM classification

In the case of linearly separable samples, the optimal hyperplane is the one which maximizes the distance between the hyperplane and the nearest sample points to it of each class. This problem can be formulated as minimization of the following function:

$$Min(\frac{1}{2}\mathrm{w}^T.\mathrm{w}) \qquad s.t.\ y_i(\mathrm{w}.\mathrm{x}_i + b) \geq 1 \qquad (2\text{-}25)$$

where w is the weight vector which defines the boundary and is in the general form of equation (2-26) in which α_i are the parameters of the hyperplane.

$$\mathrm{w} = \sum_{i=1}^{n} \alpha_i y_i x_i \quad , \alpha_i \geq 0 \qquad (2\text{-}26)$$

The data points for which equation (2-25) is an equality are called the support vectors. Conceptually these are the samples that define the location of the decision surface and are most difficult to classify. An example of the optimal hyper-plane of two linearly separable data sets is presented in figure 2-13.

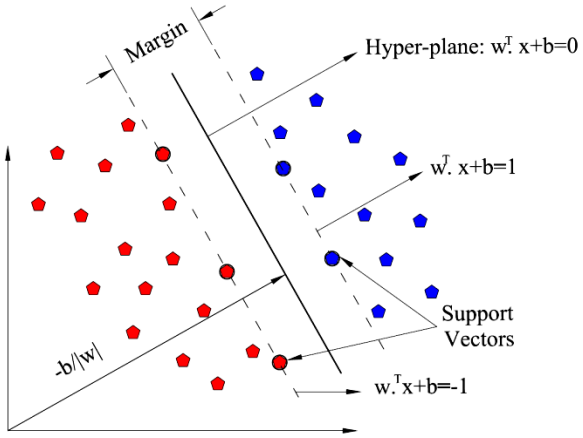

Figure 2-13. Linearly separable SVM classification

Finding the optimal hyperplane for separable data points is a quadratic optimization problem with linear constraints. It is noted that for very high dimensional spaces the problem should be translated into its dual form which is finding parameters α_i that maximize the functional

$$L(\alpha) = \sum_{i=1}^{n} \alpha_i - 1/2 \sum_{i,j=1}^{n} \alpha_i \alpha_j y_i y_j (\mathrm{x}_i . \mathrm{x}_j) \qquad s.t. \sum_{i=1}^{n} y_i \alpha_i = 0, \qquad \alpha_i \geq 0 \qquad (2\text{-}27)$$

The optimal hyperplane is then given by equation (2-28).

$$f(x) = \sum_{i=1}^{n} \alpha_i y_i (\mathrm{x} . \mathrm{x}_i) + b \qquad (2\text{-}28)$$

where *b* is given by equation (2-29).

$$b = y_s - \sum_{i=1}^{n} \alpha_i y_i (\mathrm{x}_i . \mathrm{x}_s) \qquad (2\text{-}29)$$

To construct the optimal hyperplane in the case that the samples are linearly non-separable, slack variables are introduced as shown in equation (2-30) to allow miss-classification of difficult or noisy data points (Vapnik, 1995).

$$Min(\frac{1}{2}\mathrm{w}^T.\mathrm{w} + C\sum_{i=1}^{n}\xi_i) \qquad s.t.\ y_i(\mathrm{w}.\mathrm{x_i} + b) + \xi_i - 1 \geq 0 \quad , \quad \xi_i \geq 0 \qquad (2\text{-}30)$$

where $\xi_i = \max(1 - y_i f(x_i, w), 0)$ and C is a user selected parameter that controls the trade-off between complexity and proportion of non-separable samples. The dual form of this quadratic optimization problem is to find the parameters α_i that maximize the following functional (Vapnik, 1995).

$$L(\alpha) = \sum_{i=1}^{n}\alpha_i - 1/2\sum_{i,j=1}^{n}\alpha_i\alpha_j y_i y_j(\mathrm{x}_i.\mathrm{x}_j) \qquad s.t.\ \sum_{i=1}^{n} y_i\alpha_i = 0, 0 \leq \alpha_i \leq C \qquad (2\text{-}31)$$

Figure 2-14 shows the optimal hyper-plane of two non-separable data sets.

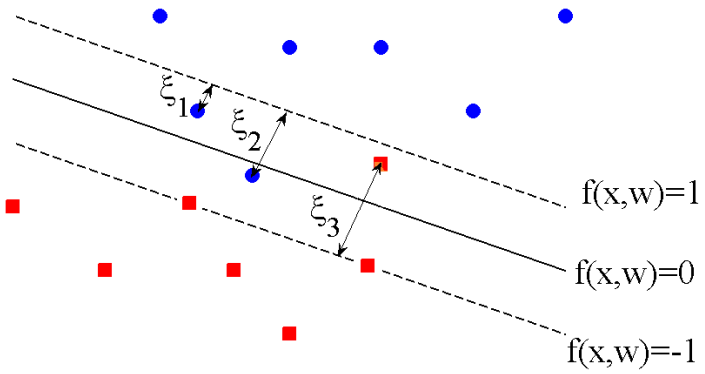

Figure 2-14. Non-separable SVM classification

2.7.3 NONLINEAR SVM CLASSIFICATION

In case of non-linearly separable data points, the input vectors are mapped into a high dimensional feature space using the nonlinear transform $\boldsymbol{x} \rightarrow \Phi(\boldsymbol{x})$. The optimal hyperplanes in the feature space will then result in nonlinear decision boundaries in the input space. Building the optimal hyperplanes in the feature space only involves calculating the inner product of two vectors in this space. For this purpose, Kernel functions are used as shown in equation (2-32).

$$(z_i . z_j) = \left(\Phi(x_i) . \Phi(x_j)\right) = K(x_i, x_j) \quad (2\text{-}32)$$

where z_i and z_j are two vectors in the feature space Z and $K(x_i, x_j)$ is the Kernel function of two variables in the input sapce. The selection of the type of kernel function corresponds to the selection of the class of functions used for feature construction. Table 2-1 presents some commonly used functions for learning machines that are considered in this study.

Table 2-1. Formulation of Kernel Functions

Kernel Function	K(x,x_j)
Linear	$x^T . x_j$
Polynomial	$(\gamma x^T . x_j + r)^d, \gamma > 0$
Gaussian RBF	$\exp(-\left\|\left\|x - x_j\right\|\right\|^2 / 2\gamma^2)$

After the kernel function is selected, the optimal hyperplane is a nonlinear function in the input space, which is equivalent to the linear function in feature space for the nonlinear separable training data and is formulated as equation (2-33).

$$f(x) = \sum_{i=1}^{n} \alpha_i y_i K(\mathrm{x} \,.\, \mathrm{x}_i) + b \quad (2\text{-}33)$$

2.7.4 SVM MODEL SELECTION

The quality of the SVM models depends on the proper tuning of SVM parameters such as the appropriate kernel function, kernel parameter (γ) and penalty parameter (C). The performance of a SVM classifier is usually measured in terms of its prediction error. Therefore, the problem of model selection includes selecting the parameters that form the model with lowest prediction error. However, the prediction error cannot be exactly calculated for most real world problems, and its estimation is required. For this purpose, resampling techniques can be used as they make no assumptions on the statistics of the data or on the type of the function being estimated (Cherkassky and Mulier, 2007). The basic idea is to learn a model using a portion of the available samples and then use the

remaining samples to estimate the prediction error of this model. A comparison of different resampling methods can be found in a study by Molinaro et. al (2005). It concludes that 10 fold cross validation generally performs well and is preferred especially for computationally burdensome analyses. Moreover, Rodrıguez et. al (2010) studied the statistical properties such as bias and variance of the k-fold cross-validation and recommended to use a 10-fold cross validation technique for estimating the error because of its small bias.

In this study optimal parameters of the SVM model are selected using grid search in combination with 10-fold cross validation (Chang and Lin, 2001). It is noted that the minimum value of prediction risk found for model selection tends to be optimistic. In order to obtain an unbiased prediction error a double resampling technique is required (Friedman, 1994). For this purpose, the available samples are divided to 10 folds of roughly equal size. Each of these folds is used in turn as a test sample with the complement sample serving as the training sample. The training set is used for parameter selection, whereas the test set is used only for estimating the prediction risk associated with various kernel functions. In order to find the optimal parameters of (C, γ), a 9-fold cross validation is implemented to divide the training set into learning and validation set. The learning set is used to estimate the hyper-planes for every set of (C, γ) and the validation set is used to estimate the error associated with each set of parameters. (C, γ) with the lowest average of validation error are selected. Finally, the average values of prediction errors are compared to determine the best model and kernel function.

2.7.5 MULTICLASS SVMS

SVM was originally designed for binary classification and extending it to multiclass problems is an ongoing research issue. Two types of approaches may be followed in the generalization of binary SVM to solve a multiclass SVM. In the direct approach, the SVM training algorithm is reformulated to generate a multiclass version (Weston and Watkins, 1998, Crammer and Singer, 2001, Lee et. al, 2001). This approach in general yields to costly algorithms and are usually avoided (Hsu and Lin, 2002, Rifkin and Klautau, 2004, Lorena and Carvalho, 2008a, 2008b).

The simpler and more popular approach consists in dividing the original data set into two-class subsets and learning a different binary model for each new subset. The final step is to combine the outputs of these binary classifiers. These methods are known as binarization techniques. Among the most common binarization strategies, one can cite the "one-vs-one" (OVO) (Knerr et. al, 1990, Kreßel, 1999) and "one-vs-all" (OVA) (Anand et. al, 1995). The former constructs all the possible classifiers between pairs of classes and then predicts the output class based on the outputs of these classifiers, while the latter learns a classifier for each class where all of the examples in that class have positive labels, and all other examples have negative labels. Many researchers have proposed different combination methods to obtain the predicted class from the outputs of OVO or OVA binary classifiers. Friedman (1996) proposed the Voting strategy or Max-Wins rule where each binary classifier gives a vote for the predicted class and the class with the largest number of votes is predicted. Platt et. al (2000) suggested using Decision directed acyclic graph (DDAG) where a rooted binary acyclic graph is constructed and each node is associated to a list of classes and a binary classifier. Hastie and Tibshirani (1998) and Wu et. al (2004) presented the method of classification by pairwise coupling where the joint probability for all classes are calculated from the pairwise class probabilities of the binary classifiers and the class with the highest posterior probability is selected. In each level, the method removes the class that is not predicted. The final output class is the one remaining on the list. Galar et. al (2011) presented a detailed comparison of various binarization techniques used in dealing with multiclass learning machines and pointed that for most learning machines including SVM classifiers OVO strategy based methods outperform OVA ones. Duan and Keerthi (2005) compared different binarization techniques for SVM multiclass classification problem and demonstrated that pairwise coupling PSVM which is used in this study offers the best accuracy.

2.7.6 PROBABILISTIC SUPPORT VECTOR MACHINES (PSVM)

Constructing a classifier that produces a posterior probability P(class|input) is a useful tool in reliability analysis of structural systems. Unfortunately, the original SVMs only

produce a threshold value *f(x)* calculated based on equation (2-28) for linear SVMs and equation (2-33) for nonlinear SVMs. This score provides the distance of the sample point *x* to the separating hyperplane. In recent years, many researchers have proposed different methods to convert the threshold output of SVM into a probability estimate. Drish (1998) proposed the application of binning technique where the decision values are divided into several bins, and the conditional class probability is the fraction of the training examples with similar label in that bin. Zadrozny and Elkan (2002) used isotonic regression to map the SVM scores to probability estimates. Vovk et. al (2003 and 2005) introduced a new class of algorithms for online probability forecasting called "Venn Machines". Ruping (2004) compared various scaling methods to obtain estimates of conditional class probabilities from SVM decision function and concluded that the method proposed by Platt (2000) offers the best scaling for SVM outputs. Platt (2000) and Lin et. al. (2003) proposed an algorithm to map the *f* value into the positive class posterior probability by applying a sigmoid function to the SVM output as presented in equation (2-34).

$$\Pr(y=1|\mathbf{x}) \approx P_{A,B}(f) \equiv p(\mathbf{x}) = \frac{1}{1+\exp(A f(\mathbf{x})+B)}, \quad \text{where } f = f(\mathbf{x}). \tag{2-34}$$

The best parameter setting $Z^*=(A^*,B^*)$ is determined by solving the following regularized maximum likelihood problem in which N_+ and N_- are the number of positive and negative training data respectively.

$$\min_{z=(A,B)} F(z) = -\sum_{i=1}^{l}(t_i \log(p_i) + (1-t_i)\log(1-p_i))$$

$$t_i = \begin{cases} \dfrac{N_+ + 1}{N_+ + 2} & \text{if } y_i = 1 \\ \dfrac{1}{N_- + 2} & \text{if } y_i = -1 \end{cases}, i = 1,2,...,l. \tag{2-35}$$

Regarding multi-class classification problems, Hastie and Tibshirani (1998) proposed pairwise coupling to combine the probabilistic outputs of all the one-versus-one binary classifiers in order to estimate the posterior probabilities $P_i=\text{prob}(w_i|x)$, i=1,…, *k*. In which *k* is the number of classes. It is noted that for a k-class problem k(k-1)/2 binary

classifiers are required. Wu et. al., (2004) proposed the optimization problem presented in equation (2-36) to obtain the probability of x belonging to class i.

$$\min_{p} \sum_{i=1}^{k} \sum_{j:j\neq i} (r_{ji}p_i - r_{ij}p_j)^2 \quad \text{subject to} \sum_{i=1}^{k} p_i = 1,\ p_i \geq 0,\ \forall i. \tag{2-36}$$

in which r_{ij} = P(y=i| y=i or j, x) are auxiliary variable which represents the binary SVMs of the i^{th} and j^{th} classes and are calculated based on equation (2-34) and (2-35).This optimization problem provides a vector of multi-class probability estimates.

In this study Platt's algorithm is used to produce probabilistic outputs for the trained binary SVM. In case of multiclass SVM classification, OVO binarization strategy is applied to obtain pair-wise class probabilities of the binary classifiers, then equation (2-36) is used to calculate the probability of x belonging to class i.

CHAPTER 3: MANUSCRIPT 1

UNCERTAINTIES IN SEISMIC FRAGILITY ANALYSIS OF EXISTING BRIDGES

S.N. Mahmoudi[1], L. Chouinard[2], D. Mitchell[3], P. Tehrani[1], A. De la Puente[1]

ABSTRACT

Seismic fragility analysis of bridges provides a powerful tool to identify critical structural components and to assess the reliability of structures. This paper represents the fragility analysis of a typical Montreal bridge built in the 1960's. The main objective of this paper is to address the structural deficiencies under seismic demands considering all significant sources of uncertainties in modeling and evaluating the demands and capacities.

Based on the design plans, the existing bridge bent has three major design deficiencies: 1) large spacing of ties in the column, 2) absence of shear reinforcement in cap beams, and 3) lack of shear reinforcement in the beam-column joints. A 2-dimensional bridge model is developed which is validated with results of a laboratory test performed on a half scale model of the existing bridge bent. An Incremental Dynamic Analysis (IDA) is performed to account for record-to-record variability in seismic inputs on engineering demand parameters (EDP).

Component fragility curves are developed for each critical bridge component by utilizing probabilistic demand models (PDMs) obtained from regression analyses of component response. Component fragility curves are used to identify the weak components that require strengthening. Finally, the system fragility curve of the bridge is generated to estimate the overall reliability of the bridge structure.

[1] Graduate Student, Department of Civil Engineering and Applied Mechanics, McGill University, Montreal, QC, H3A 2K6
[2] Associate Professor, Department of Civil Engineering and Applied Mechanics, McGill University, Montreal, QC, H3A 2K6
[3] Professor, Department of Civil Engineering and Applied Mechanics, McGill University, Montreal, QC, H3A 2K6

The results demonstrate that the bridge is vulnerable and likely to be damaged under seismic demands and that brittle shear failure of the cap beam is the dominant failure mode of the structure. In the second part of this paper, a retrofit strategy is suggested which requires minimal interference with the normal function of the bridge and the fragility curves are developed for the retrofitted structure.

Keywords: Bridge, Component Fragility Curves, System Fragility Curve, Incremental Dynamic Analysis (IDA), Model Validation, Hypothesis Test, Bayesian, Monte Carlo

3.1 INTRODUCTION

Much research has been conducted to assess and address seismic deficiencies of existing structures in high seismic regions as a result of increased awareness of potential damages after the occurrence of major earthquakes such as the 1989 Loma Prieta (Houser and Thiel, 1990; Mitchell *et. al.,* 1995), the 1994 Northridge (Mitchell *et. al.*, 1994) and the 1995 Kobe (Mitchell *et. al.,* 1995) earthquakes. However, seismic deficiencies of highway bridges have been traditionally neglected in moderate seismic regions such as eastern Canada.

According to Tavares et. al. (2010), 75% of bridges in Quebec have more than thirty years of service and have some form of deterioration. Moreover, the design codes which were applicable at the time of the original construction of older bridges are considered inadequate today. With the new code requirements, the focus of decision-makers should be to evaluate and retrofit bridges to improve their seismic performance together with rehabilitation for deterioration problems.

Uncertainties involved in determining the demands of earthquakes and in evaluating the capacity of structures under cyclic loads lead designers to use probabilistic methods to quantitatively assess the structural reliability. Fragility curves represent the state-of-the-art in seismic risk assessment (SRA) and are defined as the conditional probability that a structure will meet or exceed a certain level of damage for a given ground motion intensity. Fragility curves are also useful tools to identify weak parts of the structure and to guide the efficient allocation of funds to strengthen or retrofit an existing structure.

Through this study, the seismic behaviour of a typical bridge built in the 1960's in Montreal is determined. The 4-span overpass investigated is considered a lifeline bridge due to the fact that it provides a major access route to a hospital and also crosses two national railway lines. It is one among several similar bridges, which makes it possible to extend the conclusions of this study to other bridges in the area.

3.2 STRUCTURE AND STRUCTURAL COMPONENTS DESCRIPTION

The bridge is composed of a reinforced concrete deck supported by a grid of steel beams. The three spans (21.3, 26.2 and 21.3 m) are supported by two concrete abutments, one at each end, and two concrete moment resisting frames. These frames each consist of twelve slender columns supported by a wall. The columns are interconnected at their tops by a cap beam (Figure 3-1). The load from each steel beam is directly supported by one concrete column, which transmits the load directly to the wall and then to the foundations. Due to the symmetry of the bridge, it is assumed that each of the two frames shares equally the lateral loads.

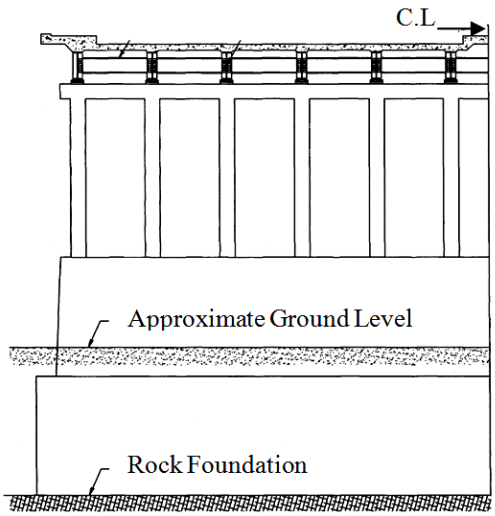

Figure 3-1. Frame elevation of bridge

The square-shaped concrete columns have dimensions of 457 x 457 mm and contain a longitudinal reinforcement ratio of 3.52% and a volumetric ratio of transverse reinforcement of 0.557%, with #4 ties spaced at 305 mm (Figure 3-2a). The bottom portion of the columns are within the splash exposure zone for water and deicing

chemicals caused by vehicles on a service road that runs under the bridge which resulted in corrosion of the reinforcing steel and spalling of the concrete cover (Figure 3-3). The effect of the deterioration of the existing structure is accounted for in the analyses by considering the spalled concrete section of the columns and a 10% reduction of the gross steel area (Mahmoudi et. al, 2015 B).

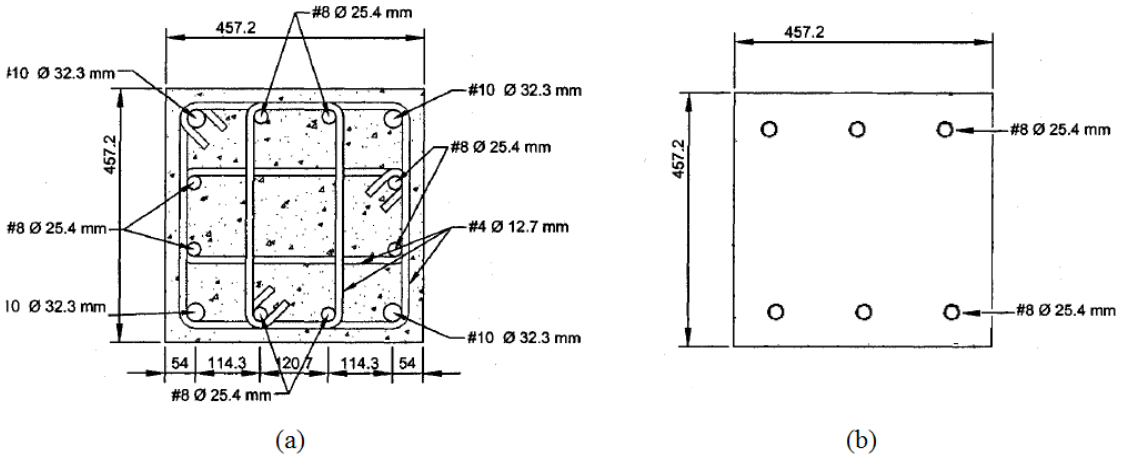

Figure 3-2. Details of as-built bridge components: (a) Column cross section (b) Beam cross section

Figure 3-3. Deterioration in one of the bridge columns

The top of each column is connected to a 457 x 457 mm cap beam composed of eleven segments. This beam has only longitudinal reinforcement (1.464%) without any transverse reinforcement, and hence is expected to have a brittle failure mode (Figure 3-2b).

The wall supporting the twelve columns has a thickness of 610 mm at the top and increases to 915 mm at the base. The wall has a height of 3658 mm. The wall reinforcement consists of #6 vertical bars at 305 mm and #6 horizontal bars at 710 mm on each face. The mean value of the concrete compressive strength is assumed to be 25 MPa which is typical of structures built in the 1960' s (Griezic 1996) and a mean value of 300 *MPa* is assigned to yield-strength of the steel reinforcement.

3.3 FINITE ELEMENT MODELING AND LABORATORY TEST

The bridge is modeled with finite elements using Ruaumoko 3D (Carr, 2001). The moment-resisting frame is idealized with 69 elements divided into six types (Figure 3-4), of which, 23 have possible non-linear behaviour. These elements correspond to the 12 columns and the 11-segments of the cap beam. The nonlinear behaviour of the concrete component is determined with the *Response 2000* software (Bentz, 2001). Moment-Curvature and Force- Displacement diagrams for the beams and columns are shown in Figure 3-5. It is noted that moment-curvature responses presented in Figure 3-5 are developed for the components when they are subjected to an average dead load of 465 kN for columns and 0 kN for beams as well as when they are subjected to tension or compression axial loads. The grid of steel beams that support the concrete deck have elastic linear behaviour and are connected to the moment-resisting frame by rocker supports.

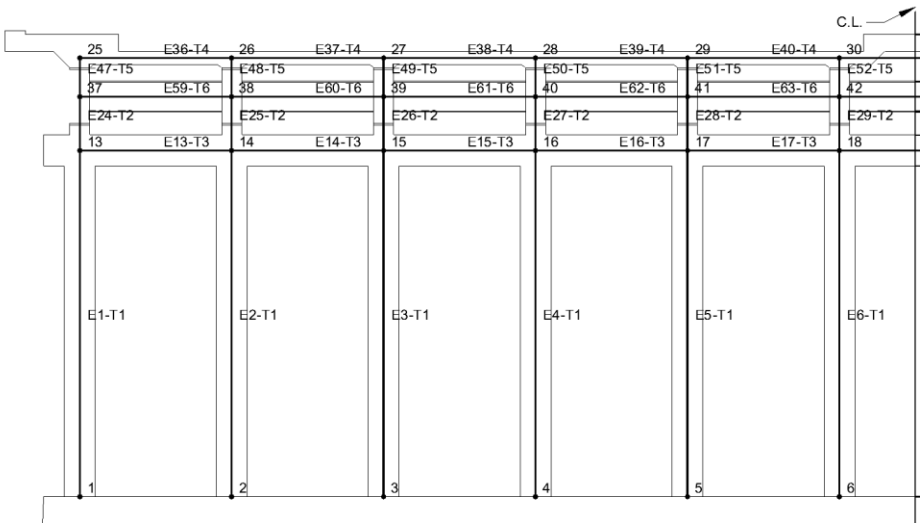

Figure 3-4. Structural idealization of moment-resisting frame (Left side)

Uncertainties arise from the selection of the conceptual model and the formulation of the mathematical model as well as the input parameters of the selected model. Traditional statistical theories have provided solutions to find a set of input parameters which result in responses consistent with a given sample of data. However, they usually differ only in the parameter values and the mathematical model is assumed known. However, in practice, model uncertainty can be more significant than other sources of uncertainty (Chatfield, 1995).

A half scale model of the existing bridge bent was designed and constructed in the structural laboratory at McGill University and the model was tested under reversed cyclic loading (Itagawa, 2005). The axial load was kept constant during the test and the lateral load level was increased gradually to determine the loads corresponding to various cracking events and to determine the dominant failure mechanism.

This test provides the required information to investigate and quantify the goodness of the developed finite element model. However, in order to assess and reduce the uncertainties resulted from selected input variables, such as material strengths and stiffness of components, field testing of the actual existing bridge structure is required.
The results obtained from the laboratory test of the half scale structure demonstrate that the shear failure in the beam is the dominant failure mode which occurs at a lateral load of about 60 kN. Finite element model results in the same failure mode at a lateral load of 55.89 kN. The ratio of the results obtained from the test to the model is equal to 1.073 which represents a good agreement. However, since a defined acceptable ratio or distance between the results is not provided in the literature, a stochastic approach is required to validate and verify the model.

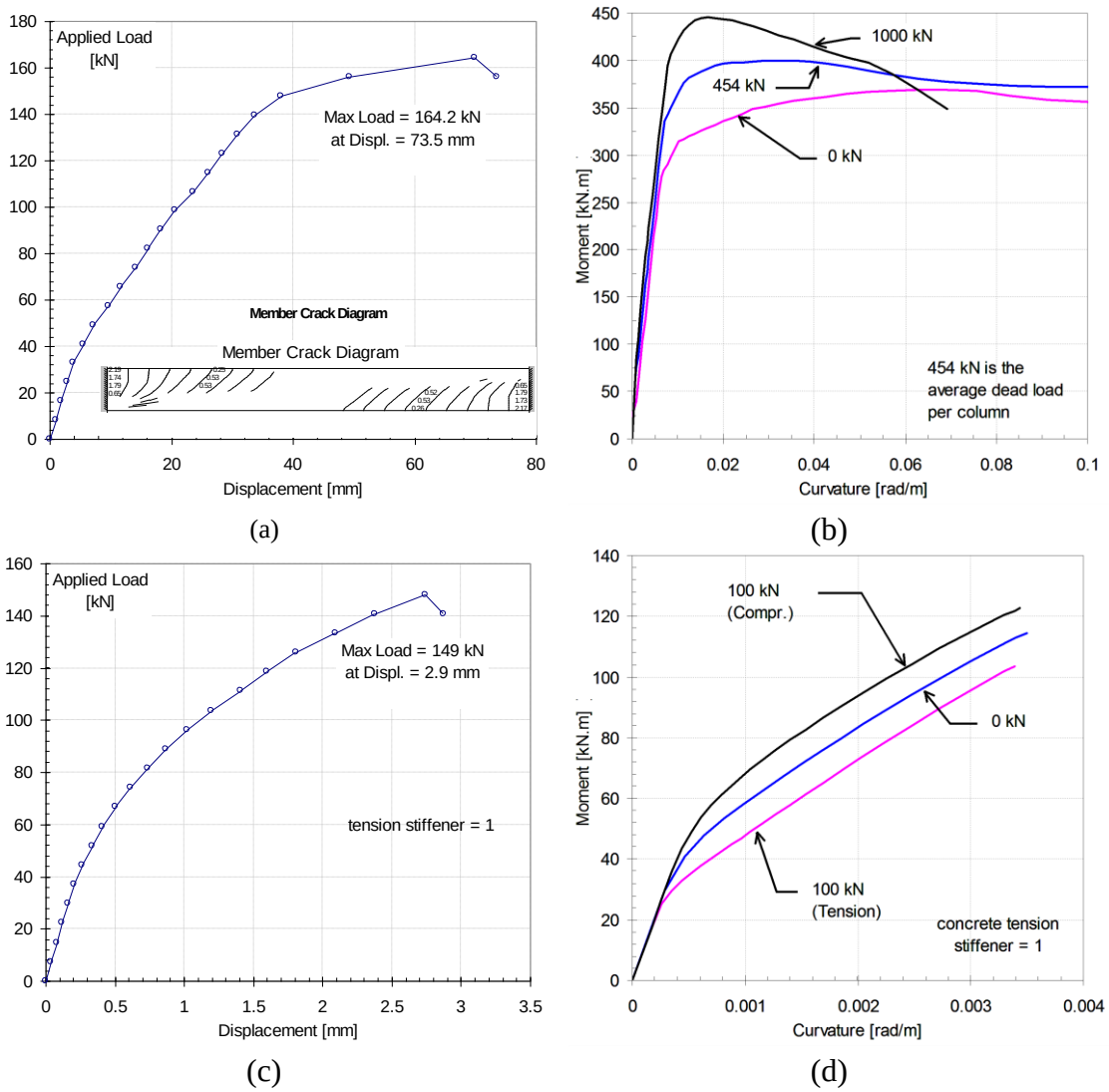

Figure 3-5. Predicted Component Response: (a) Force- Displacement of Columns (b) Moment- Curvature of Columns (c) Force- Displacement of Beams (d) Moment- Curvature of Beams

3.4 FINITE ELEMENT MODEL VALIDATION

Traditionally, computer models have been verified using subjective or quantitative comparison approaches (Chen et. al., 2004). The former is based on a visual comparison of the plots or contours of the predicted model and observations. This approach neither presents the uncertainties involved in the predicted model nor demonstrates the confidence in the model. The latter uses some measures such as the ratio of the results obtained from the model and observations. However, a prescribed acceptable measure cannot be found in the literature for every case.

Two stochastic approaches are used in this study to validate the finite element model of the bridge structure. These approaches can be utilized for either single or multiple available observations. The first approach is based on classical hypothesis testing which provides valuable information about goodness of fit of the model and the confidence of predicted model. However, Edwards et. Al. (1963) and Zhang and Mahadevan (2003) argue that this method can be sometimes misleading and hard to interpret. In addition, they suggest that this approach can be biased and inclined toward rejecting the null hypothesis. The second approach however is based on Bayesian hypothesis testing which addresses the mentioned issues and provides an unbiased model validation test.

It is noted that there may not be a unique acceptable model and every model validation method accepts a variety of models. However, the mentioned methods present statistics which can be a representation of the goodness of each model. Classical hypothesis test uses the confidence bound or p-value of the test while Bayesian hypothesis approach introduces the Bayes factor for this purpose.

3.4.1 CLASSIC HYPOTHESIS APPROACH

Hills and Trucano (1999) stated that if an experiment falls inside a given confidence bound of the predicted model, the experiment and the model are consistent; otherwise the model will be rejected. This test is the foundation of the methods which reject incorrect models.

An uncertainty propagation technique should be used to evaluate confidence bounds of the predicted model. Hence, various uncertainties involved in finite element modeling of the bridge are assessed and the effect of them on the predicted model is evaluated through Monte Carlo Simulation (MCS). However, since performing MCS of finite element model is not computationally feasible, MCS is performed on a metamodel which is developed using Response Surface Method (RSM) as suggested by Chen et. al. (2004).

After a brief sensitivity analysis, the compressive strength of the concrete (f_c), the shear resistance of beams (V_c) and the axial dead load of the bridge deck (L_d) are considered as variables since they have significant effect on the predicted lateral load which causes

failure in the structure. A polynomial regression method is used for developing a RSM in order to model the finite element predicted response by polynomials.

f_c and L_d are assumed to have normal distributions. The mean value and standard deviation of f_c and the mean value of L_d are obtained from tests which were performed by Itagawa (2005). Song and Kang (2010) demonstrated that the shear capacity of a reinforced concrete beam without shear reinforcement has a lognormal distribution. The mean value of Vc is determined by the Response 2000 software and the standard deviation is assumed according to Song and Kang (2010). Distribution parameters of the variables are presented in Table 3-2.

Since this test is based on the assumption of normality of the response, all the input variables are transformed into normal space. Hence, Vc is transformed using natural logarithm function. In addition, in order to give each predictor an equal share in determining the response, an appropriate coding transformation of the data should be used. So, all the normalized input variables are transferred to a space with a range of -1 to 1. A response surface regression analysis is performed using 200 data points and the resulting RSM is shown in equation 3-1 in which index 1 represents the normalized variables. Estimates of the regression coefficients are provided in Table 3-1. It is noted that 216 data points are used for design of the developed response surface.

$$\begin{aligned} Log(F) = {} & R_1.Log(V_{c1})^2 + R_2.\log(V_{c1}) + R_3.f_{c1}^2 + R_4.f_{c1} + R_5.{L_{d1}}^2 \\ & + R_6.L_{d1} + R_7.Log(V_{c1}).f_{c1} + R_8.Log(V_{c1}).L_{d1} + R_9.f_c.L_{d1} \\ & + R_{10} \end{aligned} \quad (3\text{-}1)$$

Table 3-1. Parameters of the input variable distributions in prior and posterior states

	R_1	R_2	R_3	R_4	R_5
μ	$2.368*10^{-3}$	0.682	$7.21*10^{-5}$	$-3.51*10^{-4}$	$4.44*10^{-5}$
σ ($*10^{-5}$)	2.841	1.681	2.855	1.722	2.845

	R_6	R_7	R_8	R_9	R_{10}
μ	$-3.34*10^{-3}$	$-9.23*10^{-4}$	$-1.75*10^{-4}$	$4.7*10^{-4}$	4.065
σ ($*10^{-5}$)	1.721	2.461	2.461	2.442	16.878

The standard deviation of residuals and the coefficient of determination (R^2) for this regression model are $2.8*10^{-8}$ and 1.00 respectively. It is inferred from Table 3-1 that the variance on R2 and R10 which correspond to the design variables with the highest influence on the response, are negligible. It is noted that performing a hypothesis test on the coefficients demonstrates that R_8 and R_9 are statistically insignificant at the 5% significance level and the corresponding values shown in Table 3-1 are the values of those variables if they were considered in the regression model. This result is consistent with the physics of the structure, as L_d is uncorrelated with V_c and f_c. Figure 3-6 shows the relationship of the variables in the model.

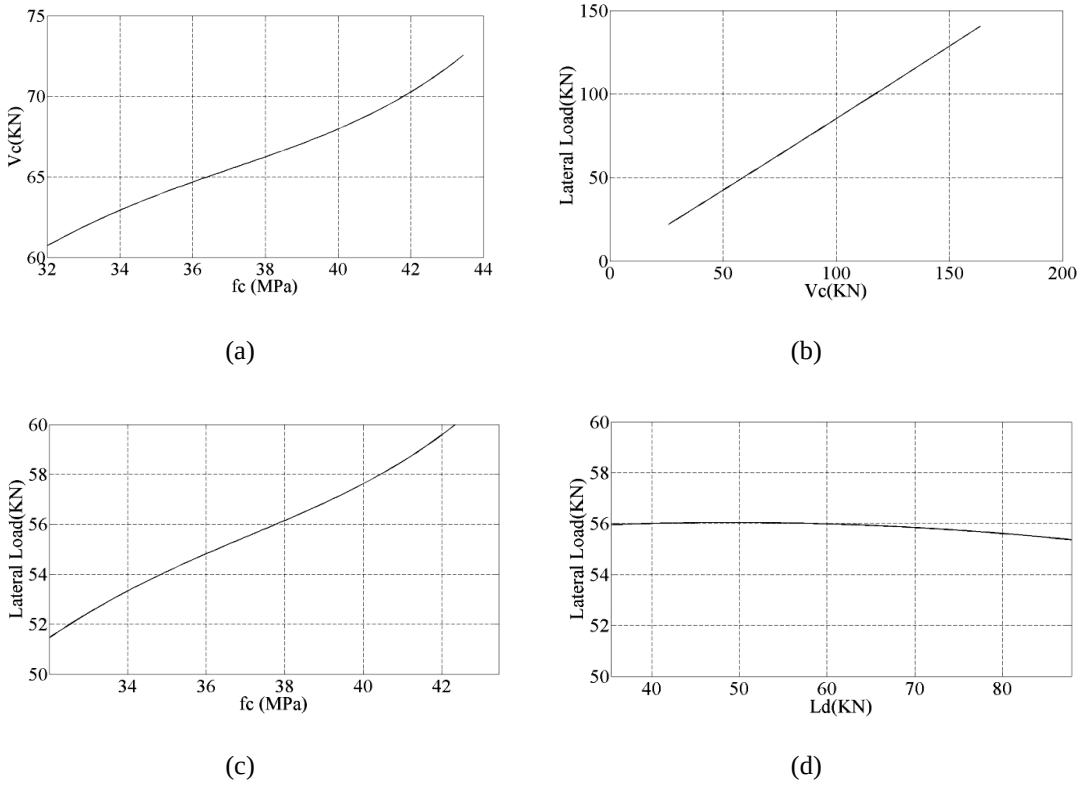

Figure 3-6. Relationships of the variables which are considered in RSM

The histogram and consequently the distribution of the predicted lateral load corresponding to failure are obtained from a MCS which is performed with 400,000 samples. The predicted lateral load has a lognormal distribution with the mean value of 55.89 kN and standard deviation of 11.75 kN. The histogram of natural logarithm of the response is shown in figure 3-7.

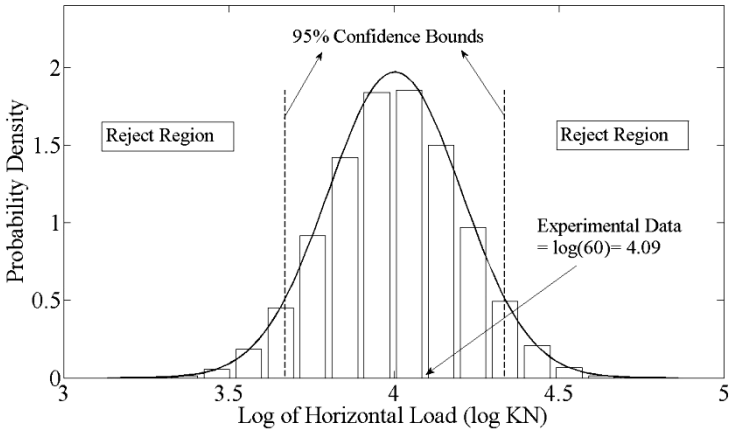

Figure 3-7. Model Validation using classic hypothesis approach

It is noted that considering a narrow acceptable confidence interval increases the probability of type I error or rejecting the correct model, while considering wide acceptable confidence interval increases the probability of type II error or accepting an incorrect model.

According to the results of MCS, the observation of 60 kN corresponds to 63.7% confidence limit or a p-value of 0.182. So, if the significant level is set at 95%, the experiment fails to reject the model under the null hypothesis.

3.4.2 BAYESIAN MODEL VALIDATION APPROACH

The classic hypothesis approach provides a powerful method to represents the confidence in the model. However, as mentioned earlier, it has been suggested that hypothesis testing method may be misleading and can be biased toward rejection of the models because this method neglects prior distribution under the alternative hypothesis. In other words, classical hypothesis approach only considers the likelihood of the observation if the null hypothesis is true and neglects the likelihood of the observation in case that the null hypothesis is false (Zhang and Mahadevan, 2003). Bayesian hypothesis approach is also used in this study to address the mentioned issue. This approach compares the likelihood of the observation under null and alternative hypotheses.

According to Mahadevan and Rebba (2004), a model is accepted if the observation favors

the model. In other words, if the probability density of the predicted value increases given new observation, the model will be acceptable. Mahadevan and Rebba (2004) and Rebba and Mahadevan (2006) demonstrated that the Bayes factor can be calculated from equation 3-2:

$$B(x_0) = \frac{f(x|y)}{f(x)}|_{x=x_0} \tag{3-2}$$

in which x_0 is the predicted value, f(x) represents the prior Probability Density Function (PDF) and f(x|y) represent posterior PDF. It is noted that the $B(x_0)$ higher than unity validates the model.

In this study, the posterior PDF is obtained from a MCS similar to the one of the previous part considering updated input variables. Input variables- fc, Vc and Ld- are updated using the following Bayesian equation:

$$f(\theta_i|y) = \frac{L(y|\theta_i).f(\theta_i)}{\int_{\theta_i} L(y|\theta_i).f(\theta_i)\ d\theta_i} \tag{3-3}$$

in which θ_i represents the input variable, $L(y|\theta_i)$ is the likelihood of the observation in prior system and $f(\theta_i)$ represents the prior PDF of the input. The PDF of input variables are updated based on equation 3 using MCS. The results are shown in Table 3-2.

Table 3-2. Parameters of the input and output variable distributions in prior and posterior states

		Distribution	Prior		Posterior	
			Mean Value	Standard Deviation	Mean Value	Standard Deviation
Inputs	f_c (MPa)	Normal	37.7	1.34	43.9	5.44
	V_c (kN)	Lognormal	66	13.39	73.5	6.48
	L_d (kN)	Normal	60	6	71.71	8.31
Output	Lateral Load (kN)	Lognormal	55.89	11.75	62.24	5.56

The resulted posterior PDF of the predicted lateral load corresponding to failure has a lognormal distribution with the mean value of 62.24 kN and standard deviation of 5.56 kN and is shown in figure 3-8. The PDF of prior and posterior at x=55.89 kN is equal to 0.0407 and 0.0341 respectively. Hence, the Bayes ratio at the predicted point is equal to 1.19 and the model is validated.

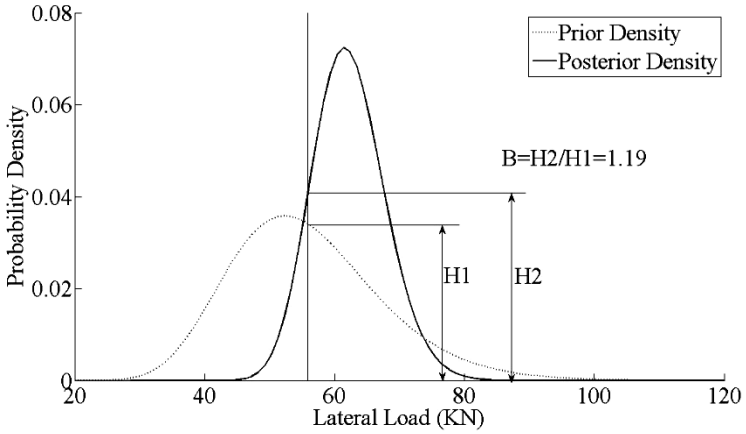

Figure 3-8. Model Validation using Bayesian hypothesis approach

3.5 INCREMENTAL DYNAMIC ANALYSIS (IDA)

Variability in seismic inputs is a significant source of uncertainty in the seismic evaluation of structures. The IDA technique (Vamvatsikos and Cornell, 2002) addresses the record-to-record variability by using a set of scaled input ground motions to evaluate the response of the structure. By performing non-linear dynamic analyses with increasing scaling factors for each ground motion record, the relationship of the Intensity Measure (IM) and the Engineering Demand Parameter (EDP) is obtained. The selection of the proper ground motion records, EDP and IM for the structure should be done carefully since they can all affect the results.

3.5.1 SELECTION OF GROUND MOTION RECORDS

Since there are few available ground motion records in the Montreal area and none of them is considered as a strong ground motion, a variety of artificial and simulated ground motion records developed by Atkinson and Bersenev (1998) are used in this study. The effect of using artificial records on the resulting fragility curves is investigated by

comparing the obtained fragility curves to developed fragilities using a set of actual ground motion records suggested by ATC63. IDA methods are applicable to either artificial, natural, or modified natural ground motion records. In this paper, three sets of records including ATC-63 records (44 natural records), Atkinson-6C2 records (45 artificial records) and Atkinson-7C2 records (45 artificial records) (Atkinson and Beresnev, 1998) are used.

The epsilon-based record selection method recommended by Baker and Cornell (2006) was used to include the effects of spectral shapes. The records that have mean epsilon values similar to those obtained from the seismic deaggregation analysis at the fundamental period of the structure are selected. Epsilon, ε, is the number of logarithmic standard deviations of a target ground motion from a median ground motion prediction equation (GMPE) for a given magnitude, M and distance (R). It has been shown that $\varepsilon(T_1)$ is a proxy for spectral shape (Baker and Cornell, 2006).

Mean epsilon values for Montreal are reported in Tehrani and Mitchell (2012) based on the updated seismic hazard data provided by Atkinson and Goda (2011) (Table 3-3).

Table 3-3. Mean epsilon values at different hazard levels from seismic deaggregation for Montreal (Tehrani and Mitchell, 2012)

	Hazard level		
Period (sec)	10% in 50 years	2% in 50 years	0.5% in 50 years
0.2	0.89	0.93	0.95
0.5	0.85	1.03	1.1
1	0.88	1.16	1.3
2	0.84	1.04	1.18
3	0.76	1.22	1.24

It is inferred from the Table 3-3 that the mean epsilon values from the seismic deaggregation are around 1.0 to 1.3 at 0.5% probability of exceedance in 50 years for different periods. The mean epsilon values of the records predicted using the Atkinson-6C2 records (Atkinson and Boore, 2006) are very similar to those computed from the seismic deaggregation for the period range of bridges studied in this research (Figure 3-

9). Therefore the mean spectral shape of the records used for the analysis is expected to be appropriate for Montreal (Tehrani and Mitchell, 2012).

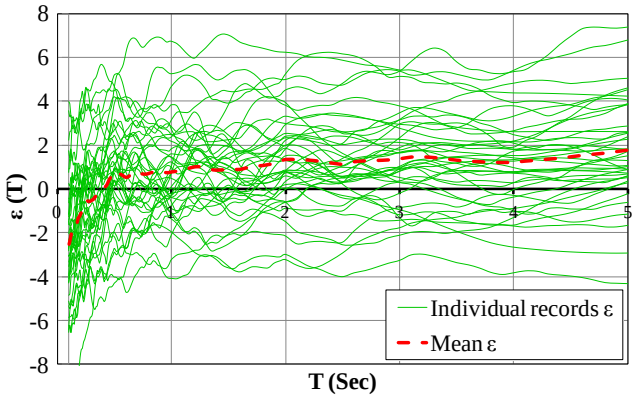

Figure 3-9. Epsilon values of all records and mean epsilon values computed using the AB06 GMPE for Eastern North America (Tehrani and Mitchell, 2012)

3.5.2 SELECTION OF EDPS AND IM

Mackie and Stojadinovic (2003) developed fragility curves considering various IM-EDP pairs and demonstrated that there may not be a single choice which is appropriate for all cases. In this study, curvature ductility, axial force and shear force are considered as EDPs to account for various failure scenarios in each structural component.

Peak Ground Acceleration (PGA) and Spectral Acceleration (Sa) at the first period of the structure are the most popular choices of IM in the literature (Nielson, 2005). The efficiency of each candidate is evaluated using the method proposed by Giovenale and Cornell (2004) to select the better IM for the structure. In IDA, the IM of the records is scaled up from 0.001g until they cause the bridge to collapse.

It has been suggested by Cornell et. al. (2002) that the estimate of the median demand ($\widehat{EDP}$) can be represented by a power model as:

$$\widehat{EDP} = a.\,IM^{b} \tag{3-4}$$

where IM is the seismic intensity measure of choice and both a and b are regression coefficients. Given the IM, the demand is assumed to be lognormally distributed with a logarithmic standard deviation $\beta_{EDP|IM}$. Therefore, the logarithm of the demand is

normally distributed.

$$Ln(\widehat{EDP}) = Ln(a) + b.Ln(IM) \quad (3\text{-}5)$$

The variance about the median ($\beta_{EDP|IM}$) is a measure of the effectiveness of the selected IM to estimate the seismic demand. The higher the variability of the EDP for a given IM, the lower is the effectiveness of the selected IM to estimate seismic demand. The effectiveness of PGA and Sa at the dominant structural mode are compared as IM for this bridge. For this purpose, the first natural period of the structure was obtained by modal analysis and estimated at T=0.87 sec.

Figure 3-10 presents the results of IDA for a typical component under the ATC36 ground motion set of records. The curvature ductility of an interior column (column-5) with respect to both PGA and Sa is shown. It is noted that in Figure 3-10, only the points in the specified box are considered for the regression analysis as they have higher contribution to the total probability of failure of the component. The regression coefficients (a,b) for PGA and Sa cases are equal to (0.707,0.162) and (3.178,0.732) and the $\beta_{EDP|IM}$ are equal to 0.314 and 0.190 respectively and hence, Sa is the more efficient IM for this component. In addition, Padgett et. al. (2007) suggests that the parameter b which represents the correlation between the natural logarithm of the EDP and natural logarithm of the IM, can be an indicator of practicality of the selected IM. Therefore, Sa is the more practical choice as it results in higher coefficient (b). Since this result is consistent for all of the structural components, Sa is selected as the IM in this study.

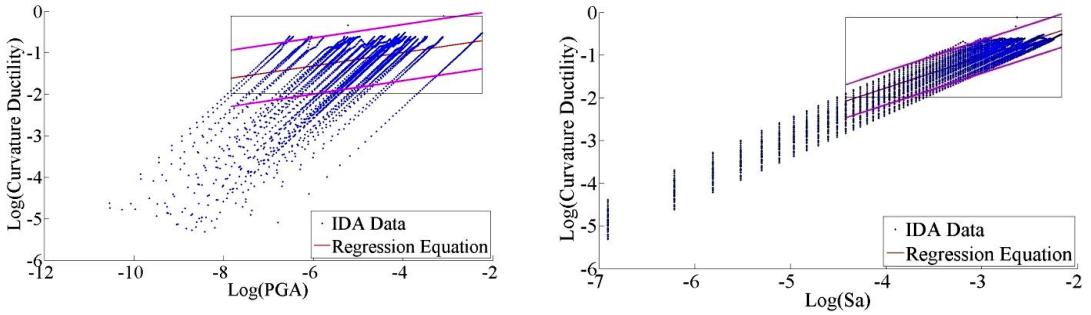

Figure 3-10- Comparison of PGA and Sa as candidate IM for ATC-63 ground motions for an Interior Column Component (Element 5).

3.5.3 IDA RESULTS

As predicted, IDA results demonstrate that the beams fails in shear before significant yielding in the columns is attained. After failure in the beam, the columns behave as cantilevers and the subsequent large deflections of the frame constitute failure.

The IDA results for an interior column (Element 5) and a beam (Element 13) under ATC36 ground motion records are shown in figure 3-11. It is noted that a sudden change in column behavior after failure of the beam prevents columns from developing their ductility. Figure 3-11 also presents the 16, 50 and 84 percentile curves of the IDA. These are determined by calculating curvature ductilities associated with a given acceleration level for different earthquakes and repeating the calculations for increasing acceleration levels.

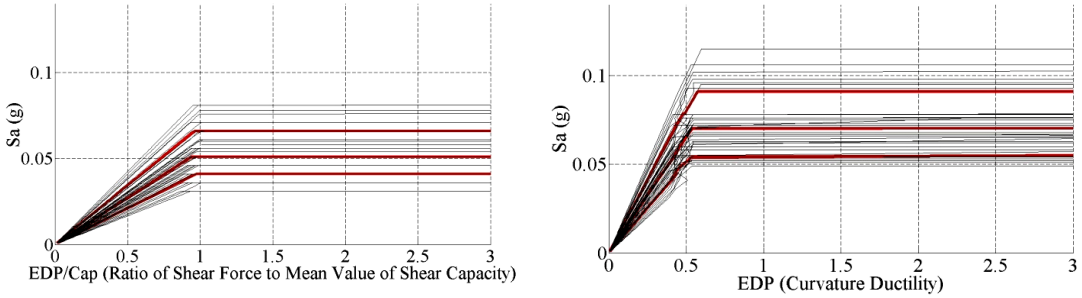

(a) (b)

Figure 3-11. IDA results associated with the 16, 50 and 84 percentiles for: (a) Beam Component (Element 13) (b) Interior Column Component (Element 5).

3.6 FRAGILITY CURVES

A fragility curve is the conditional probability that the structure or structural component sustains the specified damage-level or limit state for a given ground motion intensity. Assuming lognormal distributions for the probabilistic seismic demand model and the structural capacity, fragility curves are determined from equation 3-6.

$$P\left[\frac{D}{C} \geq 1 \mid IM\right] = \Phi\left(\frac{Ln(E\widehat{D}P/S_c)}{\sqrt{\beta_{D|IM}{}^2 + \beta_c{}^2}}\right) \tag{3-6}$$

in which $\widehat{EDP}$ is the median of demand at the selected IM, S_c is the median of capacity for the selected limit state, $\beta_{D|IM}$ is the logarithmic standard deviations of demands and β_c is the logarithmic standard deviation of the limit state (capacity).

Fragility curves can be developed for structural components as well as for the structure as a whole system. By considering the variability in seismic inputs, structure response, and material capacity into account, component fragility curves are useful tools to identify weak parts of the structure while system fragility curves are useful in seismic risk assessment of the structure.

3.6.1 COMPONENT FRAGILITY

Component fragility curves are developed for the columns and the beams of the frame for the limit state of dynamic instability (collapse). It is assumed that component fragility curves have lognormal distribution as represented in equation 3-6. The median demand ($\widehat{EDP}$) is estimated at various IMs using equation 3-5 in which a and b coefficients are calculated by a regression analysis over the results of IDA. Component fragility curves are developed for each element. To illustrate the vulnerability of the beams, fragility curve of a beam (Element 13), an interior column (Element 5) and an exterior column (Element 1) under ATC63 ground motion records are compared and shown in figure 3-12. Values of $\beta_{D|IM}$ and β_c are given in Table 3-4. The value of β_c for columns and beams are chosen based on Zhu (2005) and Song and Kang (2010) respectively.

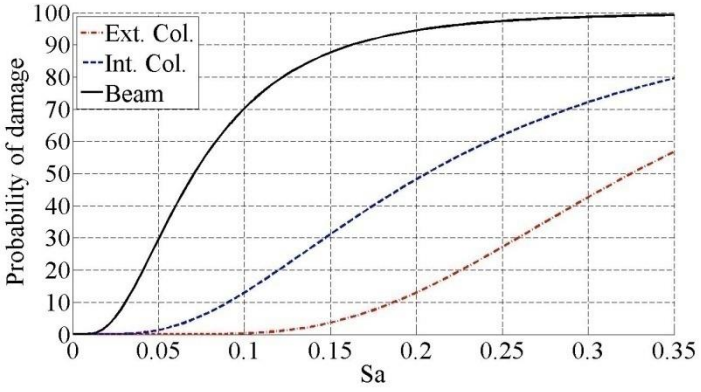

Figure 3-12. Comparison of the fragility curves of a Beam Component (Element 13), an Interior Column Component (Element 5) and an Exterior Column Component (Element 1) under ATC36 ground motion records

Table 3-4. Dispersion values used in developing component fragility curves under ATC63 records

	$\beta_{D\|IM}$	β_c
Exterior Column	0.1895	0.0699
Interior Column	0.1904	0.0699
Beam	0.1838	0.1980

From the component fragility curves, it is inferred that the beams fail in shear at a spectral acceleration level of 0.07g (490 year return period earthquake in Montreal), while interior and exterior column failure occur at Sa levels of 0.2g (2620 year return period) and 0.32g (5540 year return period) respectively.

Component fragility curves are developed using 3 sets of ground motion: ATC-63 records (44 natural records), Atkinson-6C2 records (45 artificial records) and Atkinson-7C2 records (45 artificial records). Figure 3-13 indicates the comparison of fragility curves resulting from the ground motion record sets for the beam and interior column. It is inferred that the fragility curves from the natural ground motion records have slightly higher mean values and standard deviations. So, the artificial ground motion records result in slightly more conservative results in this case.

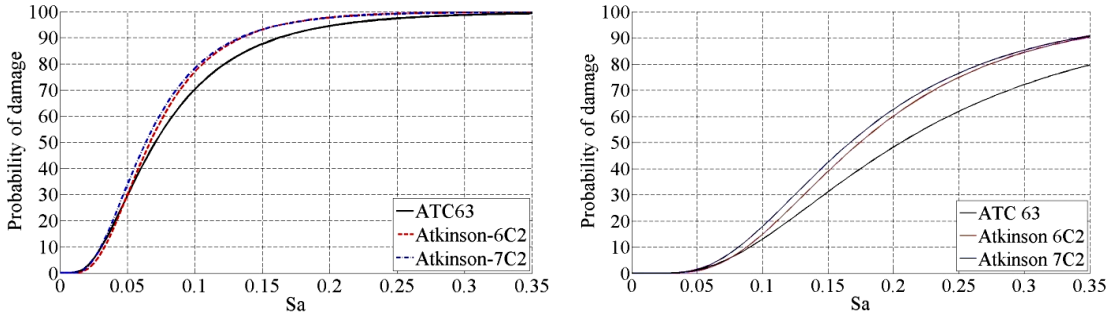

(a) (b)

Figure 3-13. Comparison of component fragility curve for three different ground motion set: (a) Beam component (Element 13) (b) Interior column (Element 5)

3.6.2 SYSTEM FRAGILITY

Correlations between seismic demands of various components in a structure make it difficult to calculate the system fragility by combining component fragilities directly. There are three established flexible and robust approaches to obtain system fragility: Nielson and DesRoches (2007) have developed joint probability distribution of seismic demands which accounts for correlations between components and have performed Monte Carlo Simulation (MCS) to integrate over all failure domains; Song and Kang (2009) have introduced a Matrix-based System Reliability (MSR) which considers the correlations between components by introducing common source random variables using Dunnett–Sobel correlation coefficient matrix; And Dueñas-Osorio and Padgett (2011) have proposed a nonrecursive combinatorial closed-form method to consider all the possible failure modes for a limit state.

In aforementioned studies, correlations between components are assumed to be constant over the range of spectral accelerations. However in this study, correlations are calculated at each Sa using IDA results which provide a set of demands for each component at each Sa. Resulted correlations between a beam, an interior column and an exterior column are presented in figure 3-14. It is inferred from Figure 3-14 that there is a strong correlation between components (over 90%) which slightly varies over the range of spectral accelerations. The reason is the linearity in structural behavior before brittle failure of the beams.

In this study, system fragility is obtained considering Sa-dependent component correlations and using the approach proposed by Nielson and DesRoches (2007). In other words, a Joint Probabilistic Seismic Demand Model (JPSDM) of natural logarithm of $\widehat{EDP}$s are simulated by MCS with 50,000 samples considering the obtained distributions with mean value (from equation 3-5), variance $\beta_{D|IM}$ and correlations between components. Then, corresponding capacities are also simulated by MCS and the probability of having at least one failure in the system is calculated over the range of Sa. It is noted that the component capacities are assumed to be independent in this study.

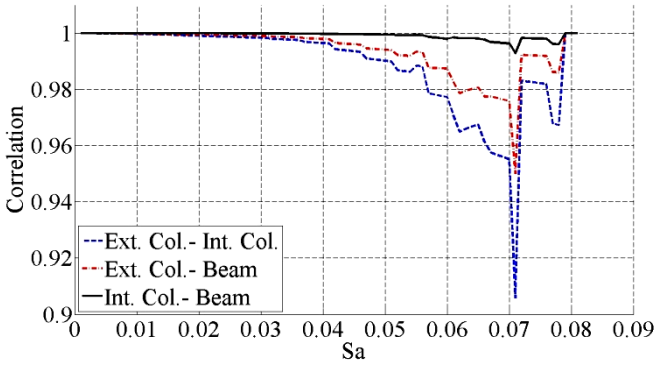

Figure 3-14. Correlations between natural logarithm of demands for elements 1, 5 and 13 (Exterior Column, Interior Column and Beam) over a range of Sa

Finally, having the probability of failure at various spectral accelerations, a lognormal distribution is fitted to obtain the system fragility of the bridge structure. Figure 3-15 represents the system fragility of the bridge under ATC63 ground motion records accompanied with 95% prediction intervals. Prediction intervals present the range of the new or future observations and the width is a measure of the regression quality and numerical uncertainty of the analysis.

It is noted that Canadian Highway Bridge Design Code (CSA-S6-06) requires that lifeline bridges remain open to all traffic after a design earthquake with a return period of 475 years and usable by emergency and security vehicles after a large earthquake with a return period of 1000 years. Based on the data provided by Boore and Atkinson (2008), Atkinson and Boore (2006) and Atkinson (2008), natural logarithm of Sa at the first period of the studied structure (T_1=0.876 sec) has a normal distribution with the mean value and standard deviation of –2.98 and 0.72 respectively.

Hence, the studied bridge is required to remain serviceable after an earthquake with a Sa(T_1)=0.4g and withstand an earthquake with a Sa(T_1)=0.47g while as it is shown in Figure 3-15, the bridge is not expected to withstand such ground motions. So, the bridge structure should be retrofitted to meet the code requirements.

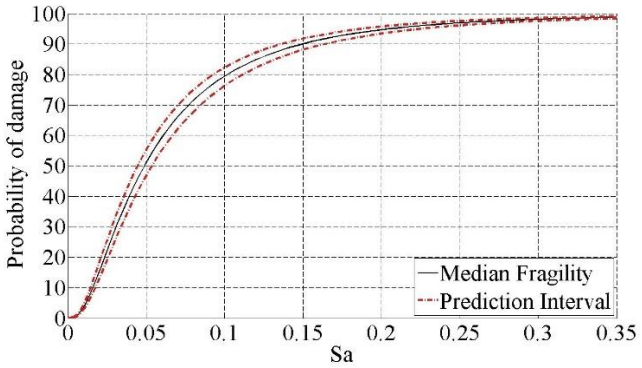

Figure 3-15. System fragility curve with confidence and prediction intervals under ATC63 ground motion records

Contribution of each component in system fragility can be visually investigated by comparison of component fragilities with system fragility as it is presented in figure 3-16 (a). A Component Importance Measure (CIM) is also quantitatively evaluated using equation 3-7 as proposed by Kang et. al. (2008).

$$CIM_i = P(f_i|f_{sys}) = \frac{P(f_i \cap f_{sys})}{P(f_{sys})} \tag{3-7}$$

in which f_i denotes the event of having failure in component *i* and f_{sys} represents the event of occurrence of system failure. CIMs of the selected exterior column, interior column and beam are calculated over a range of Sa and are presented in Figure 3-16(b). It is inferred that the beam failure is dominant and in almost all the cases the shear failure of the beam causes the failure.

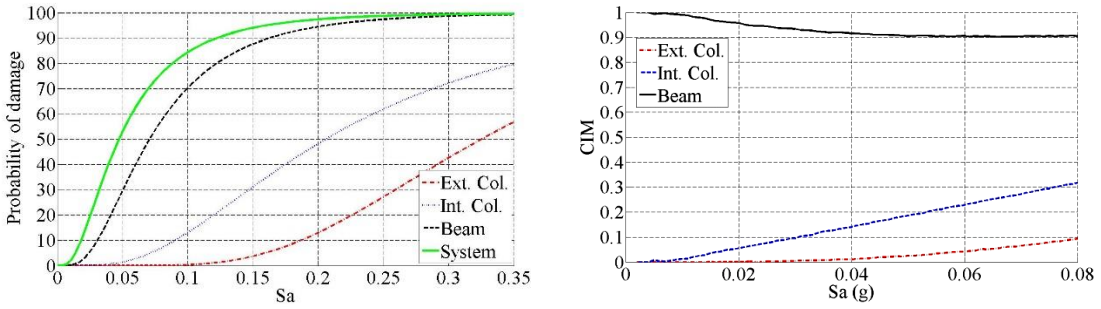

(a) (b)

Figure 3-16. Contribution of component failures in system failure under ATC63 records (a) Visual comparison of system fragility versus component fragility curves (b) CIM of components over Sa

Moreover, system fragility curves are also developed for the 3 sets of ground motion records: ATC-63 records (44 natural records), Atkinson-6C2 records (45 artificial records) and Atkinson-7C2 records (45 artificial records). Figure 3-17 presents the comparison of the resulting system fragility curves. It is inferred that the difference between system fragility curves obtained from the mentioned record sets are negligible.

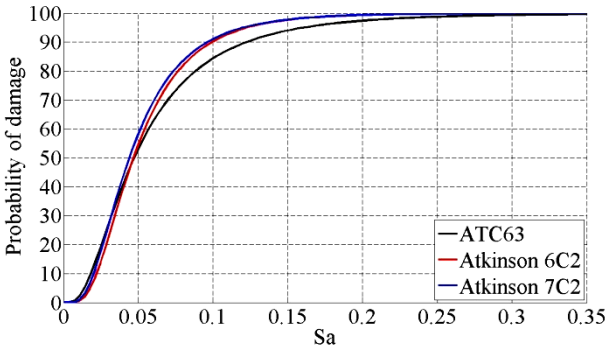

Figure 3-17. Comparison of system fragility curve for three different ground motion sets of: ATC-63 (natural records), Atkinson-6C2 (artificial records) and Atkinson-7C2 (artificial records)

3.7 CONCLUSION

In this study, fragility curves of a typical existing highway bridge located in Montreal are developed considering the significant uncertainties involved in modeling and evaluating the component seismic demand and capacities.

It is demonstrated that laboratory tests can be used to quantify the goodness of computer models as well as to display the actual behavior of a structure or a structural component. A classic hypothesis test and a Bayesian model approach are used to validate the developed finite element model of the bridge structure.

Record-to-record variability in seismic inputs is addressed and assessed through an IDA and the associated uncertainty is minimized by choosing a proper IM-EDP. IDA is performed on the model and component and system fragility curves are developed considering Sa-dependent correlation between structural components.

It is demonstrated that beam failure is the dominant failure mode with a Component

Importance Measure (CIM) above 0.9 over Spectral Accelerations and earthquakes with Sa higher than 0.07 g (at T = 0.876 sec) are predicted to cause the beams to fail prematurely in shear before any yielding occurs in columns, creating the potential of structural instability or collapse. This limit is below the requirements of Canadian standards and brittle shear failure is unacceptable in structures; hence, the frame should be retrofitted.

In moderate seismic areas in which there are not enough available ground motion records, reliable artificial seismic records are suitable alternatives for designers. It is shown in this paper that in comparison with natural ground motion records, using artificial ground motion sets developed by Atkinson and Boore (2006) result in slightly conservative component fragility curves with lower mean and standard deviation values. However, the difference in system fragility curves is negligible. This result should be further investigated for other cases.

CHAPTER 4: MANUSCRIPT 2

UNCERTAINTIES IN SEISMIC FRAGILITY ANALYSIS OF RETROFITTED BRIDGES

S. Mahmoudi, L.Chouinard, D. Mitchell, P. Tehrani, A. De la Puente

ABSTRACT

This paper presents fragility analysis of a typical Montreal bridge after an appropriate seismic retrofit. Laboratory tests are used to address the model uncertainty associated with finite element modeling of the structure by adopting two stochastic approaches. A detailed description of the existing highway bridge is provided in the companion paper (Mahmoudi et. al, 2015 A). The companion paper also demonstrates that the bridge is vulnerable and likely to be damaged under seismic demands and that brittle shear failure of the cap beam is the dominant failure mode of the structure. In deciding upon the retrofitting strategy, an approach using minimum intervention is studied which involves the strengthening of the concrete cap beam to avoid shear failure and to provide sufficient flexural resistance so that yielding occurs in the columns rather than shear and flexural failure in the beams.

A 3-dimensional bridge model is developed which is validated with results of a laboratory test performed on a half scale model of the retrofitted bridge bent. The effects of corrosion on structural components are assessed and addressed in a probabilistic context and an Incremental Dynamic Analysis (IDA) is performed to account for record-to-record variability in seismic inputs on engineering demand parameters (EDP). Component fragility curves are developed for each critical bridge element to identify the weak components. And the system fragility curve of the bridge is generated to estimate the overall reliability of the bridge structure.

The results demonstrate that the retrofit of the beam completely changes the performance of the frame. The as-built frame suffers a brittle shear failure at a predicted spectral acceleration of 0.07g whereas the retrofitted frame is predicted to experience general

yielding of the columns with the ability to undergo spectral accelerations in excess of 0.57g. In addition, this study demonstrates the importance of considering the corrosion effects in assessment of older bridges.

Keywords: Bridge, Component Fragility Curves, System Fragility Curve, Incremental Dynamic Analysis (IDA), Model Validation, Hypothesis Test, Bayesian, Monte Carlo, retrofit design

4.1 INTRODUCTION

In recent years, developed countries such as US, Japan and Canada have made significant efforts to retrofit existing highway bridges to withstand seismic events. As a result, various retrofit strategies and methods have been proposed and applied based on the deficiencies of the structures and the objectives of the retrofit. Common retrofit methods which have been used for reinforced concrete bents are concrete, steel and fiber-reinforced polymer (FRP) composite jacketing, external prestressing steel and infill shear walls.

Numerous studies have been carried out to demonstrate the effectiveness of various retrofit methods. Priestley et. al (1993) performed experimental and analytical studies on a retrofitted double-deck viaduct and demonstrated the enhancement of the shear and flexural capacity of cap beams which are retrofitted by prestressed tendons; Gergely et. al (1998, 2000) studied the effectiveness of CFRP composite jackets on the behavior of cap beams, columns and joints in an existing bridge structure; and Mitchell (2002) tested cap beams, retrofitted by reinforced concrete sleeving, under reversed cyclic loading.

Shinozuka et. al (2002) investigated the fragility curves of concrete bridges retrofitted with column jacketing; Pan et. al (2010) compared the effectiveness of two retrofit strategies on a typical bridge in New York State by comparing analytical fragility curves of the retrofitted structure with the two methods; and Billah et. al (2012) studied the effectiveness of concrete, steel, FRP and Engineered Cementitious Composites (ECC) jacketing by comparing fragility curves of a multi-column bridge bent retrofitted with each method.

Through this study, a retrofit strategy with minimum intervention is proposed for a typical highway bridge built in the 1960's in Montreal and the seismic behaviour of the retrofitted frame is investigated. A Finite Element Model of the bridge which is verified by experimental data obtained from a half scale laboratory test is used to develop analytical component and system fragility curves.

4.2 STRUCTURE AND STRUCTURAL COMPONENTS DESCRIPTION

The bridge is composed of a reinforced concrete deck supported by a grid of steel beams. The three spans (21.3, 26.2 and 21.3 m) are supported by two concrete abutments, one at each end, and two concrete moment resisting frames. These frames each consist of twelve slender columns supported by a wall. The columns are interconnected at their top by a cap beam (Figure 4-1). Details of as-built columns and beam sections are shown in figure 4-2. In this study, it is assumed that failure of the bridge occurs in moment resisting frames, so their fragility curves represent the system fragility curve of the bridge structure.

Figure 4-1. Lateral view of the bridge

The mean value of the concrete compressive strength is assumed to be 25 MPa which is typical of structures built in the 1960' s (Griezic 1996) and a mean value of 300 *MPa* is assigned to the yield-strength of the steel reinforcement.

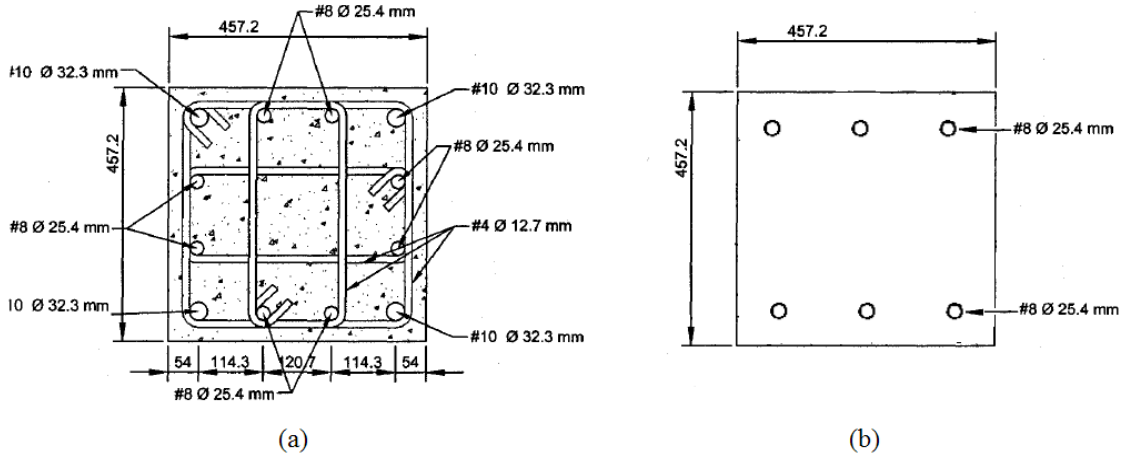

Figure 4-2. Details of as-built bridge components: (a) Column cross section (b) Beam cross section

4.3 CORROSION EFFECT

The bridge is exposed to the frequent use of deicing salts in the winter on the deck. Moreover, the lower portion of the columns are in the splash zone from water and deicing from a service road that runs under the bridge. Deicing salts are sources of chloride ions which results in the corrosion of the reinforcing steel and results in spalling of the concrete cover (Figure 4-3). According to Tutti (1982), the service life of a bridge in northern climates can be divided into two phases: Phase 1 which corresponds to the time period from the completion of original construction to initiation of corrosion (T_i) in the structure, and phase 2 which is the time period starting from the initiation of corrosion and onward. Corrosion begins when chloride concentration (C) at the level of reinforcing bars reaches the critical value (C_{cr}). Fick's second law of diffusion can be used to predict the time variation of chloride concentration through semi-infinite solid as shown in equation 4-1. (Stewart and Rosowsky 1998).

$$\frac{\partial C(x,t)}{\partial t} = -D_C . \frac{\partial^2 C(x,t)}{\partial x^2} \qquad (4\text{-}1)$$

in which C represents chloride ion concentration, D_C is diffusion coefficient and x represents the depth. Hence, T_i can be obtained from equation 4-2.

$$T_i = \frac{x^2}{4D_C}[erf^{-1}\left(\frac{C_0 - C_{cr}}{C_0}\right)]^{-2} \quad (4\text{-}2)$$

in which erf is the Gaussian error function and C_0 represents surface chloride concentration. Once corrosion begins, the diameter of corroding bar at the time t, D(t) can be estimated from equation 4-3.

$$D(t) = D_0 - \int_{T_i}^{t} r_{corr} \, . \, dt \quad (4\text{-}3)$$

in which D_0 is the initial diameter of the bar and r_{corr} represents the rate of corrosion. Rate of corrosion is a time-dependent variable, however, it is assumed to be constant in this study due to lack of data.

Figure 4-3. Deterioration in one of the bridge columns

It is noted that the time to initiation of corrosion and rate of corrosion depend on environmental conditions and are random variables. Therefore, a probabilistic model is developed to predict the effect of corrosion on the reliability of structural components. Variables adopted for this study are shown in Table 4-1. (Lounis and Mirza 2001, Lounis et. al. 2004, Ismail and Soleymani 2002 and Flis et. al. 1995).

Table 4-1. Parameters of the input variable distributions in corrosion effect prediction

Variable	X (cm)	D_C (cm^2/year)	C_0 (kg/m^3)	C_{cr} (kg/m^3)	R_{corr} (mm/year)
Distribution	Constant	LogNormal	LogNormal	LogNormal	Normal
Mean	5.4	0.51	4.56	1.35	0.062
COV	0	0.3	0.4	0.1	0.25

A Monte Carlo Simulation (MCS) with a sample size of 100,000 is developed to predict the time to initiation of corrosion and subsequently the change in area of reinforcement as a function of time. The results demonstrate that the distribution of T_i is approximated by a lognormal distribution with mean value and standard deviation of 34 and 19 years respectively. The histogram of resulting T_i is shown in figure 4-4(a).

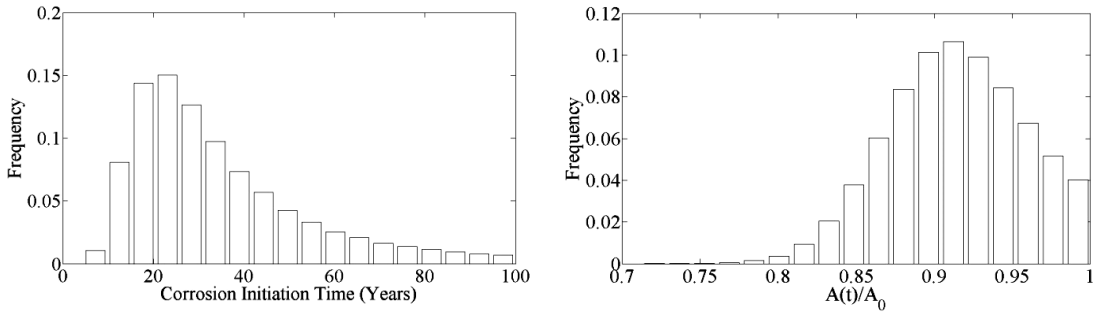

(a) (b)

Figure 4-4. Histogram of: a) time to initiation of corrosion (T_i) b) ratio of the area of the remaining reinforcing bars to the area of intact bars after 50 years of service life.

The results of the simulation also indicate that the ratio of the area of the remaining reinforcing bars (A(t)) to the area of intact bars (A_0) follows a beta distribution (β(45.67,4.52)) with mean value and standard deviation of 0.91 and 0.04 respectively. The effect of the deterioration of the existing structure is accounted for in the analyses by considering the spalled concrete section of the columns and a 10% reduction of the gross steel area. Figure 4-5 compares predicted behaviour of as-built column in its original condition and when corrosion and cover spalling takes place using Response 2000 (Bentz, 2001) software.

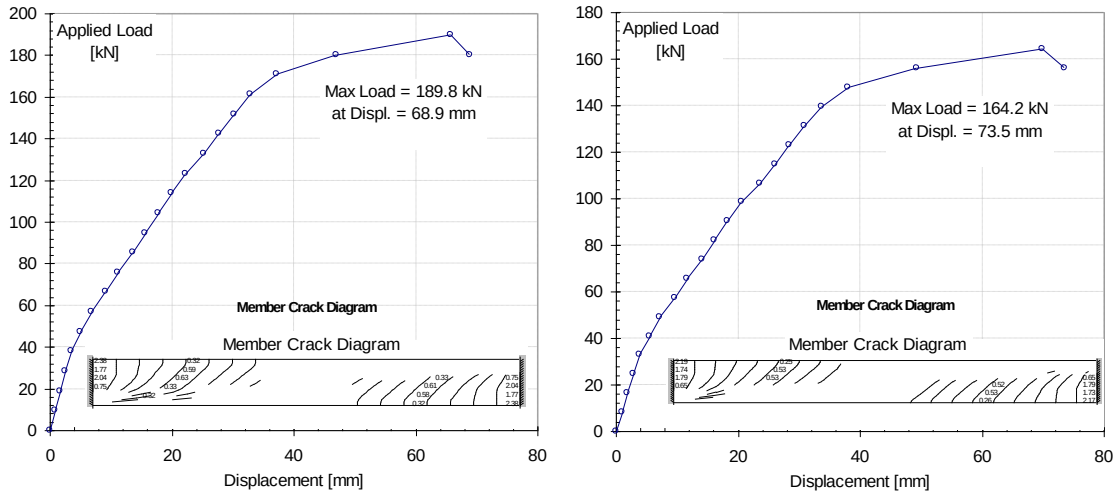

(a) (b)

Figure 4-5. Predicted force-displacement response of as-built column: a) Intact b) Spalled and corroded

4.4 BRIDGE RETROFITTING STRATEGY

In the companion paper (Mahmoudi et. al., 2015 A), it is shown that the early shear failure of the concrete beam dominates the overall response of the frame. The objective of the retrofit is to improve the performance of the frame with minimum intervention. The retrofitting strategy is based on strengthening the reinforced concrete beam and beam-column joints so that yielding occurs in the columns rather than a brittle shear failure in the cap beams. It is noted that the bridge is located over railroad tracks and a municipal street so a retrofit method which requires minimum interference with traffic is essential.

Mitchell (2002) demonstrated that retrofitting cap beams with reinforced concrete sleeves results in an increase in strength and ductility of the beam. The same approach is used in this study. It is noted that due to the geometry of the frame structure, the additional longitudinal reinforcement can only be added to the sides and bottom of the beams. Four 30M and two 35M bars are placed in three layers as shown in figure 4-6(a). To ensure that the added reinforced concrete is fully composite with the existing beam, horizontal bars with a fixed head on one end and a threaded head at the other end are used. Additional 15M U-stirrups at a spacing of 80mm for edge beams and 150mm for interior beams are added to increase the shear resistance. To facilitate placement, self-levelling concrete with a minimum specified compressive strength of 60 *MPa* is used. In addition, a grid of

15M double-legged stirrups spaced at 55 mm in horizontal and vertical directions is used to enhance the shear resistance at the joints. Figure 4-6(b) illustrates the retrofitted beam detail at the location of the joint. Figure 4-7 compares the behaviour of as-built and retrofitted beams and shows that the retrofitted beam demonstrates significantly higher capacity and ductility.

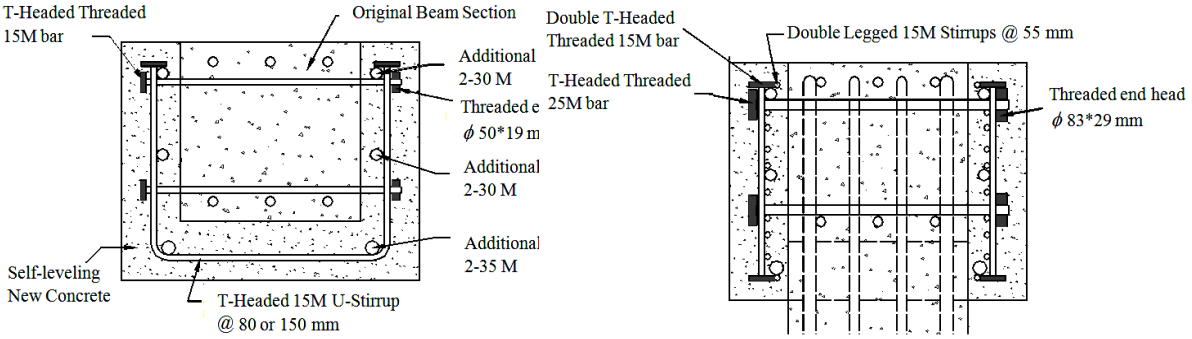

(a) (b)

Figure 4-6. Detail of a) Retrofitted beam section b) Retrofitted beam at joint location

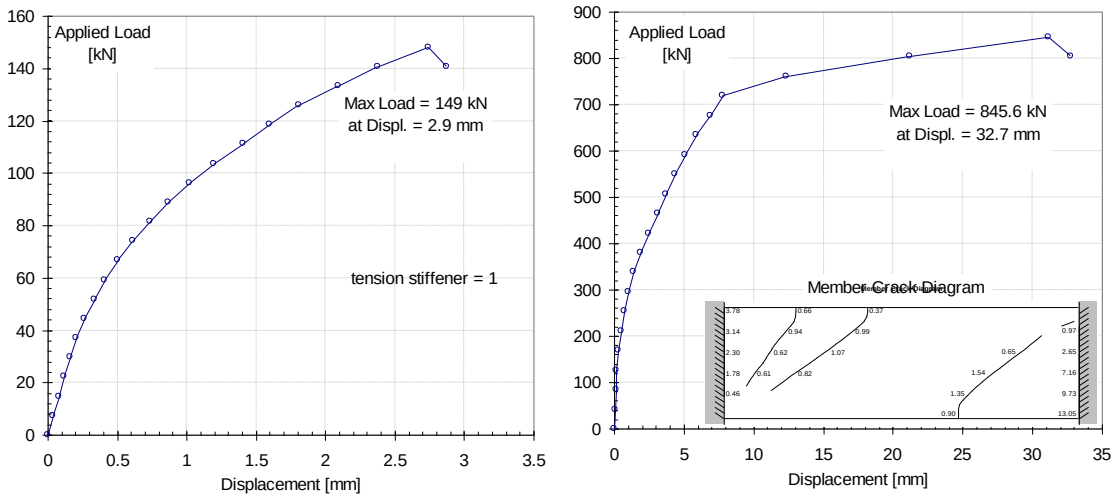

(a) (b)

Figure 4-7. Predicted force-displacement response of a) as-built beam with a brittle shear failure b) Retrofitted beam

4.5 FINITE ELEMENT MODELING AND LABORATORY TEST

The bridge is modeled with finite elements using Ruaumoko 3D (Carr, 2001). The moment-resisting frame is idealized with 69 elements divided into six types (Figure 4-8),

of which, 23 have possible non-linear behaviour. These elements correspond to the 12 column and the 11 cap beam segments whose nonlinear response are determined with the *Response 2000* software (Bentz, 2001) (figures 4-5(b) and 4-7(b)). The grid of steel beams that support the concrete deck have elastic linear behaviour and are connected to the moment-resisting frame by rocker supports.

A modal analysis of the Finite Element Model demonstrates that the retrofit increases the stiffness of the structure and the first natural period of the structure decreases from T=0.87 sec to T=0.83 sec.

Traditional statistical theories have assumed that the formulation of the model is known and tried to find the input parameters which result in responses consistent with a given sample of data. However, in practice, model uncertainty can be more significant than other sources of uncertainty (Chatfield, 1995). Laboratory testing provides information which can be used to quantify the goodness of a model.

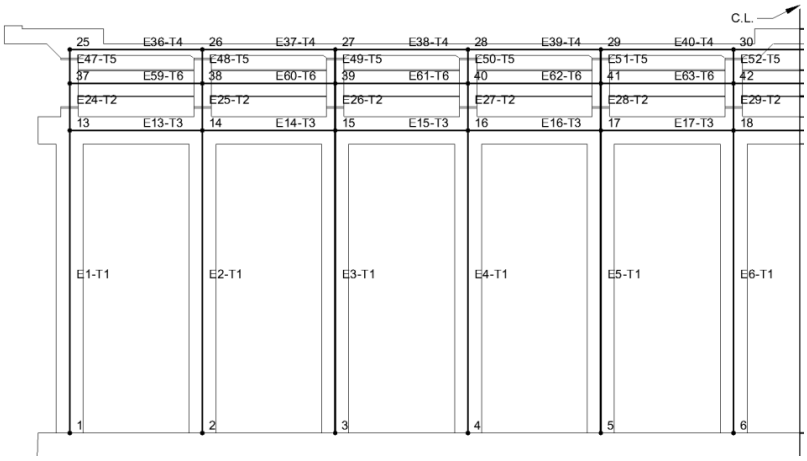

Figure 4-8. Structural idealization of the moment-resisting frame (Left side)

In order to investigate the goodness of the finite element model and to display the actual behavior of the existing structure, a half-scale model of the retrofitted frame was designed and constructed in the structural laboratory at McGill University and the model was tested under reversed cyclic loading (Coulombe, 2007). The axial load was kept constant during the test and the lateral load level was increased gradually to determine the loads corresponding to various cracking events and to determine the dominant failure mechanism.

The results obtained from the laboratory test of the half-scale structure demonstrate that the retrofitted beams are stronger than the columns, so column failure is the dominant failure mode. The test also demonstrated that although as-built columns do not meet the requirements for ductile columns, they exhibited a displacement ductility of about 2.3 (Coulombe, 2007).

According to the results from the laboratory test, the first and second yielding of the columns occur at lateral load levels of 120 kN and 142.5 kN respectively while the finite element model predictions are for lateral loads of 117.8 and 140.9 kN, respectively indicating good agreement. However, since a defined acceptable ratio or accuracy of the results is not provided in the literature, a stochastic approach is required to validate and verify the model.

4.6 FINITE ELEMENT MODEL VALIDATION

Two stochastic approaches are applied in this study to validate the finite element model of the bridge structure. The first approach is based on classical hypothesis tests and provides useful information about the confidence of the predicted model. However, this approach may be misleading and hard to interpret (Zhang and Mahadevan, 2003 and Edwards, 1963). The second approach however is based on Bayesian hypothesis testing and provides an unbiased model validation test. These approaches can be utilized for either single or multiple output data. In the companion paper (Mahmoudi et. al. 2015 A), finite element model validation is performed for a single output of the lateral load corresponding to shear failure of the beam; however, the aforementioned methods are applied using two observations in this paper. Lateral loads which result in the first and second yielding in columns are considered as the observations and the input variables are the ratio of the component height to its core height (α), compressive strength of concrete (fc), yielding stress of reinforcing bars (fy) and axial dead load (Ld). Distribution parameters of the variables are presented in Table 4-2. For each method, the power of test is also investigated to demonstrate their effectiveness. Power of test is defined as the probability that the test will reject a model when the model is incorrect.

4.6.1 CLASSIC HYPOTHESIS APPROACH

Hills and Trucano (1999) stated that if an experiment falls inside a given confidence bound of the predicted model, the experiment and the model are consistent; otherwise the model will be rejected. This test is the foundation of the methods which reject incorrect models.

An uncertainty propagation technique should be used to evaluate the confidence interval of the predicted model. Hence, the effect of uncertainties of input variables on the predicted model is evaluated through Monte Carlo Simulation (MCS). However, since performing MCS of finite element model is not computationally feasible, MCS is performed on a metamodel which is developed using the Response Surface Method (RSM) as suggested by Chen et. al. (2004). All the input variables are transferred to a space with a range of -1 to 1 so that each predictor have an equal share in determining the response. The predicted lateral loads are represented by quadratic polynomial functions of the variables. The resulted RSMs are shown in equations 4-4 and 4-5 in which index 1 represents the transformed variables.

$$\begin{aligned} F_1 = {} & 0.292{\alpha_1}^2 - 3.088\alpha_1 - 0.048f_{c1}^2 + 0.991f_{c1} - 0.109f_{y1}^2 + 5.632f_{y1} \\ & + 0.003{L_{d1}}^2 + 0.754L_{d1} + 0.189\alpha_1.f_{c1} - 0.459\alpha_1.f_{y1} \\ & - 0.059\alpha_1.L_{d1} + 0.155f_{c1}.f_{y1} + 0.033f_{c1}.L_{d1} \\ & - 0.047f_{y1}.L_{d1} + 74.22 \end{aligned} \tag{4-4}$$

$$\begin{aligned} F_2 = {} & 0.512{\alpha_1}^2 - 6.548\alpha_1 + 0.127f_{c1}^2 + 3.094f_{c1} - 0.584f_{y1}^2 + 3.068f_{y1} \\ & - 0.018{L_{d1}}^2 + 0.191L_{d1} + 0.134\alpha_1.f_{c1} - 1.103\alpha_1.f_{y1} \\ & - 0.093\alpha_1.L_{d1} - 0.152f_{c1}.f_{y1} + 0.01f_{c1}.L_{d1} - 0.183f_{y1}.L_{d1} \\ & + 94.95 \end{aligned} \tag{4-5}$$

in which F1 and F2 represent the lateral forces corresponding to the first and second yielding of the columns. The standard deviation of residuals for the regression models are 0.003 and 0.017 and the coefficient of determination (R^2) for them are 1 and 0.999, respectively. It is noted that performing a hypothesis test with 5% significance level on

the coefficients demonstrates that neither F_1 nor F_2 depend on L_d^2 and F_2 doesn't depend on $f_{c1}.L_{d1}$, so corresponding coefficients are regarded as zeros.

MCSs with a sample size of 1E6 are developed to obtain the Probability Density Function (PDF) of F_1 and F_2 from equations 4-4 and 4-5. The results show that they follow a joint normal distribution with the following parameters,

$$\begin{Bmatrix}\mu_{F_1}\\ \mu_{F_2}\end{Bmatrix} = \begin{Bmatrix}117.88\\ 141.1\end{Bmatrix} \text{ and } \sum = \begin{bmatrix}4.66^2 & 0.89*4.66*7.79\\ 0.89*4.66*7.79 & 7.79^2\end{bmatrix} \quad (4\text{-}6)$$

In which μ_{F_1} and μ_{F_2} and $\sum$ are the mean values and covariance matrix of F_1 and F_2. Figure 4-9 illustrates the classic hypothesis test for F_1 and F_2 individually and indicates that the test fails to reject the model in both instance at the 5% confidence level.

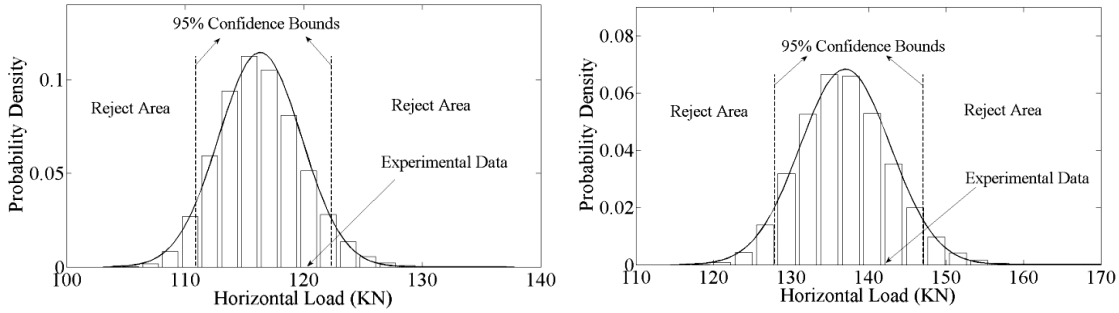

Figure 4-9. Model Validation using classic hypothesis testing based on: a)F_1 b)F_2

Figure 4-10(a) shows the 95% confidence interval of the joint distribution of F_1 and F_2 and figure 4-10(b) demonstrates the power of classic hypothesis test to validate the model. The power of test value at a given point presents the probability of rejection given that the model is false. In calculation of the power of test, the same covariance matrix as shown in Equation 4-6 is assumed for the false model. It is noted that if the significant level is set at 95% confidence interval the joint experiments fail to reject the model.

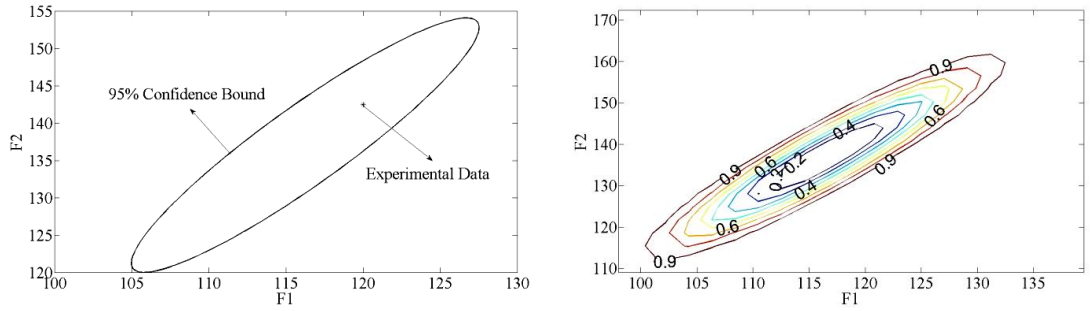

(a) (b)

Figure 4-10. a) Classic Hypothesis test for multiple observations of F_1 and F_2 b) Power of the test

4.6.2 BAYESIAN MODEL VALIDATION APPROACH

As mentioned earlier, despite the fact that the classic hypothesis testing approach provides a powerful method to represent the confidence of the model and to reject incorrect models, it does not validate or accept the model. Hence, the Bayesian approach is also used in this study.

According to Mahadevan and Rebba (2004), a model is accepted if the observation favors the model. In other words, if the probability density of the predicted value increases as the condition of the new observations, the model will be acceptable. Mahadevan and Rebba (2004) demonstrated that for a single observation test the Bayes factor can be calculated from equation 4-7:

$$B(x_0) = \frac{f(x|y)}{f(x)}|_{x=x_0} \tag{4-7}$$

In which x_0 is the predicted value, f(x) represents the prior PDF and f(x|y) represent posterior PDF. It is noted that a value of $B(x_0)$ greater than 1 validates the model. Rebba and Mahadevan (2006) suggested that for multiple observations, the Bayes factor is equal to the ratio of the posterior joint probability density to the prior joint probability density for the observations.

The prior joint PDF of outputs is obtained in the previous section. In order to estimate the posterior joint PDF, first, input variables are updated given the observation points using Bayesian updating with equation 4-8 and then, the posterior joint PDF is obtained from

the updated input variables using MCS,

$$f(\theta_i|y) = \frac{L(y|\theta_i).f(\theta_i)}{\int_{\theta_i} L(y|\theta_i).f(\theta_i)\ d\theta_i} \quad (4\text{-}8)$$

in which θ_i represents the input variable, y is the vector of observations, L(y|θ_i) is the likelihood of the observations given the parameter and f(θ_i) represents the prior PDF of the input parameter θ_i. The PDF of input variables are updated based on equation 4-8 using the MCS method. The results are shown in Table 4-2. It is noted that the posterior distribution parameters obtained in the companion paper (Mahmoudi et. al, 2015 A) are used as prior parameters in this paper since the same model is retrofitted and used in this study.

Table 4-2. Parameters of the input variable distributions in prior and posterior states

Input variables	Distribution type	Prior		Posterior	
		Mean Value	Standard Deviation	Mean Value	Standard Deviation
α	Normal	1.41	0.07	1.39	0.05
f_c (MPa)	Normal	43.9	5.44	43.13	3.43
F_y (kN)	Normal	513	15.39	522.06	7.24
L_d (kN)	Normal	71.71	8.31	73.09	8.04

MCSs with a sample size of 1E6 are developed to obtain the posterior Probability Density Function (PDF) of F_1 and F_2 from equations 4-4 and 4-5 and using the updated PDF of the input variables. The results show that they follow a joint normal distribution with the following parameters (the index p represents the posterior state).

$$\begin{Bmatrix} {\mu_{F_1}}^p \\ {\mu_{F_2}}^p \end{Bmatrix} = \begin{Bmatrix} 119.83 \\ 142.11 \end{Bmatrix} \text{ and } \sum{}^p = \begin{bmatrix} 3.05^2 & 0.93 * 3.05 * 5.28 \\ 0.93 * 3.05 * 5.28 & 5.28^2 \end{bmatrix} \quad (4\text{-}9)$$

Hence, posterior and prior joint probability density values at the experimental point [117.88 141.1] are equal to 2.71E-2 and 7.83E-3 respectively which results in a Bayes factor of 1.23 which validates the model. The power of the Bayesian model validation test is obtained assuming the same covariance matrix as presented in Equation 4-9 for the false model. The resulted power of test for Bayesian hypothesis test is presented in Figure

4-11.

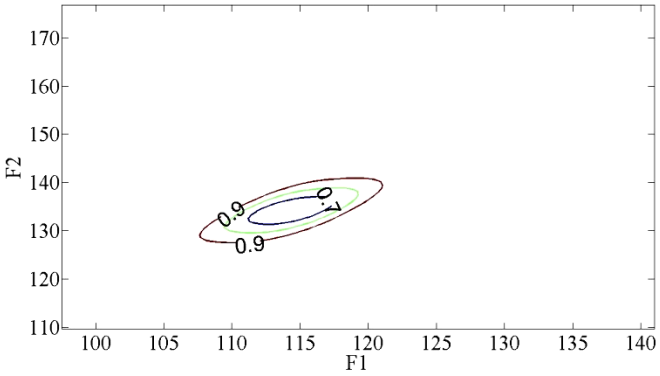

Figure 4-11. Power of Bayesian Test

Comparing powers of the two applied model validation methods, it is inferred that Bayesian method demonstrates a higher test power. Another way to present the effectiveness of the methods is to obtain the domain of observations which result in acceptance of the finite element model. The acceptable region for hypothesis test corresponds to 95% confidence bound whereas the acceptable region resulted from Bayesian hypothesis test demonstrates the region which results in a Bayes factor of 1 and higher. Figure 4-12 presents the acceptable observation domain for the two methods.

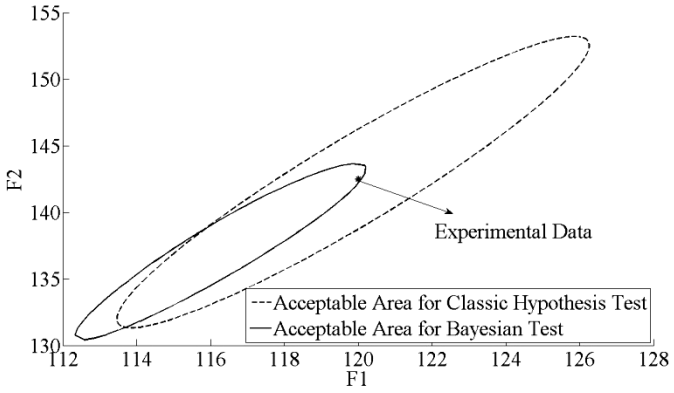

Figure 4-12. Domain of observations which result in acceptance of the finite element model

From figure 4-12, it is inferred that Bayesian model validation method presents stricter criteria for model acceptance. However, since there may not be a unique acceptable model and each of the mentioned methods accepts a variety of models and as it is shown in Figure 4-12, the acceptable domain of Bayesian method is not a subset of the hypothesis

test acceptable domain, it is favorable to use both methods in validating finite element models.

4.7 INCREMENTAL DYNAMIC ANALYSIS (IDA)

Variability in seismic inputs is a significant source of uncertainty in the seismic evaluation of structures. The IDA technique (Vamvatsikos and Cornell, 2002) defines the relationship between the Intensity Measure (IM) and the Engineering Demand Parameter (EDP) while taking into account the record-to-record variability. IDA uses non-linear dynamic analyses with increasing scaling factors for each input ground motion record to evaluate the response of the structure. It has been suggested by Cornell et. al. (2002) that the estimate of the median demand ($\widehat{\mathrm{EDP}}$) can be represented by a power model as:

$$\widehat{\mathrm{EDP}} = \mathrm{a}.\,\mathrm{IM}^{\mathrm{b}} \tag{4-10}$$

where a and b are regression coefficients. Given the IM, the demand is assumed to be lognormally distributed with a logarithmic standard deviation $\beta_{EDP|IM}$. Therefore, the logarithm of the demand is normally distributed.

$$Ln\left(\widehat{EDP}\right) = Ln(a) + b.Ln(IM) \tag{4-11}$$

The selection of proper ground motion records, EDP and IM for the structure should be done carefully since they can all affect the results. In the companion paper, it is shown that the ground motion record set suggested in ATC-63 is appropriate for the studied bridge located in Montreal.

Peak Ground Acceleration (PGA) and Spectral Acceleration (Sa) at the first natural period of the structure are the most popular choices of IM in the literature (Nielson, 2005). Giovenale and Cornell (2004) suggested that the variation about the median ($\beta_{EDP|IM}$) is a measure of effectiveness of the selected IM to estimate the seismic demand. The higher the variability of the EDP for a given IM, the lower is the effectiveness of the selected IM to estimate seismic demand. According to the results presented in the companion paper, Sa at the first natural period of the structure is the better IM for the studied structure when curvature ductility of structural components is considered as the EDP.

4.7.1 IDA RESULTS

IDA results demonstrate that the beams do not suffer any shear distress or any flexural yielding while initial yielding in the columns is attained at 0.15g. The IDA results for an exterior column (Element 1), an interior column (Element 5) and a beam (Element 13) under ATC36 ground motion records are shown in figure 4-13. It is noted that the flexural demand of the beam remains constant after yielding occurs in the columns. Figure 4-13 also presents the 16, 50 and 84 percentile curves of the IDA. These are determined by calculating curvature ductilities associated with a given acceleration level for different earthquakes and repeating the calculations for increasing acceleration levels.

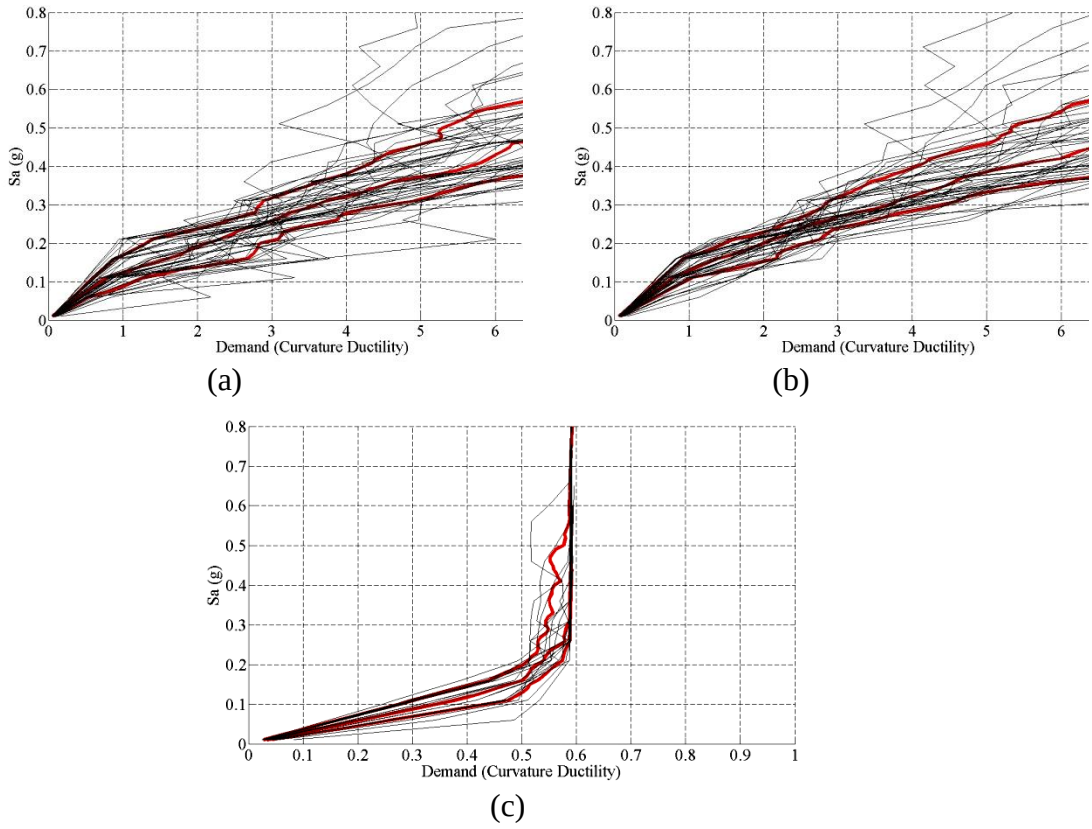

Figure 4-13- IDA results associated with the 16, 50 and 84 percentiles for: (a) Exterior Column (Element 1) (b) Interior Column Component (Element 5) (c) Beam Component (Element 13)

4.8 FRAGILITY CURVES

A fragility curve is the conditional probability that the structure or structural component sustains a specified damage-level or limit state for a given ground motion intensity. Fragility curves can be developed for structural components as well as for the structure as a whole system. Taking into account the variability in seismic inputs, structural behaviour and component capacities, component fragility curves are useful tools to identify weak parts of the structure while system fragility curves are useful in seismic risk assessment of the structure.

Assuming lognormal distributions for EDP and the structural capacity, fragility curves are determined from equation 4-12.

$$P\left[\frac{D}{C} \geq 1 \mid IM\right] = \Phi\left(\frac{Ln(\widehat{EDP}/S_c)}{\sqrt{{\beta_{D|IM}}^2 + {\beta_c}^2}}\right) \tag{4-12}$$

in which $\widehat{EDP}$ is the median of demand at the selected IM, S_c is the median of capacity for the selected limit state, $\beta_{D|IM}$ is the logarithmic standard deviations of demands and β_c is the logarithmic standard deviation of the limit state (capacity).

4.8.1 COMPONENT FRAGILITY

Component fragility curves are developed for each element for the limit state of dynamic instability (collapse). It is assumed that component fragility curves have lognormal distribution as presented in equation 4-12. Curvature ductility is considered as the EDP and is estimated at various IMs using equation 4-11 in which a and b coefficients are calculated by a regression analysis over the results of IDA. Values of S_c, $\beta_{D|IM}$ and β_c are given in Table 4-3. It is noted that according to figure 4-13(c), beam components remain elastic. Hence, the high margin of safety results in negligible probability of failure in beams. Fragility curves of an interior column (Element 5) and an exterior column (Element 1) under ATC63 ground motion records are compared and shown in figure 4-14.

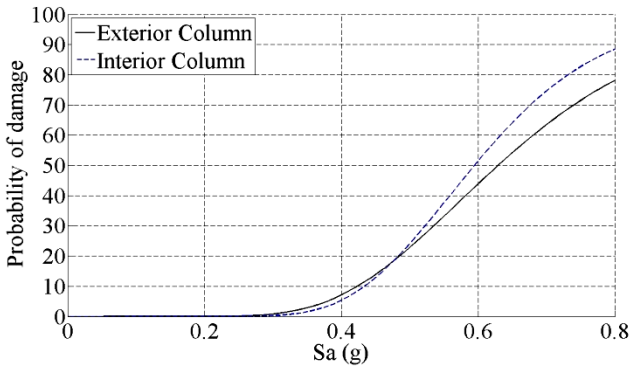

Figure 4-14- Comparison of the fragility curves of interior and exterior columns (Element 5 and 1) under ATC36 ground motion records

Table 4-3. Distribution values used in developing component fragility curves under ATC63 records

	S_c	$\beta_{D\|IM}$	β_c
Exterior Column	6.43	0.2610	0.0699
Interior Column	6.43	0.2363	0.0699
Beam	7.10	0.0395	0.0633

From figure 4-14, it is inferred that exterior columns are the most critical components under lower spectral accelerations. However, interior columns become the most critical components under higher spectral accelerations which lead to yielding and load redistribution in the structure.

4.8.2 SYSTEM FRAGILITY

In this study, the structural system is modelled as a series system. In other words, the system fragility represents the probability of having at least one failure at a given Sa. System fragility is obtained by comparing the Joint Probabilistic Seismic Demand Model (JPSDM) of natural logarithm of $\widehat{EDP}$s with the corresponding probabilistic models of natural logarithm of component capacities as proposed by Nielson and DesRoches (2007). JPSDM is obtained by considering the mean value vector (from equation 4-11), the variance ($\beta_{D|IM}$) and Sa-dependent correlation between components. Correlations are calculated at each Sa using IDA results which provide a set of demands for each component at each Sa. The correlations between an interior column and an external

column are presented in figure 4-15. It is noted that the correlation between columns decrease at spectral accelerations which cause the columns enter their plastic behavior zone. A MCS is used to simulate the JPSDM and component capacities and to calculate the probability of having at least one component failure at a given Sa.

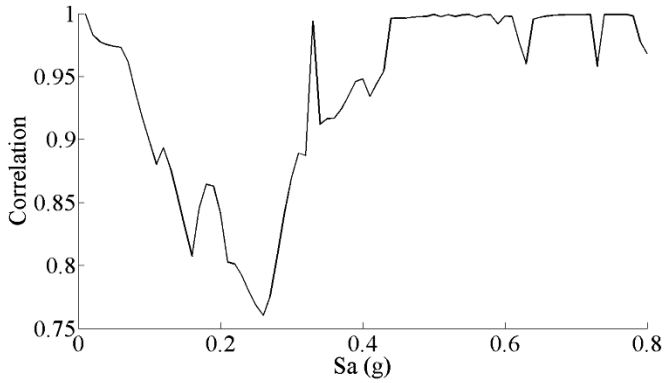

Figure 4-15. Correlations between natural logarithm of demands for elements 1 and 5 and 13 (an exterior Colum and an interior Column) over a range of Sa

Finally, having probability of failure at various spectral accelerations, a lognormal distribution is fitted to obtain the system fragility of the bridge structure. Figure 4-16 represents the system fragility of the bridge under ATC63 ground motion records accompanied with 95% prediction intervals. Prediction intervals present the range of the new or future observations and the width is a measure of the regression quality and numerical uncertainty of the analysis.

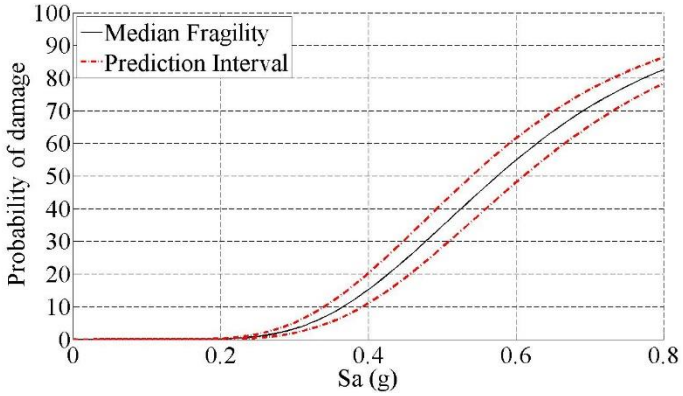

Figure 4-16. System fragility curve with confidence and prediction intervals under ATC63 ground motion records

The contribution of each component to the system fragility can be visually investigated by comparing of component fragilities with the system fragility as it is presented in figure 4-17 (a). However, Component Importance Measure (CIM) can be quantitatively evaluated using equation 4-13 proposed by Kang et. al. (2008).

$$CIM_i = P(f_i|f_{sys}) = \frac{P(f_i \cap f_{sys})}{P(f_{sys})} \tag{4-13}$$

in which f_i denotes the event of having failure in component i and f_{sys} represents the event of occurrence of system failure. CIMs of the selected exterior column and interior column are calculated over a range of Sa and are presented in Figure 4-17(b). It is inferred that under low spectral accelerations, exterior columns are the most critical components while the failure of an interior column is the dominant failure mode under higher spectral accelerations.

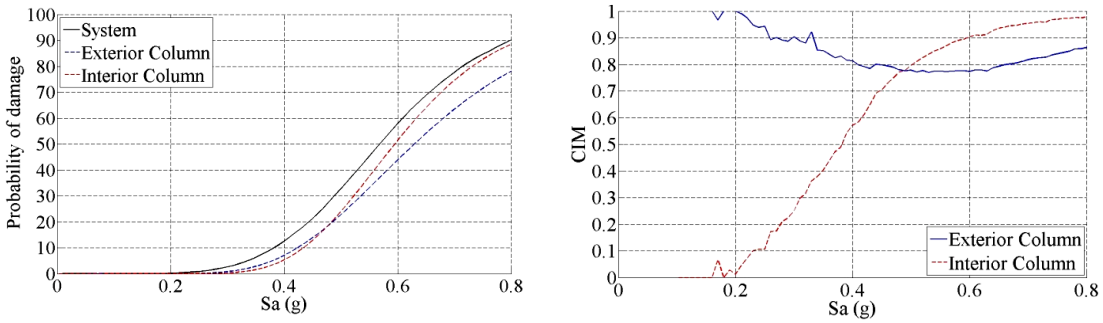

(a) (b)

Figure 4-17. Contribution of component failures in system failure under ATC63 records (a) Visual comparison of system fragility versus component fragility curves (b) CIM of components over Sa

In order to demonstrate the overall effect of the proposed retrofit on reliability of the highway bridge, system fragility curves of the existing and the retrofitted structures are compared in figure 4-18. It is noted that by retrofitting the beams of the frames with minimal interference with the normal function of the highway bridge, the Sa (at T=0.83 sec) with 50% probability of causing a failure in the structure increases from 0.07g to 0.57g.

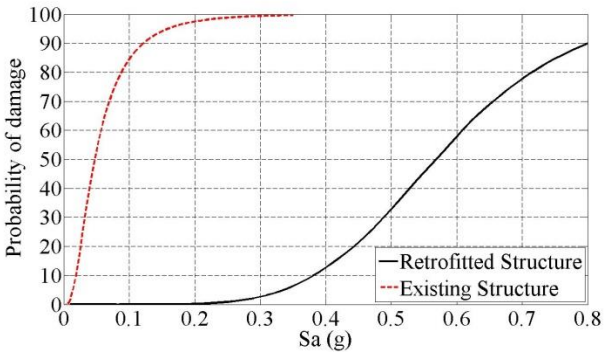

Figure 4-18- Comparison of the system fragility curves of the existing and the retrofitted structures underATC36 ground motion records

4.9 CONCLUSION

A retrofit strategy using minimum intervention is proposed for an existing deficient highway bridge located in Montreal and seismic fragility curves of the retrofitted structure are developed considering significant uncertainties involved in modeling and evaluating structural demands and capacities. Uncertainties arising from finite element modeling are addressed through model validation analyses; uncertainties associated with seismic inputs are assessed by IDA and are reduced by proper selection of IM-EDP pair; and uncertainties involved in component capacities are accounted for in component and system fragility analysis.

The selected retrofitting strategy involves the strengthening of the concrete cap beams to avoid shear failure and to provide sufficient flexural resistance so that yielding occurs in the columns rather than in the beams. The retrofitted structure is modeled by a nonlinear Finite Element model and a laboratory tests is used to quantify the goodness of a finite element model as well as to display the actual behavior of a structure or a structural component. The model is validated with laboratory test results using a classic hypothesis test and a Bayesian model verification approach.

Moreover, the effects of corrosion of the reinforcing steel and spalling of the concrete cover on the columns are investigated in a probabilistic context. It is demonstrated that the corrosion initiation time for the studied structure follows a lognormal distribution with mean value of 34 years and the corroded reinforcement area follows a beta distribution

with mean value of 9%.

IDA is performed on the model and component and system fragility curves are developed considering Sa-dependent correlation between structural components. It is demonstrated that the retrofit of the beam completely changes the performance of the frame. The as-built frame suffers a brittle shear failure at a predicted spectral acceleration (at T=0.83 sec) of 0.07g whereas the retrofitted frame is predicted to experience general yielding of the columns with the ability to undergo spectral accelerations in excess of 0.57g.

CHAPTER 5: MANUSCRIPT 3

BAYESIAN UPDATING AND STRUCTURAL MODEL VALIDATION OF BRIDGES BASED ON AMBIENT VIBRATION TESTS

S. N. Mahmoudi, L. Chouinard

ABSTRACT:

Analytical seismic fragility analysis of bridges provides a powerful tool to identify weak structural components and to assess the reliability of existing structures. To decrease uncertainties relative to structural models, analysts often acquire field data to validate their models. Ambient vibration test provides a nonintrusive and inexpensive procedure to assess the dynamic behaviour of full-scale structures. The objective of this paper is to utilize Bayesian methods as a robust approach to update input variables of the model and to assess the confidence and the uncertainties involved in a structural model based on ambient vibration test results. In this study, the total mass of the structure, concrete strength and rotational stiffness of the bearings are considered as variables which are updated based on the first natural frequency of the structure. This approach is applied to a typical 5-span concrete bridge as a case study.

5.1 INTRODUCTION

Many developed countries are struggling with the issue of deteriorated bridges in their transportation system due to aging and damage caused by increased magnitude and volume of vehicular loads. Moreover, seismic deficiencies of existing bridges must be assessed and addressed. In both cases, these require some assessment that often requires a model that offers an accurate representation of the current condition and response of the bridge.

Ambient vibration testing has recently become a popular method for assessing the dynamic behaviour of full-scale structures. This test is used to estimate the modal parameters of structures which are natural frequencies, mode shapes and corresponding

damping ratios. Ambient vibration surveys are non-intrusive because no excitation equipment is needed since the natural or environmental excitations are used which translates into minimal interference with the normal function of the structure.

Modal parameters are related to stiffness, mass and damping of the structure. Hence, the results of this test can be used to validate and update the parameters which have significant influence on structural stiffness, mass or damping. Moreover, comparing the modal information obtained from ambient vibration testing and computer models can provide an insight into model uncertainties of the structural model when all components are minimally loaded.

In addition, any major structural damage which affect the structural stiffness can be detected and located using ambient vibration data.

In this paper, the Finite Element model of the bridge and the ambient vibration survey results are first presented. Then, validation of the model is performed using two stochastic approaches: a Classical hypothesis testing approach and a Bayesian hypothesis testing approach. Updating of input parameters of the structural model and major deficiency detection are also discussed in the Bayesian hypothesis test section.

5.2 FINITE ELEMENT MODELING AND AMBIENT VIBRATION TEST

The bridge under study has three lanes as well as a bicycle path and a pedestrian walkway. The heavy pedestrian walkway and the light bicycle path result in a non-uniform weight distribution of the bridge section and are expected to affect the natural frequencies, dominant modes and generally the behavior of the structure.

The bridge is designated as a lifeline structure and needs to meet the highest standards in terms of reliability. This Bridge consists of 5 spans with a total length of 232 meters. The superstructure consists of a concrete deck with 0.203 m thickness which is supported by 5 steel girders with varying depth. Except for the bearing at pier 2, which is a low type fixed bearing, all other bearings at the piers and abutments are high steel bearings. The piers located in the river bed are supported by regular footings on hard rock.

The bridge is modeled with finite elements with the computer program SAP2000. A three dimensional view of the model is shown in Figure 5-1. The bridge deck and the girders are modeled with 4-node shell elements. The piers are modeled with nonlinear multi layered shell elements. Cap beams are modeled with beam elements and the bearings and the abutments are modeled using Nllink elements which have six independent springs, one for each of six deformational degrees of freedom (SAP2000, 1996). Non-confined concrete material behaviour is assumed to model the behaviour of the piers (Mander, 1988). The behaviour of bearings is determined by finite element simulation in ABAQUS program. And the behaviour of the abutments is determined based on the proposed model by Shamsabadi et. al. (2007) for granular soils. The behaviour of abutments and bearing are shown in Figure 5-2. Detailed analytical modeling of bridge components are provided in Appendix A.

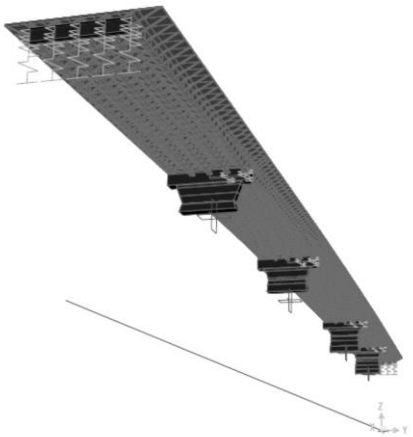

Figure 5-1. Three Dimensional view of Finite Element model

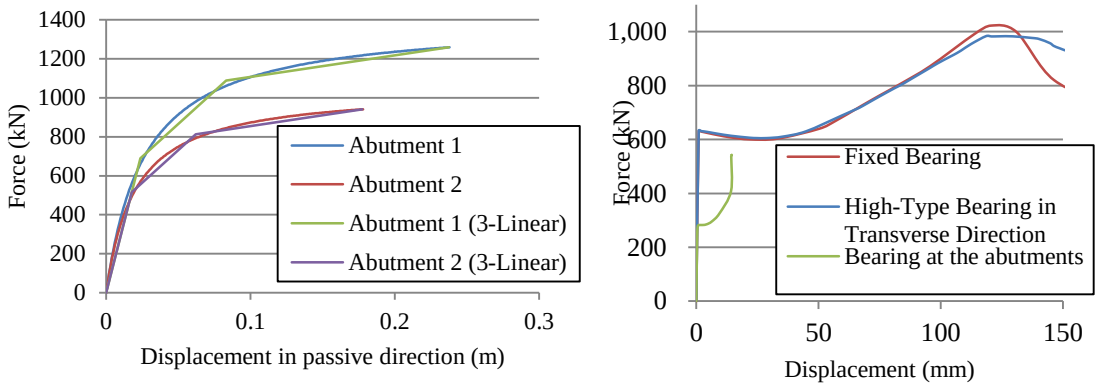

(a) (b)

Figure 5-2. Force-Displacement relationship in a) Abutments b) Bearings

Ambient vibration test was performed using 6 sensors, 4 of which were roving sensors and 2 reference sensors. A total of 11 setups were used to cover 21 points on each side of the bridge and the movements in 3 directions were recorded. More details regarding ambient vibration testing of the studied bridge are provided in Appendix B. Saeed and Chouinard (2013) obtained the natural frequencies and the mode shapes using Enhanced Frequency Domain Decomposition (EFDD) analysis. Figure 5-3 presents the first three mode shapes of the structure and Table 5-1 compares natural periods of the bridge obtained with the ambient vibration test and with the finite element model for the first twenty natural modes of the bridge which correspond to 76%, 73% and 50% mass participation factors in x, y and z directions, respectively. From figure 5-3, it is inferred that the natural modes of the bridge are combined with the torsion resulted from non-uniform weight distribution of the bridge section.

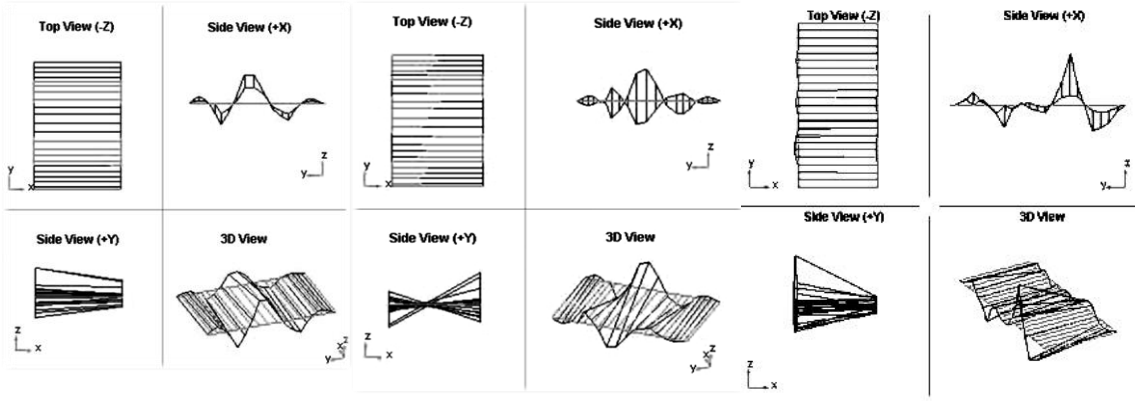

(a) (b) (c)

Figure 5-3. Results of EFDD analysis for the (a) first, (b) second and (c) third mode shapes of the bridge

In AVT, the system identification is based on the assumption that the structure behaves linearly under environmental excitations. However, it is noted that although only natural excitations, mostly due to traffic and wind, are used in ambient vibration surveys and resulting forces are minimal, large structures with numerous joints may demonstrate nonlinear behaviour. Because in some cases all of the structural components and joints may not be engaged under such low loading. This nonlinear behaviour could result in inaccuracy in test results.

In addition, input excitations in ambient vibration testing are assumed to be a Gaussian White Noise with uniform power over the frequency domain which can excite all of the structural modes. However, in practice, it is possible that the test cannot detect some of the natural modes of the structure. It is seen in table 5-1 that the fourth mode of the structure was not detected in the performed ambient vibration test.

Table 5-1. Comparison of natural periods obtained by ambient vibration test and the Finite Element model

Mode number		1	2	3	4	5	6	7	8	9	10
Measured Period	Sec	0.69	0.63	0.46	-	0.40	0.36	0.30	0.28	0.26	0.26
Model Period	Sec	0.70	0.62	0.51	0.42	0.39	0.37	0.31	0.28	0.26	0.26
Error	(%)	0.76	1.13	10.34	-	2.98	1.62	3.71	1.41	0.86	1.57

Mode number		11	12	13	14	15	16	17	18	19	20
Measured Period	Sec	-	0.21	0.19	0.18	0.16	0.15	0.14	0.13	0.11	0.10
Model Period	Sec	0.23	0.20	0.20	0.18	0.18	0.14	0.13	0.13	0.13	0.12
Error	(%)	-	1.37	1.48	1.66	13.21	3.74	6.04	2.85	10.45	24.16

5.3 FINITE ELEMENT MODEL VALIDATION

Two stochastic approaches are used in this study to validate the finite element model of the bridge structure. These approaches can be utilized for either single or multiple observations. The first approach is based on classical hypothesis tests and demonstrates the confidence level of the model. However, this approach focuses on rejecting incorrect models. Conversely, the second approach focuses on accepting appropriate models using Bayesian hypothesis testing.

In this paper, concrete density, concrete strength and rotational stiffness of the bearings are considered as updating parameters. It is noted that concrete strength is selected because it affects the stiffness of the structural components.

Moradalizadeh (1990), Slastan (1993) and Slawu (1993) argued that lower modes are best suited for damage detection in structures. Hence, in this study, the first natural period of the structure is considered as the single experimental modal data point

5.3.1 CLASSIC HYPOTHESIS APPROACH

Hills and Trucano (1999) stated that if an experiment falls inside a given confidence bound of the predicted model, the experiment and the model are consistent; otherwise the model will be rejected. This test is the foundation of the methods which reject incorrect models.

An uncertainty propagation technique is used to evaluate confidence bounds of the predicted model. Hence, the probabilistic model of the first natural period of the structure is evaluated through Monte Carlo Simulation (MCS). However, since performing MCS of a finite element model is not computationally feasible, MCS is performed on a metamodel which is developed using Response Surface Method (RSM) as suggested by Chen et. al. (2004).

In this study, concrete density and concrete strength are assumed to have normal distributions. The prior distribution variables are presented in Table 5-2. For each of the mentioned variables, the range of mean value minus standard deviation to mean value plus standard deviation is uniformly divided into 7 points for the full factorial design of natural period of the structure.

Ambient vibration test results are also used to detect damage in bearings. Steel bearings are prone to rust and get locked up or frozen such that no movement is possible. In order to detect frozen bearings in the studied bridge, the rotational stiffness of the bearings is considered as either free or fixed. Hence, the structural results are provided for two models of M_1 and M_2 corresponding to free rotation and fixed rotation of the bearings. This approach is also applicable to detect other types of major deficiencies in the bridge i.e. cracking or delamination of the concrete or loss of prestress.

The histogram and distribution of the predicted first natural period of the structure are obtained from a MCS which is performed with 1.000,000 samples for each model of bearing stiffness. The predicted natural period has a normal distribution with the mean value of 0.662 sec and standard deviation of 0.023 sec for the first model and 0.647 sec and 0.023 sec for the second model. The histograms of the response is shown in Figure 5-4.

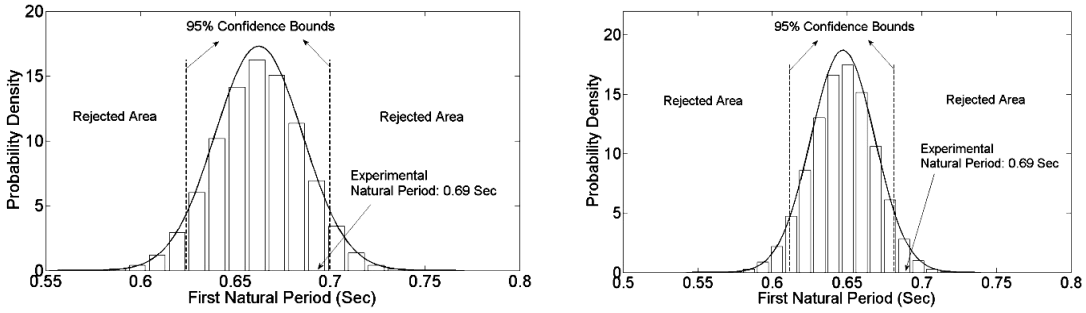

(a) (b)

Figure 5-4. Model Validation using classic hypothesis approach (a) Free rotation at the bearings (b) Fixed rotation at the bearings

According to the results of MCS, the observation of 0.69 Sec corresponds to 92.2% and 98.2% confidence limits in the first and second model respectively. So, if the significant level is set at the 95% confidence interval, the experimental data fails to reject the first model while the second model is rejected by this test.

5.3.2 BAYESIAN APPROACH

The classic hypothesis approach provides a powerful method to represent the confidence of the model and to reject incorrect models but it does not validate or accept the model. Hence, the Bayesian approach is also used in this study.

According to Mahadevan and Rebba (2004), a model is accepted if the observation favors the model. In other words, if the probability density of the predicted value increases as the condition of the experimental data, the model will be acceptable. Mahadevan and Rebba (2004) and Rebba and Mahadevan (2006) demonstrated that the Bayes factor can be calculated from equation 5-1:

$$B(x_0) = \frac{f(x|y)}{f(x)}|_{x=x_0} \tag{5-1}$$

in which x_0 is the predicted value, f(x) represents the prior Probability Density Function (PDF) and f(x|y) represent posterior PDF. It is noted that the $B(x_0)$ higher than unity validates the model. In this study, the posterior PDF is obtained from a MCS similar to

the one of the previous part but considering updated input variables. The parameters of the input variables, concrete density and strength, are updated as shown in equation 5-2:

$$f(\theta_i|y) = \frac{L(y|\theta_i).f(\theta_i)}{\int_{\theta_i} L(y|\theta_i).f(\theta_i)\ d\theta_i} \quad (5\text{-}2)$$

in which θ_i represents an input variable, $L(y|\theta_i)$ is the likelihood of the observation given an input parameter and $f(\theta_i)$ represents the prior PDF of the input. The PDF of input variables are updated based on equation 5-2 using MCS method.

Zhang and Mahadevan (2000) suggested to assume equal prior likelihood for M_i when there is no available data. Hence, in order to demonstrate the probability of having frozen bearings in the bridge, an equal prior probability of 0.5 is assigned to each model of free and fixed bearings and the posterior probability is calculated based on Bayesian equation as presented in equation 5-3.

$$P(M_i|y) = \frac{P(M_i).\int_{\theta_i} L(y|\theta_i).f(\theta_i|M_i)\,d\theta_i}{\sum P(M_i).\int_{\theta_i} L(y|\theta_i).f(\theta_i|M_i)\,d\theta_i} \quad (5\text{-}3)$$

By evaluating $P(M_i|y)$ in equation 5-3 using MCS results, the posterior probability of the models are equal to 0.808 and 0.192 respectively. So, there is a 0.192 probability of having frozen bearings. This result is consistent with the result obtained in the previous method. Hence, the model with free rotation at bearings will be used for the purpose of updating input variables and model validation in this paper. The PDF of the input variables are updated based on equation 5-2 using MCS method. The results are shown in Table 5-2.

The resulting posterior PDF of the first natural period has a normal distribution with the mean value of 0.674 sec and standard deviation of 0.018 kN and is shown in figure 5-5. The PDF of the prior and posterior at x=0.662 sec is equal to 17.345 and 17.7471 respectively. Hence, the Bayes ratio at the predicted point is equal to 1.023 and the model is validated.

Table 5-2. Parameters of the input variable distributions in prior and posterior states

		Distribution	Prior		Posterior	
			Mean Value	Standard Deviation	Mean Value	Standard Deviation
Inputs	Concrete density	Normal	24 (kN/m^3)	2.4 (kN/m^3)	26.23 (kN/m^3)	1.85 (kN/m^3)
	Concrete strength	Normal	34.5 (MPa)	6.9 (MPa)	32.15 (MPa)	6.58 (Mpa)
Output	First Natural Period	Normal	0.662 (Sec)	0.023 (Sec)	0.674 (Sec)	0.018 (Sec)

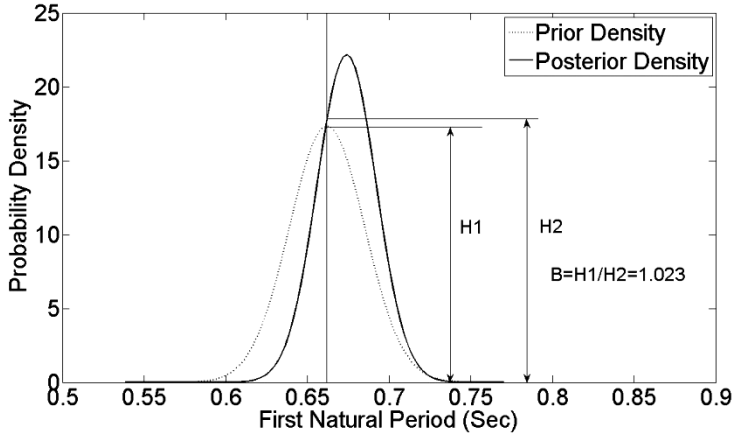

Figure 5-5. Model Validation using Bayesian hypothesis approach

5.4 CONCLUSION

A typical bridge is modeled with Finite Elements as a case study and the model is validated by two stochastic methods. Moreover, based on the first natural period of the structure which is obtained from ambient vibration test, the input variables which are concrete density and concrete strength have been updated using Bayesian method and the probability of a specific major deficiency of having frozen bearings is calculated. It is shown that the Finite Element model is acceptable in the range of elastic behaviour and the probability of having frozen bearings is less than 20%.

The proposed methodology is also applicable for multiple experimental data i.e. a set of natural periods or modal shapes.

It is shown that the proposed methodology reduces the variance of model input variables and subsequently the parameter uncertainties of the structural model. In addition, by rejecting inappropriate probable models, such as the one with frozen bearings in this study, model uncertainty of the reliability analysis is also reduced. Hence, performing ambient vibration surveys and model validation is an inexpensive test which can significantly increase the accuracy of structural assessments.

CHAPTER 6: MANUSCRIPT 4

SEISMIC FRAGILITY ASSESSMENT OF HIGHWAY BRIDGES USING SUPPORT VECTOR MACHINES

S. N. Mahmoudi, L. Chouinard

ABSTRACT

Seismic fragility curves provide a powerful tool to assess the reliability of structures. However, conventional fragility analysis of structures comprising a large number of components requires enormous computational efforts. In this paper, the application of Probabilistic Support Vector Machines (PSVM) for the system fragility analysis of existing structures is proposed. It is demonstrated that SVM based fragility curves provide accurate predictions compared to component based fragilities developed by Monte Carlo Simulations (MCS).

The proposed method is applied to an existing bridge structure in order to develop fragility curves for serviceability and collapse limit states. In addition, the efficiency of using the PSVM method in the application of vector-valued ground motion Intensity Measures (IM) as well as traditional single-valued IM are investigated. The results obtained from an Incremental Dynamic Analysis (IDA) of the structure are used to train PSVMs. The application of PSVM in binary and multi-class classifications is used for the fragility analysis and reliability assessment of the bridge structure.

Keywords: System Fragility, Bridge Structure, Incremental Dynamic Analysis (IDA), Probabilistic Support Vector Machines (PSVM)

6.1 INTRODUCTION

Uncertainties involved in determining the demands of earthquakes and in evaluating the capacity of structures under cyclic loads lead designers to use probabilistic methods to quantitatively assess the structural reliability. Fragility curves represent the state-of-the-

art in seismic risk assessment (SRA) and are defined as the conditional probability that a structure will meet or exceed a certain level of damage for a given ground motion intensity. Fragility curves are also useful tools to guide the efficient allocation of funds to strengthen or retrofit an existing structure.

Fragility analysis was first introduced in the seismic evaluation of nuclear facility vulnerabilities in the late 1970s and early 1980s and since then has expanded into other areas of structural engineering. The methodologies for developing fragility curves of bridge structural systems which have been proposed in the past can be divided into two different approaches.

The first approach is to develop fragility curves directly from structural analysis data. Hwang and Huo (1998) performed a time history analysis on a bridge structure and used a Bernoulli random variable with 0 and 1 outcomes to show whether or not the bridge sustains the defined damage-state at each level of the ground motion Intensity Measure (IM). They estimated the probability of failure based on the number of zeros and ones at each IM value and fitted a logistic probability distribution to present the fragility curve of the structural system. Shinozuka (1998) also considered the event of bridge damage as a realization from a Bernoulli experiment. However, he applied the maximum likelihood method to fit a lognormal distribution. This approach doesn't account for uncertainties in component capacities.

The second approach is to develop a probabilistic model for the seismic demands and obtain the fragility curve by comparing the distributions of demands and capacities at various IM levels. The probabilistic seismic demands can be generated from ground motion parameters and peak structural component responses by using regression analysis or parameter estimation techniques like maximum likelihood method. Hwang et. al. (2000), Shinozuka et. al. (2003), Bignell et. al. (2004) and Choi et. al. (2004) followed this approach. Nielson and DesRoches (2007) introduced a component based approach to develop system fragility curves. They developed joint probability distribution of seismic demands which accounts for correlations between components and have performed Monte Carlo Simulation (MCS) to integrate over all failure domains. Song and Kang (2009) have introduced a Matrix-based System Reliability (MSR) which considers the

correlations between components by introducing common source random variables using Dunnett–Sobel correlation coefficient matrix.

Fragility analysis of structures comprising a large number of components using the aforementioned methods requires enormous computational effort. Moreover, numerous structural analysis data is required to estimate the component correlations at each IM level.

In order to discover patterns in highly dimensional and complex data such as the relationship between ground motion intensities and peak structural responses, Machine Learning and Soft Computing methods such as Support Vector Machines (SVM) and Neural Networks (NN) can be used. Mitropoulou and Papadrakakis (2011) applied NN methods on the results of Incremental Dynamic Analysis (IDA) of a structure to accurately predict the structural responses. Jack and Nandi (2002) and Widodo and Yang (2007) proposed the application of SVM classification for machine condition monitoring and fault diagnosis. Ge et. al. (2004) compared the efficiency of NN and SVM methods in fault detection in a manufacturing process and demonstrated the superiority of SVM classification method. Hong-Shuang et. al. (2006) proposed SVM based MCS and SVM based FORM analyses for reliability assessment of simple structures.

In this study, IDA results of 40 selected ground motion records are used to train Probabilistic Support Vector Machines (PSVM) in order to develop fragility curves. Binary PSVMs are used to develop system fragility curves for serviceability and collapse limit states and a multi-class PSVM is developed to estimate the damage state of the structure subjected to a given level of ground motion intensity. Fragility curves for single-valued and multi-valued IMs are developed in this study. The structure of this paper is as follows: Section 2 presents a brief review of SVM and PSVM learning methods and model selection; Section 3 describes the modeling of the structure, ground motion selection and IDA and fragility analyses of the studied bridge; Section 4 presents the results obtained from PSVMs and component based system fragility methods and demonstrates the efficiency of PSVM method in reliability analysis and Section 5 presents the conclusion of the paper.

6.2 REVIEW ON SVMS

SVM introduced by Vapnik (1995) is an increasingly popular machine learning technique which has widespread applications in classification, regression and density estimation. Unlike traditional methods (e.g. Neural Networks), which minimize the empirical training error, SVMs are based on the structural risk minimization (SRM) principle and aim at minimizing an upper bound of the generalization error (Vapnik, 1995 and Cortes and Vapnik, 1995).

A binary SVM uses a number of support vectors which are a subset of the training data to construct a hyper-plane to define the boundary between the two classes. In SVMs, some nonlinear kernel functions are used to map the training data into a higher dimensional feature where the data are linearly separable. There can be more than one possible hyper-plane to separate the data so the one with the maximum margin on separation will be selected. The use of nonlinear kernel function enables the SVMs to define complex decision functions and optimally separate two classes of data samples. Multiclass SVMs are usually implemented by combining several binary SVMs and direct multiclass SVM formulation is avoided due to various complexities. Probabilistic Support Vector Machines (PSVM) are also based on the results of binary SVMs.

6.2.1 SVM CLASSIFICATION

Given data input x_i where $x_i \in R^d$, the samples are assumed to have two classes namely positive class and negative class which are labelled as $x_i \in \{-1,+1\}$. SVM finds the optimal hyper-plane that separates one class from the other based on quadratic programming technique which is mathematically presented in equation (6-1).

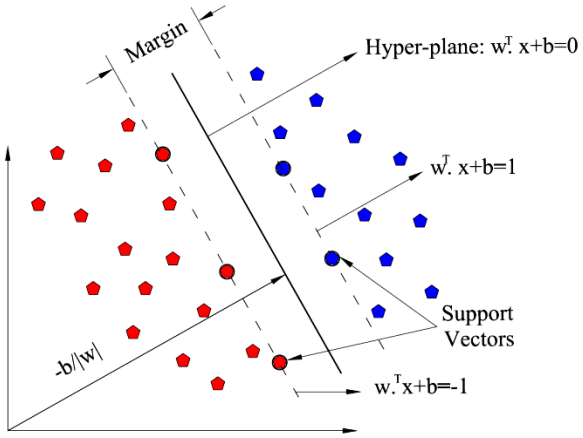

Figure 6-1. Binary SVM classification

$$Min(\frac{1}{2}w^T.w + C\sum_{i=1}^{N}\xi_i) \qquad s.t.\ y_i(w\Phi(x_i)+b)+\xi_i-1\geq 0 \quad , \quad \xi_i \geq 0 \qquad (6\text{-}1)$$

where $\Phi(x_i)$ maps data from the input space into a high dimensional feature space, b is the bias term, ξ_i is the slack variable which is added to allow miss-classification of difficult or noisy data points (Vapnik, 1995), C is the penalty for the error term that is a control to prevent over-fitting, and w is the weight vector which defines the boundary. The weight vector is defined as,

$$w = \sum_{j=1}^{n} \alpha_j y_j \Phi(x_j) \qquad (6\text{-}2)$$

in which x_j are the support vectors. An example of the optimal hyper-plane for two data sets is presented in figure 6-1. In order to solve equation 6-1, a dual formulation is used which is obtained by Lagrange technique. Then, the Sequential Minimization Optimization (SMO) method is applied as suggested by Platt (1998) to obtain the decision hyper-plane. Once the optimal hyper-plane is constructed, the classification decision score is calculated by equation (6-3).

$$f(x) = \sum_{j=1}^{n} \alpha_j y_j K(x, x_j) + b \qquad (6\text{-}3)$$

where $K(x,x_j)=\Phi(x)^T.\Phi(x_j)$ represents the kernel function which corresponds to a dot product of two feature vectors in some expanded feature space. In this paper, polynomial and Gaussian Radial Basis Function (RBF) kernel functions are used which are formulated in Table 6-1. In binary classification, the sign of *f* in equation (6-3) determines whether the point x belongs to the positive or the negative class. However, the value of *f* is required in PSVM analysis.

Table 6-1. Formulation of Kernel Functions

Kernel Function	$K(x,x_j)$
Linear	$x^T.x_j$
Polynomial	$(\gamma x^T.x_j + r)^d, \gamma > 0$
Gaussian RBF	$\exp(-\left\|x - x_j\right\|^2 / 2\gamma^2)$

6.2.2 PROBABILISTIC SUPPORT VECTOR MACHINES (PSVM)

In equation (6-3), f(x) represents an uncalibrated distance measurement of x to the separating hyper-plane in the feature space. Platt (2000) and Lin et. al. (2003) proposed an algorithm to map the *f* value into the positive class posterior probability by applying a sigmoid function to the SVM output as presented in equation (6-4).

$$\Pr(y=1|\mathbf{x}) \approx P_{A,B}(f) \equiv p(\mathbf{x}) = \frac{1}{1+\exp(A f(\mathbf{x})+B)}, \quad \text{where } f = f(\mathbf{x}). \tag{6-4}$$

The best parameter setting $Z^*=(A^*,B^*)$ is determined by solving the following regularized maximum likelihood problem in which N_+ and N_- are the number of positive and negative training data points respectively.

$$\min_{z=(A,B)} F(z) = -\sum_{i=1}^{l}(t_i \log(p_i) + (1-t_i)\log(1-p_i))$$

$$t_i = \begin{cases} \dfrac{N_+ + 1}{N_+ + 2} & \text{if } y_i = 1 \\ \dfrac{1}{N_- + 2} & \text{if } y_i = -1 \end{cases}, i = 1, 2, ..., l. \tag{6-5}$$

Hastie and Tibshirani (1998) proposed Pairwise coupling for multi-class classification

problems. Pairwise coupling combines the probabilistic outputs of all the one-versus-one binary classifiers in order to estimate the posterior probabilities P_i=prob(w_i|x), i=1,…, k. In which *k* is the number of classes. It is noted that for a k-class problem k(k-1)/2 binary classifiers are required. Wu et. al. (2004) proposed the optimization problem presented in equation (6-6) to obtain the probability of *x* belonging to class *i*.

$$\min_{p} \sum_{i=1}^{k} \sum_{j:j\neq i} (r_{ji}p_i - r_{ij}p_j)^2 \quad \text{subject to} \sum_{i=1}^{k} p_i = 1,\ p_i \geq 0,\ \forall i. \qquad (6\text{-}6)$$

in which r_{ij} = P(y=i| y=i or j, x) are auxiliary variables which represents the binary SVMs of the i^{th} and j^{th} classes and are calculated based on equation (6-4) and (6-5).This optimization problem provides a vector of multi-class probability estimates. Duan and Keerthi (2005) demonstrated that this pairwise PSVM technique is the most reliable SVM multiclass classification procedure.

6.2.3 MODEL SELECTION

A Model Selection technique is required to select the appropriate kernel function, kernel parameter (γ) and penalty parameter (C). A double re-sampling procedure with application of a K-fold method is used in this paper. First, a 10-fold Cross Validation is used to divide the data into training and test set. The training set is used for parameter selection, whereas the test set is used only for estimating the prediction risk associated with various kernel functions. In order to find the optimal parameters of (C, γ), a 9-fold cross validation is implemented to divide the training set into learning and validation sets. The learning set is used to estimate the hyper-planes for every set of (C, γ) and the validation set is used to estimate the error associated with each set of parameters. (C, γ). Those with the lowest average validation error are selected. Finally, the average values of prediction errors are compared to determine the best model and kernel function for the input data of this study.

6.3 CASE STUDY

The PSVM method is applied to obtain fragility curves of an existing highway bridge located in Montreal for serviceability and the onset of collapse limit states. In order to

train PSVM, damage states of the structural system given various ground motion intensities are required. Hence, a finite element model of the bridge is developed in SAP2000, 40 appropriate ground motion records are selected and an IDA on the structure is performed to define the damage states at various ground motion intensities. It is assumed that the structural system functions as a series system which implies that the system exceeds a limit state once any of its components exceeds that limit state.

6.3.1 BRIDGE DESCRIPTION AND FINITE ELEMENT MODELING

The bridge consists of 5 spans with a total length of 232 meters. The superstructure consists of a concrete deck which is supported by 5 steel girders with varying depth. Except for the bearing at the second pier, which is a low type fixed bearing, the other bearings at the piers and abutments are high steel bearings. The piers are located in the river bed and are supported by regular footings on hard rock.

A three dimensional view of the model in SAP2000 is shown in Figure 6-2. The bridge deck and the girders are modeled with 4-node shell elements. The piers are modeled with nonlinear multi-layered shell elements. Cap beams are modeled with beam elements and the bearings and the abutments are modeled using NLlink elements which have six independent nonlinear springs, one for each of six deformational degrees of freedom (SAP2000, 1996). Non-confined concrete material behaviour is assumed for the piers (Mander, 1988). The behaviour of the bearings is determined by finite element simulation in ABAQUS and the behaviour of the abutments is based on the model by Shamsabadi et. al. (2007) for granular soils. The behaviour of abutments and bearing are shown in Figure 6-3. Detailed analytical modeling of bridge components are provided in Appendix A.

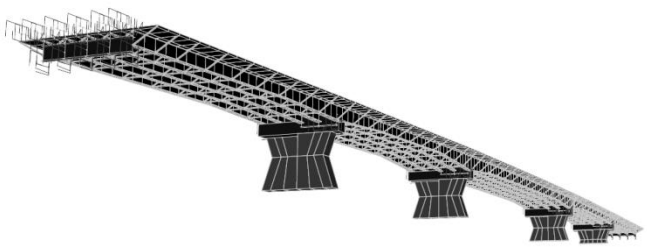

Figure 6-2. Three Dimensional view of Finite Element model of the bridge

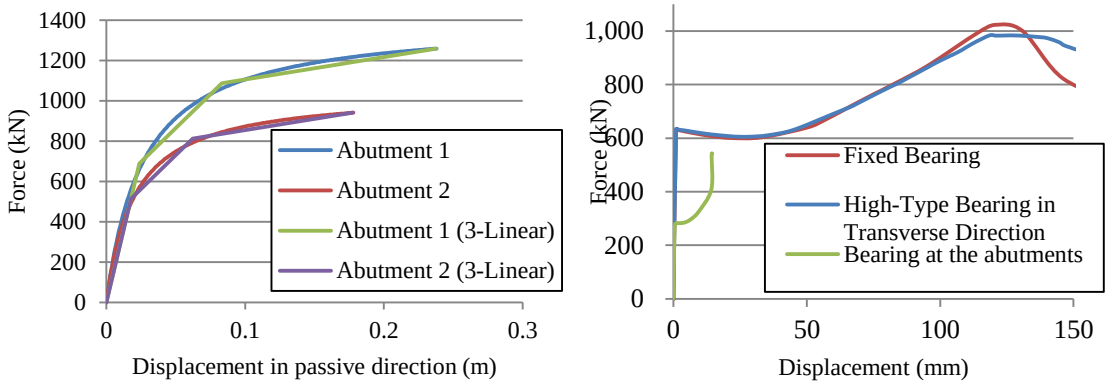

(a) (b)

Figure 6-3. Force-Displacement relationship in a) Abutments b) Bearings

6.3.2 GROUND MOTION SELECTION AND IDA

The IDA technique (Vamvatsikos and Cornell, 2002) addresses the record-to-record variability which is a significant source of uncertainty in seismic evaluations by using a set of scaled input ground motions to evaluate the response of a structure. By performing non-linear dynamic analyses with increasing scaling factors for each ground motion record, the relationship between the IM and the Engineering Demand Parameter (EDP) is obtained. The selection of the proper ground motion records, EDP and IM for the structure should be done carefully since they can all affect the results.

Mackie and Stojadinovic (2003) developed fragility curves considering various IM-EDP pairs and demonstrated that there may not be a single choice which is appropriate for all cases. In this study, fragility curves for single-valued and vector-valued IM are developed. Spectral Acceleration at the first natural period of the structure ($Sa(T_1)$) is considered as the single-valued IM and the pair of Sa and unscaled Epsilon (ε) is selected as the multi-valued IM as suggested by Baker and Cornell (2005). Epsilon (ε) is the number of logarithmic standard deviations by which a target ground motion differs from a median ground motion and is an indicator of spectral shape as it shows whether an Sa at a specified period is in a peak or a valley of the spectrum. Ground motions are assumed

to occur in the transverse direction and the $Sa(T_1)$ of the records is scaled up from 0.03g to 1.5g. Displacements of piers, bearings and abutments are considered as EDPs in this paper.

The Uniform Hazard Spectrum (UHS) has been traditionally used as a target spectrum to determine appropriate set of ground motions. However, it is conservative to use the UHS as the target response spectrum because traditional probabilistic seismic hazard analysis ignores the joint probability of exceedance of spectral ordinates at different periods.

Baker and Cornell (2006) introduced the "Conditional Mean Spectrum" (CMS) as a suitable alternative for the target spectrum. The main purpose of introducing CMS is to provide the expected response spectrum, conditioned on occurrence of a target spectral acceleration value at the period of interest (e.g. at the first natural period of the structure). CMS is defined by the conditional mean and standard deviation of spectral ordinates which are obtained using deaggregation of seismic hazard and ground motion prediction model based on the observations of correlations between spectral ordinates (Baker and Jayaram 2008). In this study, the ground motion prediction model developed by Atkinson and Boore (2006, 2008) are used for both ground motion selection and ground motion hazard assessment. The predicted median spectrum, UHS and CMS are presented in figure 6-4(a).

Finally, a procedure suggested by Baker (2011) is applied to select ground motions from PEER-NGA database which offers 3541 ground motion records from 175 earthquakes. Figure 6-4(b) represents the CMS and the Sa of the selected earthquake records. Appendix C provides more details about ground motion selection analysis and selected records which are used for IDA.

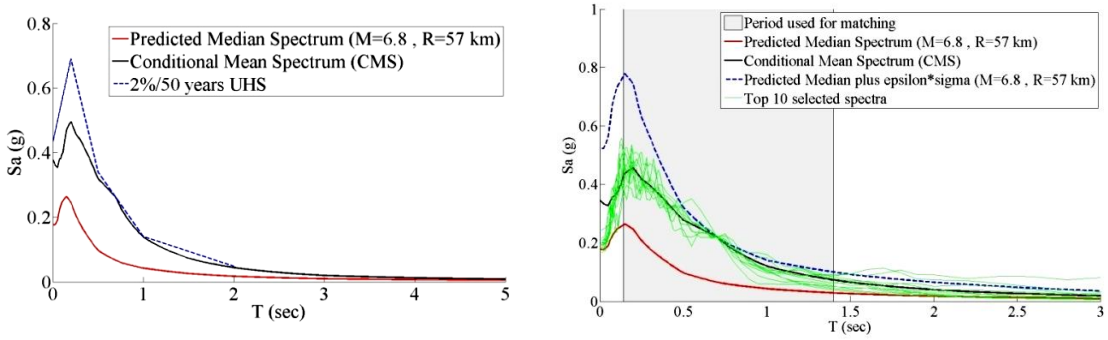

(a) (b)

Figure 6-4. a)CMS and UHS b)CMS and Sa of the top ten selected ground motion records

Figure 6-5 presents the IDA results for a typical bearing at an abutment and a column and the 16, 50 and 84 percentile curves of the IDA results. Appendix D presents more details about IDA results for various bridge structural components.

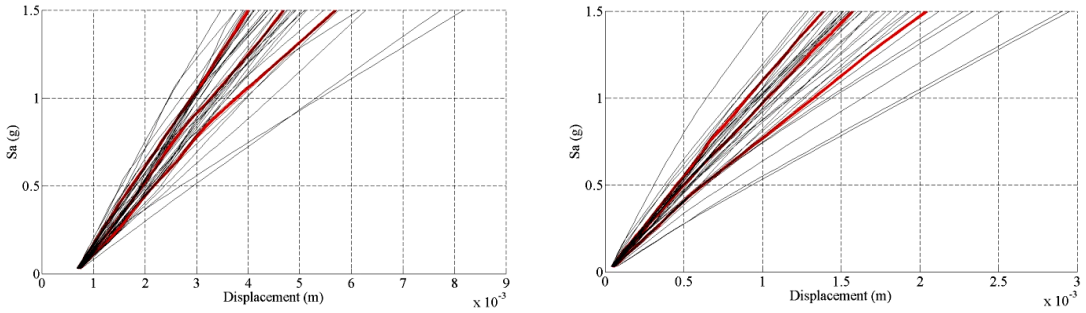

(a) (b)

Figure 6-5. IDA results associated with the 16, 50 and 84 percentiles for: (a) Bearing at the second abutment (b) First Column

6.3.3 FRAGILITY CURVES

A fragility curve, $P[D/C \geq 1 \mid IM]$ is the conditional probability that the structure or structural component sustains the specified damage-level or limit state for a given ground motion intensity. Limit states are assumed to have log-normal distributions. For each component, the mean value of serviceability and onset of collapse limit states are derived based on qualitative damage definitions for slight and complete damages offered by HAZUS-MH. Table 6-2 presents the mean values used for each of the respective distributions. The coefficient of variation (COV) is assumed to be smaller for the serviceability than for the collapse limit state. The COV of the bearings and the columns

are assumed to be equal to 0.05 and 0.1 for serviceability and 0.1 and 0.15 for collapse limit states respectively (Zhu, 2005). It is noted that since the structural system is assumed to be a series system, the system exceeds a limit state once any of its components exceeds that limit state.

Table 6-2. Quantitative Limit states for structural components

Component	Direction	Serviceability (mm)	Onset of Collapse (mm)
Bearing at the Abutments	Longitudinal	-	60
	Transverse	2.85	14.2
High-Type Bearing at the Columns	Longitudinal	-	40
	Transverse	1.4	124
Fixed Bearing at the Columns	Longitudinal	-	45
	Transverse	1	45
Column 1	Longitudinal	20.2	36.15
	Transverse	9.3	12.4
Column 2	Longitudinal	20.1	30.95
	Transverse	9	10
Column 3	Longitudinal	19.8	24.9
	Transverse	8.6	10.5
Column 4	Longitudinal	5	9.5
	Transverse	5.6	7.45

Traditionally, fragility curves are developed for single-valued IMs such as $Sa(T_1)$. In this study, system fragility curves are developed for single IM of $Sa(T_1)$ using PSVM with polynomial and RBF kernel functions and are compared to a system fragility curve developed by a component based method. In addition, system fragility curves for vector-valued IM of ($Sa(T_1)$, ε) using PSVM with polynomial and RBF kernel functions are developed to demonstrate the superiority of using vector-valued IM in reliability analysis.

6.3.3.1 *COMPONENT-BASED FRAGILITY ANALYSIS*

In order to perform component-based fragility analysis, a Joint Probabilistic Seismic Demand Model (JPSDM) of natural logarithm of component demands is developed. Median values and standard deviations of component demands are obtained by performing a regression analysis on IDA results of each component as shown in equation (6-7) in which EDP represents the estimated component demand and both a and b are regression coefficients (Cornell et. al., 2002). Seismic demand and capacity distributions

of the bridge components at various IMs are provided in Appendix D.

$$\widehat{EDP} = a.IM^{b} \quad (6\text{-}7)$$

Since IDA provides a set of demands for each component at each Sa, correlations between component demands at each Sa can be calculated. Assuming a joint lognormal distribution as JPSDM with obtained mean value, standard deviation ($\beta_{D|IM}$) and Sa-dependent correlations, natural logarithm of demands are simulated by MCS. Then, corresponding component capacities are also simulated by MCS and the probability of having at least one failure in the system is calculated over the range of Sa. It is noted that the fragility curves developed by this method have lognormal distributions.

6.3.3.2 *PSVM-BASED FRAGILITY ANALYSIS*

In PSVM method, damage states of the structural system subjected to the given ground motion intensities are defined by comparing the component demands obtained from IDA results with corresponding simulated limit states. These damage states are used to train PSVMs and develop fragility curves. The PSVM method uses sigmoid functions (equation 6-4) to develop fragility curves.

6.4 RESULTS AND DISCUSSION

6.4.1 FRAGILITY CURVES USING SINGLE-VALUED IM

The optimal kernel parameter (γ) and penalty parameter (C) are determined using a double re-sampling method in order to minimize misclassifications in fragility analysis for serviceability and collapse limit states based on single-valued and vector-valued IMs. For this purpose, prediction errors of SVMs with various pairs of (γ,C) are calculated and the pair with the minimum prediction error is selected. Figure 6-6 shows the prediction errors of the fragility analysis with single-valued IM using PSVM with the RBF kernel function. Optimal SVM parameters and associated prediction errors are shown in Table 6-3.

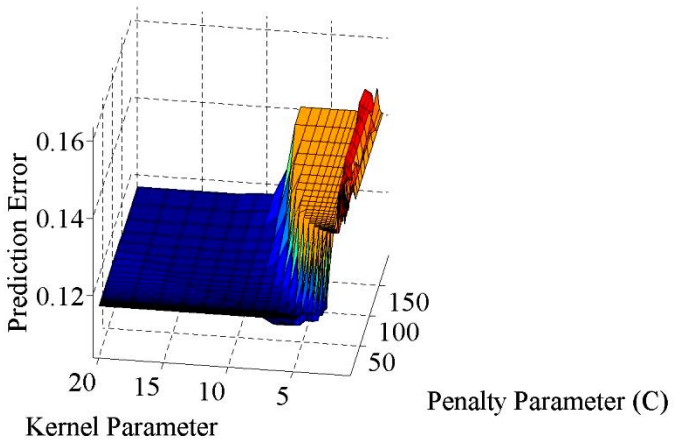

Figure 6-6. Prediction errors of the PSVM in fragility analysis with single-valued IM

Table 6-3. Optimal SVM parameters and associated prediction errors in classifications

Method	IM	Kernel	Serviceability			Collapse		
			γ	C	Prediction Error	γ	C	Prediction Error
SVM	Sa (T1)	RBF	1	1	0.0295	5.1	1	0.116
		Polynomial	4	1.2	0.0311	2	0.1	0.116
SVM	[Sa (T1),ε]	RBF	2	1	0.0274	4.6	1	0.111
		Polynomial	3	1	0.0273	2	0.2	0.124
Component Based MCS	Sa (T1)	-	-	-	0.0327	-	-	0.1433

It is noted that the prediction error in Table 6-3 represents the classification error which is equal to the fraction of untrained data that are misclassified by the analysis. So, in order to compare the results of PSVM to component based fragility analysis, the fragility curve is considered as a classifier. In other words, it is assumed that the structure exceeds the limit state if the probability of exceedance subjected to the given ground motion intensity is higher than 0.5.From table 6-3, it is inferred that PSVM offers more accurate classification. Moreover, RBF and polynomial kernel functions demonstrate similar predictions and the difference in their resulting fragility curves are negligible. So, there is not a superior kernel function choice for this problem.

Figure 6-7 compares the system fragility curves obtained from PSVM analysis (based on equations 6-4 and 6-5) with component based system fragility cures for serviceability and collapse limit states assuming Sa as the IM. It is noted that the points in figure 6-7

represent the sample cumulative distribution (stepped curve) which are obtained from comparison of IDA results and simulated component capacities. Fragility curves obtained from both methods pass Kolmogorov–Smirnov (K-S) goodness of fit test at the 5% significance level, so they are acceptable. Table 6-4 presents the p-value of K-S tests.

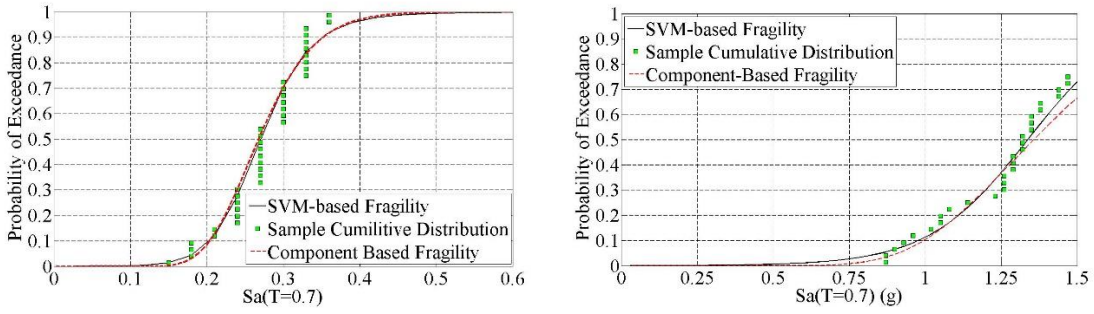

(a) (b)

Figure 6-7. System fragility curves based on PSVM method (RBF kernel function) and the sample cumulative distribution (stepped curve) a) Serviceability limit state b) Onset of Collapse limit state

Table 4. Results of Kolmogorov–Smirnov goodness of fit test

Fragility Analysis Method	Serviceability		Collapse	
	P-Value	K-S Statistic	P-Value	K-S Statistic
PSVM	0.187	0.172	0.777	0.103
Component based MCS	0.185	0.173	0.696	0.111

In order to estimate the reliability of the bridge based on the fragility curves, a PSVM based MCS is performed. For this purpose, samples of $Sa(T_1)$ are generated with MCS based on Atkinson ground motion prediction model and the probability of exceeding any limit state is estimated by the developed PSVM models. According to Atkinson and Boore (2006 and 2008), natural logarithm of $Sa(T_1)$ at the location of the bridge has a normal distribution with the mean value and standard deviation of -2.718 and 0.725 respectively. Hence, the mean value of annual probability of exceeding serviceability and onset of collapse limit states are 3.67 E -2 and 6.76 E -4 which are equivalent to reliability indices (β) of 1.79 and 3.2 respectively.

6.4.2 FRAGILITY CURVES USING VECTOR-VALUED IM

Figure 6-8 demonstrates the damage states of the structure for various pairs of ($Sa(T_1)$,ε) and the decision hyper-planes provided by SVM with RBF kernel function for serviceability and collapse limit states. Figure 6-8 also shows the support vectors used in SVM analysis. Figure 6-9 presents the resulting fragility contours for serviceability and collapse limit states which offer the probability of exceeding the limit states at every ($Sa(T_1)$,ε) pair.

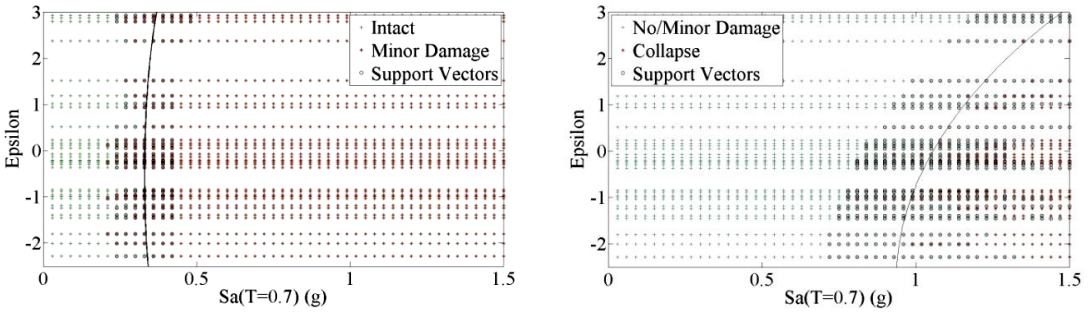

(a) (b)

Figure 6-8. Decision hyper-planes for (a) serviceability and (b) collapse limit states

It is inferred from figure 6-8 that both of Sa and ε, which are measures of ground motion intensity and spectral shape respectively, have significant effects on the response of structures. For a fixed $Sa(T_1)$, records with higher ε cause smaller demands in structures, therefore, they have smaller probability of damage. This was predictable because a higher epsilon means larger than expected Sa at T_1, thus smaller Sa at other periods. In other words, a ground motion record with a high epsilon is likely to have a peak at T_1 while a record with a low epsilon has a valley at T_1. So, when all records are scaled to a certain $Sa(T_1)$, the records with higher epsilons will likely have smaller Sa over a range of periods and cause smaller demands on the structure. However, the effect of ε is not equal over the range of Sa and ε is more important for higher range of Sa. This is also evident in figure 6-9 which shows the fragility contours for serviceability and collapse limit states.

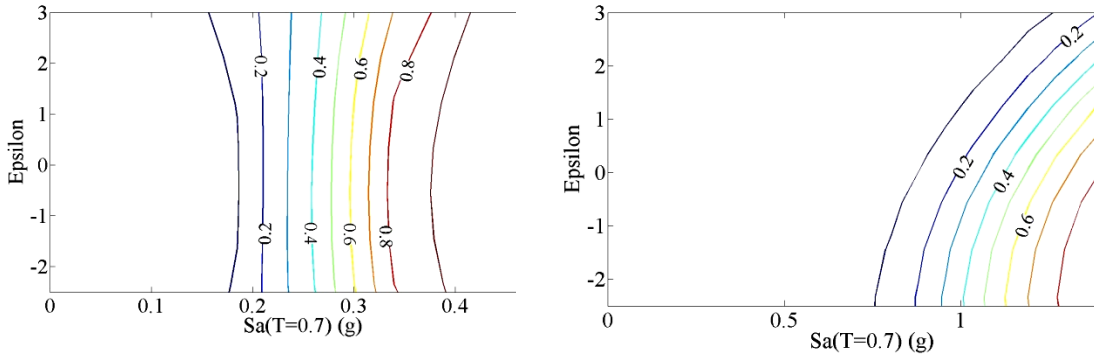

(a) (b)

Figure 6-9. Fragility contours for a) serviceability b) onset of collapse limit states

6.4.3 MULTI-CLASS RELIABILITY ASSESSMENT

PSVMs can also be used in multi-class classification problems by using pairwise coupling and combining the probabilistic outputs of all the one-versus-one binary classifiers, based on equation (6-6). The results can be used to classify the damage state of the given structure subject to ground motions. In this study, three binary classification analyses are performed to develop a 3-class probability assessment. Figure 6-10 shows the probability of sustaining defined damage states over the range of Sa and figure 6-11 demonstrates the probability of sustaining each level of damage as functions of Sa and ε.

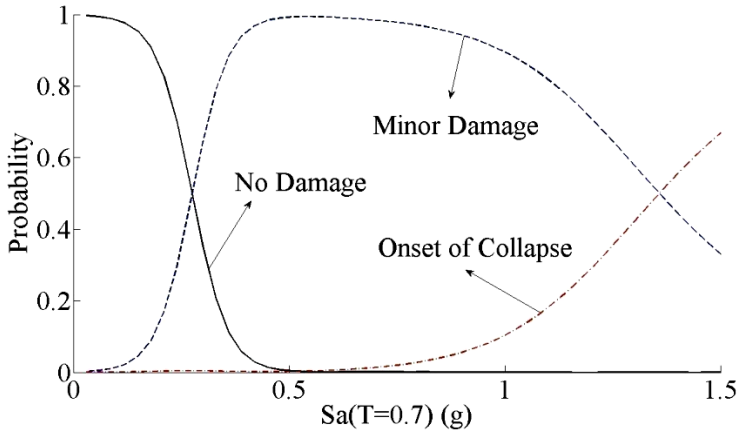

Figure 6-10. Probability of sustaining various damage states assuming Sa as the IM

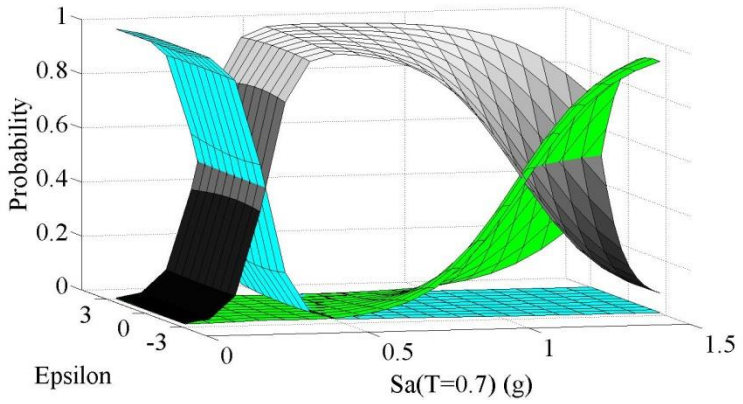

Figure 6-11.Probability of sustaining various damage states assuming (Sa,ε) as the IM

6.5 CONCLUSION

In this paper, application of PSVMs is proposed in reliability assessment of structures and particularly in developing system fragility curves. It is demonstrated that the application of PSVM in reliability assessment reduces the algorithmic or numerical uncertainties. The proposed methodology also reduces the analysis time and computational effort in fragility analysis of structures comprising large number of components significantly.
The proposed methodology is applied in fragility and reliability analysis of an existing bridge located in Montreal as a case study. The results demonstrate that the bridge exceeds serviceability and collapse limit states with the mean annual probability of 3.67 E -2 and 6.76 E -4 respectively.

By considering fragility curves as classifiers and by comparing prediction errors of PSVMs and conventional component based fragility curves, the superiority of PSVM method is demonstrated.

Moreover, it is shown that for the studied case study, polynomial and RBF kernel functions produce similar results. Classic SVM and PSVM are binary classifiers. However, by using pairwise coupling and combining the probabilistic outputs of all the one-versus-one binary classifiers, PSVMs can be used in multi-class classification problems such as fragility analysis for multiple limit states.

SVMs generalize well even in high dimensional spaces and for small training sample

data. So, they can be conveniently applied in fragility analysis with vector-valued IMs. It is demonstrated that considering the pair of ($Sa(T_1)$,ε) as opposed to Sa as IM, reduces the prediction errors and enhances the reliability of the analyses because ε, as in indicator of spectral shape, has a significant effect on the response of structures. This effect is more considerable for higher limit states. It is shown through the case study that for a fixed $Sa(T_1)$, records with higher εs leads to smaller demands and smaller probability of damage. So, for reliability assessment of structure, the effect of epsilon should not be neglected in ground motion selection.

CHAPTER 7: CONCLUSIONS AND RECOMMENDATIONS

This thesis explains methodologies to develop reliable fragility curves of highway bridge structures, considering all the significant uncertainties involved. The proposed methodologies are applied in seismic vulnerability assessment of two existing highway bridges located in Montreal. Parameter uncertainties, Model uncertainties, and algorithm uncertainties are addressed through the case studies.

Parameter uncertainties arise from variability in input parameters of the model and include variability in seismic inputs, structural behaviour, and component limit states. Seismic input uncertainties are quantified through IDA of the structure and reduced by applying a proper ground motion selection method. The variability in structural behaviour is assessed and minimized through the proposed model validation and input parameter updating schemes. In addition, a probabilistic corrosion model is used to further reduce the uncertainties associated with component behaviour of existing structures. And uncertainties involved in component limit state definitions are addressed in developing both component and system seismic fragility curves of the structures.

Model uncertainties come from discrepancies between the mathematical model and the underlying true physics of the structural behaviour. The effect of model uncertainties becomes more significant if there are unaccounted major deficiencies in an existing structure. To address this issue, ambient vibration testing is suggested which provides modal information about full scale structures. The test results are used in the proposed model validation and parameter updating technique to discover and locate probable major structural deficiencies.

Finally, algorithm or numerical uncertainties come from numerical errors and approximations. In order to reduce these uncertainties, a modification to existing component-based fragility analysis methods is proposed in which dependencies in component demands are properly considered at various ground motion intensities.

In addition, a new methodology is proposed for developing fragility curves which reduces numerical uncertainties as well as the required computational effort compared to existing fragility assessment methods. This approach applies soft computing and machine learning

methods such as SVM and PSVM in fragility assessment of structures.

The conclusions from each manuscript were stated at the end of the chapters. The main conclusions of this thesis are summarized as follows:

- Application of stochastic model validation techniques reduces the model uncertainty and quantifies the confidence of the developed model. The Classic hypothesis approach provides a powerful tool to present the confidence of the models. However, this approach is more focused and biased toward rejecting models. The Bayesian approach provides a proper alternative model validation method which uses an unbiased indicator for accepting or rejecting computer models based on available observations.

- Ambient vibration surveys present modal information of structures such as natural frequencies, damping and vibration mode shapes. The obtained information can be used for validating computer models, updating model input parameters which have significant influence on dynamic behaviour of the structure, and for detecting major damages in the studied structure.

- In aggressive environments such as Montreal, corrosion effects may significantly change the behaviour of structural components in older bridges. Estimation of corrosion initiation time and subsequent corrosion propagation in a probabilistic context can provide a realistic model of component behaviours as well as the confidence of the obtained models.

- Structural response under seismic events highly depends on the spectral shape of the ground motion as well as its magnitude. Hence, an appropriate ground motion scheme should consider magnitude, distance and spectral shape of the ground motion records. Conditional Mean Spectrum is a proper ground motion selection method which takes into account the influence of all three main parameters of M, R and ε (ε as an indicator of spectral shape).

- Incremental Dynamic Analysis (IDA) involves numerous nonlinear dynamic analyses of the structure and requires a high computational effort. However, this method provides invaluable data for reliability and fragility evaluation. The results present the seismic demands of each component over the desired range of Intensity Measure (IM) levels as well as the effect of inherent randomness in seismic inputs (record-to-record variability), which is the main source of aleatory uncertainty in the seismic evaluation of structures.

- The data provided by IDA can be used for determining efficiency, practicality and sufficiency of selected Intensity Measures (IM) in order to determine the most proper IM for the studied case. For the case studies in this research, Spectral Acceleration (Sa) proved to be a better choice than Peak Ground Acceleration (PGA). However, the use of (Sa, ε) as a pair increases the accuracy of predictions, especially for higher limit states.

- Component fragility curves can be used to identify the weak structural components of the system which require special attention in order to strengthen or retrofit the structure. Retrofitting the weak element(s) of the structure may alter the local and global load distribution in the structure and subsequently the seismic response of the structural system; such retrofitting can significantly improve the reliability of the system. Hence, component fragility curves are very useful tools to guide the efficient allocation of funds in order to retrofit an existing structure.

- Component-based fragility analysis provides the required information in order to estimate the reliability importance of each component. This measure presents the contribution of each component in the event of a system failure over the desired IM levels. Components may not have the same contribution at different limit states. Hence, the results provide the required information for goal-oriented planning of the retrofit design.

- System fragility curves provide a probabilistic model of structural system failure

under given seismic intensity and can easily be translated into system reliability. Hence, system fragility is a useful tool to demonstrate the structural performance as a system under seismic events, considering all the significant sources of uncertainties in seismic inputs, structural behaviours and component capacities.

- Support Vector Machine (SVM) learning is an outstanding method in pattern detection in complex systems and can be adopted for recognition of relationships between ground motion intensities and peak structural responses. In comparison to conventional fragility assessment techniques, the application of Probabilistic SVMs (PSVM) in fragility analysis of complex structures comprising numerous components reduces the computational effort significantly and increases the prediction accuracy.

- SVMs can be implemented conveniently for systems with high dimensional inputs. Hence, vector-valued IMs can be easily used in fragility assessment of structures without causing any additional computational cost. Vector-valued IMs result in more accurate and reliable fragility curves, as demonstrated in a comparison of Sa and (Sa,ε) as IM candidates.

- SVMs are applicable for both binary classification and multiclass classification problems. Hence, in addition to having the ability to develop classic fragility curves, which represent the conditional probability of exceeding a certain level of damage in the structure at the given ground motion intensity levels, multiclass PSVMs can present the probability of sustaining any level of damage at any given intensity level simultaneously.

APPENDIX A: ANALYTICAL MODEL OF HIGHWAY BRIDGE COMPONENT

This Appendix presents the behavior of the various components of the studied bridge in chapters 5 and 6 accompanied by the analytical models which are used in SAP2000 to represent the behavior of the individual components.

A.1 SUPERSTRUCTURE

The superstructure of a bridge refers to the portion of the bridge which directly receives the live load and is located above the bearings. The superstructure of the studied bridge consists of a concrete deck with 0.203 m thickness which is supported by 5 steel girders with depth varying from 1.37 m at the mid-span of exterior spans to 2.594 m at the interior piers. Cross-bracing is provided between the girders. The girders and deck are constructed such that they operate in composite action. Figure A-1 represents a schematic view of superstructure section of the bridge.

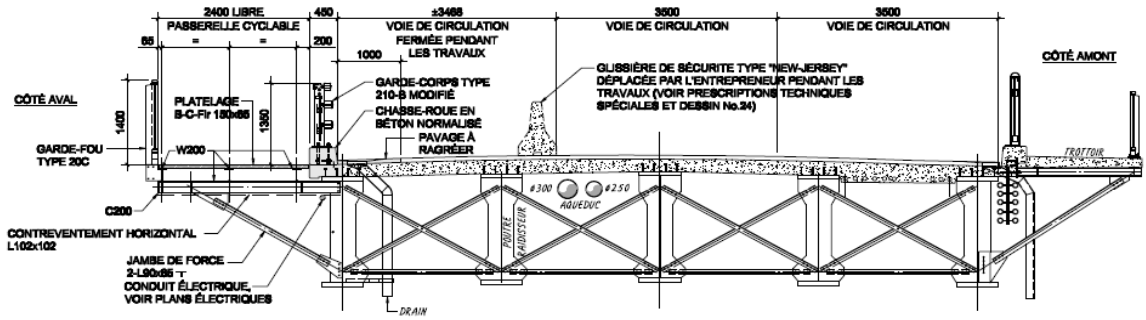

Figure A-1. Typical cross-section geometry of the bridge

In this study, the bridge deck and the girders are modeled with 4-node shell elements. Figure A-2 shows the superstructure section at the location of an interior column and Figure A-3 demonstrates the elevation view of the bridge superstructure as defined in SAP2000. It is noted that the superstructure is expected to remain linearly elastic under seismic loading. Hence, for time integration time history analyses implemented by IDA,

an equivalent beam section is used to simplify the model. Table A-1 presents the section properties of the superstructure at end spans and middle span of the studied bridge.

As it is seen in figure A-1, a heavy pedestrian walkway and a light bicycle path were added to the original structure and resulted in a non-uniform weight distribution of the bridge section. This has affected the natural frequencies, dominant modes and generally the behavior of the structure from the original design assumptions.

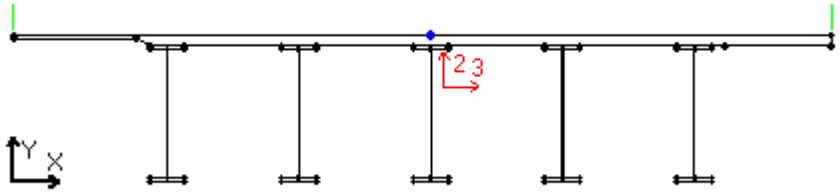

Figure A-2. Typical Superstructure Section Definition in SAP2000

It is noted that although the mass and the mass distribution of the deck have significant effect on structural response of the bridge, the response is not sensitive to longitudinal and transverse stiffness of the deck because the superstructure is much stiffer than the other components of the bridge in those directions and the deck almost behaves as a rigid link.

Figure A-3. Elevation View Bridge Superstructure

Table A-1. Section Properties of the Superstructure at End Spans and Middle Span

Location	A	J	I33	I22	I23	Z33	Z22	r33	r22	Xcg	Ycg	Xpna	Ypna
Mid-Span	4.564	0.0451	1.473	70	0.514	0.4033	11.022	0.5682	3.916	8.347	1.181	8.085	1.452
Column 1 and 4	6.853	0.0477	5.481	99.3	1.128	0.938	11.732	0.894	3.806	8.216	1.415	8.013	1.962
Column 2 and 3	7.074	0.0477	9.454	102.1	1.496	1.166	11.891	1.156	3.799	8.208	1.816	7.802	2.564

A.2 STEEL BEARINGS

Bearings are responsible for transmitting vertical and horizontal loads or displacements from superstructure to substructure. Hence, they have a significant contribution in reliability and vulnerability of bridge structures. Various types of bearings are available based on their shapes, sizes and functionality.

Based on the movements that the bearings allow, they are categorized into two classes: Fixed Bearings (which only permit rotational movements) and Expansion Bearing (which permit both rotations and horizontal translations). A typical steel bearing connects a masonry plate (which is attached to the column or abutment) and a sole plate (which is attached to the underside of the steel girders) in a way to enable the desired motions.

Four types of steel bearings are used in the studied bridge: one type of Low-type fixed bearing and three types of high-type expansion bearings. Figure A-4 presents the as-built plans of the bearings used in the studied bridge.

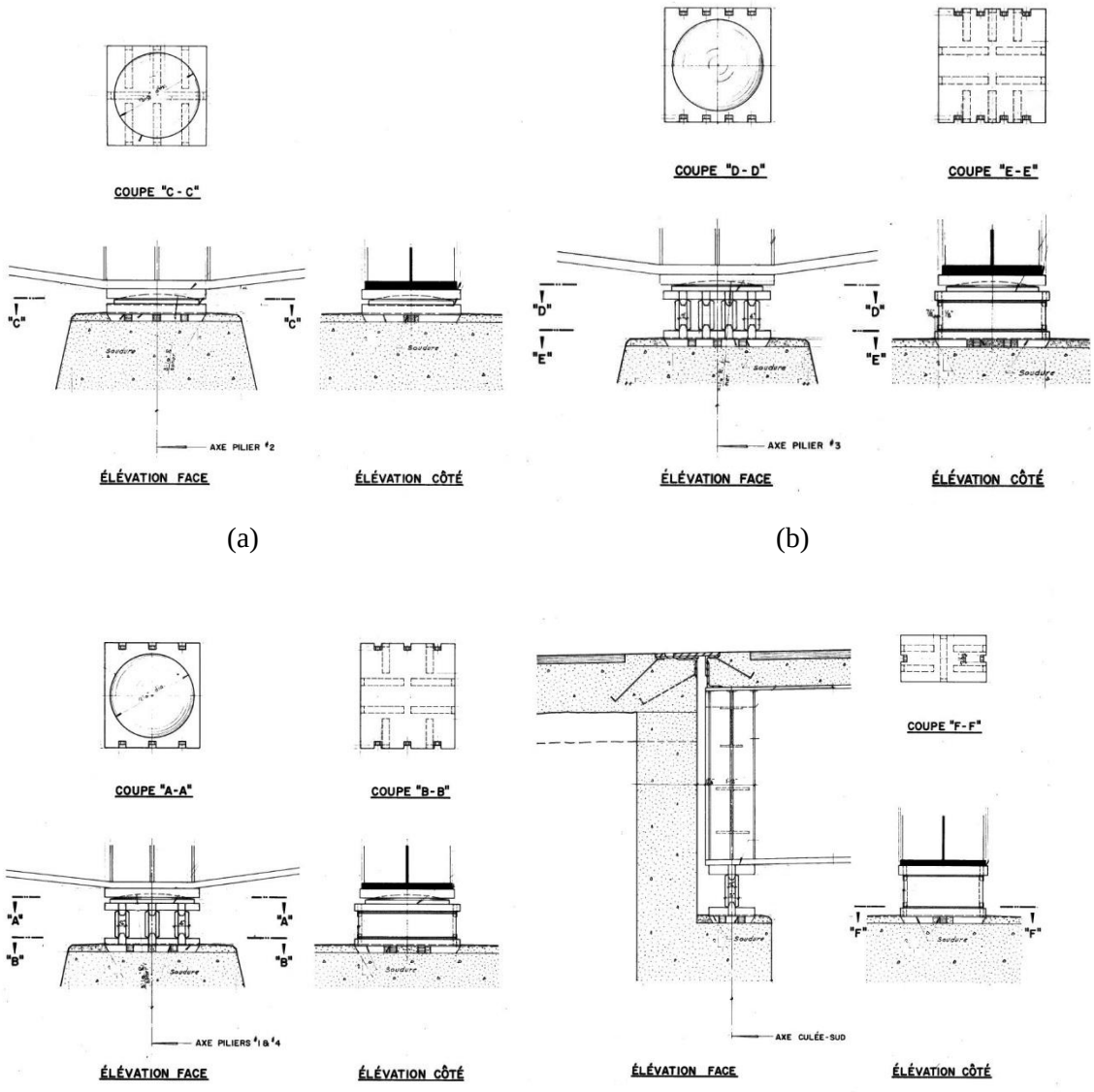

Figure A-4. As-built plans of the bearings a) low-type fixed bearing b) High-type expansion bearing (I) c) High-type expansion bearing (II) d) high-type expansion bearing (at the abutments)

Steel bearings usually demonstrate don-ductile behavior and are prone to corrosion and deterioration. Hence, they are vulnerable to seismic loadings and they are no longer used in design of new bridges or retrofitting the old structures (Mander et. al., 1996).

Figure A-5 presents the current condition of the bearings of the studied bridge.

(a) (b)

Figure A-5. Current condition of the bearings a) at an abutment b) at an interior column

The bearings are modeled with Finite Elements using ABAQUS software and analyzed using a pushover method to obtain the component behaviors. The bearings are then modeled in SAP2000 using Nllink elements which have six independent nonlinear springs, one for each of six deformational degrees of freedom. Figure A-6 shows a modeled high-type expansion bearing in ABAQUS.

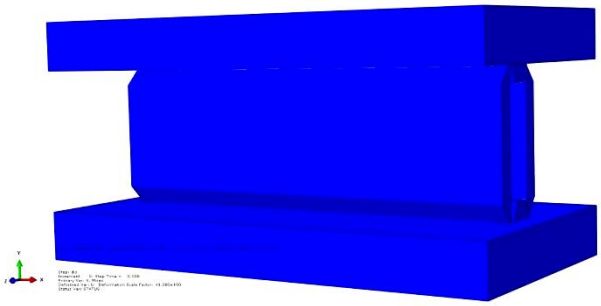

Figure A-6. ABAQUS model of the bearing located at abutment of the bridge

A.2.1 LOW-TYPE FIXED BEARINGS

As it is shown in figure A-4 (a), a spherical cap which is attached to the masonry plate is locked in the sole plate in order to prevent horizontal movements while allowing rotations. This component will fail if the ratio of the horizon load to the vertical pressure (due to the superstructure weight and live load) exceeds a certain limit by enduring

excessive displacements through sliding on spherical surface. Figure A-7 demonstrates the failure mechanism of this component.

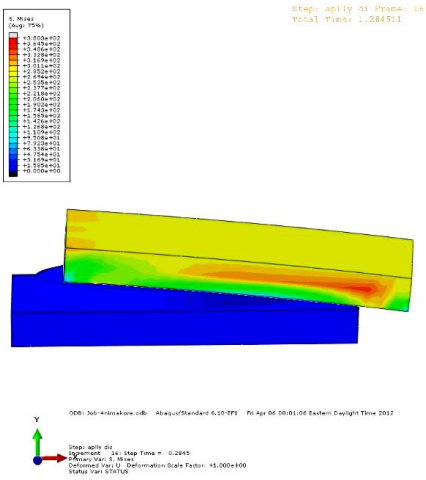

Figure A-7. Failure mechanism of the fixed bearing

Figure A-9 demonstrates the nonlinear behavior of this component obtained from the pushover analysis in ABAQUS software. This bearing has an initial stiffness of 630 kN/mm and yields at 1mm displacement followed by a perfectly plastic behavior (which models the sliding with a friction coefficient of 0.37). It is noted that the behavior of this component in longitudinal and transverse directions are similar.

A.2.2 HIGH-TYPE EXPANSION BEARINGS AT THE ABUTMENTS

As it is shown in figures A-4 (d) and A-6, masonry plate and sole plate are connected with a thick plate anchored at the ends. The behavior of this type of bearing consists of the deformation of the anchors due to bending and shear and overturning of the plate.

Figure A-8 demonstrates the failure mechanism of this bearing.

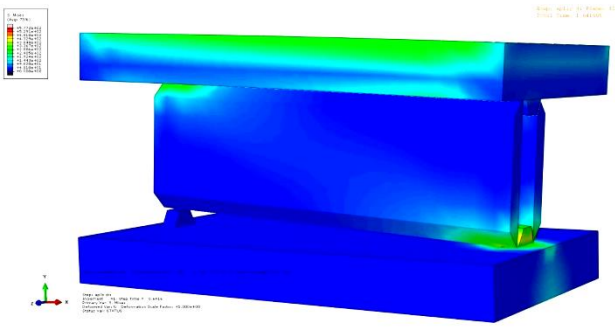

Figure A-8. Failure mechanism of high-type expansion bearings at the abutments

Figure A-9 demonstrates the nonlinear behavior of this component obtained from the pushover analysis in ABAQUS software. This bearing has an initial stiffness of 481.3 kN/mm and the first yielding occurs at 0.58mm displacement followed by a strain hardening behavior until the brittle shear failure of the anchor. It is noted that this component allows longitudinal displacement with an insignificant stiffness.

A.2.3 HIGH-TYPE EXPANSION BEARINGS AT THE COLUMNS

The bearings at the columns as shown in figure A-4 (a) and (b), consist of three or four thick plates similar to the bearing located at abutments accompanied with a spherical cap at the top similar to the fixed bearings. Hence, the behavior of these bearings is a combination of the two previously mentioned bearings. However, as the stiffness of the group of plates is significantly higher than the stiffness of the sliding mechanism in spherical cap surface, the sliding mechanism is the dominant mode of failure and the behavior of these bearings in transverse direction is very similar to the fixed bearings as shown in figure A-9. It is noted that the stiffness of this component in longitudinal direction is insignificant.

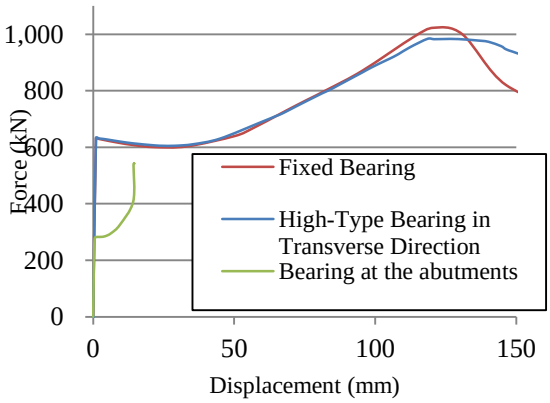

Figure A-9. Force-Displacement Relationship in Bearings

A.3 REINFORCED CONCRETE COLUMNS

The studied bridge crosses a river and hammerhead columns with various lengths support its superstructure. Figure A-10 shows the as-built plan of a typical column. It is noted that this type of column demonstrates very low ductility. Figure A-10 presents as-built plans of a typical column of the structure.

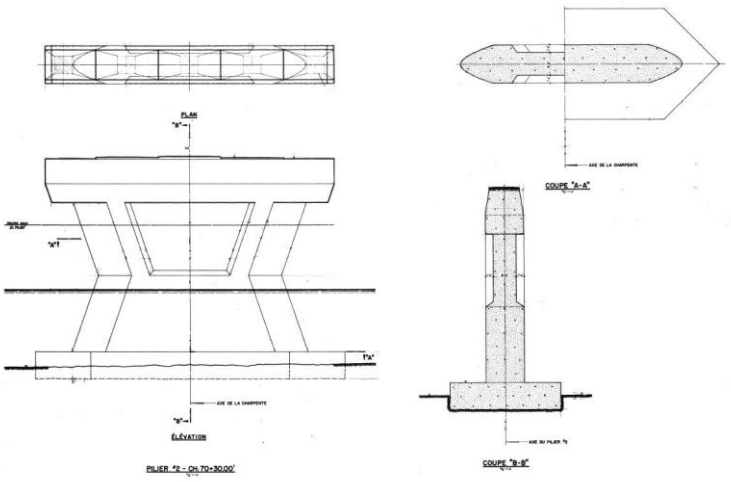

Figure A-10. As-built plans of a typical pier

The columns are modeled with multilayer nonlinear shell elements in SAP2000 as shown in figure A-11. First, each column is divided into six areas with uniform thickness and reinforcement details and every section is modeled by multilayer nonlinear shell elements. Non-confined concrete material behaviour is assumed in modeling the behaviour of the piers (Mander, 1988).

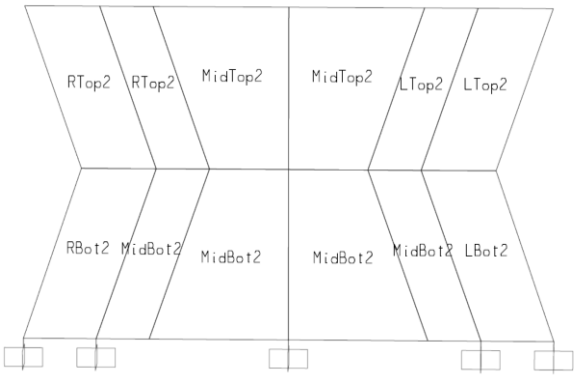

Figure A-11. Typical pier model in SAP2000

In order to demonstrate the behavior of the piers in longitudinal and transverse directions, push over analyses is performed on the pier model shown in figure A-11 in both directions assuming a constant vertical load. Figure A-12 presents the obtained force displacement curves.

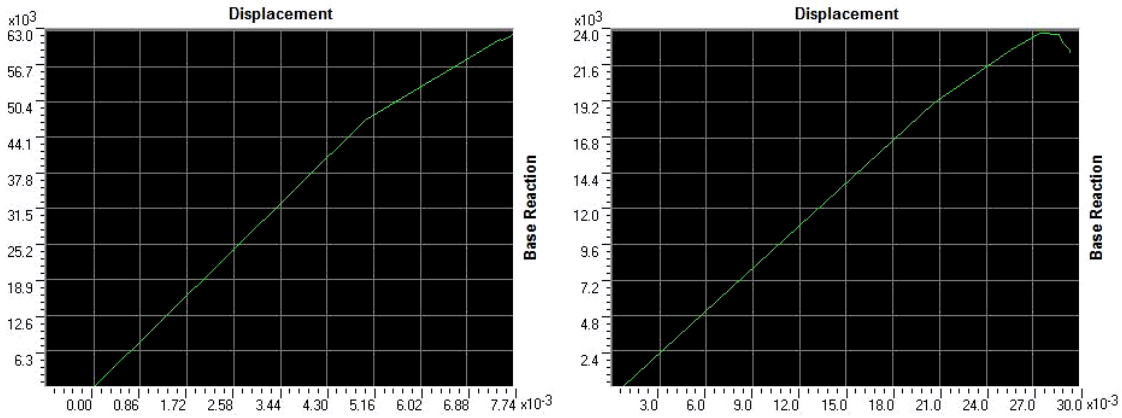

(a) (b)

Figure A-12. Force-Displacement curves of a typical pier in a) transverse b) longitudinal directions

A.4 ABUTMENTS

Abutments are important elements of highway bridges which support the superstructure at bridge ends in both vertical and horizontal directions. Typical abutments are either built in the form of seat type or integral abutments. In seat type abutments, there is a gap between the superstructure and the abutment and they are connected to the by bearings while in integral abutments, the abutment is built integral with the bridge superstructure.

Typical highway bridges are mostly supported by seat type abutments. Several types of seat type abutments can be found based on their structural form and their foundation type. The studied bridge is supported by U-shape abutments as shown in figure A-13 and A-14, one of which is supported by a pile cap while the other one is located on spread footing on bed rock.

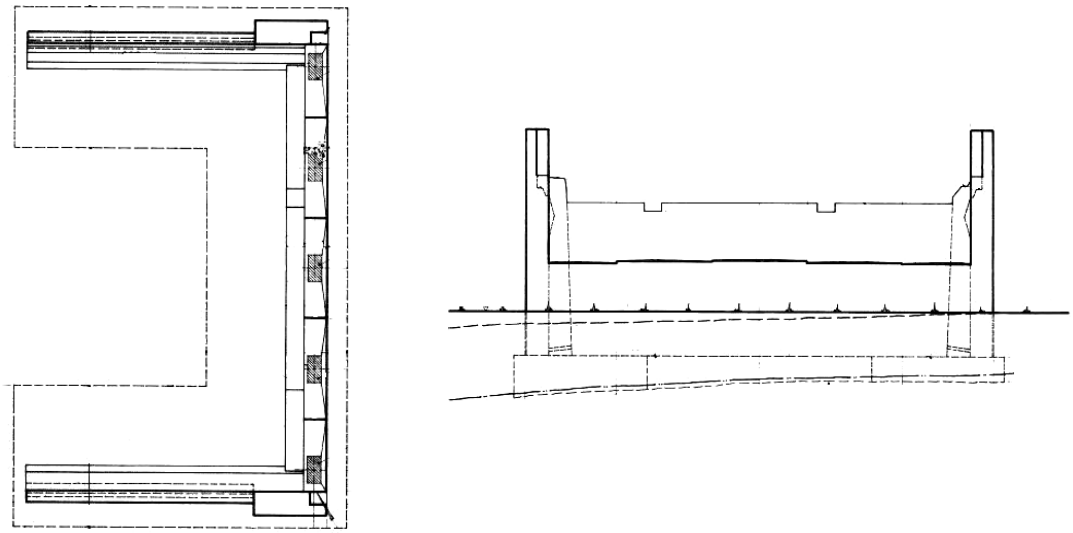

(a) (b)

Figure A-13. Abutment located on hard rock a) plan view b) elevation view

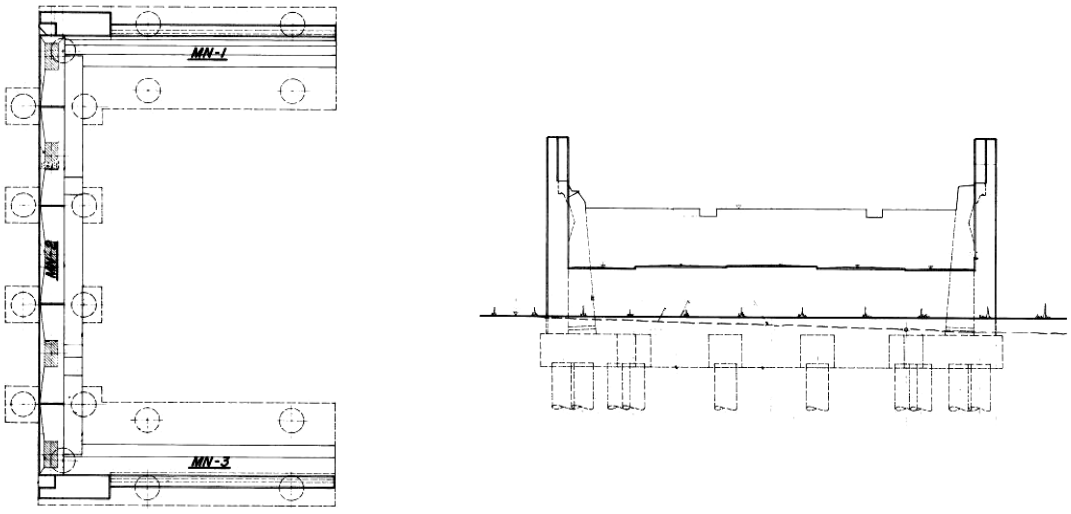

(a) (b)

Figure A-14. Abutment supported by pile group a) plan view b) elevation view

Past experience in 1994 Northridge earthquake (U.S.A.), the 1995 Kobe earthquake (Japan), the 1999 Izmit and Duzce earthquake (Turkey), and 1999 Chi-Chi earthquake (Taiwan) demonstrated that abutments have significant contribution in vulnerability of the bridges. Several studies such as Faraji et. al. (2001), El-Gamal and Siddharthan (1998)

have demonstrated that the assumptions in nonlinear interaction of soil-structure have a significant effect on overall structural response and seismic performance of highway bridges.

Damages to the abutment are generally either due to the foundation failure or structural failures in abutment. The first type of damage is caused by excessive soil deformation and results in tilting, sliding, settling or overturning of the abutment and leads to a serious disruption in functionality of the bridge. However, the second type of damage which is cause by excessive soil pressure on the abutment structure is easily repairable.

Hence, analytical modeling of abutments in both longitudinal and transverse directions are further discussed in the following subsection.

A.4.1 LONGITUDINAL DIRECTION

When the bridge deck moves longitudinally toward the abutment during a seismic event, the abutment wall is pressed into the soil back-fill and mobilizes passive resistance which is partially provided by the soil and partially provided by the piles.

Strong earthquakes may result in permanent soil displacements and nonlinear soil-structure interaction which affects the overall performance of the bridge.

A.4.2 PASSIVE SOIL BEHAVIOR AT ABUTMENTS

A hyperbolic force-displacement model developed by Shamsabadi et. al. (2007) which is compatible with Caltrans provision is adopted in this study. Equation A.1 and figure A-15 presents the applied force-displacement model.

$$F(y_i) = \frac{F_{ult}(2Ky_{max} - F_{ult})y_i}{F_{ult}y_{max} + 2(Ky_{max} - F_{ult})y_i} \quad \text{(A.1)}$$

In which F_{ult}, K and y_{max} are maximum abutment force, average soil stiffness and maximum displacement respectively. These 3 geotechnical parameters are selected as shown in table A-2 for granular soil based on Shamsabadi et. al. (2007) suggestion. It is noted that H represents abutment backwall height which is equal to 4.75 m and 3.55 m for the studied abutments.

Table A-2. Selected geotechnical parameters for passive soil behaviour modeling

Backfill Soil Type	Maximum Pressure KPa (F_{ult}/H)	K kN/cm/m	Maximum Displacement (y_{max}/H)
Granular	265	290	0.05
Cohesive	265	145	0.1

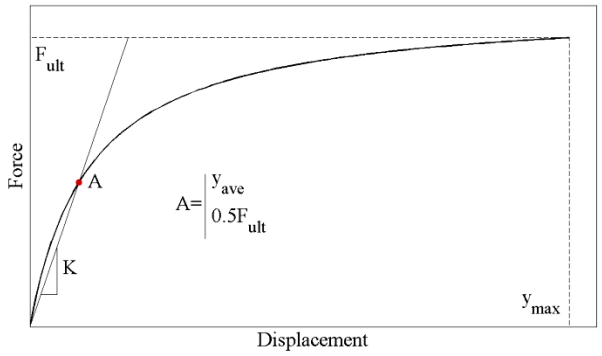

Figure A-15. Hyperbolic force-displacement behavior of abutment backfill soil as suggested by Shamsabadi et. al. (2007)

In order to model the passive soil behavior of the abutment backfill in SAP2000, Nlink element with nonlinear behavior are used and the hyperbolic function is estimated by tri-linear model as shown in figure A-16. It is noted that the first two points in tri-linear models correspond to $0.1y_{max}$ and $0.35y_{max}$ respectively and the slope of the first two lines are equal to K and 0.7K as shown in Table A-3.

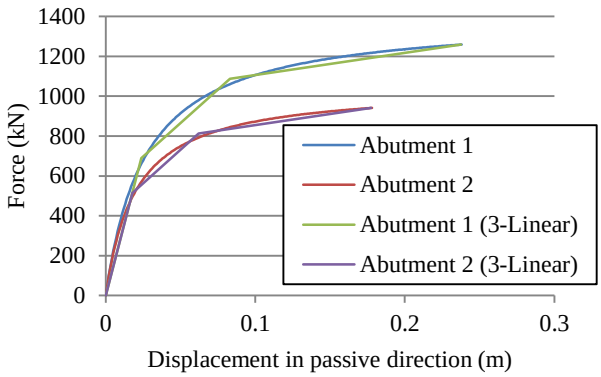

Figure A-16. Force-displacement relationship of the abutments backfill soil

Table A-3. Model properties of soil passive action

Properties	Notations	Values
Initial Stiffness	K_{P1}	K (=290 kN/cm/m)
Displacement 1	Δ_{P1}	$0.1y_{max}$
Second Stiffness	K_{P2}	0.7K
Displacement 2	Δ_{P2}	$0.35y_{max}$
Third Stiffness	K_{P3}	$\frac{F_{ult} - 0.275Ky_{max}}{0.65y_{max}}$
Displacement 3	Δ_{P3}	y_{max}

A.4.3 PILE BEHAVIOR

In this study, pile behavior is defined according to Caltrans provision. (Caltrans, 1990). Hence, an effective stiffness (K_{eff}) of 7 kN/mm/pile and ultimate strength of 119 kN/pile is assumed and the force-displacement relationship is defined by a tri-linear model as suggested by Choi (2002) and Nielson (2005). The defined model properties are shown in Table A-4.

Table A-4. Model properties of soil passive action

Properties	Notations	Values
Initial Stiffness	K_1	$2.33K_{eff}$
Displacement 1	Δ_1/H	7.62 mm
Second Stiffness	K_2	$0.428K_{eff}$
Displacement 2	Δ_2/H	25.4 mm
Third Stiffness	K_3	0
Displacement 3	Δ_3/H	-

In order to consider the interaction of piles in a pile group a p-multiplier (Brown et. al. 1988) can be introduced. The value of the p-multiplier depends on the position of the pile in the pile group. However, since the front and rear rows alternate during a cyclic loading, an average multiplier can be used to simplify the calculation. Hence, a p-multiplier of 0.7 is considered for all piles regardless of their position as suggested by Curras et. al. (2001).

A.4.4 TRANSVERSE DIRECTION

Piles and wing walls are the components which contribute in the stiffness of abutments in transverse direction. The behavior of piles is the same in longitudinal and transverse directions. Hence the same pile model is used in transverse direction.

However, according to Caltrans the effect of wing-walls decreases as the width of the abutment increases because they cannot fully mobilize passive behavior of the soil. Hence, as suggested by Maroney and Chai (1994), the abutment stiffness and strength obtained for the longitudinal direction are modified by wing-wall effectiveness and participation factors of 2/3 and 4/3 respectively.

APPENDIX B: AMBIENT VIBRATION TEST

This appendix provides details about ambient vibration survey of the bridge studied in chapters 5 and 6. It includes a description of the equipments used during the test, measurement scheme and the results of the system identification analysis.

B.1 TEST EQUIPMENT AND MEASUREMENT SCHEME

In order to perform ambient vibration test on the studied bridge, 6 TROMINO® velocity meters were used. Since these sensors have Data Acquisition Systems (DAS) with radio transceivers, they can communicate and synchronize their internal clock with one millisecond precision. So, the obtained data from the sensors is always synchronized.

In order to detect structural mode shapes with sufficient resolutions a total of 42 equally spaced points, 21 on each side, were identified on the bridge for ambient measurement. Multiple setups of sensors were required as the number of points exceeded the number of available sensors. Hence, 2 reference sensors were located in the middle of the bridge on each side and the remaining 4 sensors were used as roving sensors.

11 setups were used to cover 21 points on each side of the bridge as shown in figure B-1. Two sets of data were recorded for each setup each of which for approximately six minute. The sampling frequency was set to 128 Hz and the movements in 3 directions were recorded.

Figure B-1 schematically presents the setups used in ambient vibration survey. Reference and roving sensors are presented with green and yellow labels respectively.

B.2 RESULTS OF THE SYSTEM IDENTIFICATION ANALYSIS

The Enhanced Frequency Domain Decomposition (EFDD) technique was performed by Saeed (2013) for system identification. Table B-1 demonstrates the obtained structural natural periods. The obtained first singular value plots and first ten mode shapes of the structure are presented in figures B-2 to B-12.

Setup 1	Bridge End 1	0	1	2	3	4	5	6	7	8	9	10	11	12	13	14	15	16	17	18	19	20	21	80	Bridge End 2
			S2			S3			S4			S5	S6												
													S7												
		0'	1'	2'	3'	4'	5'	6'	7'	8'	9'	10'	11'	12'	13'	14'	15'	16'	17'	18'	19'	20'	21'	80'	
Setup 2	Bridge End 1	0	1	2	3	4	5	6	7	8	9	10	11	12	13	14	15	16	17	18	19	20	21	80	Bridge End 2
				S2			S3			S4			S6												
													S7												
		0'	1'	2'	3'	4'	5'	6'	7'	8'	9'	10'	11'	12'	13'	14'	15'	16'	17'	18'	19'	20'	21'	80'	
Setup 3	Bridge End 1	0	1	2	3	4	5	6	7	8	9	10	11	12	13	14	15	16	17	18	19	20	21	80	Bridge End 2
					S2			S3			S4		S6	S5											
													S7												
		0'	1'	2'	3'	4'	5'	6'	7'	8'	9'	10'	11'	12'	13'	14'	15'	16'	17'	18'	19'	20'	21'	80'	
Setup 4	Bridge End 1	0	1	2	3	4	5	6	7	8	9	10	11	12	13	14	15	16	17	18	19	20	21	80	Bridge End 2
													S6				S5		S4		S3		S2		
													S7												
		0'	1'	2'	3'	4'	5'	6'	7'	8'	9'	10'	11'	12'	13'	14'	15'	16'	17'	18'	19'	20'	21'	80'	
Setup 5	Bridge End 1	0	1	2	3	4	5	6	7	8	9	10	11	12	13	14	15	16	17	18	19	20	21	80	Bridge End 2
													S6			S5		S4		S3		S2			
													S7												
		0'	1'	2'	3'	4'	5'	6'	7'	8'	9'	10'	11'	12'	13'	14'	15'	16'	17'	18'	19'	20'	21'	80'	
Setup 6	Bridge End 1	0	1	2	3	4	5	6	7	8	9	10	11	12	13	14	15	16	17	18	19	20	21	80	Bridge End 2
											S5	S4	S6	S3	S2										
													S7												
		0'	1'	2'	3'	4'	5'	6'	7'	8'	9'	10'	11'	12'	13'	14'	15'	16'	17'	18'	19'	20'	21'	80'	
Setup 7	Bridge End 1	0	1	2	3	4	5	6	7	8	9	10	11	12	13	14	15	16	17	18	19	20	21	80	Bridge End 2
													S6												
													S7				S5		S4		S3		S2		
		0'	1'	2'	3'	4'	5'	6'	7'	8'	9'	10'	11'	12'	13'	14'	15'	16'	17'	18'	19'	20'	21'	80'	
Setup 8	Bridge End 1	0	1	2	3	4	5	6	7	8	9	10	11	12	13	14	15	16	17	18	19	20	21	80	Bridge End 2
													S6												
													S7			S5		S4		S3		S2			
		0'	1'	2'	3'	4'	5'	6'	7'	8'	9'	10'	11'	12'	13'	14'	15'	16'	17'	18'	19'	20'	21'	80'	
Setup 9	Bridge End 1	0	1	2	3	4	5	6	7	8	9	10	11	12	13	14	15	16	17	18	19	20	21	80	Bridge End 2
													S6												
											S5	S4	S7	S3	S2										
		0'	1'	2'	3'	4'	5'	6'	7'	8'	9'	10'	11'	12'	13'	14'	15'	16'	17'	18'	19'	20'	21'	80'	
Setup 10	Bridge End 1	0	1	2	3	4	5	6	7	8	9	10	11	12	13	14	15	16	17	18	19	20	21	80	Bridge End 2
													S6												
			S2		S3		S4		S5				S7												
		0'	1'	2'	3'	4'	5'	6'	7'	8'	9'	10'	11'	12'	13'	14'	15'	16'	17'	18'	19'	20'	21'	80'	
Setup 11	Bridge End 1	0	1	2	3	4	5	6	7	8	9	10	11	12	13	14	15	16	17	18	19	20	21	80	Bridge End 2
													S6												
				S2		S3		S4		S5			S7												
		0'	1'	2'	3'	4'	5'	6'	7'	8'	9'	10'	11'	12'	13'	14'	15'	16'	17'	18'	19'	20'	21'	80'	

Figure B-1. Schematic representation of setups for ambient vibration measurements

Table B-1. Structural natural periods obtained from EFDD analysis

Mode number		1	2	3	4	5	6	7	8	9	10
Measured Period	Sec	0.69	0.63	0.46	-	0.40	0.36	0.30	0.28	0.26	0.26
Mode number		11	12	13	14	15	16	17	18	19	20
Measured Period	Sec	-	0.21	0.19	0.18	0.16	0.15	0.14	0.13	0.11	0.10

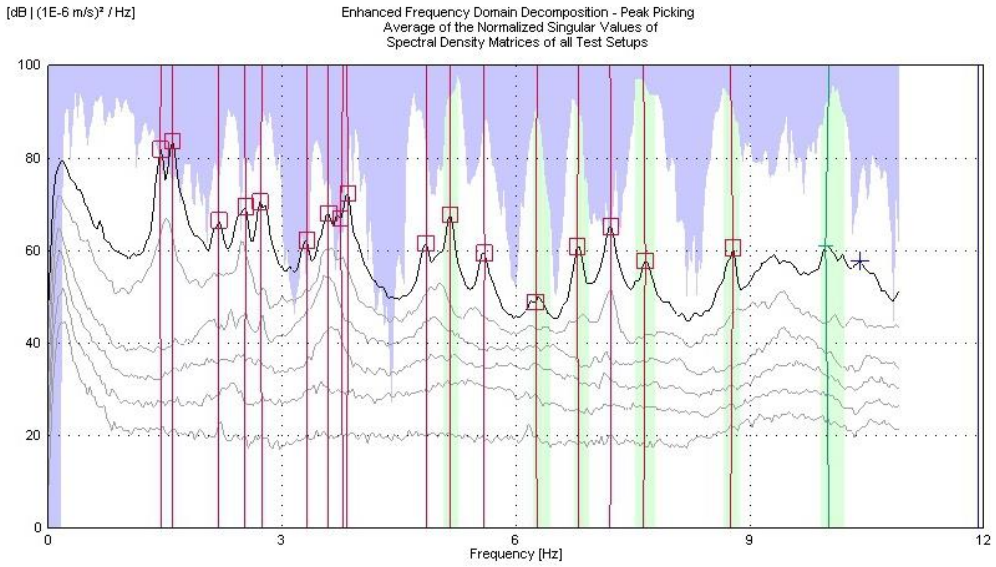

Figure B-2. Singular value plot obtained from EFDD analysis

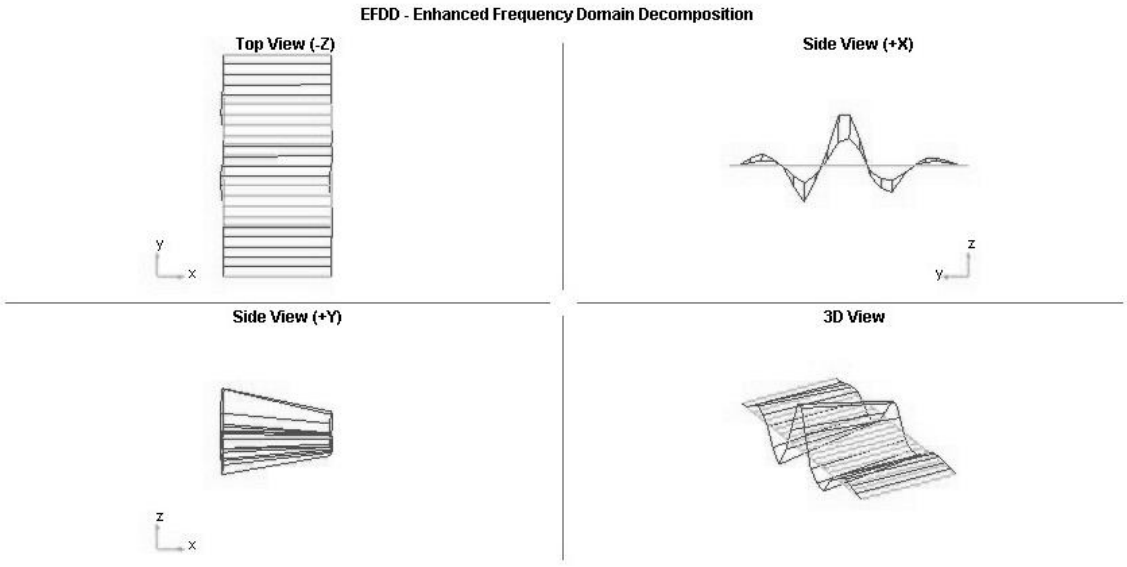

Figure B-3. First structural mode shape obtained from EFDD analysis

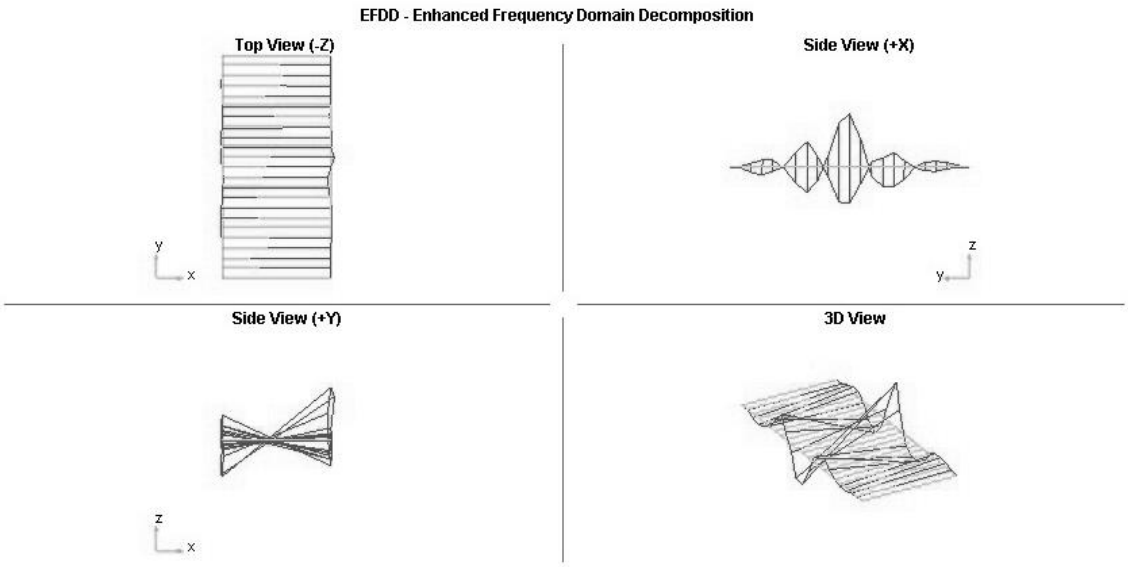

Figure B-4. Second structural mode shape obtained from EFDD analysis

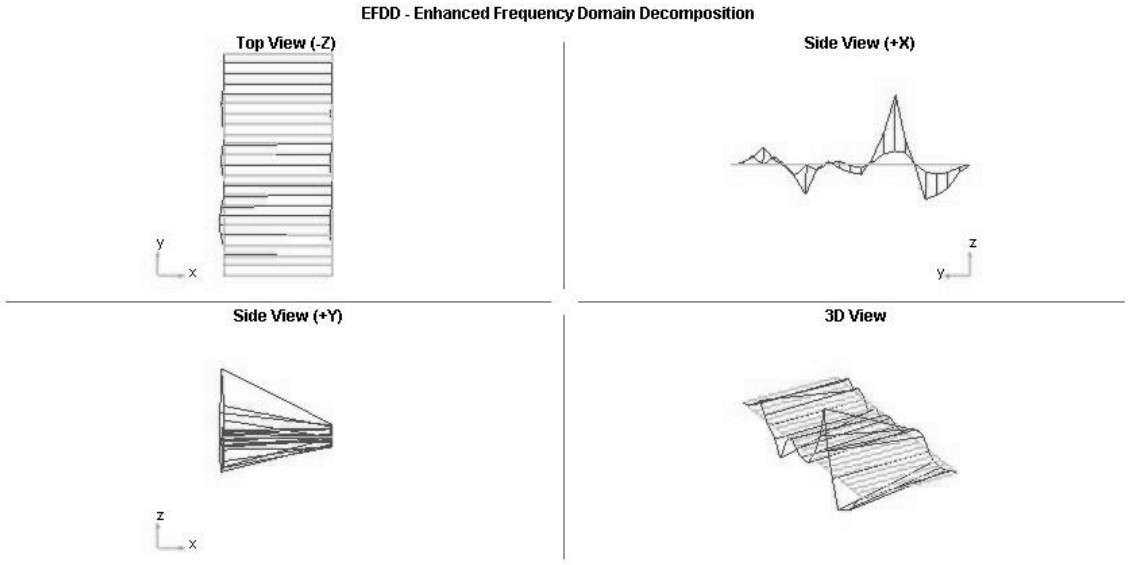

Figure B-5. Third structural mode shape obtained from EFDD analysis

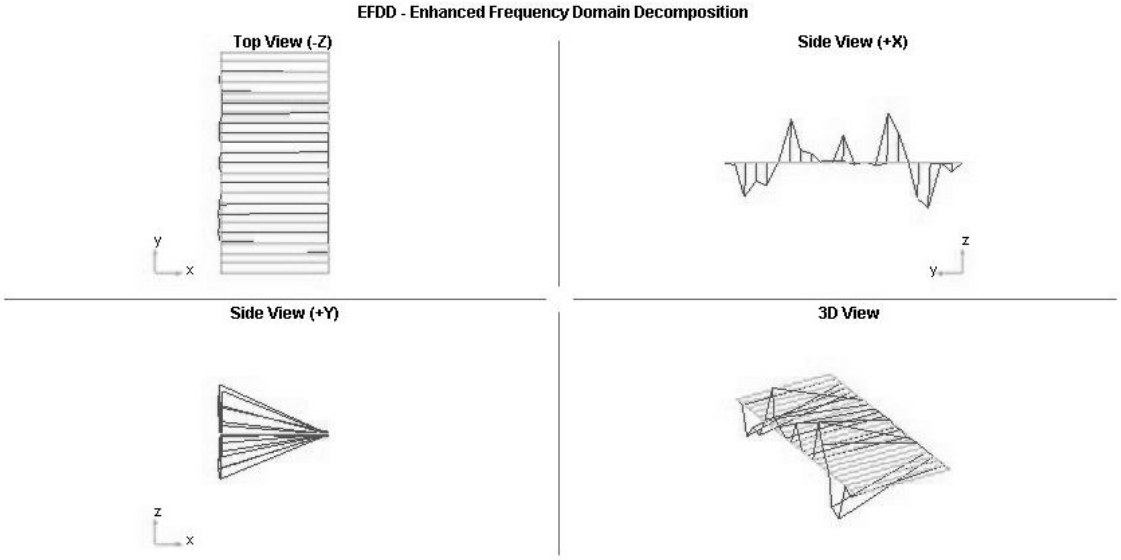

Figure B-6. Fourth structural mode shape obtained from EFDD analysis

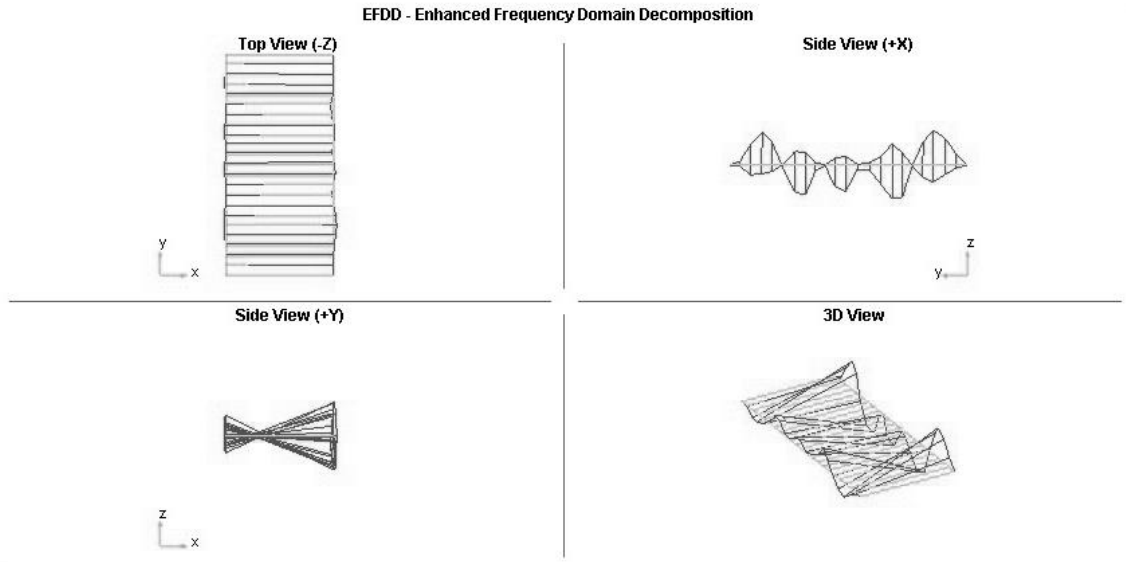

Figure B-7. Fifth structural mode shape obtained from EFDD analysis

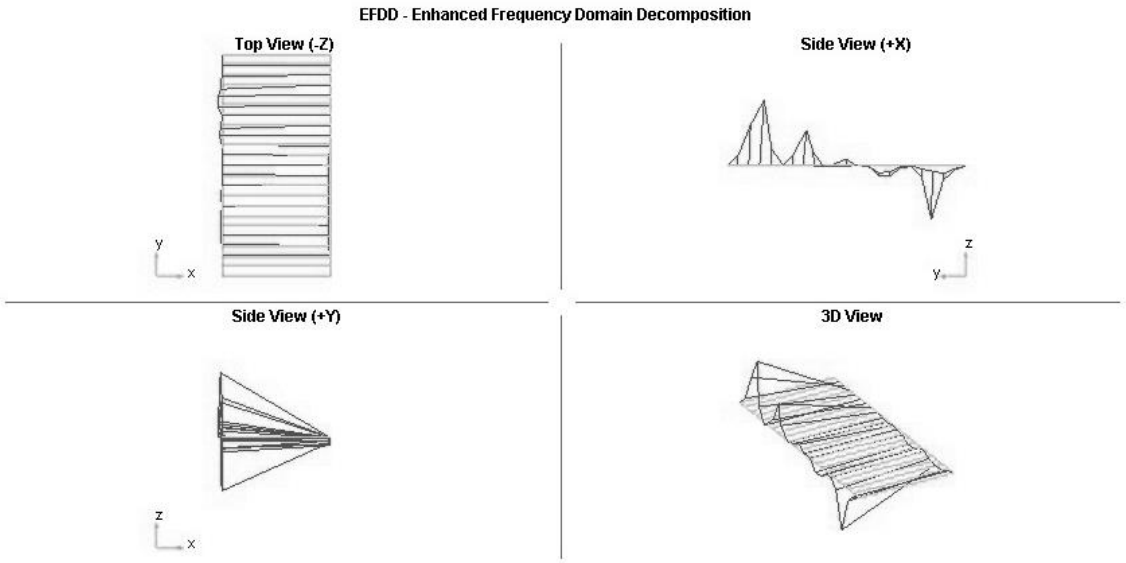

Figure B-8. Sixth structural mode shape obtained from EFDD analysis

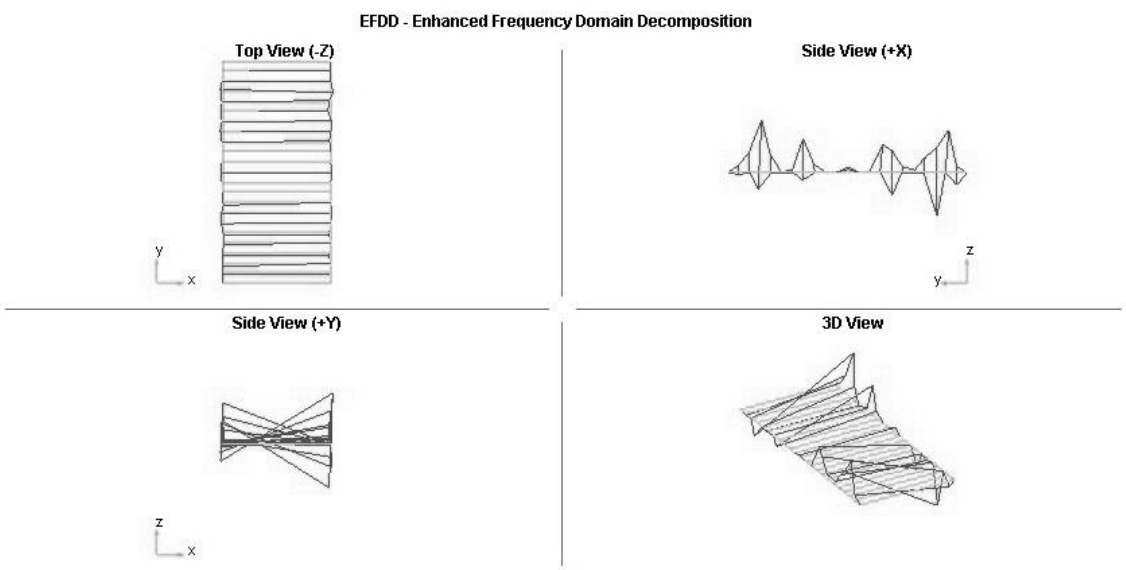

Figure B-9. Seventh structural mode shape obtained from EFDD analysis

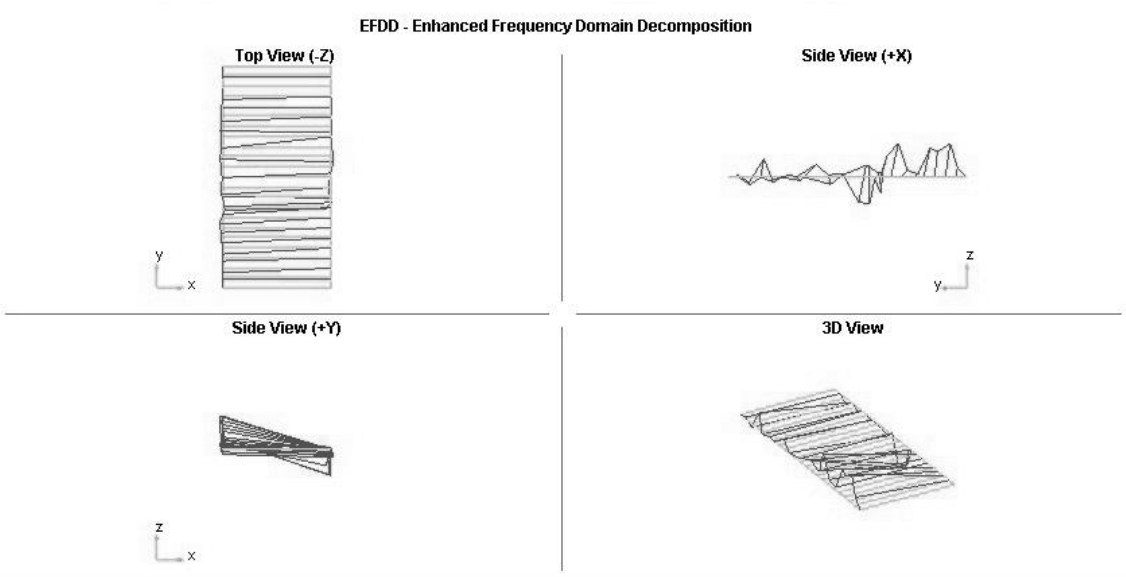

Figure B-10. Eighth structural mode shape obtained from EFDD analysis

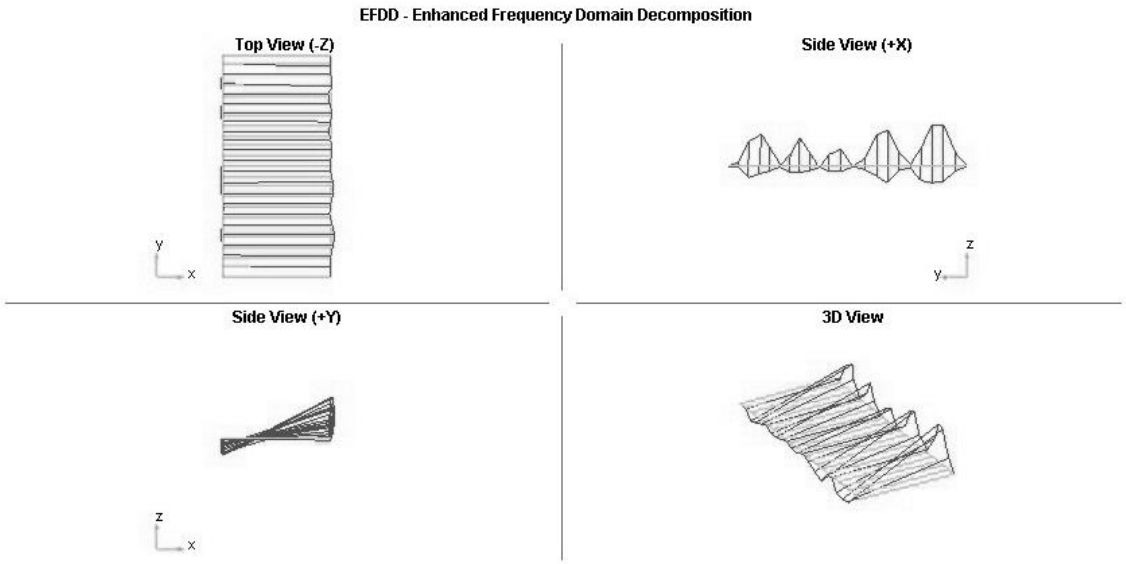

Figure B-11. Ninth structural mode shape obtained from EFDD analysis

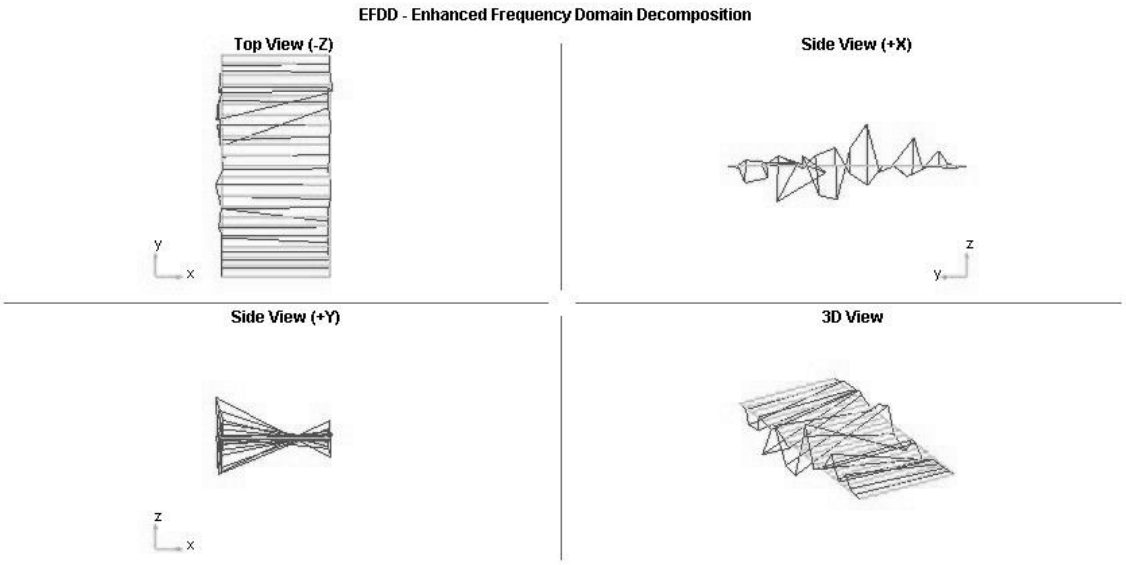

Figure B-12. Tenth structural mode shape obtained from EFDD analysis

APPENDIX C: GROUND MOTION SELECTION

This appendix provides detailed information about Conditional Mean Spectrum (CMS) based ground motion selection performed in chapter 6. It includes seismic hazard deaggregation used in the analysis as well as the MATLAB code developed for ground motion selection. This computer codes selects the most appropriate available ground motion records from PEER-NGA database which offers 3541 ground motion records from 175 earthquakes. Detailed information about the selected ground motion records for the studied bridge in chapter 6 is also provided in this appendix.

C.1 DEAGGREGATION OF MONTREAL SEISMIC HAZARD

Seismic hazard deaggregation provides helpful information regarding the relative contributions of the earthquake sources in terms of distance and magnitude which can be used in various ground motion selection strategies. In this study, the information provided by Geological Survey of Canada (GSC) and the results of Halchuk and Adam's study (2007) is used for deaggregation of Montreal seismic hazard. Figure C-1 presents the deaggregation of Montreal for the probability of 2% in 50 years for various periods.

Hence, for the studied bridge with the first period of 0.7 sec, the mean value of earthquake magnitude and distance of 6.8 and 57 are selected respectively.

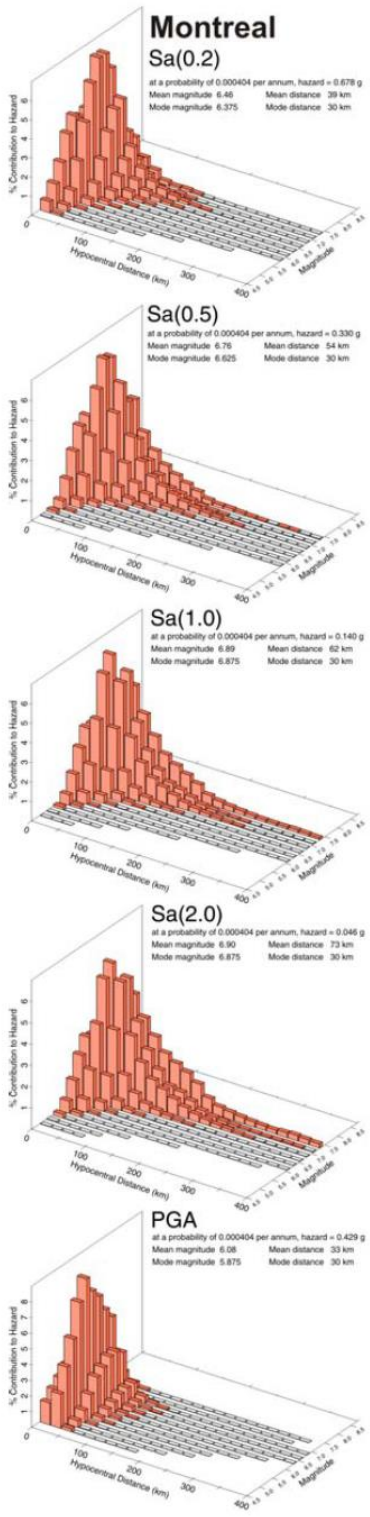

Figure C-1. Deaggregation of Montreal for the probability of 2% in 50 years for various periods (Halchuk and Adam, 2007)

C.2 MATLAB PROGRAM FOR CMS BASED GROUND MOTION SELECTION

A MATLAB code is developed to perform a CMS based ground motion selection analysis. This program uses the Ground Motion Prediction Equations (GMPE) developed by Boore and Atkinson (2006) and Atkinson (2008) to estimate the CMS. The inputs and outputs of the program are as follows:

C.2.1 PROGRAM INPUTS

- Mean values of the magnitude and distance of the earthquake based on seismic hazard deaggregation analysis of the location
- Uniform Hazard Spectrum (UHS) data of the location
- Number of required ground motion records and the range of periods for which the spectrum matching should be done
- Location of the database Excel file

C.2.2 PROGRAM OUTPUTS

- Name of the selected Earthquakes and their record label
- Magnitude, Distance and Epsilon of the selected records
- The address of the selected ground motion records in order to be used in SAP2000 for dynamic time history analysis
- Plots of CMS in comparison with UHS and Predicted Median Spectrum in regular and log-log scales
- Plots of the selected ground motion records spectra in comparison with CMS, UHS and Predicted Median Spectrum

The explained code is presented below:

```
clear all
clc

% INPUTS↙
_____________________________________________________________

% Mean Value of the Seismic Deaggregation
M=6.8;
Rjb=57;

% Vs30 of the Soil and the First Period of the Structure
Vs30=750;
period=0.7;

% Montreal UHS Values
uhs=[0 0.2 0.5 1 2;0.43 0.69 0.34 0.14 0.048];

% Period Range to Match and the Number of Requird Records
high=2; low=0.2; numrec=100;

% The location of the database and the required data in the Excel File
adddata='NGA_Flatfile.xlsx';
adddatasheet='Flatfile';
adddatarange1='DV2:DV10000';
adddatarange2='DY2:HY10000';
adddatarange3='DY1:HY1';
adddatarange4='A2:A10000';
adddatarange5='C2:C10000';
adddatarange6='D2:D10000';
adddatarange7='G2:G10000';
adddatarange8='J2:J10000';
adddatarange9='AV2:AV10000';
adddatarange10='CB2:CB10000';
adddatarange11='DE2:DE10000';


% Ground Motion Prediction Equations (GMPE) _____________________________
% Based on Boore & Atkinson (2006) and Atkinson (2008)
U=1; SS=0; NS=0; RS=0;
time=[0 0.01 0.02 0.03 0.05 0.075 0.1 0.15 0.2 0.25 0.3 0.4 0.5 0.75 ...
    1 1.5 2 3 4 5 7.5 10];
blin=[-0.360 -0.360 -0.340 -0.330 -0.290 -0.230 -0.250 -0.280 -0.310 ...
    -0.390 -0.440 -0.500 -0.600 -0.690 -0.700 -0.720 -0.730 -0.740 ...
    -0.750 -0.750 -0.692 -0.650];
b1=[-0.640 -0.640 -0.630 -0.620 -0.640 -0.640 -0.600 -0.530 -0.520 ...
    -0.520 -0.520 -0.510 -0.500 -0.470 -0.440 -0.400 -0.380 -0.340 ...
    -0.310 -0.291 -0.247 -0.215];
```

```
b2=[-0.14 -0.14 -0.12 -0.11 -0.11 -0.11 -0.13 -0.18 -0.19 -0.16 -0.14 ...
   -0.10 -0.06 0 0 0 0 0 0 0 0 0];
a1=0.03;
pgalow=0.06;
a2=0.09;
V1=180;
V2=300;
Vref=760;
Mref=4.5;
Rref=1;
Mrefpga=5;
c1=[-0.66050 -0.66220 -0.66600 -0.69010 -0.71700 -0.72050 -0.70810 ...
   -0.69610 -0.58300 -0.57260 -0.55430 -0.64430 -0.69140 -0.74080 ...
   -0.81830 -0.83030 -0.82850 -0.78440 -0.68540 -0.50960 ...
   -0.37240 -0.09824];
c2=[0.1197 0.12 0.1228 0.1283 0.1317 0.1237 0.1117 0.09884 0.04273 ...
   0.02977 0.01955 0.04394 0.0608 0.07518 0.1027 0.09793 0.09432 ...
   0.07282 0.03758 -0.02391 -0.06568 -0.13800];
c3=[-0.01151 -0.01151 -0.01151 -0.01151 -0.01151 -0.01151 -0.01151 ...
   -0.01113 -0.00952 -0.00837 -0.00750 -0.00626 -0.00540 -0.00409 ...
   -0.00334 -0.00255 -0.00217 -0.00191 -0.00191 -0.00191 ...
   -0.00191 -0.00191];
h=[1.35 1.35 1.35 1.35 1.35 1.55 1.68 1.86 1.98 2.07 2.14 2.24 2.32 ...
   2.46 2.54 2.66 2.73 2.83 2.89 2.93 3 3.04];
e1=[-0.53804 -0.52883 -0.52192 -0.45285 -0.28476 0.00767 0.20109 0.46128 ...
   0.5718 0.51884 0.43825 0.3922 0.18957 -0.21338 -0.46896 -0.86271 ...
   -1.22652 -1.82979 -2.24656 -1.28408 -1.43145 -2.15446];
e2=[-0.50350 -0.49429 -0.48508 -0.41831 -0.25022 0.04912 0.23102 0.48661 ...
   0.59253  0.53496 0.44516 0.40602 0.19878 -0.19496 -0.43443 -0.79593 ...
   -1.15514 -1.74690 -2.15906 -1.21270 -1.31632 -2.16137];
e3=[-0.75472 -0.74551 -0.73906 -0.66722 -0.48462 -0.20578 0.03058 0.30185 ...
   0.4086 0.3388 0.25356 0.21398 0.00967 -0.49176 -0.78465 -1.20902 ...
   -1.57697 -2.22584 -2.58228 -1.50904 -1.81022 -2.53323];
e4=[-0.50970 -0.49966 -0.48895 -0.42229 -0.26092 0.02706 0.22193 0.49328 ...
   0.61472 0.57747 0.5199 0.4608 0.26337 -0.10813 -0.39330 -0.88085 ...
   -1.27669 -1.91814 -2.38168 -1.41093 -1.59217 -2.14635];
e5=[0.28805 0.28897 0.25144 0.17976 0.06369 0.0117 0.04697 0.1799 0.52729 ...
   0.6088 0.64472 0.7861 0.76837 0.75179 0.6788 0.70689 0.77989 0.77966 ...
   1.24961 0.14271 0.52407 0.40387];
e6=[-0.10164 -0.10019 -0.11006 -0.12858 -0.15752 -0.17051 -0.15948 ...
   -0.14539 -0.12964 -0.13843 -0.15694 -0.07843 -0.09054 -0.14053 ...
   -0.18257 -0.25950 -0.29657 -0.45384 -0.35874 -0.39006 -0.37578 -0.48492];
e7=[0 0 0 0 0 0 0 0 0.00102 0.08607 0.10601 0.02262 0 0.10302 0.05393 ...
   0.19082 0.29888 0.67466 0.79508 0 0 0];
Mh=[6.75 6.75 6.75 6.75 6.75 6.75 6.75 6.75 6.75 6.75 6.75 6.75 6.75 ...
   6.75 6.75 6.75 6.75 6.75 6.75 8.5 8.5 8.5];
std1=[0.566 0.569 0.569 0.578 0.589 0.606 0.608 0.592 0.596 0.592 0.608 ...
```

```
    0.603 0.615 0.649 0.654 0.684 0.702 0.7 0.702 0.73 0.781 0.735];

tt=[5 2 1 0.5 0.2 0.1 0];
jcc1=[-1.07E-03 5.20E-04 5.56E-04 1.13E-03 1.44E-03 1.24E-03 1.20E-03];
jcc2=[1.49E-06 3.76E-07 7.44E-07 6.98E-07 1.27E-06 1.99E-06 2.30E-06];
jcc0=[-0.271 -0.419 -0.376 -0.364 -0.102 0.143 0.287];
jstd2=[0.284 0.379 0.288 0.368 0.290 0.234 0.331];

for i=1:max(size(time))
    R(i)=sqrt(Rjb^2+h(i).^2);
    Fd(i)=(c1(i)+c2(i)*(M-Mref))*log(R(i)/Rref);

    if M<=Mh(i)
        Fm(i)=e1(i)*U+e2(i)*SS+e3(i)*NS+e4(i)*RS+e5(i)*(M-Mh(i))+...
            e6(i)*(M-Mh(i))^2;
    else
        Fm(i)=e1(i)*U+e2(i)*SS+e3(i)*NS+e4(i)*RS+e7(i)*(M-Mh(i));
    end
end

pga4nl=exp(Fm(1)+Fd(1));
deltax=log(a2/a1);

for j=1:max(size(time))
    Flin(j)=blin(j)*log(Vs30/Vref);
    if Vs30<=V1
        bnl(j)=b1(j);
    elseif Vs30<=V2
        bnl(j)=(b1(j)-b2(j))*log(Vs30/V2)/log(V1/V2)+b2(j);
    elseif Vs30<=Vref
        bnl(j)=b2(j)*log(Vs30/Vref)/log(V2/Vref);
    else
        bnl(j)=0;
    end
    deltay(j)=bnl(j)*log(a2/pgalow);
    c(j)=(3*deltay(j)-bnl(j)*deltax)/(deltax^2);
    d(j)=-(2*deltay(j)-bnl(j)*deltax)/(deltax^3);
    if pga4nl<=a1
        Fnl(j)=bnl(j)*log(pgalow/0.1);
    elseif pga4nl<=a2
        Fnl(j)=bnl(j)*log(pgalow/0.1)+c(j)*(log(pga4nl/a1))^2+d(j)*...
            (log(pga4nl/a1))^3;
    else
        Fnl(j)=bnl(j)*log(pga4nl/0.1);
    end
    Fs(j)=Flin(j)+Fnl(j);
end
```

```
for k=1:max(size(time))
   cc1(k)=interp1(tt,jcc1,time(k));
   cc2(k)=interp1(tt,jcc2,time(k));
   cc0(k)=interp1(tt,jcc0,time(k));
   std2(k)=interp1(tt,jstd2,time(k));
   F(k)=cc0(k)+cc1(k).*Rjb+cc2(k).*Rjb^2;
end
mmxx1=Fm+Fd+Fs;
mmxx=Fm+Fd+Fs+F;
ssxx=sqrt(std1.^2+std2.^2);
% ssxx=std1;

mmxx(end-1:end)=[];
mmxx1(end-1:end)=[];
ssxx(end-1:end)=[];
time(end-1:end)=[];


% Calculation of CMS↙
_____________________________________________________

time2=linspace(0,5,400);
mmx=interp1(time,mmxx,time2);
ssx=interp1(time,ssxx,time2);


median=logninv(normcdf(0,0,1),mmx,ssx);
[mean,sstd]=lognstat(mmx,ssx);
std=sqrt(sstd);

% Epsilon
epsilon1=(interp1(log(uhs(1,:)),log(uhs(2,:)),log(period))- ...
   interp1(time2,mmx,period))/interp1(time2,ssx,period);
% epsilon1=(log(interp1(uhs(1,:),uhs(2,:),period))- ...
%   interp1(time2,mmx,period))/interp1(time2,ssx,period);


% Correlation of Epsilon at various Periods
for l=1:max(size(std))
   tmax=max(period,time2(l));
   tmin=min(period,time2(l));
   D1(l)=1-cos(pi/2-0.366*log(tmax/max(tmin,0.109)));
   if tmax<0.2
      D2(l)=1-0.105*(1-1/(1+exp(100*tmax-5)))*(tmax-tmin)/(tmax-0.0099);
   else
      D2(l)=0;
```

```
    end
    if tmax<0.109
        D3(l)=D2(l);
    else
        D3(l)=D1(l);
    end
    D4(l)=D1(l)+0.5*(sqrt(D3(l))-D3(l))*(1+cos(pi*tmin/0.109));
    if tmax<0.109
        weight(l)=D2(l);
    elseif tmin>0.109
        weight(l)=D1(l);
    elseif tmax<0.2
        weight(l)=min(D2(l),D4(l));
    else
        weight(l)=D4(l);
    end
%     weight2(l)=1-cos(pi/2-(0.359+0.163*floor((tmin-0.189)/tmin)*...
%         log(tmin/0.189))*log(tmax/tmin));
end


epsilon=epsilon1.*weight;

% CMS Vector
CMS=exp(mmx+epsilon.*ssx);

mm=logninv(normcdf(0,0,1),mmx,ssx);
sigmacond=ssx.*sqrt(ones(size(ssx))-weight.^2);

% Log-Log plot of CMS Vs UHS
loglog(time2,mm,'r','LineWidth',2.5)
% axes('FontName','Times New Roman','FontSize',25)
hold on
% loglog(time2,median,'o')
loglog(time2,CMS,'g','LineWidth',2.5)
uu2=logninv(normcdf(epsilon1,0,1),mmx,ssx);
% loglog(time2,uu2,'c')
loglog(uhs(1,:),uhs(2,:),'LineWidth',2.5)
grid on
legend('Predicted Median Spectrum (M=6.8 , R=57 km)', ...
    'Conditional Mean Spectrum (CMS)', ...
    '2%/50 years UHS');

% Plot of CMS Vs Predicted Median Spectrum
figure
axes('FontName','Times New Roman','FontSize',35)
hold on
```

```
% plot(time2,uu)
plot(time2,mm,'r','LineWidth',2.5)
% plot(time2,medianint,'o')
plot(time2,CMS,'k','LineWidth',2.5)
uu2=logninv(normcdf(epsilon1,0,1),mmx,ssx);
% plot(time2,uu2,'--','LineWidth',2.5)
plot(uhs(1,:),uhs(2,:),'--','LineWidth',2.5)
% legend('Predicted Median Spectrum (M=6.8 , R=57 km)', ...
%     'Predicted Median plus epsilon*sigma (M=6.8 , R=57 km)', ...
%     '2%/50 years UHS');
legend('Predicted Median Spectrum (M=6.8 , R=57 km)', ...
   'Conditional Mean Spectrum (CMS)', ...
   'Predicted Median plus epsilon*sigma (M=6.8 , R=57 km)');
% legend('Predicted Median Spectrum (M=6.8 , R=57 km)', ...
%     'Predicted Median plus epsilon*sigma (M=6.8 , R=57 km)', ...
%     '2%/50 years UHS');
legend('Predicted Median Spectrum (M=6.8 , R=57 km)', ...
   'Conditional Mean Spectrum (CMS)', ...
   '2%/50 years UHS');
xlabel('T (sec)');
ylabel('Sa (g)');
% ll=logninv(normcdf(-1,0,1),mmx,ssx);
% ll2=logninv(normcdf(-2,0,1),mmx,ssx);
% plot(time2,ll,'--')
% plot(time2,ll2,'c--')

% Reading Data from Database
data3=xlsread(adddata,adddatasheet,adddatarange1);
data4=xlsread(adddata,adddatasheet,adddatarange2);
[~,data5]=xlsread(adddata,adddatasheet,adddatarange3);
number=xlsread(adddata,adddatasheet,adddatarange4);
[~,recname]=xlsread(adddata,adddatasheet,adddatarange5);
[~,recyear]=xlsread(adddata,adddatasheet,adddatarange6);
[~,recstat]=xlsread(adddata,adddatasheet,adddatarange7);
recmag=xlsread(adddata,adddatasheet,adddatarange8);
recdis=xlsread(adddata,adddatasheet,adddatarange9);
recvs30=xlsread(adddata,adddatasheet,adddatarange10);
[~,recadd]=xlsread(adddata,adddatasheet,adddatarange11);

timer(1,1)=0;
for i=1:max(size(data5))
   as=data5{i};
   timer(i+1,1)=str2num(as(2:end-1));
end
data(:,1)=data3; data(:,2:size(data4,2)+1)=data4;
data(find(isnan(data3)),:)=[];
number(find(isnan(data3)),:)=[];
```

```
% figure
% hold on
% plot(time2,mm,'r')
% for i=25:35
% plot(timer,data(i,:))
% end

% Matching Available Ground Motion Records with CMS and Ground Motion
% Selection Procedure _____________________________________________
[~,index1]=min(abs(timer-low*period));
[~,index2]=min(abs(timer-high*period));
[~,index3]=min(abs(timer-period));

CMS2=interp1(time2,CMS,timer(index1:index2));
scale=interp1(time2,CMS,period).*ones(size(data,1),1)./data(:,index3);
% receps=(log(data(:,index3))-(interp1(time2,mmx,period) ...
%     .*ones(size(data,1),1))./interp1(time2,ssx,period);
scaleddata=scale*ones(1,size(data,2)).*data;
res1=(scaleddata(:,index1:index2)-ones(size(data,1),1)*CMS2').^2;
res=sum(res1');
[~,sortrec]=sort(res);
select=sortrec(1:numrec);

% Plotting the Selected Ground Motion Records Vs CMS
figure
axes('FontName','Times New Roman','FontSize',25)
hold on
ha=area([period/5 2*period],[1 1]);
set(ha,'FaceColor',[0.9 0.9 0.9])
plot(time2,mm,'r','LineWidth',2.5)
plot(time2,CMS,'k','LineWidth',2.5)
plot(time2,uu2,'--','LineWidth',2.5)
for i=1:10
plot(timer,scaleddata(select(i),:),'g')
end
legend('Period used for matching',...
   'Predicted Median Spectrum (M=6.8 , R=57 km)', ...
   'Conditional Mean Spectrum (CMS)', ...
   'Predicted Median plus epsilon*sigma (M=6.8 , R=57 km)', ...
   'Top 10 selected spectra');
xlabel('T (sec)');
ylabel('Sa (g)');
axis([0 3 0 1])
% ha=area([period/5 2*period],[1 1]);

figure
```

```
axes('FontName','Times New Roman','FontSize',25)
hold on
ha=area([period/5 2*period],[1 1]);
set(ha,'FaceColor',[0.9 0.9 0.9])
plot(time2,CMS,'k','LineWidth',2.5)
for i=1:10
plot(timer,scaleddata(select(i),:),'g')
end
plot(time2,exp(log(CMS)+sigmacond),'LineWidth',2.5);
plot(time2,exp(log(CMS)-sigmacond),'LineWidth',2.5);
axis([0 3 0 1])
legend('Period used for matching',...
   'Period used for matching',...
   'Conditional Mean Spectrum (CMS)', ...
   'CMS +/- conditional sigma', ...
   'Top 10 selected spectra');
xlabel('T (sec)');
ylabel('Sa (g)');


% Outputs↙
```

```
line=number(select);
numtot=size(number,1);
selname=recname(line);
selyear=recyear(line);
selstat=recstat(line);
selmag=recmag(line);
seldis=recdis(line);
selvs30=recvs30(line);
seladd=recadd(line);
meanmag=sum(selmag)/numrec;
meandis=sum(seldis)/numrec;
meanvs30=sum(selvs30)/numrec;
magsort=sort(selmag);
dissort=sort(seldis);
vs30sort=sort(selvs30);
if numrec/2==floor(numrec/2)
   medmag=sum(magsort(numrec/2)+magsort(numrec/2+1))/2;
   meddis=sum(dissort(numrec/2)+dissort(numrec/2+1))/2;
   medvs30=sum(vs30sort(numrec/2)+vs30sort(numrec/2+1))/2;
else
   medmag=magsort((numrec+1)/2);
   meddis=dissort((numrec+1)/2);
   medvs30=vs30sort((numrec+1)/2);
end
```

C.3 DETAILED INFORMATION OF THE SELECTED GROUND MOTION RECORDS

Table C-1. Detailed information of 40 selected ground motion records for dynamic time history analysis of the studied bridge

NO.	Earthquake Name	Event ID	Mag. (M)	Distance (km)	PGA	PGV	ε (T=0.7)
1	'Chi-Chi, Taiwan-06'	3302	6.3	84.3	0.15	9.8	-1.39
2	'Chi-Chi, Taiwan-06'	3471	6.3	36.0	0.08	4.7	-0.61
3	'Chi-Chi, Taiwan-02'	2211	5.9	88.2	0.03	1.7	0.94
4	'Imperial Valley-07'	201	5.01	15.3	0.14	6.7	-1.03
5	'Chi-Chi, Taiwan-02'	2162	5.9	80.5	0.03	1.5	1.19
6	'Chi-Chi, Taiwan-02'	2170	5.9	82.3	0.02	1.1	1.51
7	'Imperial Valley-07'	195	5.01	11.9	0.09	6.5	-0.85
8	'Coalinga-05'	412	5.77	16.2	0.43	24.2	-2.94
9	'Chi-Chi, Taiwan-05'	2982	6.2	84.1	0.09	8.1	-1.04
10	'Hector Mine'	1832	7.13	93.9	0.05	8.0	-0.22
11	'Victoria, Mexico'	268	6.33	58.9	0.08	8.3	-0.96
12	'Irpinia, Italy-01'	284	6.9	33.1	0.06	6.1	-0.29
13	'Chi-Chi, Taiwan-05'	3251	6.2	92.3	0.05	2.5	0.12
14	'Hector Mine'	1836	7.13	68.4	0.06	6.0	-0.26
15	'Chi-Chi, Taiwan-06'	3473	6.3	17.9	0.34	26.2	-2.95
16	'Northridge-01'	1032	6.69	52.7	0.14	11.8	-1.80
17	'Big Bear City'	2125	4.92	85.6	0.01	0.5	2.79
18	'Hector Mine'	1842	7.13	127.9	0.05	5.3	-0.01
19	'Northridge-01'	1051	6.69	20.4	1.43	75.5	-4.89
20	'Big Bear City'	2135	4.92	119.4	0.01	0.5	2.87
21	'Mammoth Lakes-07'	253	4.73	4.6	0.03	1.9	1.01
22	'Chi-Chi, Taiwan-05'	3171	6.2	73.7	0.04	3.3	0.05
23	'Chi-Chi, Taiwan'	1281	7.62	62.2	0.14	8.5	-1.24
24	'Chi-Chi, Taiwan-03'	2635	6.2	10.5	0.09	6.6	-0.88
25	'Whittier Narrows-01'	658	5.99	66.4	0.04	2.3	0.16
26	'Chi-Chi, Taiwan-05'	2988	6.2	99.4	0.05	6.2	-0.21
27	'Chi-Chi, Taiwan-02'	2375	5.9	41.5	0.04	2.9	0.23
28	'Landers'	855	7.28	121.0	0.13	12.4	-1.45
29	'Chi-Chi, Taiwan-03'	2541	6.2	63.6	0.01	0.6	2.37
30	'Chi-Chi, Taiwan-05'	2950	6.2	60.0	0.10	7.2	-0.99
31	'Tabas, Iran'	139	7.35	20.6	0.35	28.2	-2.97
32	'Chi-Chi, Taiwan-02'	2303	5.9	90.3	0.01	0.4	2.93
33	'San Fernando'	51	6.61	71.1	0.03	3.7	0.51
34	'Denali, Alaska'	2115	7.9	189.7	0.08	12.4	-0.37
35	'Chi-Chi, Taiwan-05'	3025	6.2	47.2	0.05	4.1	-0.07
36	'Loma Prieta'	737	6.93	40.1	0.15	21.1	-2.01
37	'Imperial Valley-06'	164	6.53	24.8	0.18	14.0	-2.28
38	'Northridge-01'	964	6.69	47.5	0.11	7.2	-1.18
39	'Whittier Narrows-01'	692	5.99	11.7	0.43	28.3	-3.34
40	'Chi-Chi, Taiwan-05'	2948	6.2	84.4	0.06	4.8	-0.13

APPENDIX D: DETAILED RESULTS OF INCREMENTAL DYNAMIC ANALYSIS OF THE STUDIED BRIDGE IN CHAPTER 5 AND 6

In chapter 6, IDA was used to evaluate seismic response of the studied bridge over a range of ground motion intensities. The IDA was performed on the studied bridge using 40 ground motion records each scaled by 50 various scaling factors to evaluate the component damage states at various ground motion intensities in the range of $Sa(T_1)$= (0,1.5g).

The damage states of the following 15 components are evaluated at each ground motion intensity:

- 4 columns
- 4 bearings on top of the columns
- 2 abutments
- 2 bearings on the abutments
- 2 Wing walls
- The pile group at one end of the bridge (The other end is supported by a footing located on the bed rock)

This appendix provides detailed results obtained from IDA. It includes tables demonstrating the seismic intensities at which each structural component exceeds the specified limit states. In addition, probabilistic model of structural demands and capacities at selected ground motion intensities are presented in this appendix.

D.1 GROUND MOTION INTENSITIES CORRESPONDING TO DIFFERENT COMPONENT FAILURES

Table D-1 and D-2 present the ground motion intensities at which each component exceeds serviceability and collapse limit states respectively. It is noted that over the specified range of Sa, only bearings exceed the defined limit states and the other components are protected and remain in the range of serviceability.

Table D-1. Spectral Accelerations at which the bearings exceed serviceability limit state

Earthquake NO.	Bearing 1 (at the abutment 1)	Bearing 2	Bearing 3	Bearing 4	Bearing 5	Bearing 6 (at the abutment 2)
1	1.44	0.57	0.40	0.31	0.66	0.76
3	0.30	0.59	0.51	0.35	0.64	0.80
4	0.22	0.32	0.32	0.22	0.36	0.48
5	0.41	0.53	0.42	0.29	0.62	0.87
6	0.36	0.48	0.34	0.25	0.54	0.78
7	0.40	0.39	0.48	0.33	0.42	0.83
8	0.30	0.32	0.29	0.19	0.34	0.53
9	0.38	0.64	0.56	0.43	0.72	0.95
10	0.44	0.54	0.44	0.30	0.59	0.94
11	0.38	0.57	0.33	0.24	0.59	0.88
12	0.34	0.64	0.50	0.33	0.64	0.96
13	0.28	0.55	0.28	0.18	0.53	0.76
14	0.37	0.47	0.29	0.20	0.50	0.86
15	0.30	0.50	0.29	0.23	0.57	0.71
16	0.32	0.46	0.28	0.20	0.49	0.73
17	1.93	0.66	0.38	0.27	0.81	1.05
19	0.47	0.67	0.46	0.33	0.63	0.98
20	0.43	0.70	0.38	0.27	0.63	0.98
21	1.91	0.87	0.54	0.36	0.90	1.19
22	0.34	0.59	0.46	0.32	0.56	0.91
23	0.33	0.53	0.46	0.32	0.57	0.83
24	0.34	0.45	0.51	0.36	0.50	0.87
25	0.22	0.46	0.36	0.27	0.52	0.59
26	0.38	0.46	0.38	0.28	0.53	0.91
27	0.36	0.53	0.34	0.22	0.50	0.96
28	0.35	0.58	0.39	0.30	0.63	0.94
29	0.32	0.61	0.45	0.31	0.67	0.98
30	0.36	0.60	0.40	0.28	0.70	1.17
31	0.41	0.60	0.48	0.31	0.60	0.99
32	0.42	0.63	0.51	0.34	0.71	0.81
33	0.40	0.66	0.47	0.32	0.57	0.96
34	0.33	0.61	0.40	0.27	0.56	0.96
35	0.29	0.57	0.34	0.25	0.54	0.81
36	0.25	0.45	0.31	0.23	0.50	0.64
37	0.36	0.60	0.45	0.34	0.65	0.74
38	0.33	0.59	0.38	0.28	0.64	0.77
39	0.39	0.57	0.36	0.25	0.75	0.79
40	0.24	0.48	0.45	0.31	0.51	0.70

Table D-2. Spectral Accelerations at which the bearings exceed collapse limit state

Earthquake NO.	Bearing 1 (at the abutment 1)	Bearing 2	Bearing 3	Bearing 4	Bearing 5	Bearing 6 (at the abutment 2)
1	1.44	-	-	-	-	-
3	0.84	-	-	-	-	0.88
4	1.23	-	-	-	-	1.31
5	-	-	-	-	-	-
6	1.02	-	-	-	-	1.08
7	0.88	-	-	-	-	0.81
8	1.41	-	-	-	-	-
9	-	-	-	-	-	-
10	1.40	-	-	-	-	1.32
11	-	-	-	-	-	-
12	1.37	-	-	-	-	1.48
13	1.47	-	-	-	-	1.45
14	1.23	-	-	-	-	1.19
15	1.21	-	-	-	-	-
16	-	-	-	-	-	-
17	-	-	-	-	-	-
19	-	-	-	-	-	-
20	1.23	-	-	-	-	-
21	1.20	-	-	-	-	1.24
22	1.10	-	-	-	-	1.21
23	1.18	-	-	-	-	1.29
24	1.13	-	-	-	-	1.26
25	1.42	-	-	-	-	-
26	-	-	-	-	-	-
27	1.48	-	-	-	-	-
28	1.48	-	-	-	-	-
29	-	-	-	-	-	-
30	-	-	-	-	-	-
31	-	-	-	-	-	-
32	-	-	-	-	-	-
33	1.16	-	-	-	-	1.30
34	1.02	-	-	-	-	1.21
35	1.44	-	-	-	-	1.39
36	-	-	-	-	-	-
37	1.40	-	-	-	-	-
38	1.19	-	-	-	-	1.21
39	0.39	0.57	0.36	0.25	0.75	0.79
40	0.24	0.48	0.45	0.31	0.51	0.70

D.2 COMPONENT PROBABILISTIC DEMAND AND CAPACITY MODELS AT SELECTED GROUND MOTION INTENSITIES

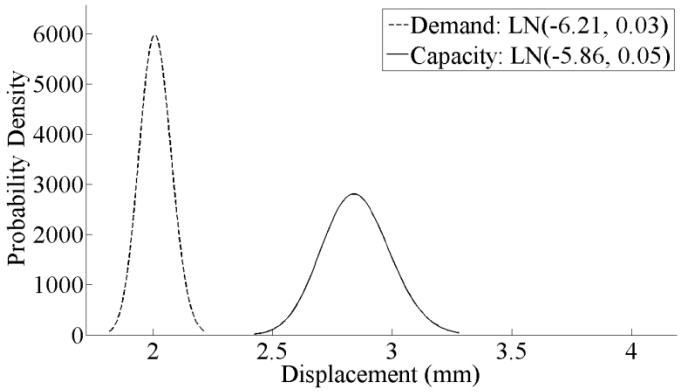

(a) Sa=0.09g

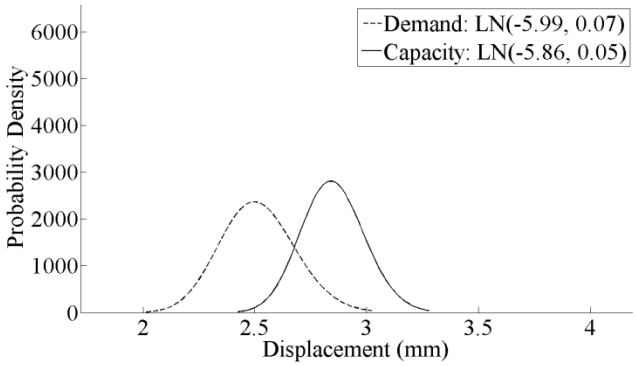

(b) Sa=0.24gg

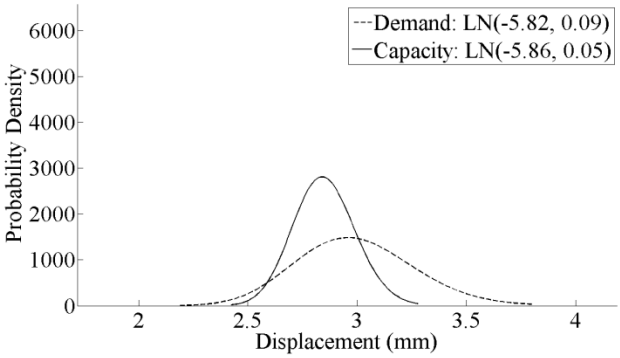

(c) Sa=0.39g

Figure D-1. Probabilistic models of the demand and capacity of bearing 1 for serviceability limit state, given that a) Sa=0.09, b) Sa=0.24 and c) Sa=0.39

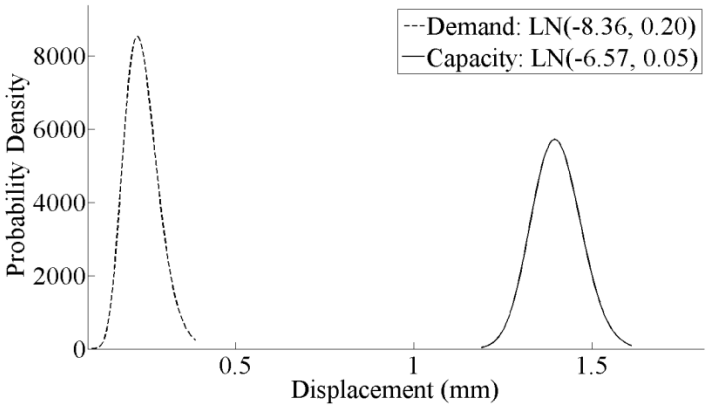

(a) Sa=0.09g

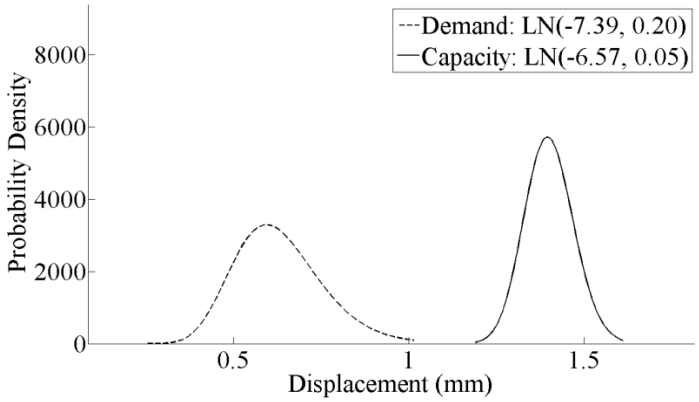

(b) Sa=0.24g

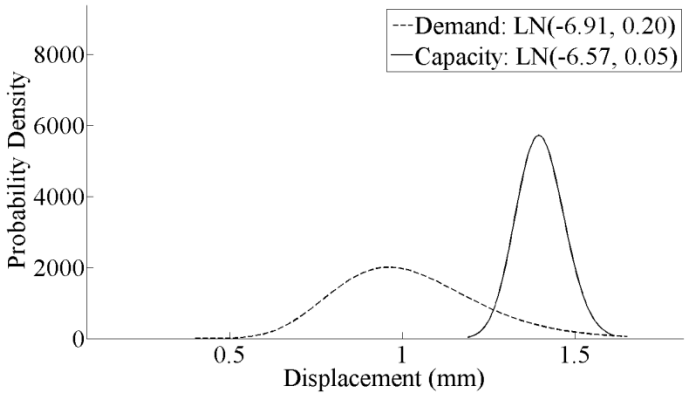

(c) Sa=0.39g

Figure D-2. Probabilistic models of the demand and capacity of bearing 2 for serviceability limit state, given that a) Sa=0.09, b) Sa=0.24 and c) Sa=0.39

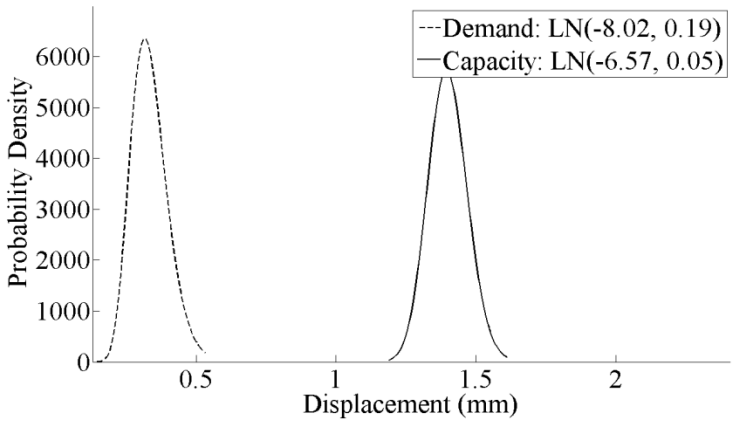

(a) Sa=0.09g

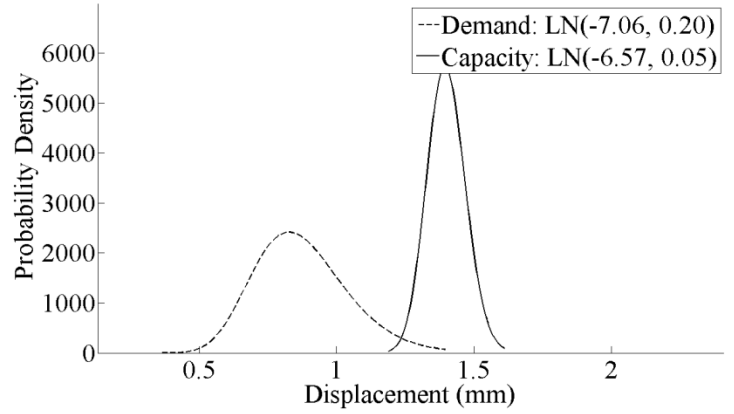

(b) Sa=0.24g

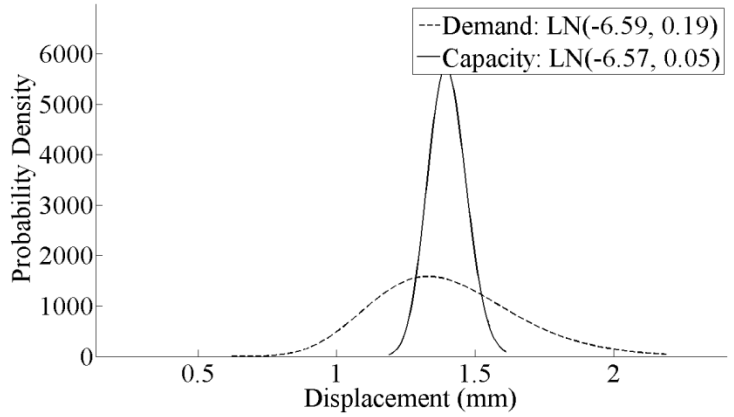

(c) Sa=0.39g

Figure D-3. Probabilistic models of the demand and capacity of bearing 3 for serviceability limit state, given that a) Sa=0.09, b) Sa=0.24 and c) Sa=0.39

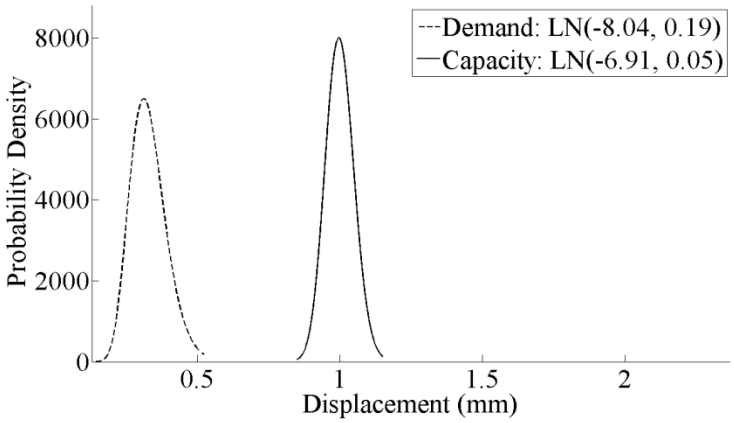

(a) Sa=0.09g

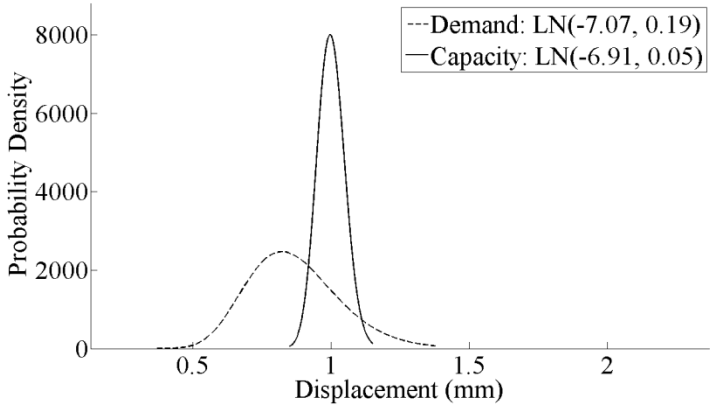

(b) Sa=0.24g

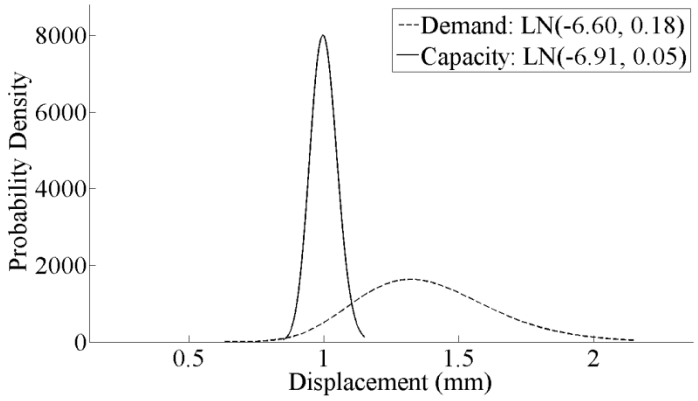

(c) Sa=0.39g

Figure D-4. Probabilistic models of the demand and capacity of bearing 4 for serviceability limit state, given that a) Sa=0.09, b) Sa=0.24 and c) Sa=0.39

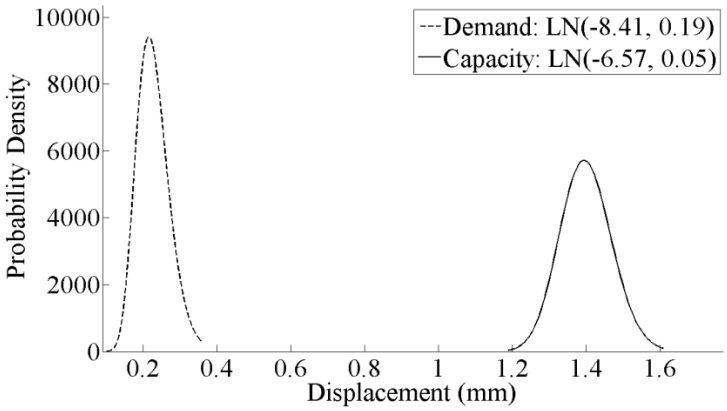

(a) Sa=0.09g

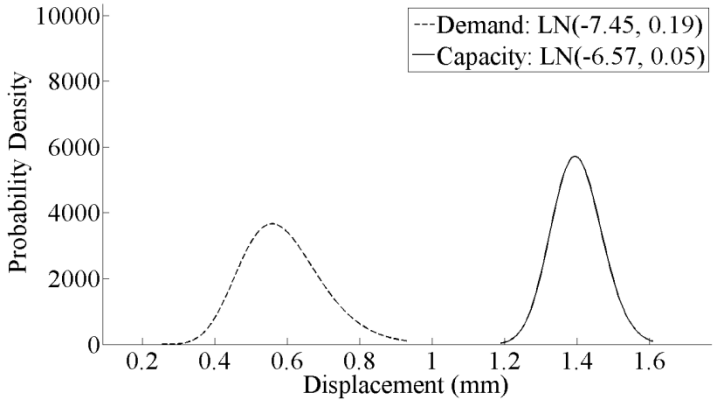

(b) Sa=0.24g

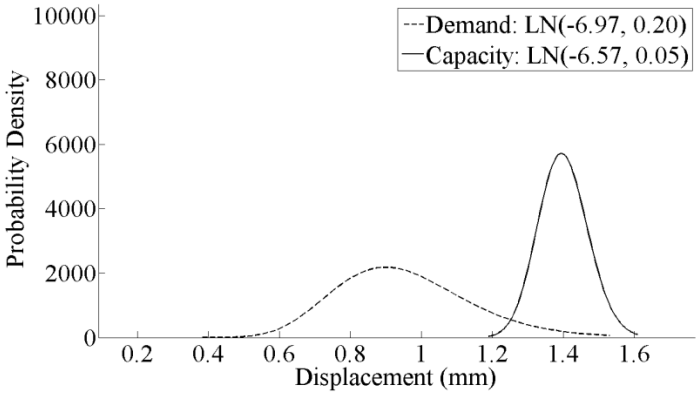

(c) Sa=0.39g

Figure D-5. Probabilistic models of the demand and capacity of bearing 5 for serviceability limit state, given that a) Sa=0.09, b) Sa=0.24 and c) Sa=0.39

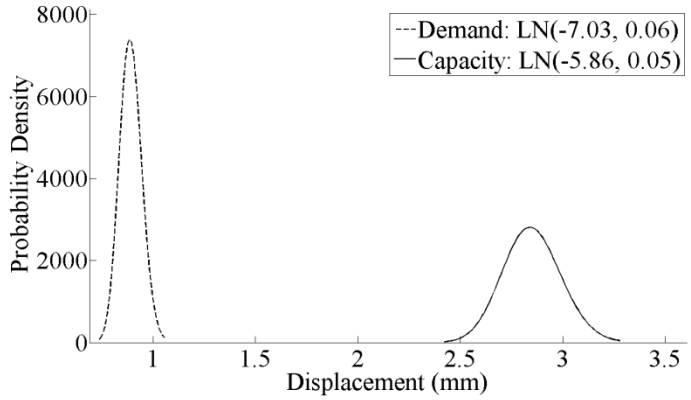

(a) Sa=0.09g

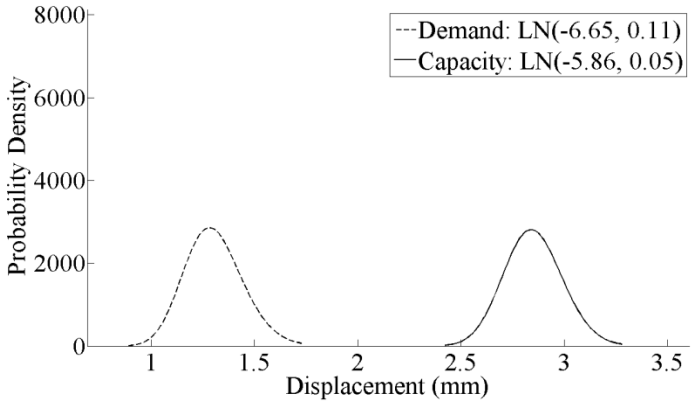

(b) Sa=0.24g

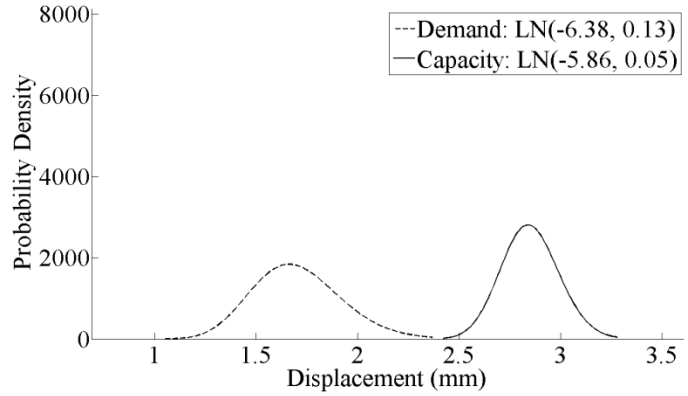

(c) Sa=0.39g

Figure D-6. Probabilistic models of the demand and capacity of bearing 6 for serviceability limit state, given that a) Sa=0.09, b) Sa=0.24 and c) Sa=0.39

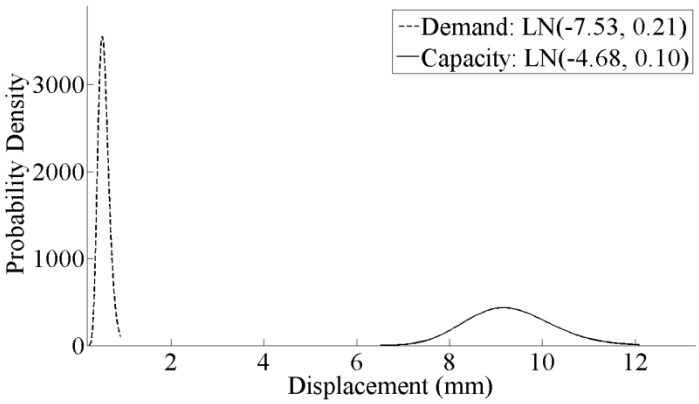

(a) Sa=0.51g

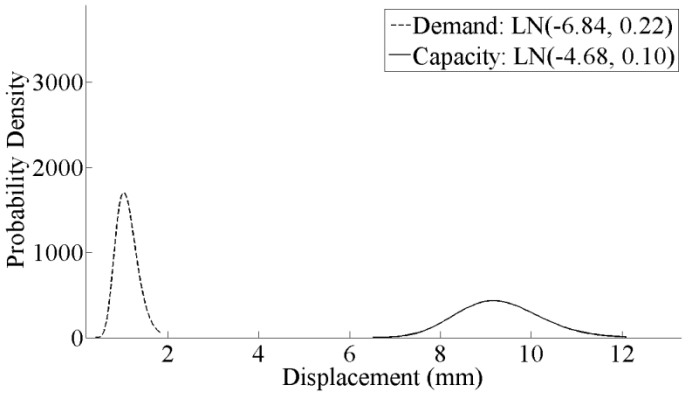

(b) Sa=0.99g

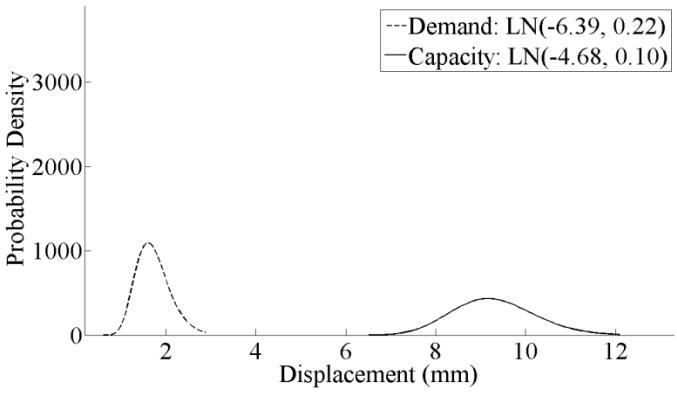

(c) Sa=1.5g

Figure D-7. Probabilistic models of the demand and capacity of column 1 for serviceability limit state, given that a) Sa=0.51, b) Sa=0.99 and c) Sa=1.5

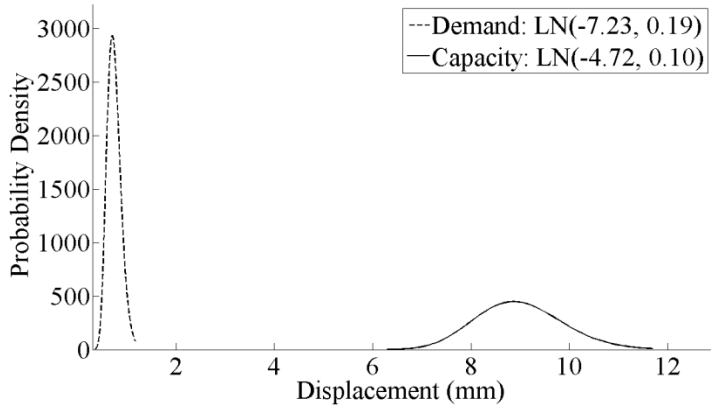

(a) Sa=0.51g

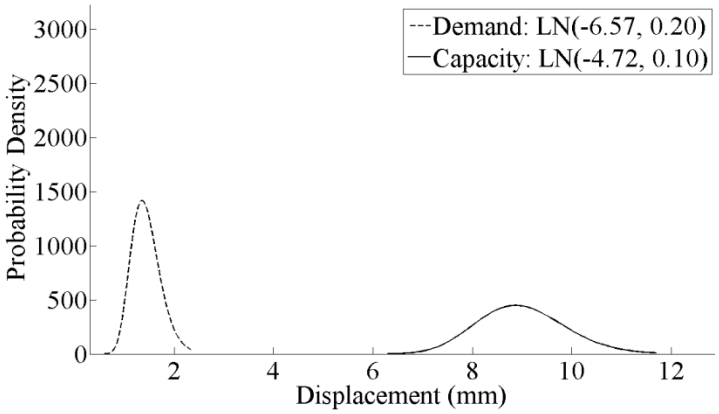

(b) Sa=0.99g

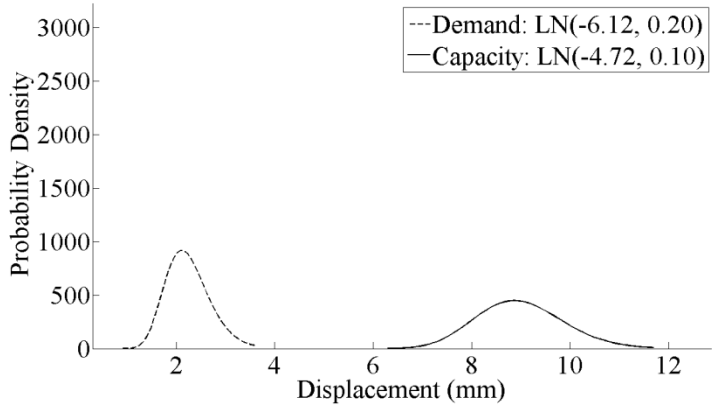

(c) Sa=1.5g

Figure D-8. Probabilistic models of the demand and capacity of column 2 for serviceability limit state, given that a) Sa=0.51, b) Sa=0.99 and c) Sa=1.5

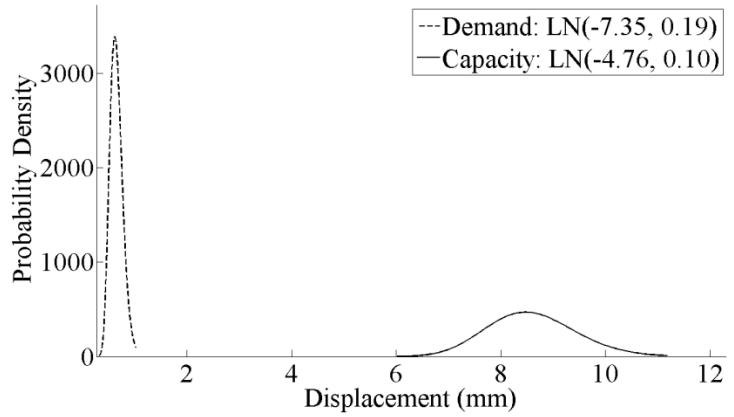

(a) Sa=0.51g

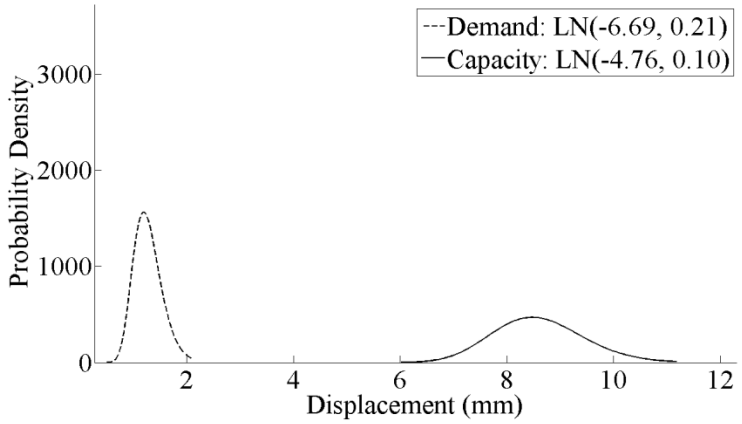

(b) Sa=0.99g

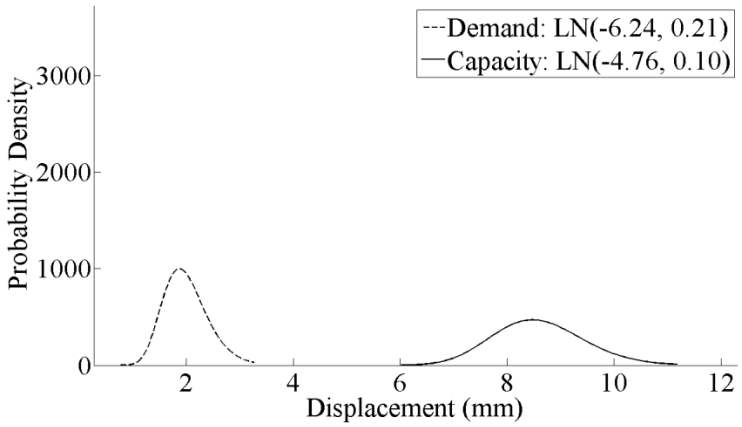

(c) Sa=1.5g

Figure D-9. Probabilistic models of the demand and capacity of column 3 for serviceability limit state, given that a) Sa=0.51, b) Sa=0.99 and c) Sa=1.5

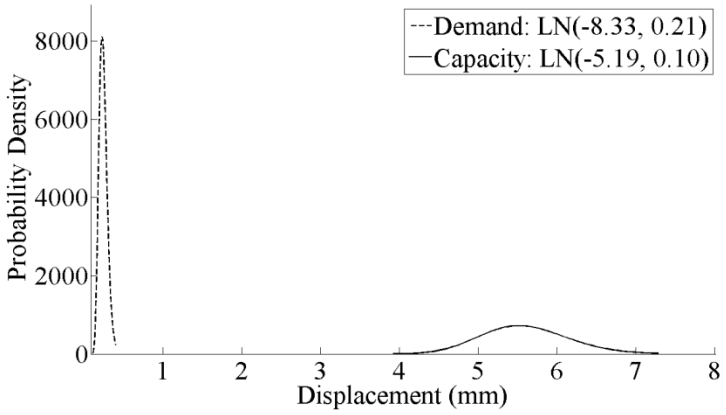

(a) Sa=0.51g

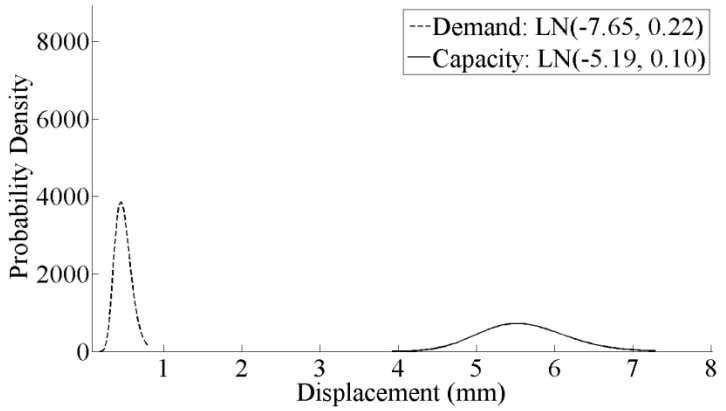

(b) Sa=0.99g

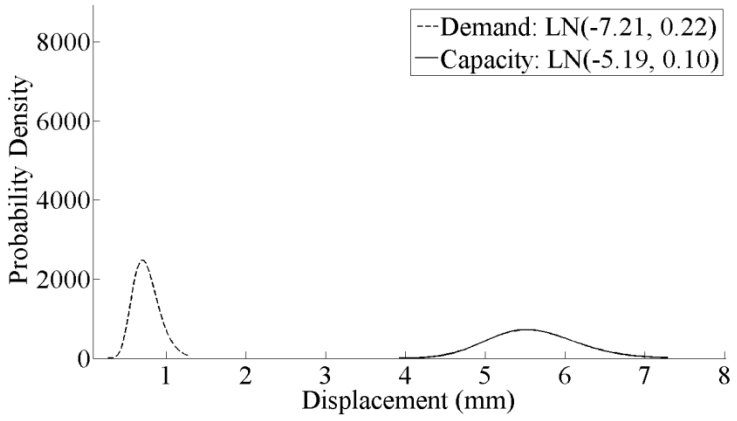

(c) Sa=1.5g

Figure D-10. Probabilistic models of the demand and capacity of column 4 for serviceability limit state, given that a) Sa=0.51, b) Sa=0.99 and c) Sa=1.5

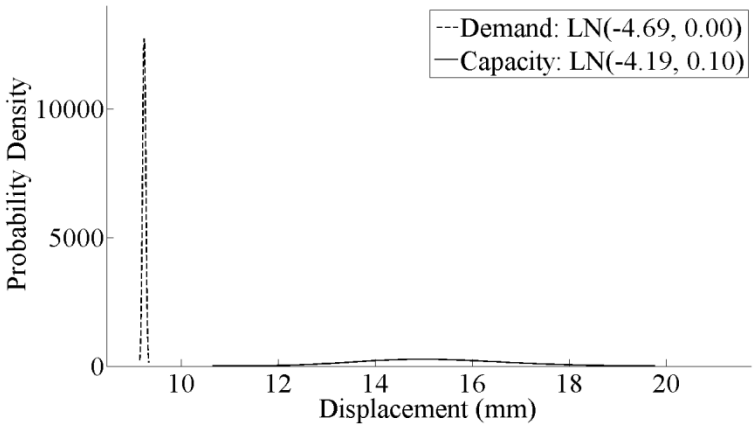

(a) Sa=0.51g

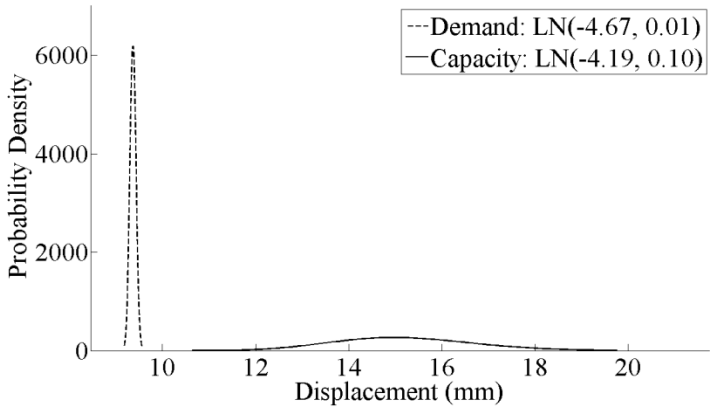

(b) Sa=0.99g

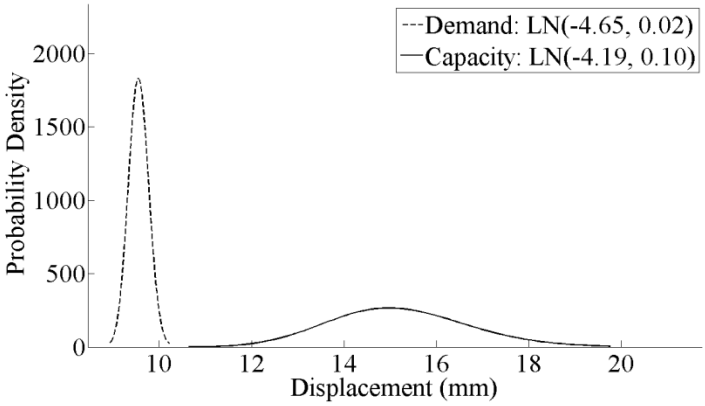

(c) Sa=1.5g

Figure D-11. Probabilistic models of the demand and capacity of the pile group for serviceability limit state, given that a) Sa=0.51, b) Sa=0.99 and c) Sa=1.5

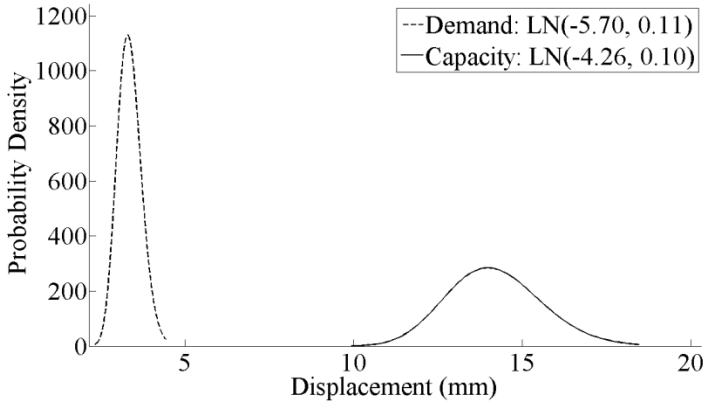

(a) Sa=0.51g

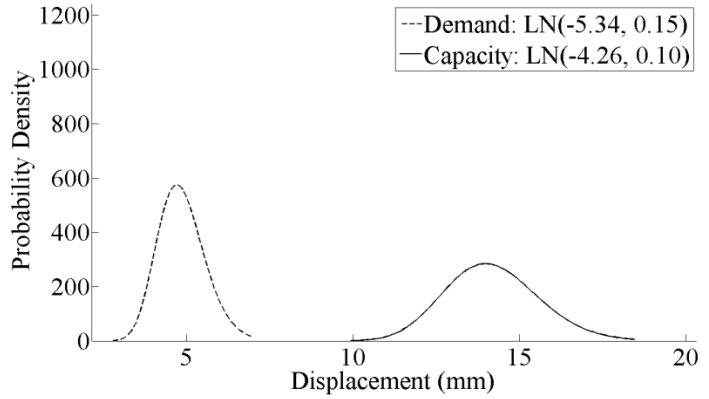

(b) Sa=0.99g

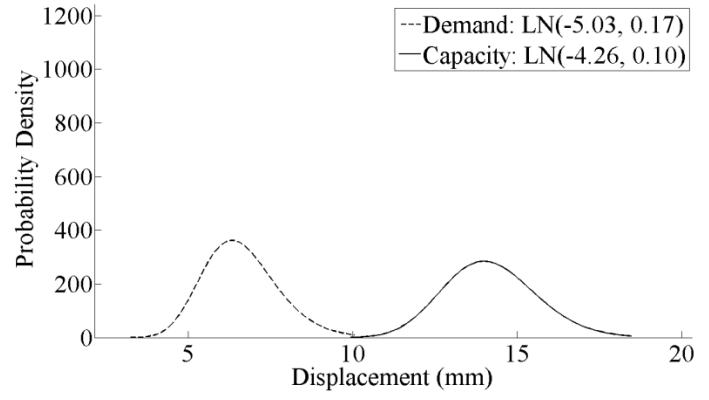

(c) Sa=1.5g

Figure D-12. Probabilistic models of the demand and capacity of bearing 1 for collapse limit state, given that a) Sa=0.51, b) Sa=0.99 and c) Sa=1.5

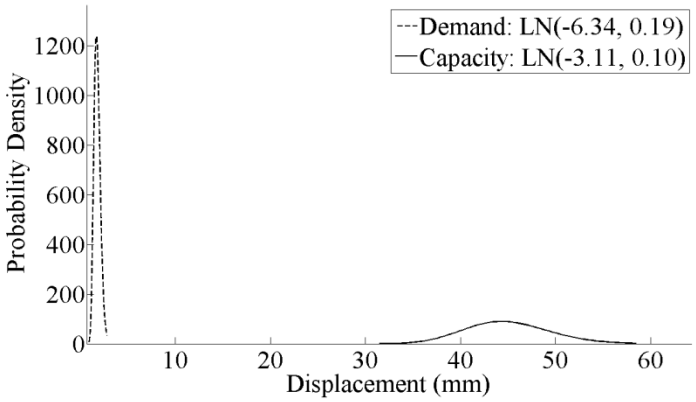

(a) Sa=0.51g

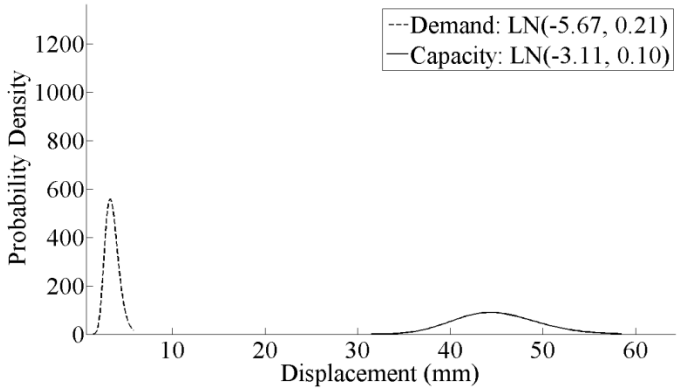

(b) Sa=0.99g

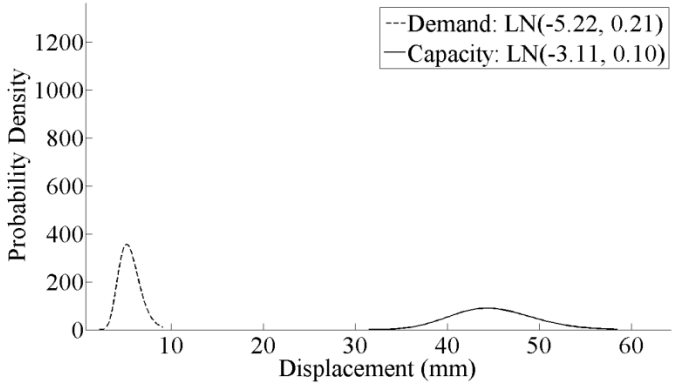

(c) Sa=1.5g

Figure D-13. Probabilistic models of the demand and capacity of bearing 4 for collapse limit state, given that a) Sa=0.51, b) Sa=0.99 and c) Sa=1.5

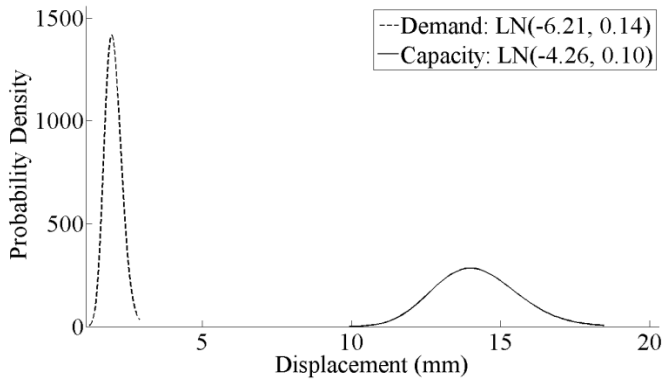

(a) Sa=0.51g

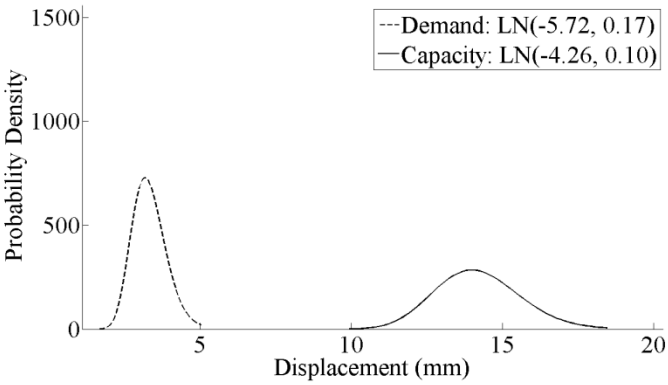

(b) Sa=0.99g

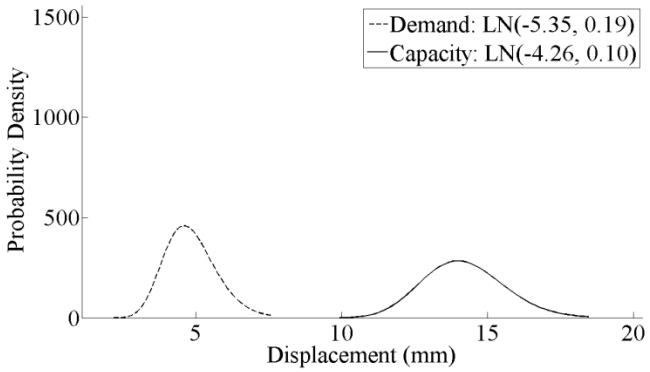

(c) Sa=1.5g

Figure D-14. Probabilistic models of the demand and capacity of bearing 6 for collapse limit state, given that a) Sa=0.51, b) Sa=0.99 and c) Sa=1.5

REFERENCES

Alipour, A., Shafei, B., and Shinozuka, M. (2011). “Performance Evaluation of Deteriorating Highway Bridges Located in High Seismic Areas”, J. Bridge Eng., 16(5), 597–611.

Alipour, A., Shafei, B., and Shinozuka, M. (2013). “Capacity loss evaluation of reinforced concrete bridges located in extreme chloride-laden Environments”, Structure and Infrastructure Engineering 9(1), 8–27

Anand R., Mehrotra K., Mohan C.K., Ranka S., (1995)."Efficient classification for multiclass problems using modular neural networks", IEEE Transactions on Neural Networks 6 (1) 117–124.

Andrade, C., Alonso, C., and Molina, F. J. (1993A). “Cover cracking as a function of rebar corrosion: Part 1. Experimental test” *Mater. Struct.*, 26, 453–464.

Andrade, C., Alonso, C., and Molina, F. J. (1993B). “Cover cracking as a function of rebar corrosion: Part 2. Numerical Model” *Mater. Struct.*, 26(9), 532-548

Atkinson, G.M. and Boore, D.M. (2006). “Earthquake ground-motion prediction equations for eastern North America.” *Bull. Seism. Soc. Am.*, 96(6), 2181-2205.

Atkinson, G.M. and Goda, K. (2011). “Effects of seismicity models and new ground-motion prediction equations on seismic hazard assessment for four Canadian cities.” *Bull. Seism. Soc. Am.*, 101(1), 176-189.

Baker, J.W., (2011). “Conditional Mean Spectrum: Tool for ground motion selection”Journal of Structural Engineering, 137(3), 322-331.

Baker, J. W., and Cornell, C. A. (2005) “A vector-valued ground motion intensity measure consisting of spectral acceleration and epsilon” Earthquake EngStruct. Dyn. 34, 1193–1217

Baker, J.W. and Cornell, C.A. (2006).“Spectral shape, epsilon and record selection.”Earthquake Engineering & Structural Dynamics, 34(10), 1193-1217.

Baker, J.W., and Jayaram, N. (2008). “Correlation of Spectral Acceleration Values from NGA Ground Motion Models.” Earthquake Spectra, 24(1), 299–317.Bentz, E. 2001. Response-2000, Shell-2000, Triax-2000, Membrane-2000: User Manual. Department of Civil Engineering,

University of Toronto, Toronto, Ontario, Canada.

Bignell, J. L., Lafave, J. M., Wilkey, J. P., and Hawkins, N. M. (2004).“Seismic Evaluation of Vulnerable Highway Bridges with Wall Piers on Emergency Routes in Southern Illinois.”13th World Conference on Eartquake Engineering, Vancouver, B.C. Canada.

Billah, M., Alam, S. and Bhuiyan, R. (2012). “Fragility Analysis of Retrofitted Multi-Column Bridge Bent Subjected to Near Fault and Far Field Ground Motion”, *Journal of Bridge Engineering, 10.1061*

Boore, D. M. and G. M. Atkinson (2008). “Ground-motion prediction equations for the average horizontal component of PGA, PGV, and 5%-damped PSA at spectral periods between 0.01 s and 10.0 s”, Earthquake Spectra 24, 99-138.

Box, G. E. P. and Wilson, K.B. (1951) “On the Experimental Attainment of Optimum Conditions (with discussion).”, *Journal of the Royal Statistical Society* ,Series B**13**(1):1–45.

Bucher C G, Bourgund U. A fast and efficient response surface approach for structural reliability problems[J]. Structural Safety, 1990, 7(1):57–66.

Carr, A.J. (2001). RUAUMOKO, The Maori God of Volcanoes and Earthquakes 3-Dimensional Version. Department of Civil Engineering - University of Canterbury, Christchurch, New Zealand.

Chang, C.-C. and C.-J. Lin, LIBSVM: a library for support vector machines, 2001. Software available at http://www.csie.ntu.edu.tw/_cjlin/libsvm.

Chen, W., Baghdasaryan, L., Buranathiti T., Cao, J., (2004). “Model Validation via Uncertainty Propagation and Data Transformations”, AIAA Journal Vol. 42, No. 7.

Cherkassky, V., Mulier, F., (2007). " Learning from Data: Concepts, Theory, and Methods", John Wiley & Sons, Inc., New York, NY.

Choi, E., DesRoches, R., and Nielson, B. (2004).“Seismic Fragility of Typical Bridges in Moderate Seismic Zones.”Engineering Structures, 26(2), 187–199.

Christensen P, Baker MJ (1982). “Structural reliability theory and its applications.”, Springer, New York

Cornell, A. C., Jalayer, F., and Hamburger, R. O. (2002). “Probabilistic Basis for 2000 SAC Federal Emergency Management Agency Steel Moment Frame Guidelines.” *Journal of Structural Engineering*, 128(4), 526–532.

Cortes, C., Vapnik, V. N., (1995). "Support vector networks". Machine Learning, 20(3) 273–297

Coulombe, C., (2007). “Seismic Retrofit of a Reinforced Concrete Bridge Bent”, M.Sc. Thesis, Department of Civil Engineering and Applied Mechanics, McGill University, Montreal, Canada, 85pp.

Crammer K., Singer Y., (2001). "On the algorithmic implementation of multiclass kernel-based vector machines". Journal of Machine Learning Research, 2:265:292.

De la Puente Altez, AG. (2005). “Study of the Seismic Vulnerability of Highway Overpass Bridges in Montreal”, Ph.D. thesis, Department of Civil Engineering and Applied Mechanics, McGill University, Montreal.

Drish, J. (1998) "Obtaining calibrated probability estimates from Support Vector Machines", Technical report, University of California, San Diego, June 2001.

Duan, K.B., Keerthi, S. (2005). “Which Is the Best Multiclass SVM Method? An Empirical Study” N.C. Oza et. al. (Eds.): MCS 2005, LNCS 3541, pp. 278–285.

Dueñas-Osorio, L. and Padgett, J.(2011). “Seismic Reliability Assessment of Bridges with User-Defined System Failure Events.” Journal of Engineering Mechanics, Vol. 137, No. 10, pp.680-690.

Duprat, F. (2007). "Reliability of RC beams under chloride-ingress." Construction and Building Materials 21(8): 1605-1616.

Edwards W., Lindman H., Savage L. J., (1963). “Bayesian statistical inference for psychological research.”, Psychol Rev, 7(3), 193–342.

FEMA. HAZUS-MH MR1: Technical Manual, Federal Emergency Management Agency, Washington, DC, 2003

Flis. J.. Pickering, H. W. and Osseo-Asare, K(1995) "Assessment of dada from three electrochemical instruments for evaluation of reinforcement corrosion rates in concrete bridge

componrnts". Corrosion. 5 l(8): 603-609

Friedman, J. H. , (1994). An overview of predictive learning and function approximation, in: V. Cherkassky, J. H. Friedman, and H.Wechsler (Eds.), From Statistics to Neural Networks, NATO ASI Series F, 136, New York: Springer.

Friedman J.H.,(1996), Another approach to polychotomous classification, Technical Report, Department of Statistics, StanfordUniversity.URL: /http:// www stat.stanford.edu/_jhf/ftp/poly.ps.ZS.

Ge, M., Du R., Zhang, G., Xu, Y., (2004). "Fault diagnosis using support vector machine with an application in sheet metal stamping operations" Mechanical Systems and Signal Processing 18, 143–159

Gergely, I., Pantelides, C. P., Nuismer, R. J., and Reaveley, L. D. (1998). "Bridge pier retrofit using fiber-reinforced plastic composites", *J. Compos. Constr.,* 2(4), 165–174.

Gergely, J., Pantelides, C. P., and Reaveley, L. D. (2000). "Shear strengthening of RC T-joints using CFRP composites", *J. Compos. Constr.,* 4(2), 56–64.

Ghanem R. G., Spanos P. D., (1991). "Stochastic finite elements: a spectral approach.", Springer, New York

Ghosh, J., Padgett, J. E. (2010). "Aging Considerations in the Development of Time-Dependent Seismic Fragility Curves", Struct. Eng. 136(12), 1497–1511

Giovenale, P., Cornell, A. C., and Esteva, L. (2004). "Comparing the Adequacy of Alternative Ground Motion Intensity Measures for the Estimation of Structural Responses." *Earthquake Engineering & Structural Dynamics*, 33, 951979.

Griezic, A (1996). "Seismic Evaluation and Retrofit of Concrete Bridge Columns and Joints", Ph.D. Thesis, Department of Civil Engineering and Applied Mechanics, McGill University, Montreal, Canada, September 1996, 341pp.

Guan XL, Melchers RE. (2001). "Effect of response surface parameter variation on structural reliability estimates". Structural Safety; 23:429–44.

Halton, J. H., (1960). "Onthe Efficiency of Certain Quasi-Random Sequences of Points in

Evaluating Multi-Dimensional Integrals,", *Numerische Mathematik*, 2, 84–90.

Hammersley, J. M., (1960). "Monte Carlo Methods for Solving Multivariate Problems.", *Ann. New York Acad. Sci. 86, 844-874.*

Hastie T., Tibshirani R., (1998) "Classification by pairwise coupling", Annals of Statistics 26 (2) 451–471.

Hills RG, Leslie IH. (2003). "Statistical validation of engineering and scientific models: validation experiments to application." Report no. SAND2003-0706. Albuquer- que, NM: Sandia National Laboratories.

Hills, G. R., and Trucano, T. G., (1999). "Statistical Validation of Engineering and Scientific Models: Background", Sandia National Labs., Rept. SAND99- 1256, Albuquerque, NM.

Hastie T., Tibshirani R., (1998) "Classification by pairwise coupling", Annals of Statistics 26 (2) 451–471.

Hong-shuang, L., Zhen-zhou, L., Zhu-feng, Y., (2006). "Support Vector Machine For Structural Reliability Analysis" Applied Mathematics and Mechanics (English Edition), 27(10) 1295–1303

Housner, G.W., and Thiel, C.C. (1990). "Competing Against Time: Report of the Governor's Inquiry on the Loma Prieta Earthquake", *Earthquake Spectra,* Vo1.6, *No.4,* pp. 681-711.

Hsu, C.-W., Lin, C.-J. (2002). "A comparison of methods for multi-class support vector machines". IEEE Transactions on Neural Networks 13, 415–425.

Huang, R. and C. C. Yang (1997). "Condition assessment of reinforced concrete beams relative to reinforcement corrosion." Cement & concrete composites. 19(2): 131.

Hurtado J E. An examination of methods for approximating implicit limit state functions from the viewpoint of statistical learning theory[J]. Structural Safety, 2004, 26(3):271–293.

Hurtado J E, Alvarez D A. Classification approach for reliability analysis with stochastic finite-element modeling. Journal of Structural Engineering 2003; 129(8): 1141-1149.

Hwang, H. and Huo, J. R. (1998). "Probablistic Seismic Damage Assessment of Highway Bridges," the 6t h U.S. National Conference on Earthquake Engineering, Seattle, Washington,

June, 1998.

Hwang, H., Jernigan, J. B., and Lin, Y. (2000a). "Evaluation of Seismic Damage to Memphis Bridges and Highway Systems," Journal of Bridge Engineering, Vol. 5, No. 4, ASCE, November, 2000, p322-330.

Ismail, M.E. and Soleymani, H.R. (2002) "Laboratory Monitoring Of Corrosion Rate In Portland Cement Concrete Specimens Subjected To Chloride Attack", Annual Conference of the Canadian Society for Civil Engineering, Montréal, Québec, Canada

Itagawa, W., (2005). "Seismic response of a concrete bridge bent", M.Sc. Thesis, Department of Civil Engineering and Applied Mechanics, McGill University, Montreal, Canada, 92pp.

Jack, L. B., Nandi, A. K., "Fault Detection Using Support Vector Machines and Artificial Neural Networks, Augmented By Genetic Algorithms" Mechanical Systems and Signal Processing 16(2–3), 373–390

Kang W.H., Song J., Gardoni, P., (2008). "Matrix-based system reliability method and applications to bridge networks.", Reliability Engineering and System Safety 93 (2008) 1584–1593

Kiureghian A. D. (1996). "Structural reliability methods for seismic safety assessment: a review.", Eng Struct 18:412–424

Kleijnen J. (1995). "Verification and validation of simulation models", European Journal of Operational Research 82, 145-162

Kleijnen J. (1995). "Statistical validation of simulation models", European Journal of Operational Research 87, 21-34

Knerr S., Personnaz L., and Dreyfus G., (1990). "Single-layer learning revisited: A stepwise procedure for building and training a neural network", in Neurocomputing: Algorithms, Architectures and Applications, J. Fogelman, Ed. New York: Springer-Verlag.

Kreßel U., (1999) "Pairwise classification and support vector machines", in Advances in Kernel Methods—Support Vector Learning, B. Schölkopf, C. J. C. Burges, and A. J. Smola, Eds. Cambridge, MA: MIT Press, pp. 255–268.

Lee S. H., Chen W., (2009). “A comparative study of uncertainty propagation methods for black-box-type problems.”, Struct Multidisc Optim, 37:239–253

Lee, Y., Lin, Y. and Wahba, G. (2001). "Multicategory support vector machines". Technical Report 1043, Department of Statistics, University of Wisconsin.

Li, C. Q. (2004). “Reliability Based Service Life Prediction of Corrosion Affected Concrete Structures”, *J. Struct. Eng.*, 130(10), 1570–1577.

Lin, H.-T., Lin, C.-J., Weng, R.C.:(2003). “A note on Platt’s probabilistic outputs for support vector machines “ Available: http://www.csie.ntu.edu.tw/˜cjlin/papers/plattprob.ps

Lorena A.C., Carvalho A.C. (2008a) Investigation of strategies for the generation of multiclass support vector machines. In: The twenty first international conference on industrial, engineering & other applications of applied intelligent systems (IEA/AIE), 1st edn, vol. 134 of studies in computational intelligence. Springer, New York, pp 319–328.

Lorena A.C., Carvalho A.C., Gama J.M., (2008b). "A review on the combination of binary classifiers in multiclass problems", Artificial Intelligence Review 30 (1–4) 19–37.

Lounis, Z., (2003). “Probabilistic modeling of chloride contamination and corrosion of concrete bridge structures”, Inst. for Res. in Constr., Nat. Res. Council of Canada, Ottawa, Ont.

Lounis, Z, and Mirza, M.S. (2001), “Reliability-based Service Life Prediction of Deteriorating Concrete Structures”, In Concrete under Severe Conditions, Banthia, N (ed.), pp. 965-972.

Lounis, Z, Zhang J., and Daigle, L. (2004). “Probabilistic Study of Chloride-Induced Corrosion of Carbon Steel in Concrete Structures”, 9th ASCE Joint Specialty Conference on Probabilistic Mechanics and Structural Reliability, Albuquerque, New Mexico, pp. 1-6

Mackie K. &Stojadinovic B. (2002). “Relation between probabilistic seismic demand analysis and incremental dynamic analysis”, 7th US National Conference on Earthquake Engineering, Boston, MA.

Mackie K, Stojadinovic B. (2003). “Seismic demands for performance-based design of bridges.” PEER Report. 2003/16, August, Pacific Engineering Earthquake Center, University of California, Berkeley.

Madsen HO, Krenk S, Lind NC (2006), "Methods of structural safety." Dover, Mineola, NY

Mahadevan, S., Rebba, R., (2004). "Validation of reliability computational models using Bayes networks", Reliability Engineering and System Safety Vol. 87, pp.223–232

Mander, J.B., Priestley, M.J.N., and Park, R. (1988). Theoretical stress-strain model of confined concrete. J. Struct. Eng., 114(8), 1804-1826.

Mitchell, D., Bruneau, D., Williams, M., Anderson, D.L., and Sexsmith, R. (1995). "Performance of the Bridges in the 1994 Northridge Earthquake", *Canadian Journal of Civil Engineering,* Vol. 22, No. 2, pp. 415-427.

Mitchell, D., Sexsmith, R., and Tinawi, R. (1994). "Seismic Retrofitting Techniques for Bridges-A State-of-the-Art Report", *Canadian Journal of Civil Engineering,* Vol. 21, No. 5, pp. 823-835.

Mitchell, D., Tinawi, R., and Sexsmith, R. (1991). "Performance of Bridges in the 1989 Loma Prieta Earthquake - Canadian Design Concerns", *Canadian Journal of Civil Engineering,* Vol. 18, *No.4,* pp.711-734.

Mitchell, D. (2002). "Aspects of seismic evaluation and retrofit of Canadian bridges", in proceedings of behaviour and design of concrete structures for seismic performance, *ACI special publication,* SPI-197, 169-179.

Mitropoulou, C., Papadrakakis, M., (2011) "Developing fragility curves based on neural network IDA predictions" Engineering Structures, 33(12), 3409–3421

Molinaro, A. M., Simon, R., and Pfeiffer, R. M. (2005). Prediction error estimation: A comparison of resampling methods. Bioinformatics 21, 3301–3307.

Nielson B.G. and DesRoches R., (2007). "Seismic fragility methodology for highway bridges using a component level approach", *Earthquake Eng Struct. Dyn.* 36 pp. 823–839

Nielson, B. (2005). "Analytical fragility curves for highway bridges in moderate seismic zones." Ph.D. thesis, Georgia Institute of Technology, Atlanta.

Oberkampf WL, Barone MF. (2006). "Measures of agreement between computation and experiment: validation metrics.", Journal of Computational Physics, 217(1), 5–36

Oberkampf WL, Trucano TG. (2002). “Verification and validation in computational fluid dynamics.”, Progress in Aerospace Sciences, 38, 209–72.

Oberkampf, W. L., T. G. Trucano, and C. Hirsch (2004). Verification, validation, and predictive capability in computational engineering and physics. *Applied Mechanics Reviews*. **57**(5), 345–384.

Owen, A. B., (1998). “Latin Supercube Sampling for Very High Dimensional Simulation.”, *ACM Transactions on Modeling and Computer Simulation*, 8(1), 71–102.

Pan, Y., Agrawal A.K., Ghosn M. and Alampalli S. (2010). “Seismic Fragility of Multispan Simply Supported Steel Highway Bridges in New York State. I: Bridge Modeling, Parametric Analysis, and Retrofit Design”, *Journal of Bridge Engineering, 15, 448-461*

Pan, Y., Agrawal A.K., Ghosn M. and Alampalli S. (2010). “Seismic Fragility of Multispan Simply Supported Steel Highway Bridges in New York State. II: Fragility Analysis, Fragility Curves, and Fragility Surfaces”, *Journal of Bridge Engineering, 15*

Pilch, M., T. G. Trucano, J. L. Moya, G. K. Froehlich, A. L. Hodges, and D. E. Peercy (2001). *Guidelines for Sandia ASCI Verification and Validation Plans – Content and Format: Version 2*. Albuquerque, NM, Sandia National Laboratories, SAND2000–3101.

Platt, J.C., (1998). “Sequential minimal optimization: a fast algorithm for training support vector machines” Microsoft Research Technical Report, MSR-TR-98-14, Microsoft, Redmond, Washington

Platt, J.C., (1999). “Probabilistic outputs for support vector machines and comparison to regularized likelihood methods” In: Smola, A.J., Bartlett, P., Sch¨olkopf, B., Schuurmans, D. (eds.): Advances in Large Margin Classifiers. MIT Press 61–74.

Platt J.C., Cristianini N., Shawe-taylor J. , (2000) "Large margin dags for multiclass classification", in: Advances in Neural Information Processing Systems, MIT Press, pp. 547–553.

Priestley, M.J.N, Seible, F. and Anderson, D.L. (1993). “Proof test of a retrofit concept for the San Francisco double-deck viaducts, Part I:design concept, details and model”, *ACI Structural Journa*l, 90(5): 467-479.

Priestley, M.J.N, Seible, F. and Anderson, D.L. (1993). “Proof test of a retrofit concept for the

San Francisco double-deck viaducts, Part II: Test details and results", *ACI Structural Journal*, 90(6): 616-631.

Rajashekhar M R, Ellingwood B R. A new look at the response surface approach for reliability analysis[J]. Structural Safety, 1993, 12(3):205–220.

Rebba, R., Mahadevan, S. (2006). "Validation of models with multivariate output", *Reliability Engineering and System Safety*, 91, 861–871

Revie, R. W. (2000). Uhlig's Corrosion Handbook (2nd Edition), John Wiley & Sons.

Rifkin R., Klautau A., (2004)."In defense of one-vs-all classification", Journal of Machine Learning Research 5:101–141.

Rocco C M, Moreno J A. Fast monte carlo reliability evaluation using support vector machine. Reliability Engineering & System Safety 2002; 76(3): 237-243.

Rodrıguez, J., Pe rez, A., Lozano, J., (2010). "Sensitivity Analysis of k-Fold Cross Validation in Prediction Error Estimation," IEEE Transactions on Pattern Analysis and Machine Intelligence, 32(3):569-575, doi:10.1109/TPAMI.2009.187

Rüping S. (2004) " A Simple Method for Estimating Conditional Probabilities For SVMs", Technical Report / Universität Dortmund, SFB 475 Komplexitätsreduktion in Multivariaten Datenstrukturen,56.

SAP2000, Integrated Finite Element Analysis and Design of Structures: Analysis Reference (1996). Computers and Structures, Inc., Berkeley, CA.

Shamsabadi, A., Rollins, K. M., and Kapuskar, M. (2007). Nonlinear soil-abutment-bridge structure interaction for seismic performance-based design. Journal of Geotechnical and Geoenvironmental Engineering, 133(6), 707-720.

Shinozuka, M. (1998)."Development of Bridge Fragility Curves" University of Southern California, (Unpublished Work).

Shinozuka, M., Feng, M. Q., Kim, H., Uzawa, T., and Ueda, T. (2003)."Statistical Analysis of Fragility Curves."Report No. MCEER-03-0002, MCEER.

Shinozuka, M., Kim, S.H., Kushiyama, S. and Yi, J.H. (2002). "Fragility curves of concrete bridges retrofitted by column jacketing", *Earthquake Engineering and Engineering Vibration*, 1(2): 195-205.

Song, J., and Kang, W.-H. (2009). "System reliability and sensitivity under statistical dependence by matrix-based system reliability method." Struct. Saf., 31(2), 148–156.

Song, J. and Kang, W.H.. (2010). "Probabilistic shear strength models for reinforced concrete beams without shear reinforcement.", Structural Engineering and Mechanics, Vol. 34, No. 1, pp.15-38

Stewart, M. G., and Rosowsky, D. V. (1998). "Time-dependent reliability of deteriorating reinforced concrete bridge decks." *Struct. Safety*, 20(1), 91–109.

Stewart, M. G. (2003). "Temporal and Spatial Aspects of Probabilistic Corrosion Models.", Third IABMAS Workshop on Life-Cycle Cost Analysis and Design of Civil Infrastructure Systems and the JCSS Workshop on Probabilistic Modeling of Deterioration Processes in Concrete Structures**:** 10.

Tavares D. H., Roy N, Padgett J. E. and Paultre P., (2010). "Seismic Vulnerability Evaluation of Highway Bridges in Quebec Using Fragility Curves", *9th U.S. National and 10th Canadian Conference on Earthquake Engineering*, Toronto, Canada

Tehrani, P. and Mitchell, D. (2012). "Seismic risk assessment of four-span beridges in Montreal" submitted to *Journal of Bridge Engineering*.

Tehrani, P. (2012). "Seismic analysis and behaviour of continuous reinforced concrete bridges." PhD thesis, Department of Civil Engineering and Applied Mechanics, McGill University, Montreal.

Trucano, T. G., M. Pilch, and W. L. Oberkampf (2002). *General Concepts for Experimental Validation of ASCI Code Applications*. Albuquerque, NM, Sandia National Laboratories, SAND2002–0341.

Tuutti, K. (1982). "Corrosion of steel in concrete", *Swedish Cement and Concrete Research Inst*., 17–21.

Unnikrishnan V. U., Prasad A. M. and Rao B. N. Development of fragility curves using high-

dimensional model representation[J]. Earthquake Engineering & Structural Dynamics, 2013, 42:419–430.

Vamvatsikos, D. and Cornell, A. C. (2002). “Incremental Dynamic Analysis.”, *Earthquake Engineering* & *Structural Dynamics*, 31, 491–514.

Vapnik, V.N., (1995). “The Nature of Statistical Learning Theory” Springer Verlag, NY.

Vovk V., Gammerman A., Shafer G.,(2005). Algorithmic learning in a random world. Springer, New York.

Vovk V., Shafer G. and Nouretdinov I., (2003). Self-calibrating probability forecasting. On-line Compression Modelling Project, working paper 9, http://vovk.net/cp/09.pdf.

Weston J., Watkins C. (1998). "Multi-class support vector machines". Technical Report CSD-TR-98-04, Royal Holloway, University of London, Department of Computer Science.

Widodo, A., Yang, B. (2007) “Support vector machine in machine condition monitoring and fault diagnosis.” Mechanical Systems and Signal Processing 21, 2560–2574.

Wolofsky, R. (2011), “Corrosion Initiation of Concrete Bridge Elements Exposed to De-icing Salts”, Ph.D. thesis, McGill University, Montreal, Canada.

Wu, T.F., Lin, C.J., Weng, R.C. (2004). “Probability estimates for multi-class classification by pairwise coupling” Journal of Machine Learning Research, 5, 975–1005

Zadrozny, B., Elkan, C. (2002)"Transforming classifier scores into accurate multiclass probability estimates". In: Proceedings of the 8th ACM International Conference on Knowledge Discovery and Data Mining, pp. 694–699

Zhang, R., Mahadevan S., (2000). “Model uncertainty and Bayesian updating in reliability-based inspection”, Structural Safety Vol. 22 pp 145-160

Zhiwei G., Guangchen, B. Application of Least Squares Support Vector Machine for Regression to Reliability Analysis. Chinese Journal of Aeronautics 2009; 22:160-166.

Zhu L., (2005). “Probabilistic Drift Capacity Model For Reinforced Concrete Columns”., M.Sc. Thesis, University of British Columbia, Canada